The Thesis Committee for Phillip Wayne Pesek
Certifies that this is the approved version of the following thesis:

Temperature, Stress, and Strength Development of Early-Age Bridge Deck Concrete

APPROVED BY
SUPERVISING COMMITTEE:

Supervisor:

Kevin Folliard

Thanos Drimalas

Temperature, Stress, and Strength Development of Early-Age Bridge Deck Concrete

by

Phillip Wayne Pesek, B.S.C.E

Thesis

Presented to the Faculty of the Graduate School of

The University of Texas at Austin

in Partial Fulfillment

of the Requirements

for the Degree of

Master of Science in Engineering

The University of Texas at Austin

August 2011

Dedication

I dedicate this to my parents. Without the values they instilled in me, I never would have been able to accomplish all that I have done.

Acknowledgements

I would like to thank Kevin Pruski and Andy Naranjo from TxDOT. Andy's assistance with XRF and optimized aggregate gradations is greatly appreciated. Thank you Kevin for the work you did in finding bridge decks for our team to instrument, and for the work you did tracking down information on these bridge decks both before, and many, many months after the pour.

I would like to thank my advisor, Dr. Kevin Folliard, and my second reader, Dr. Thanos Drimalas, for the guidance and assistance in writing this thesis, and in all other matters throughout the course of this project. A very special thanks goes out to Dr. Kyle Riding and Dr. Anton Schindler. Your expertise in nearly every aspect of this project was extremely helpful. I would like to thank Benjamin Byard for his cooperation and assistance with the evaluation of rigid cracking frame stresses with his modified B3 model.

Over the last five years, I have gained some amazing friends from my coworkers at CMRG. Chris, without your help, I'd probably still be working on that new formwork. And sorry about that time we made you drive to Lubbock on your birthday. Alex, thanks for joining the team that last year. I don't know that anybody else would have gotten done what you did, in the timeframe that you had. Brenden, you and I were unstoppable on that cracking frame. Thanks for all your help, and for fighting me on almost every one of my 150 step processes. Travis, thanks for your help on the bridge deck instrumentations and for the assistance on cracking frame mixes. Anthony, I greatly appreciate our friendship, and your ability to light a fire under me when I was dragging my feet at the lab. A big thanks goes out to Fred, Andy, Jose, Max, Karla, Allie, Zach,

Reid, and Mitchell. The cracking frame has never been a one-man job, the assistance you guys provided when I needed it was a huge help. Mitch, good luck with that cracking frame bud….you're going to need it.

Finally, I'd like to thank the staff at 18B. Mike, you really came through a few times when things were hitting the fan. Your help is greatly appreciated. Sherian, thank you for all the work you put in, on both the ordering and receiving of project materials, and in handling our tuition and finances.

Abstract

Temperature, Stress, and Strength Development of Early-Age Bridge Deck Concrete

Phillip Wayne Pesek, M.S.E

The University of Texas at Austin, 2011

Supervisor: Kevin Folliard

In bridge deck concrete, early-age cracking can lead to substantial serviceability and structural integrity issues over the lifespan of the bridge. An understanding of the temperature, stress, and strength development of concrete can aid determining the early-age cracking susceptibility. This project, funded by the Texas Department of Transportation, evaluated these properties for various bridge deck materials and mixture proportions.

The research presented in this thesis involved a laboratory testing program that used a combination of semi-adiabatic calorimetry, rigid cracking frame, free shrinkage frame, and match cured cylinder testing program that allowed the research team to simulate the performance of common bridge deck mixture designs under hot and cold weather conditions. In this program, the semi-adiabatic calorimetry was used, with previously generated models, to generate the temperature profile of the mixture. The rigid cracking frame and free shrinkage frame were used to evaluate the restrained stress development and the unrestrained volume changes, respectively, under the simulated

temperatures. The match-cure cylinder testing program allowed the research team to generate a strength development profile for the concrete mixtures under the various simulated temperature profiles.

Results from the laboratory program revealed that in hot weather simulations, ground granulated blast furnace slag mixtures developed the lowest stress / strength ratios, and in cold weather simulations, Class F fly ash mixtures developed the lowest stress / strength ratios. In general, use of SCMs and limestone coarse aggregate results in mixtures that generate less heat and lower stress / strength ratios. Isothermal testing showed that shrinkage reducing admixtures were effective in reducing early-age strains from chemical shrinkage.

In addition to the laboratory testing program, a field testing program was completed to measure the temperature development of four bridge decks during the winter and summer months. The recorded concrete temperatures and the effects of the environmental conditions at the time of the pour will aid in the calibration and validation of the temperature prediction component of ConcreteWorks for bridge deck construction. In addition, experience gained through these field pours resulted in an optimized instrumentation procedure that will aid in the successful collection of data in future projects.

Table of Contents

List of Tables

List of Figures

Chapter 1: Introduction

1.1 BACKGROUND

Early-age bridge deck cracking has been found to be a prevalent problem in the United States and worldwide. Studies conducted by Krauss and Rogalla (1996) and Folliard et al. (2003) reported various cases of early-age cracking in bridge deck concrete. While early-age cracking will not cause failure of a bridge deck system independently, the penetration of deleterious substances through the early-age cracks into the bridge deck concrete and the bridge superstructure can lead to costly serviceability issues, and possibly the loss of some structural integrity.

Bridge deck cracking is a multi-mechanistic process, affected by various volume change mechanisms, strength development, and the restraint conditions of the system. Before the concrete has even set, plastic shrinkage cracking due to water loss to the environment must be avoided. At an early age, the volume changes associated with the hydration reactions taking place can lead to chemical and autogenous shrinkage. After the curing system has been removed, the concrete must be able to withstand the drying shrinkage that will occur over the life of the structure. Thermal deformations, both as a gradient and as a bulk temperature change, can lead to significant stresses in the concrete system at both early and later ages. Moisture gradients and carbonation shrinkage, though typically minor factors, will also add to the volume changes occurring in the concrete over time. Restraint conditions and a changing elastic modulus turn these various volume changes into stresses, which must be resisted by the developing strength of the concrete and through relaxation from concrete creep.

To understand the volume changes and strength development that influence early-age bridge deck cracking, one must also understand the factors that affect the rate and magnitude of early-age volume change and strength development. These factors include

mixture proportions, aggregate type and gradation, chemistry of the cements and supplementary cementitious materials used, and the changing temperature of the concrete system. While temperature of the concrete generally follows that of the environment at later ages, the early age concrete temperature that governs most of the volume changes and strength development is a complicated interaction between heat generated from concrete hydration, heat transfer with the environment, and heat transfer with elements of the bridge deck support structure.

1.2 RESEARCH OBJECTIVE

The objective of this research project was to evaluate the effects of environmental conditions, cement type, supplementary cementitious material type and dosage, and aggregate type on the temperature, stress, and strength development of early-age concrete. With this knowledge, conclusions could be drawn as to which mixture designs would have a higher probability of experiencing early-age cracking.

In addition, this research project aimed to improve the temperature prediction models found in the current version of ConcreteWorks. Instrumentation of bridge decks in the field will allow adjustments to how various factors affect the early-age temperature development of bridge deck concrete.

1.3 RESEARCH APPROACH

Semi-adiabatic calorimetry, rigid cracking frame testing, free shrinkage frame testing, and match-cured mechanical testing were implemented to evaluate the temperature, stress, and strength development of various bridge deck concrete mixture designs.

Before rigid cracking frame, free shrinkage frame, and cylinder testing were conducted, the research team would perform semi-adiabatic calorimetry testing on the

mixture design. Coupled with empirical calculations, hydration parameters for the mixture designs could be calculated. These hydration parameters were used as inputs in ConcreteWorks software, along with inputs for time, date, and element size and type, to generate a temperature profile for the various mixture designs.

Following the semi-adiabatic calorimetry and temperature profile creation, rigid cracking frame, free shrinkage frame, and match-cured mechanical testing were conducted. A computer program was used to control the water circulators that pumped fluid through the insulated formwork of the rigid and free shrinkage frames, and through the match-cure water bath. Stress and temperature development were recorded from the rigid cracking frame on the same computer that controlled the water circulators. A separate data logger system was used to record the displacement of the specimen inside the free shrinkage frame. Cylinders were taken from the match-cure water bath and tested periodically to evaluate the strength development of the concrete mixture. The results of the aforementioned testing program will be synthesized and integrated into the bridge deck cracking module being developed for ConcreteWorks under TxDOT Project 6332.

1.4 SCOPE OF REPORT

Following this introductory chapter, Chapter 2 presents a literature review of the key factors involved in early-age bridge deck cracking. Though not exhaustive, the literature review provides enough information for a general knowledge of volume changes in concrete, the development of mechanical properties, and of the key parameters affecting bridge deck cracking.

Chapter 3 provides an overview of the laboratory testing program. Physical and chemical descriptions of the materials used, followed by the mixture proportions for the

mixture designs that were evaluated. An identification system is provided to aid in uniquely identify the various mixtures that were evaluated. Chapter 3 also includes a description of the procedures that were taken before, during, and after the day of mixing. Chapter 3 concludes with physical and procedural descriptions of the semi-adiabatic, rigid cracking frame, free shrinkage frame, setting time, mechanical property, and drying shrinkage testing that were conducted.

Chapter 4 presents the results of the laboratory testing program. Fresh and hardened concrete properties, hydration parameters, restrained stresses, unrestrained strains, and setting times for each mixture are presented. In addition, Chapter 4 includes a section in which a modified creep model is evaluated against the data produced from the testing program.

Chapter 5 is a description of the field testing program. Structural details, instrumentation locations, and instrumentation preparation methods are discussed. Results of return trips to inspect for visible early-age cracking are also provided.

Chapter 6 presents and discusses the results of the field testing program. In addition to the recorded bridge deck temperatures, fresh concrete properties, hydration parameters, and mechanical strength development are detailed.

Chapter 7 presents the overall conclusions from this study and provides recommendations for future research related to bridge deck volume changes and crack potential.

Chapter 2: Literature Review

Chapter 2 includes a literature review of the aspects that affect early-age bridge deck temperature, stress, and strength development. This literature review is not intended to be exhaustive, but rather, to present a general knowledge of the subject matter covered.

2.1 VOLUME CHANGES IN CONCRETE

Concrete is a dynamic material with a microstructure that evolves with time, and a volume that changes from the from the early stages of hydration to the later stages of service life. This section briefly describes the most relevant forms of volume change that affect concrete, in general, and bridge decks, in particular.

2.1.1 Plastic Shrinkage

Plastic shrinkage occurs as water is lost from the concrete to the environment while the concrete is still plastic (e.g. prior to setting). Plastic shrinkage cracking can occur in bridge decks or other elements with high surface/volume ratios once the cumulative evaporation from the concrete surface exceeds the cumulative bleeding of the concrete. When cumulative evaporation exceeds cumulative bleeding, water is drawn from within the bulk of the concrete, and the concrete goes into tension. Unfortunately, this event usually occurs before the concrete has developed any significant tensile strength, and if the event is reached, cracking is likely to result. In order to understand and possibly prevent plastic shrinkage, one must know and take into account the bleeding rate (and capacity), evaporation rate (as a function of the surrounding environment and concrete surface temperature), and the early-age strength development.

While this thesis will not delve into the testing for plastic shrinkage (evaporation and bleeding rates, and early-age strength development), an evaluation of a prediction method for concrete setting time was conducted. When attempting to predict plastic

shrinkage cracking susceptibility, a prediction of the concrete setting time will give the engineer an idea of when the concrete mixture has developed a certain level of strength. If cumulative evaporation exceeds cumulative bleeding before initial set, the probability of plastic shrinkage cracking is much higher than if this event occurs after concrete setting. Setting time will be discussed in Section 2.3.3 of the literature review.

2.1.2 Chemical and Autogenous Shrinkage

In recent years, there has been considerable interest in early-age behavior of concrete, and much of this interest has been fueled by the use of high-performance concrete (HPC), which is often characterized by relatively low water-to-cementitious materials ratio (w/cm) of less than 0.40 and the use of supplementary cementing materials. When using such mixtures in field applications, it is important to realize that there may be insufficient water present internally to fully hydrate the portland cement. As the cement hydration proceeds and the amount of free water decreases, air takes the place of water in pores, lowering the pore relative humidity. An air-water meniscus forms with an accompanying surface tension. The surface tension imparts a tensile stress on the matrix, causing shrinkage. This is referred to as "chemical shrinkage", which is defined as the volume reduction associated with the hydration reactions in a cementitious material (Jensen & Hansen, 2004). When aggregates are present, they are placed in compression by the cement matrix, providing restraint. The degree of restraint that the aggregates provide depends on the aggregate stiffness and the percent volume (Riding, 2007).

Although they are often considered to be the same property, autogenous shrinkage is different from chemical shrinkage in that it is defined as the bulk strain of a closed, isothermal, cementitious system not subjected to external forces. Chemical shrinkage can

then be defined as “a change in the absolute volume,” while autogenous shrinkage can be defined as “a bulk change in the apparent volume” (Jensen & Hansen, 2004). The two quantities tend to be identical up until concrete sets; thereafter, they deviate, with chemical shrinkage typically being significantly larger than autogenous shrinkage. As shown in Figure 2-1, “chemical shrinkage is an *internal* volume reduction, [while] autogenous shrinkage is an *external* volume change.” (Holt, 2001)

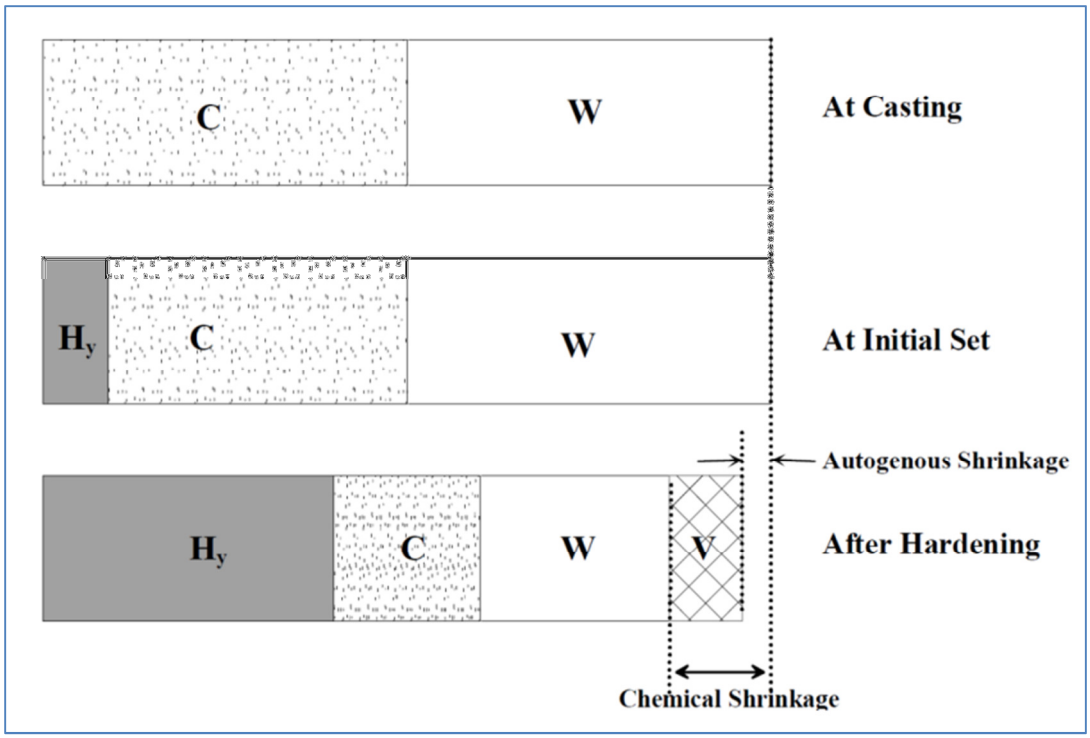

Figure 2-1: Autogenous and chemical shrinkage (Holt, 2001)

In the current version of ConcreteWorks, a modified version of the Hedlund model is used for approximating the autogenous shrinkage in concrete (Hedlund, 2000; Riding, 2007). Eq. 2-1 through Eq. 2-5 provide the autogenous shrinkage model proposed by Hedund, and the modification used in ConcreteWorks. Further explanation

of the terms, the modifications made to the model, and of the recommended parameters can be found in Hedlund (2000) and Riding (2007).

$$\varepsilon_{SH} = \varepsilon_{su} * \beta_{s0}(t_e) * \beta_{ST}(T)$$

Eq. 2-1

$$\varepsilon_{su} = \left(-0.65 + 1.3 * \frac{w}{cm}\right) * 10^{-3}$$

Eq. 2-2

$$\beta_{s0}(t_e) = exp\left(-\left[\frac{t_{s1}}{t - t_{so}}\right]^{n_{SH}}\right)$$

Eq. 2-3

$$\beta_{ST}(T) = a_0 + a_1 * \left[1 - exp\left(-\left[\frac{T}{T_1}\right]^{b_1}\right)\right] + a_2 * \left[1 - exp\left(-\left[\frac{T}{T_2}\right]^{b_2}\right)\right]$$

Eq. 2-4

$$\varepsilon_{ault} = (-0.94 + 2.238 * w/cm) * 10^{-3}$$

Eq. 2-5

2.1.3 Drying Shrinkage

Shrinkage caused by water loss from concrete has long been recognized as a cause of cracking of bridge decks and other flatwork. Although drying shrinkage has been somewhat overshadowed in recent years by concerns about autogenous shrinkage, it remains a major concern in the concrete industry. Mechanistically, the driving force behind drying shrinkage, namely the loss of internal water to the environment, is identical to the underlying cause of plastic shrinkage, the only difference being the nominal cut-off point in time when concrete transitions to a solid material (i.e. setting time). When water is lost from concrete, water is lost first from the largest pores, as the water in these pores is held with the least binding energy; water is then lost from smaller and smaller pores,

with pores below 50 nm being most responsible for drying shrinkage. As such, data on pore size distributions of the paste phase can be helpful in predicting shrinkage potential. The capillary stress theory, captured by the Kelvin/Laplace-Gibbs equation (Eq. 2-6), can be used to estimate the resultant stresses triggered by water loss as a function of pore size radius (r) and surface tension (γ) of the pore water.

$$\sigma = 2\gamma/r$$

Eq. 2-6

Various factors, such as w/cm, paste content, water content, cement type and fineness, SCM (dosage and type), chemical admixtures, aggregate type, and aggregate content affect the rate of shrinkage development and ultimate magnitude of shrinkage. One can optimize the pore size distribution to minimize the potential for drying shrinkage and shrinkage-reducing admixtures (SRAs) can be used to reduce the surface tension of the pore water (Folliard & Berke, 1997).

In field structures, factors such as curing method and regime, environmental conditions (temperature, RH, etc.) and surface/volume ratio of the structural elements play major roles in determining drying shrinkage behavior. For bridge decks, drying occurs from the top down, and as such, moisture gradients develop which can generate significant stress gradients, with the highest stress at the top of the deck.

There have been hundreds of studies on the drying shrinkage of concrete, evaluating everything from materials to mixture proportions to curing conditions. Because of this large database of shrinkage data, there have been several attempts to quantify and predict drying shrinkage as a function of time, including the following models; ACI 209, CEB 90, B3, and GL 2000 (ACI Committee 209, 2008; CEB-FIP Model Code '90, 1993; Bazant, 1995; Gardner & Lockman, 2001). Al-Manaseer and

Lam (2005) recently evaluated these four models from a statistical perspective, and found that the B3 and GL 2000 models were the best at predicting shrinkage within the RILEM database of mixtures. Mokarem (2002), using a set of mixture designs that were similar to many of those tested under TxDOT 6332, found that the CEB 90 model best predicted straight cement concrete mixtures, while the GL 2000 model most accurately predicted mixtures containing SCMs. Although there is no clear consensus on which of these models is best for predicting shrinkage (and/or creep), the B3 model (developed by Bazant and included in the RILEM recommendations) is the most recent model and has been favored by researchers and practitioners in recent years.

2.1.4 Thermal Deformations

While thermal deformations are usually thought of as a problem for mass concrete, the effects of thermal shrinkage must also be considered for bridge deck systems. Due to heat released from hydration reactions, concrete temperature will rapidly increase after concrete placement (given typical environmental conditions). After approximately 24-hours have passed, the concrete temperatures start to decrease as heat loss to the environment becomes greater than the heat generated from the hydration reactions. After several days have passed, the concrete heat production will nearly stop, and the concrete system will assume thermal behavior based on heat transfer with the surrounding environment. Although bridge decks usually do not crack due to thermal shrinkage alone, it must be realized that these strains are placed on top of drying and autogenous shrinkage strains that are occurring during the same time period (Babaei & Fouladgar, 1997). In order to predict the strains associated with the thermal changes taking place at early ages, a model was developed under TxDOT Project 4563 to predict the temperature development of concrete elements based on the progression of hydration

reactions and their interaction with the surrounding environment. Recent works by Riding and Poole have developed an extensive heat of hydration database over the last decade. This database, populated by isothermal and semi-adiabatic calorimetry data, has led to the development of hydration models for concrete mixtures containing a wide range of cement types, SCM types and dosages, and chemical admixture types and dosages (Riding, 2007; Poole, 2007). The models generated were based on both Bogue's and Rietveld analyses and were aimed at developing predictive models for quantifying the progress of hydration through the use of Eq. 2-7:

$$Q_h(t) = H_u * W_c * \left(\frac{\tau}{t_e}\right)^{\beta} * \left(\frac{\beta}{t_e}\right) * \alpha(t_e) * \exp\left(\frac{E_a}{R} * \left(\frac{1}{273 + T_r} + \frac{1}{273 + T_c}\right)\right)$$

Eq. 2-7

In Eq. 2-7, Q_h = rate of heat generation (W/m^3), H_u = total heat available (J/kg), and W_c = cementitious materials content (kg/m^3).

Equations for H_u are available in literature, but a more accurate equation is presented in Poole (2007). E_a, the apparent activation energy, describes the isothermal calorimetry testing that was developed to describe the effects of w/cm, cement chemistry, SCMs, and chemical admixtures on the E_a of Portland cement pastes. The model is also discussed in detail in work done by Poole (2007). The parameters α, β, and τ model the shape of the hydration curve from semi-adiabatic calorimetry. The model shown in Eq. 2-7 is based on a range of concrete mixtures that are typically used in mass concrete, bridge decks, and precast elements. Under TxDOT Project 4563, a finite difference-based model was developed to incorporate the heat of hydration models into field structures and to then apply advanced heat transfer principles to generate spatial, time-temperature histories throughout hydrating field elements, including mass concrete

elements, bridge decks, and precast girders (Riding, 2007). This model takes into account a wide range of boundary conditions, including solar radiation, convection, irradiation, and other mechanisms, and accounts for practical field issues such as curing conditions and formwork type and removal age. The model integrated into ConcreteWorks includes weather files for 239 cities from across the United States and includes data on temperature, relative humidity, wind speed, solar radiation, cloud cover, etc. The heat generation and transfer models have been calibrated and validated with over 35,000 hours of field data from mass concrete placements, but only minimal field validation was performed under TxDOT Project 4563 for bridge decks.

Other thermal issues that must be accounted for when modeling a bridge deck include thermal conductivity, specific heat, and coefficient of thermal expansion, all of which are already dealt with in the ConcreteWorks module for heat generation and transfer in bridge decks. ConcreteWorks, however, is lacking in that it does not address the fact that coefficient of thermal expansion (CTE) is affected by the moisture content (internal relative humidity) of concrete (Emmanuel & Hulsey, 1977). When typical concrete mixture proportions are used, the CTE of concrete in the partially dry state can be as much as 15% more than the CTE in the fully saturated state.

2.1.5 Moisture Gradients

As mentioned previously, bridge decks will be subjected to drying conditions that will impart a moisture gradient within the deck. This moisture gradient will trigger warping effects in the deck. A variety of detailed laboratory studies and modeling efforts have addressed this issue (Wittman & Roelfstra, 1980; Akita, Fujuwara, & Ozaka, 1997; Bentz, Garboczi, & Quenard, 1997; Grasley & Lange, 2004), although each has focused on laboratory testing under controlled conditions rather than realistic field conditions.

Moisture gradients were not accounted for in the mass concrete crack prediction model in ConcreteWorks, as this is a minor issue at early-ages in such elements when compared to thermal effects.

2.1.6 Carbonation Shrinkage

Though not commonly thought to be a problem in bridge deck durability, carbonation shrinkage has the ability to reduce concrete surface strength and induce differential shrinkage in concrete elements. In carbonation shrinkage, cement paste (all hydration products, starting with calcium hydroxide (C-H) will react with carbon dioxide, lowering the pH of the system. This will in turn cause corrosion if the carbonation front reaches steel reinforcement, and will result in shrinkage in the carbonated layer of concrete. Generally, this is usually not a major concern in high-quality concrete, as carbonation typically does not penetrate more than 0.5 in. into the concrete surface. If poor quality concrete is made, or if reinforcing steel is not provided with adequate cover, then carbonation shrinkage may affect a deeper section of concrete, and corrosion of the reinforcing steel my take place (ACI Committee 224, 2001). Carbonation shrinkage also requires a specific range of relative humidity in the concrete; enough to provide essential water for carbon dioxide transport, but not so high that the pore structure is saturated and carbon dioxide cannot move through the saturated pores. A relative humidity of 50% produces the greatest values of carbonation shrinkage (Mindess, Young, & Darwin, 2002). While carbonation shrinkage and resulting corrosion of steel are possible in bridge decks, it is not a common issue. The necessary environmental conditions, the low permeability of carbon dioxide into concrete, and the fact that carbonation profiles rarely exceed the cover depth for reinforced structures make carbonation a minor issue in bridge deck durability.

2.2 DEVELOPMENT OF MECHANICAL PROPERTIES

In attempting to understand the many factors and forces involved in bridge deck cracking, one must be aware of the mechanical properties of a given bridge deck system. Obtaining a full understanding of how strength development, modulus development, and the mechanisms of creep resist the buildup of tensile stresses is integral in attempting to accurately predict the cracking potential of a bridge deck system.

While it is very important to have an understanding of the failure-inducing stresses that can build up in a concrete structure, no real progress can be made unless one has a firm grasp of the concrete strength development that works to resist the stresses. Since the rate of strength development is a temperature dependent property, maturity methods are needed to calculate the development of mechanical properties. One should also have a general feel for how different factors, such as the water to cementitious products ratio (w/cm), use of supplementary cementitious materials (SCMs), and aggregate type and gradation, play a role in the long and short-term strength development of concrete. Finally, understanding the empirical relationships between compressive strength, tensile strength, modulus of elasticity, and development of creep behavior will allow the engineer to predict the concrete's ability to resist tensile stresses over time.

2.2.1 Factors Influencing Strength Development

Several factors affect the development of compressive and tensile strength. W/cm is commonly used as the main predictor for concrete strength, with high w/cm ratios producing lower strength concrete, and lower w/cm ratios producing higher strength concrete. Lower w/cm ratios also results in a faster strength development when compared to high w/cm mixtures. Testing done by Abel and Hover (1998) on lower w/cm mixtures only 2-8 hours old showed faster tensile strength development, lower deformation at failure, and higher tensile strengths. These findings are especially

relevant to bridge decks, representing the concrete behavior and stresses during the time period in which plastic shrinkage usually occurs (Abel & Hover, 1998). At different w/cm ratios, one must also consider the chemical and physical properties of the cement being used. The levels of C_3S and C_2S are the primary chemical components in influencing long and short term strength of portland cement concrete, with C_2S contributing to long-term strength and C_3S contributing to short-term strength. Focus must also be paid to the fineness of the cement being used, with high percentages of particles under 3μm resulting in high 1-day strength and high percentages of 3-30 μm particles resulting in higher 28-day strengths (Mindess, Young, & Darwin, 2002).

Aggregates are typically thought to have minor effects on concrete compressive strength. In tensile strength and fracture properties, however, aggregates hold more importance. For high strength concrete mixtures, the aggregate strength plays a larger role in the strength of the concrete, due to the fact the failure is forced to act through the aggregates. In normal strength concrete, as is typical of bridge deck mixtures, failures typically happen around the aggregate particles, such that aggregate strength is not as important a factor in the overall concrete strength. Aggregate shape and texture, and maximum aggregate size (MSA), on the other hand, typically play significant roles in the strength of normal strength concrete. Aggregate texture has a strong effect on the bond between aggregate and paste, thereby increasing the tensile strength capacity and the stress at which microcracking begins. While this alone would make for a stronger concrete, rough aggregates that would produce a stronger aggregate-paste bond also decrease workability. This creates a demand for more water in the mix, which usually offsets the strength gains due to the aggregate-paste bond improvements. Aggregate size can have an effect on both the compressive and tensile strength of the concrete. Large aggregates create larger stress concentrations when put under compressive loading, and

can also trap more bleed water, increasing the porosity in the interfacial transition zone (ITZ). Large aggregates also tend to resist the volume changes that occur in the paste, which puts larger stresses on the paste fraction. These negative effects, however, are usually offset by increased workability and lower w/cm (due to increased workability), resulting in higher strengths (Mindess, Young, & Darwin, 2002). The use of dense graded aggregates may also have an impact on concrete strength development through the potential increase in interparticle contact; however, the ultimate strength will still primarily be a function of the w/cm and aggregate strength.

2.2.2 Maturity

Concrete strength development is a product of the hydration of cement particles in a concrete mixture. From the moment water comes into contact with cement, hydration reactions take place that will, over time, transform a fluid mixture into hardened structure. The development of this strength is depended on the concrete degree of hydration and temperature development. Maturity methods are used to compare the cement hydration progress for different time-temperature histories. The two most commonly used maturity methods are the Nurse-Saul method and the Equivalent Age method (Riding, 2007). The Nurse-Saul method generates a temperature-time factor that is defined as the integral of the temperature history and may be calculated as shown in Eq. 2-8. In the Nurse-Saul method, M(t) is the maturity at t (hrs), T_a is the average concrete temperature over the time step, T_o is the datum, or baseline temperature used (°C), and Δt is the time step used (hrs).

$$M(t) = \sum (T_a - T_o) * \Delta t$$

Eq. 2-8

Equation Eq. 2-9 shows the Equivalent Age method for determining concrete maturity. Equivalent age maturity is defined as the age a concrete sample would have to be cured isothermally at a reference temperature T_r (°C) to have the same degree of reaction or properties as the sample cured at a different temperature. In this method, t_e is the equivalent age maturity (hrs), Q is the activation energy of the mixture being tested, divided by the universal gas constant (°K), T_a is the average concrete temperature over the time step, T_r is the reference temperature (°C), T_a is the average concrete temperature over the time step (°C), and Δt is the time step used (hrs). One of the advantages of the equivalent age method is that it does a better job than the Nurse-Saul method at predicting concrete strength level (Emborg, 1998; Mindess, Young, & Darwin, 2002).

$$t_e = \sum e^{-Q\left(\frac{1}{T_a+273}-\frac{1}{T_r+273}\right)} * \Delta t$$

Eq. 2-9

2.2.3 Setting Time

Setting time is another very important property in concrete strength development. Contractors often use setting time as a point from which decisions on finishing, tining, curing compounds, curing blankets / plastic, and groove cutting are based. The setting time is also important in determining the time duration during which plastic shrinkage is a major concern. Finally, setting time is used to determine when concrete no longer acts plastically, begins to retain its form, and beings to develop strength.

In order to define the time before which plastic shrinkage is a significant concern and define the point in time which tensile strength begins to develop, it becomes important from a practical and technical perspective to know when concrete sets. A setting time model, which used standard inputs from semi-adiabatic calorimetry (as shown in Eq. 2-10 and Eq. 2-11), was developed by Schindler (2004) to predict the initial

and final setting times of concrete, respectively. This approach has become more useful as an increasing number of concrete practitioners and researchers have recorded and published the heat of hydration parameters for their concrete mixtures.

$$ASTM\ C403\ Initial\ Set \qquad t_{ei} = \tau * \left(-ln\left[\frac{0.15 * w/cm}{\alpha_u}\right]\right)^{\frac{-1}{\beta}}$$

Eq. 2-10

$$ASTM\ C403\ Final\ Set \qquad t_{ef} = \tau * \left(-ln\left[\frac{0.26 * w/cm}{\alpha_u}\right]\right)^{\frac{-1}{\beta}}$$

Eq. 2-11

In Eq. 2-10 and Eq. 2-11, t_{ei} and t_{ef} stand for the equivalent age at initial and final set, respectively (hrs.), τ is the hydration time parameter (hrs.), w/cm is the water to cementitious materials ratio, α_u is the ultimate degree of hydration, and β is the hydration shape parameter.

2.2.4 Compressive Strength

Once the maturity has been determined, models can then be used to predict the compressive strength development of the concrete mixture. While many models exist, two of the more common equations are given in Eq. 2-12 and Eq. 2-13 (Viviani, 2005).

$$f_c(t) = a + b * \log\big(log\big(M(t)\big)\big)\ , f_c \geq 0$$

Eq. 2-12

$$f_c(t_e) = f_{c,ult} * \exp\left(-\left(\frac{\tau_s}{t_e}\right)^{\beta_s}\right)$$

Eq. 2-13

In Eq. 2-12 and Eq. 2-13, $f_c(t)$ is the compressive strength development (MPa), a is a fit parameter which is usually negative (MPa), b is a fit parameter (MPa/°C/hr), $f_{c,ult}$

is the ultimate compressive strength parameter fit from the compressive strength tests (MPa), τ_s is a fit parameter (hrs.), and β_s is a fit parameter. M(t) and t_e are the inputs to the predictive equations for the Nurse-Saul method and the Maturity method, respectively.

2.2.5 Elastic Modulus

Once compressive strength development has been generated, models can be used to predict the development of the elastic modulus. This value is especially important in the context of bridge deck cracking, allowing the researcher to correlate the various volume change mechanisms that are occurring with the stresses that the changes generate. Essentially, as a concrete mixture generates a higher modulus of elasticity, volume changes generate higher stresses for each unit movement. This relationship is shown in Eq. 2-14, where σ is the stress induced (psi), E is the elastic modulus of elasticity (psi), and ε is the strain in the concrete (in/in).

$$\sigma = E * \varepsilon$$

Eq. 2-14

While there are many models available for calculating the elastic modulus, most engineers and practitioners in the concrete industry are familiar with the ACI 318 (2008) calculation of elastic modulus:

$$E_c = {w_c}^{1.5} * 33 * \sqrt{f'_c}$$

Eq. 2-15

In Eq. 2-15, E_c is the elastic modulus of concrete (psi), w_c is the unit weight of the concrete (lb/ft^3), and f'_c is the compressive strength of the concrete (psi).

2.2.6 Tensile Strength

In the case of bridge deck cracking, proper modeling of the concrete tensile strength is of great importance. Without a good model for tensile strength development, the engineer cannot determine whether or not the volume changes, and the resulting stresses, occurring within a concrete system are enough to produce cracking. Raphael (1984) proposed one model for the development of tensile strength that is commonly used today:

$$f_t = l * (f_c)^m$$

Eq. 2-16

In Eq. 2-16, f_t is the tensile strength (MPa), f_c is the compressive strength of the concrete (MPa), and *l* and *m* are fit parameters.

2.2.7 Creep and Stress Relaxation

Creep and relaxation play a key role in the development of bridge deck stress, and their potential to cause cracking. Creep is a complicated mechanism, influenced by applied stresses, water / cement ratio, curing conditions, temperature, moisture gradients, cement composition, chemical admixtures, aggregate properties, and specimen geometry (Mindess, Young, & Darwin, 2002). Though complicated, its effect on bridge deck cracking must be considered as relaxation due to creep can significantly reduce the stresses that are imposed on a bridge deck due to volume changes (thermal, autogenous, etc.). Figure 2-2 shows how the process of creep helps delay cracking through stress relaxation.

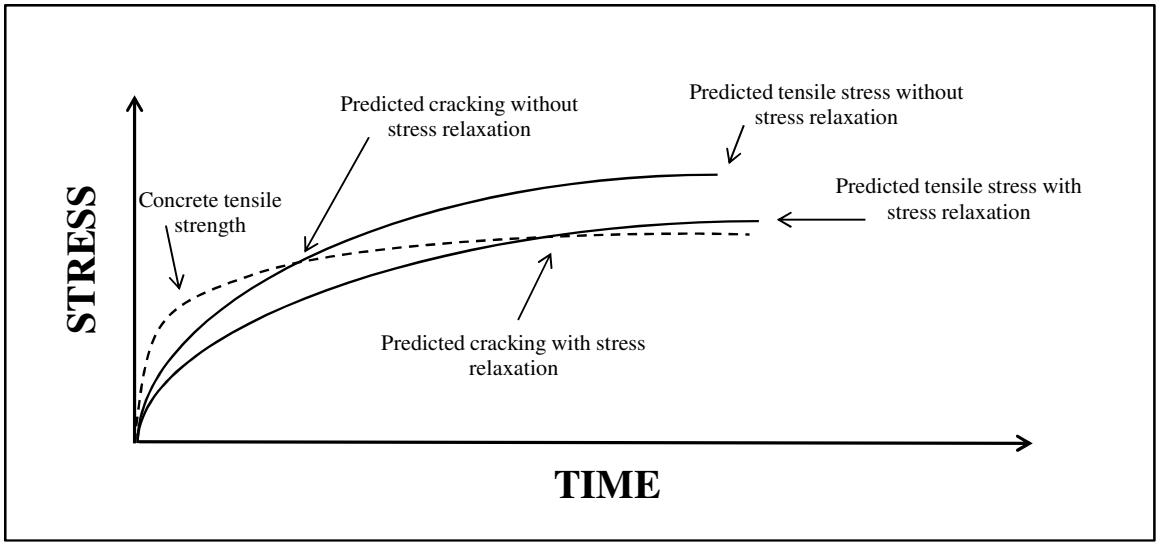

Figure 2-2: Time dependence of restrained shrinkage and creep (Mehta & Monteiro, 2005)

Many different models are available in the literature for evaluation of creep. Previous work at the University of Texas has utilized the Linear Logarithmic Model for calculating the early-age concrete stress relaxation (Larson & Jonasson, 2003). Equations are used to calculate the various slope components of the model, with adjustments for temperature modification, the aggregates used, and the Reitveld analysis of the cement used in the mixture. Further discussion, and the governing equations, of the Linear Logarithmic Model and the adjustments that have been made in ConcreteWorks can be found in (Riding, 2007).

Recent work at Auburn University has yielded a modified version of the commonly used B3 model. The modified B3 model was developed by Byard at Auburn University, and aims to better capture the early-age creep response (Byard, 2011). An abbreviated explanation of the aspects of the B3 model that are applicable to the rigid cracking frame test is provided below. Modifications to the B3 model will be presented in Section 4.10. Description of the original B3 model is made using information from

ACI Committee 209 (2008) as well as the original papers from Bazant (1995). Further explanation of the original model can be found in these sources as well. The final version of the modified B3 model will be published as a doctoral thesis by Byard at a later date.

In the B3 model, a compliance term, $J(t, t_o)$, is used to calculate the strain caused by a constant stress, σ, applied at an age of t_o. $\varepsilon_{SH}(t)$ and $\alpha * \Delta T$ are the shrinkage and temperature induced strains, respectively. In $J(t, t_o)$, q_1 is an is the instantaneous strain calculated using the 28-day elastic modulus. $C_o(t, t_o)$ is the compliance function for basic creep, and $C_d(t, t_o, t_c)$ is the additional compliance function for drying creep. For evaluation against the rigid cracking frame data, $C_d(t, t_o, t_c)$ is taken as zero and will not be explained in this thesis.

In the compliance function for basic creep, the first term is an aging viscoelastic term, the second is a nonaging viscoelastic term, and the third is an aging flow term. The aging viscoelastic term is multiplied by q_2, a function of cement content and 28-day compressive strength, and calculated with an approximation to a binomial integral. The nonaging viscoelastic term is multiplied by q_3, a function of the water to cementitious materials ratio. The last term, an aging flow term, is multiplied by q_4, a function of the aggregate to cementitious materials ratio.

$$\varepsilon(t) = J(t, t_o) * \sigma \; + \; \varepsilon_{SH}(t) + \; \alpha * \Delta T$$

Eq. 2-17

$$J(t, t_o) = \; q_1 + C_o(t, t_o) + C_d(t, t_o, t_c)$$

Eq. 2-18

$$q_1 = {}^{0.6}/_{E_{cm28}}$$

Eq. 2-19

$$C_o(t,t_o) = q_2 * Q(t,t_o) + q_3 * ln(1 + [t - t_o]^n) + q_4 * ln\left(\frac{t}{t_o}\right)$$

Eq. 2-20

$$q_2 = 86.814 * 10^{-6} * c^{0.5} * {f_{cm}}^{-0.9}$$

Eq. 2-21

$$q_3 = 0.29 * \left(\frac{w}{c}\right)^4 * q_2$$

Eq. 2-22

$$q_4 = 0.14 * 10^{-6} * \left(\frac{a}{c}\right)^{-0.7}$$

Eq. 2-23

$$Q(t,t_o) = Q_f(t_o) * \left[1 + \left(\frac{Q_f(t_o)}{Z(t,t_o)}\right)^{r(t_o)}\right]^{-\frac{1}{r(t_o)}}$$

Eq. 2-24

$$Q_f(t_o) = \left[0.086 * (t_o)^{\frac{2}{9}} + 1.21 * (t_o)^{\frac{4}{9}}\right]^{-1}$$

Eq. 2-25

$$Z(t,t_o) = (t_o)^{-m} * ln[1 + (t - t_o)^n]$$

Eq. 2-26

$$r(t_o) = 1.7 * (t_o)^{0.12} + 8$$

Eq. 2-27

2.3 BRIDGE DECK CRACKING

Bridge deck cracking is a complicated phenomenon that involves the interactions between volume changes, strength development, and the specific environment (restraint conditions) of the concrete system in use. Through the evaluation of many damaged bridge decks, researchers have been able to identify cracking patterns that are caused by the stresses generated within the concrete system, rather than those applied externally (through traffic and ground movement). Although cracking causes are numerous and

interrelated, there are some methods for modeling bridge deck systems that attempt to predict whether a specific deck will be susceptible to cracking during its lifespan. While most of these models only present a simplified approach to the bridge deck cracking problem, usually taking into account only one or two specific factors, they are a good place to start from in the attempt to make a model that accounts for all the mechanisms affecting a bridge deck system.

2.3.1 Mechanisms of Bridge Deck Cracking

As described in the introduction, bridge deck cracking has already been established as a serious concern for the nation's infrastructure. While initial deck cracking is not a failure of the bridge system, cracking allows the penetration of deleterious substances (air, water, chlorides, etc.) that can cause structural failure in bridge systems. Prediction and prevention of future bridge deck cracking issues can only be accomplished through knowledge of the various mechanisms and factors that are associated with this phenomenon. Figure 2-3 shows the many factors that affect cracking in bridge decks.

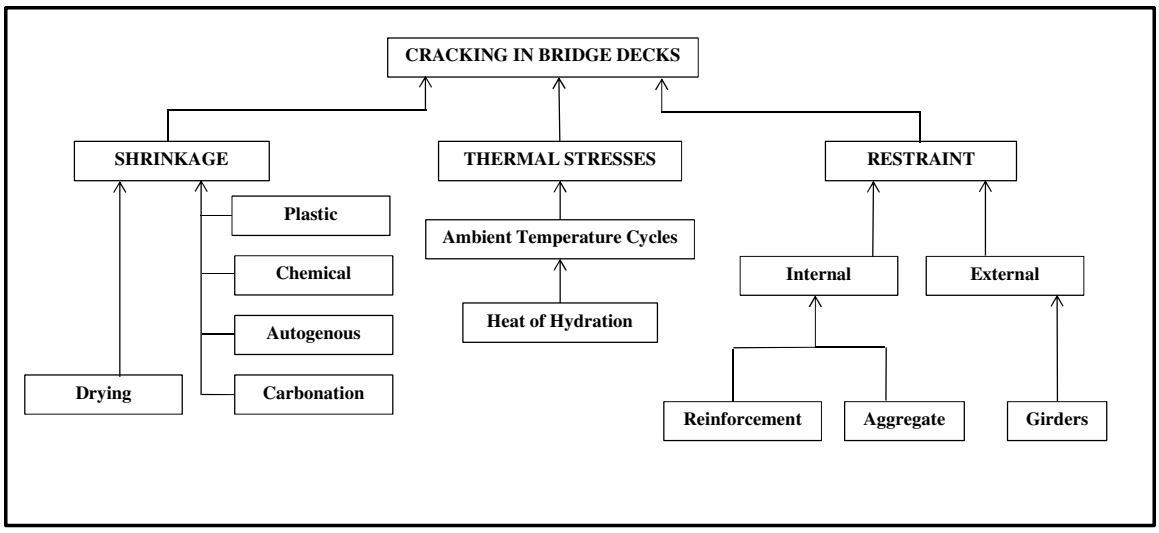

Figure 2-3: Causes of bridge deck cracking

As can be seen in Figure 2-3, and as discussed in this review, volume changes account for much of the driving force in bridge deck cracking. However, all of the volume changes are innocuous until the concrete element is restrained. In bridge deck systems, restraint is typically generated from within the concrete, by aggregate and reinforcing steel; and externally, from the sub-base or superstructure of the bridge. If strains vary though the section, as they do with moisture and temperature gradients, then the member itself may even be considered a restraint to its own internal forces. Figure 2-4 shows a typical bridge deck support structure for Texas highways.

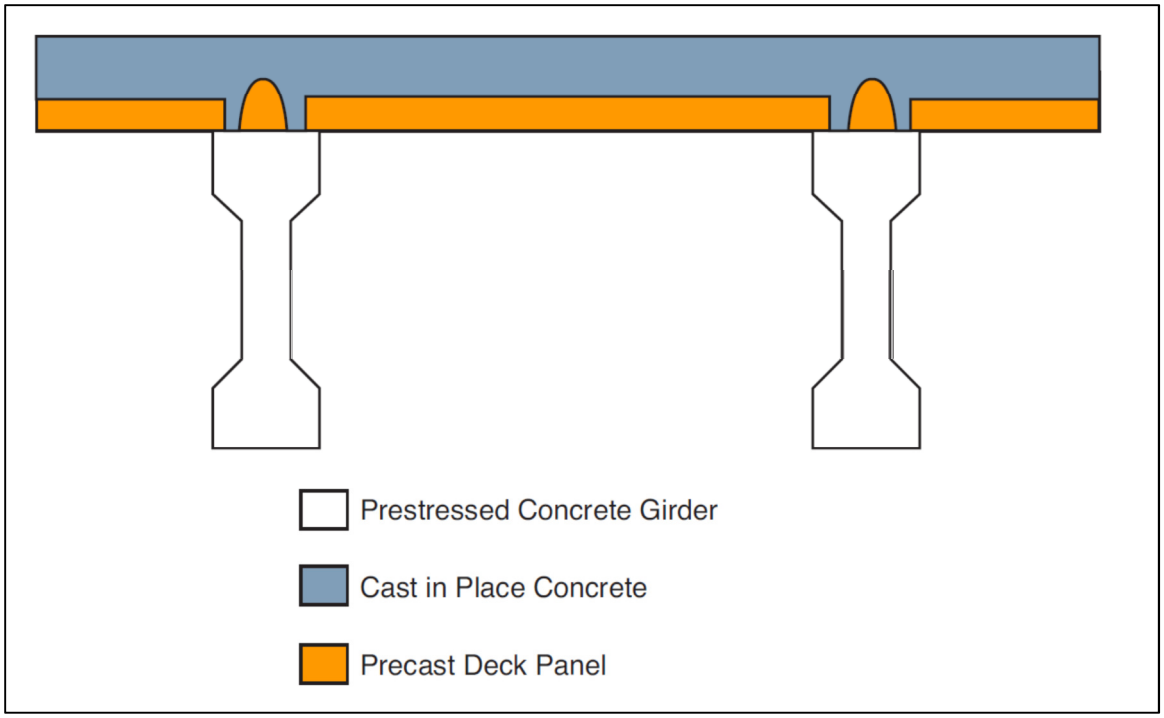

Figure 2-4: Precast, prestressed concrete panel bridge deck system. (Folliard, Smith, Sellers, Brown, & Breen, 2003)

2.3.2 Bridge Deck Cracking in Texas

Under TxDOT Project 4098, researchers evaluated several bridge decks in Texas that exhibited significant cracking. One of the structures that researchers examined had developed a series of stair step crack patterns. These cracks were located on a deck running alongside a bridge expansion joint, on both sides of the joint. The stair step cracks intersected with pairs of longitudinal cracks that were spaced about 8-10 in. apart, and ran for about 25 ft. The transverse cracks were no longer than 4 ft. long. Figure 2-5 shows the stair step cracking pattern that was common along the expansion joints of the Louetta Road Overpass in Houston, Texas. It should be noted that this deck was part of a

FHWA project aimed at high performance concrete (HPC) and within this study, it was clearly shown that HPC bridge decks are more prone to early-age cracking.

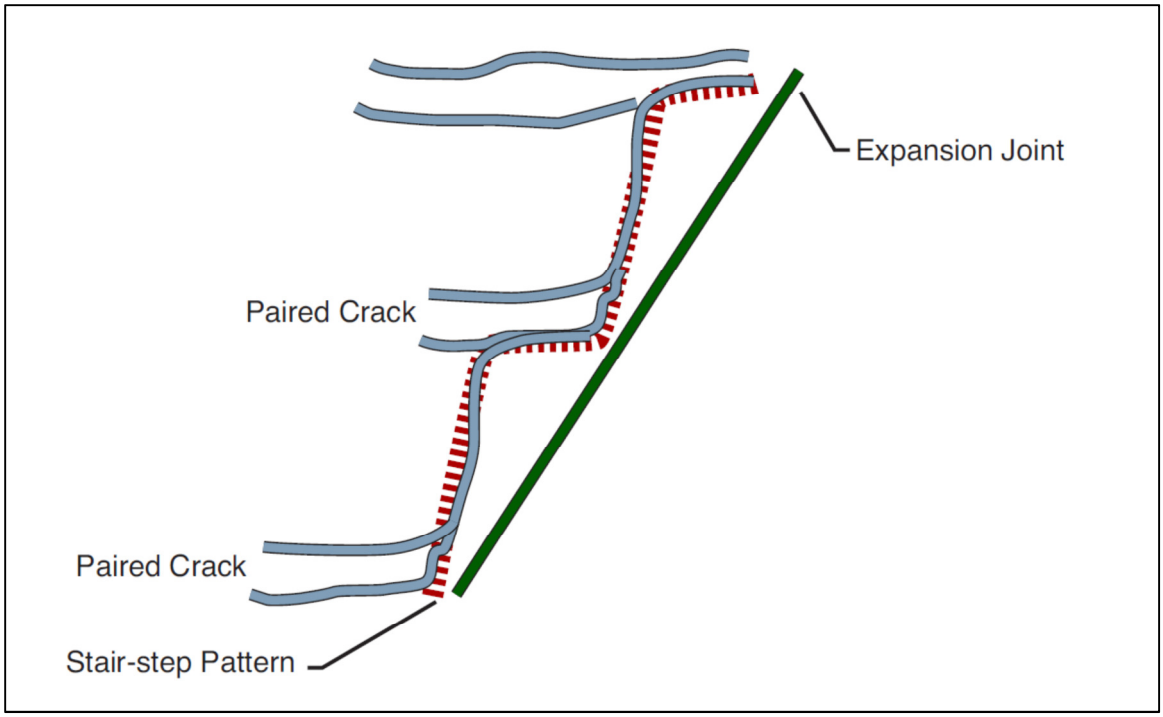

Figure 2-5: Typical stair step cracking on Louetta Bridge (Folliard, Smith, Sellers, Brown, & Breen, 2003).

The Dow Barge Canal Bridge in Freeport, Texas showed a different cracking pattern. Similar to the Louetta Bridge, the Dow Bridge had pairs of longitudinal cracks that ran along the spans. On the Dow Bridge, however, these longitudinal cracks carried much further than those on the Louetta Bridge, sometimes extending the length of the slab. The stair step pattern that was seen at the Louetta Bridge was also seen at the expansion joints of the Dow Bridge. One aspect that was different in the Dow Bridge was the occurrence of transverse cracks that spanned the length between longitudinal

cracks, with about 8 ft. separating one transverse crack from another. The cracking pattern found in the Dow Barge Canal Bridge can be seen in Figure 2-6.

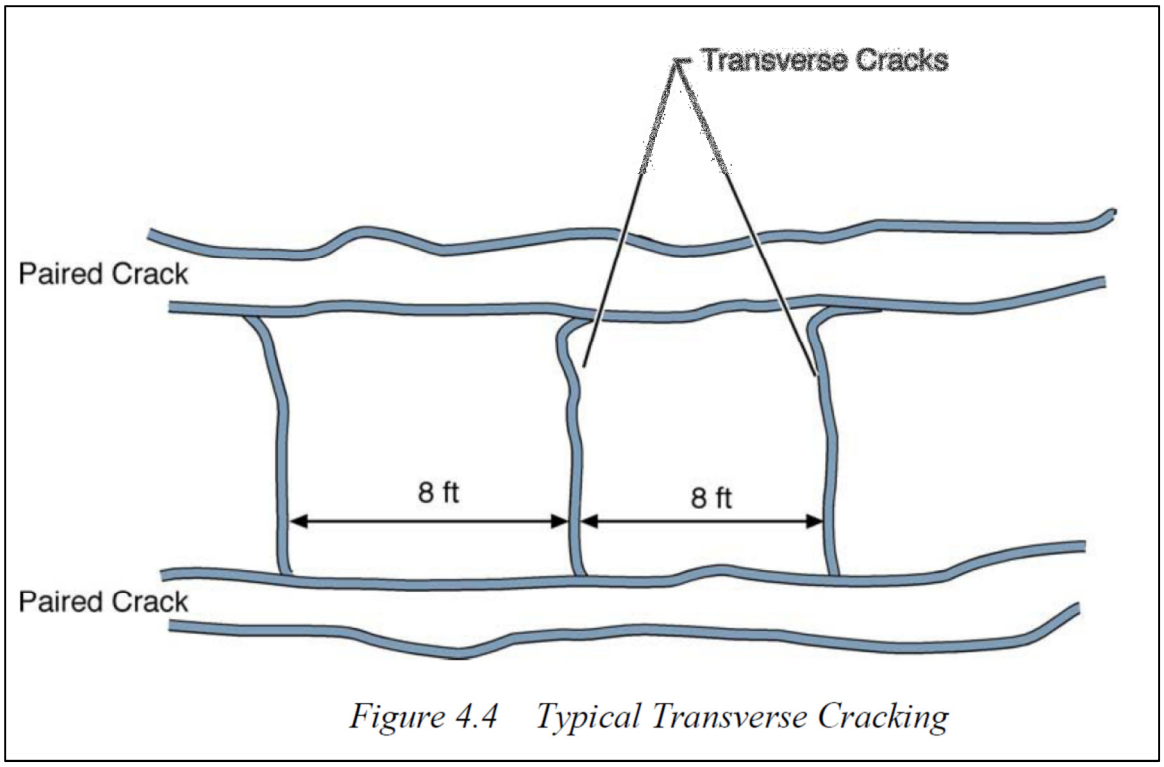

Figure 2-6: Typical transverse cracking on Dow Barge Canal Bridge (Folliard, Smith, Sellers, Brown, & Breen, 2003)

Researchers under TxDOT Project 4098 did identify the precast-prestressed concrete panels as a trigger for cracking, generally due to the restraint that the panels provide against volume changes in the new deck concrete. In addition to the differential shrinkage issues, the Dow Barge Bridge also had issues with discontinuities at the butt joints. The precast panels, which are not connected along the longitudinal direction of the bridge, would have small offsets in the height from one panel to the next. When cast-in-place (CIP) concrete was laid continuously over these panels, cracks tended to form at

the 8 ft. interval over which the butt joints were located, due to the stress concentration from the differential panel height.

Although there were significant cases of bridge deck cracking in Texas evaluated under TxDOT 4098, as depicted in Figure 2-5 and Figure 2-6, it should be noted that in Texas, bridge deck cracking is not as large an issue as can be found in other states. Regardless, any improvements that can be made to the crack resistance of bridge decks will help to prolong the service life of bridges.

2.3.3 Prediction and Modeling

While just understanding the mechanisms and factors that cause shrinkage in early-age concrete is a significant scientific achievement, it is the development of prediction and modeling systems that make this knowledge valuable to the engineering community. Unfortunately, such a tool does not exist today, at least not in a version that is user-friendly and aimed at TxDOT personnel and contractors. To develop such a tool, or in this case, a module to be integrated into ConcreteWorks, several technical issues must be addressed, as highlighted below:

- Modeling of creep and stress relaxation, bridging the gap between early-age models refined and applied under TxDOT Project 4563 and more classical long-term creep models.
- Understanding and modeling the rate of moisture loss to the environment, and the shape of the moisture gradients that develops due to this loss.
- Evaluation of how the various volume changes, individually or in combination, result in stress and potential cracking.

Chapter 3: Laboratory Testing Program

Chapter 3 details the experimental testing program that was undertaken to evaluate the early-age cracking potential of various materials and mixture proportions typically used in Texas bridge deck construction. Testing was performed to characterize each mixture's hydration properties, stress development under simulated environmental conditions, and to evaluate the strength development for the various concrete mixtures. This chapter also describes the identification scheme that was chosen to uniquely identify the various mixtures tested and presents the mixture proportions for these mixtures. The chemical analyses of the cements and SCMs tested and the gradations and physical properties of the aggregates used over the course of this project are also included in this chapter. In addition to work done under TxDOT Project 6332, an inter-agency contract from TxDOT was completed by the research team throughout the spring and summer of 2008. Information gathered from this study has been included in this thesis, and mixtures that were part of the inter-agency contract have been identified as IAC-FA.

3.1 MATERIALS TESTED

The mixture design matrix for TxDOT Project 6332 was developed to span the breadth of mixture designs used in Texas concrete bridge decks. Wherever possible, the research team obtained cements and SCMs from sources within Texas, though some materials outside of Texas were also evaluated to provide a wider range of chemical compositions. The following sections provide the chemical and physical properties of the materials used throughout this project.

3.1.1 Chemistry of Cements and SCMs Tested

Two cements were used under the TxDOT 6332 and IAC-FA studies. CEM-1, an ASTM C 150 Type I/II cement from San Antonio, Texas, was used as the low-alkali

cement. CEM-2, an ASTM C 150 Type I cement from Buda, Texas, was used as the high-alkali cement. Cement alkalinity is calculated from the sodium equivalent, Na_2Oe, for the cement. Sodium equivalent can be calculated using Eq. 3-28:

$$Na_2Oe = \%Na_2 + 0.658 * \%K_2O$$

Eq. 3-28

High and low alkalinities are defined, in this report, according to TxDOT specifications (TxDOT, 2011):

- High-alkali: > 0.60% Na_2Oe
- Low-alkali: ≤ 0.60% Na_2Oe

The cement compounds, calculated using the Bogue calculations from ASTM C150 (2011), and chemical compositions are presented in Table 3-1 and Table 3-2

Table 3-1: Chemical composition of cements.

	Cements Used	
	CEM-2	CEM-1
SiO_2	18.6	20.1
Al_2O_3	5.4	4.4
Fe_2O_3	2.6	3.6
MgO	1.1	0.7
SO_3	3.3	3.1
Na_2O	0.11	0.05
K_2O	0.98	0.64
Na_2Oe^{***}	0.78	0.47

All values aer in % by weight.
*** Na2O equivalent alkali content

Table 3-2: Bogue calculated cement phases.

Cement Phases	CEM-2	CEM-1
C_3S	62.0	62.4
C_2S	6.6	10.5
C_3A	9.9	5.4
C_4AF	7.8	11.1
Na_2Oe^{***}	0.78	0.47

All values are in % by weight.
*** Na2O equivalent alkali content

Six different SCMs were used under TxDOT 6332 and IAC-FA. These SCMs were chosen to span the breadth of options that are available for bridge deck concrete mixtures, and to provide a wide range of fly ash CaO contents. Fly ashes tested met the requirements of ASTM C 618 (2008) and the ground granulated blast furnace slag (GGBFS) met the requirements of ASTM C 989 (2010).

Table 3-3: Chemical composition of SCMs.

	SCMs Used					
	FA-1	FA-2	FA-3	FA-4	SLG120*	UFFA**
SiO_2	55.8	45.6	34.7	32.4	35.5	47.6
Al_2O_3	30.5	23.1	19.4	18.9	10.9	28.2
Fe_2O_3	4.6	3.7	6.0	6.4	0.9	2.9
CaO	1.2	15.9	22.8	24.6	43.1	12.1
MgO	0.7	2.5	4.4	4.6	7.8	2.1
SO_3	0.1	0.5	1.4	2.4	1.0	0.8
Na_2O	0.3	0.2	1.4	1.2	0.2	0.3
K_2O	2.3	0.7	0.3	0.3	0.3	1.1

All values are in % by weight.

* Ground granulated blast furnace slag

** Ultra-fine fly ash

3.1.2 Aggregates

For this project, two sources of coarse aggregate and one source of fine aggregate were used. For the majority of the mixtures tested, the coarse and fine aggregates were used as received from the producer (no additional sieving or reproportioning was done). However, for the OL-RG and OL10-RG mixture designs, the river gravel coarse aggregate and river sand were sieved and reproportioned to obtain an optimized aggregate gradation.

3.1.2.1 Coarse Aggregate

Two coarse aggregate sources were used throughout this project. An ASTM C 33 Number 57 siliceous river gravel was from Austin, Texas, sourced out of the Colorado River. An ASTM C 33 Number 57 limestone was chosen from a quarry in San Antonio,

Texas. Throughout this thesis, the coarse aggregates that were kept at ASTM C 33 Number 57 gradations will be denoted as Gr. 57. Six mixtures were tested with the Gr. 57 limestone, and thirty-four mixtures were tested with the Gr. 57 river gravel. Sieving gradations with the percent passing values for the Gr. 57 limestone and Gr. 57 river gravel, and the ASTM C33 (2011) limits, are presented in Figure 3-7 and Table 3-4. Absorption and specific gravity of the aggregates are presented in Table 3-5.

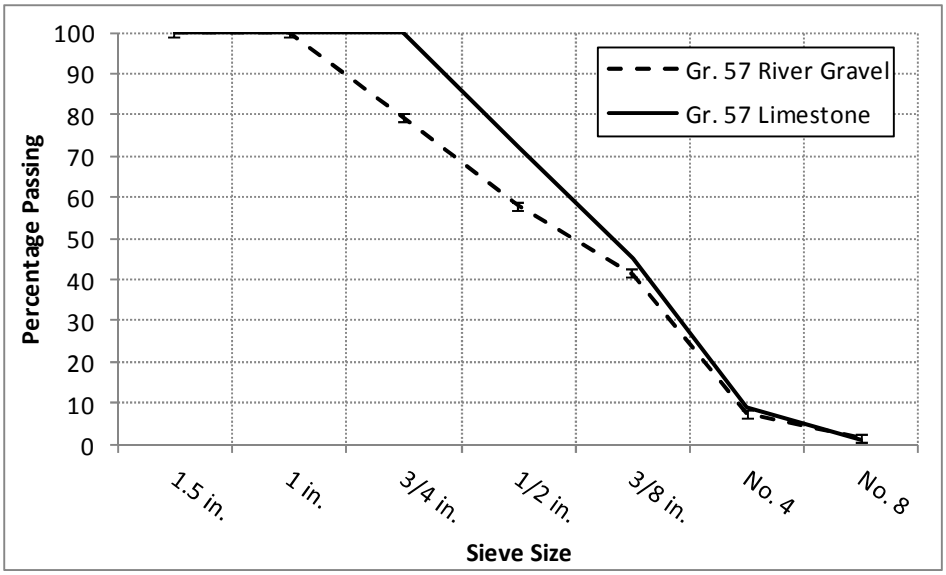

Figure 3-7: Coarse aggregate gradations.

Table 3-4: Coarse aggregate gradations and limits.

Sieve Opening	Gr. 57 River Gravel	Gr. 57 Limestone	ASTM C33 Limits for Gr. 57
1.5 in.	100	100	100
1 in.	100	100	95-100
3/4 in.	79	85	--
1/2 in.	58	44	25-60
3/8 in.	41	19	--
No. 4	7	6	0-10
No. 8	1	2	0-5

All values in percent passing.

Table 3-5: Absorption and specific gravity of aggregates.

Aggregate Source	Absorption	Specific Gravity
River Gravel	1.29%	2.60
Limestone	2.75%	2.75
River Sand	0.76%	2.61

3.1.2.2 Fine Aggregate

All mixtures tested under TxDOT 6332 and IAC-FA used a river sand from Austin, Texas, sourced from the Colorado River. The river sand passed the requirements of ASTM C 33, and had a fineness modulus of 2.71. The percent passing gradation of the river sand is shown in Figure 3-8.

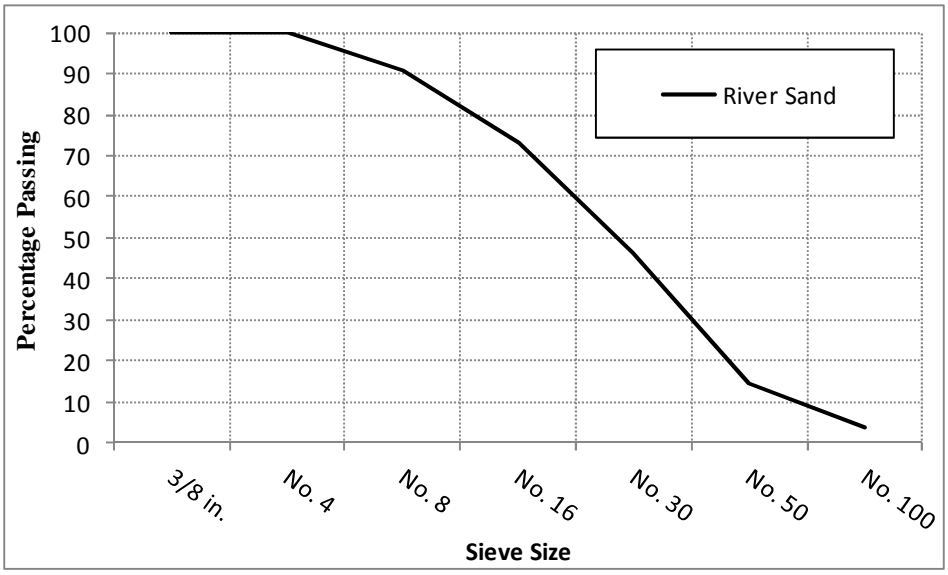

Figure 3-8: Fine aggregate gradation.

Table 3-6: Fine aggregate gradation and limits.

Sieve Size	River Sand	ASTM C33 Limits
3/8 in.	100.0	100
No. 4	99.9	95-100
No. 8	90.7	80-100
No. 16	73.1	50-85
No. 30	46.4	25-60
No. 50	14.6	5-30
No. 100	3.8	0-10

All values in percent passing.

3.1.2.3 Optimized Aggregate Gradation

Under TxDOT 6332, and with collaboration and assistance from TxDOT, two mixture designs were evaluated that used optimized aggregate gradations. While this is most commonly found in asphalt mixtures, there is recent interest in their use in portland cement concrete mixtures. If a mixture is designed properly, optimized aggregate gradations could allow for reduced paste content, while keeping the same strength and workability characteristics for a mixture. Reduced paste content results in a less expensive concrete mixture, less heat generation, and a concrete mixture that is less sensitive to deterioration of the paste fraction. In the first optimized aggregate gradation mixture, OL-RG, the paste volume was kept constant with all the other mixtures in the test matrix. In the second optimized aggregate gradation mixture, OL10-RG, the paste volume of the mixture was reduced by 10% (while keeping a 0.45 w/cm) and replaced with optimized aggregate fractions. The volumetric mixture designs of the optimized aggregate mixtures are shown in Table 3-7, and weight proportions can be found in Table 3-19.

Table 3-7: Volumetric mixture design for optimized aggregate gradation mixes.

Mix Name	Cement ft^3/yd^3	Water ft^3/yd^3	Paste Volume ft^3/yd^3	Coarse Aggregate ft^3/yd^3	Fine Aggregate ft^3/yd^3	Total Aggregate ft^3/yd^3
OL-RG	2.87	4.07	6.94	11.67	8.25	19.91
OL10-RG	2.58	3.66	6.25	12.08	8.53	20.61
			Δ -0.69			Δ 0.69

To achieve an optimized aggregate gradation, the research team sieved the Gr. 57 river gravel, and the river sand. 3/8", No. 8, and No. 16 fractions were kept, and the remaining material was discarded. The sieved fractions were then added back into the general Gr. 57 and river sand distributions in the proportions shown in Table 3-8.

Table 3-8: Weight proportioning for optimized aggregate gradation

	Coarse Aggregate % by Weight	Fine Aggregate % by Weight
Gr. 57 River Gravel	74.4%	--
River Sand	--	84.3%
3/8in. Sieve	11.1%	--
No. 8 Sieve	14.5%	--
No. 16 Sieve	--	15.7%
Total	100.00%	100.00%

After combining the sieved fractions to generate the new coarse and fine aggregate gradations, the total aggregate gradation fell within the recommended '8-18 bands' and performed much closer to the desired 'haystack' shape recommended by Shilstone (1990). This is evident in Figure 3-9 and Figure 3-10, which provide the percent retained values for the typical and optimized aggregate gradations.

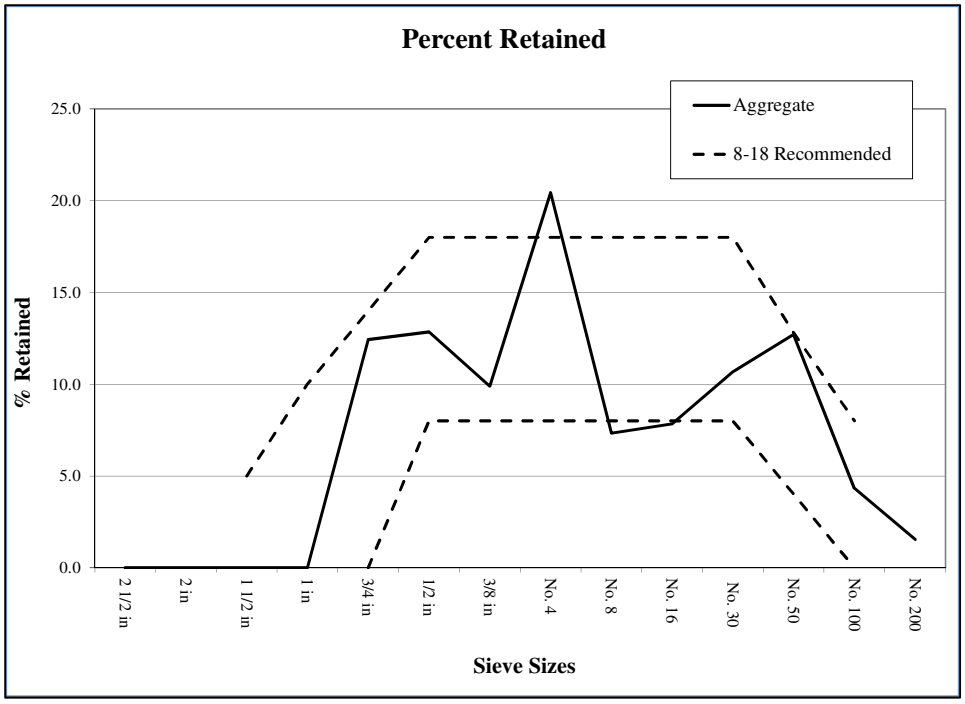

Figure 3-9: Typical aggregate distribution for testing matrix.

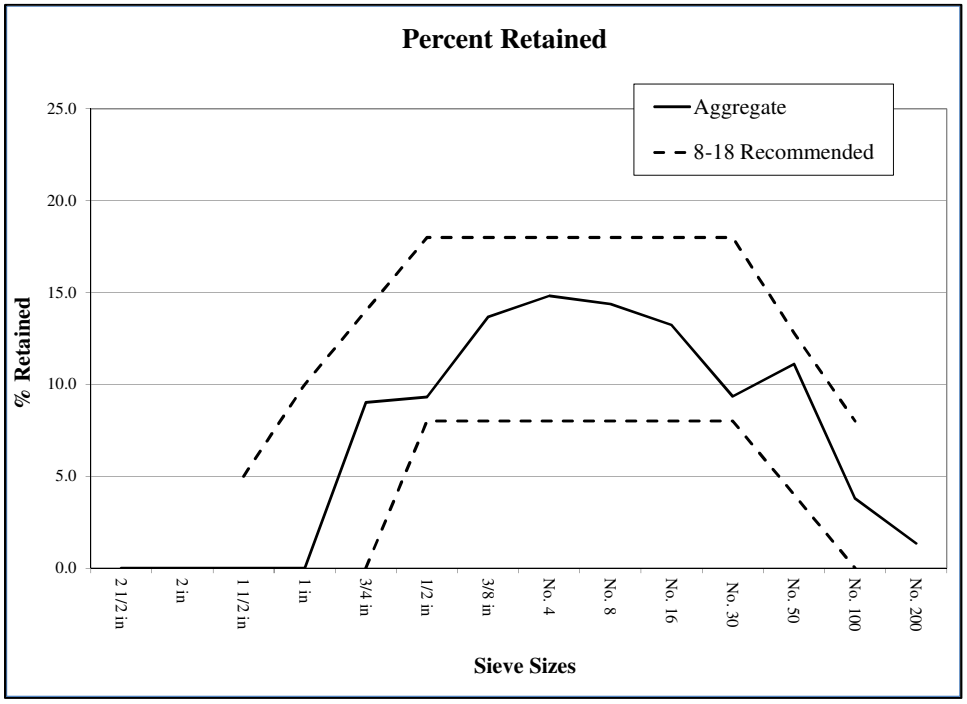

Figure 3-10: Aggregate distribution for optimized aggregate mixes.

3.1.3 Chemical Admixtures

Two admixtures were used throughout this project. WR (water reducer) is a Type A and D water-reducing and retarding admixture that was used in every mixture tested at a dosage of 3 oz./cwt of cementitious materials (ASTM C494, 2010). WR has a 44% solids content by volume (TxDOT, 2011). SRA is a shrinkage reducing admixture that works by reducing the surface tension of the pore water in the concrete. According to Eq. 2-6, this reduction results in a lower level of stress applied to the bulk concrete when menisci are formed in the concrete pore structure. SRA was added to the "S" mixtures in the testing matrix at the recommended dosage of 1.5 gal/yd^3. Also following the recommendations from the admixture data sheet, SRA was used at a 1-1 ratio as a replacement for mixture water. A summary of the chemical admixture information is shown in Table 3-9.

Table 3-9: Concrete admixture information.

Admixture	Dosage	Specific Gravity	% Solids
WR	3 oz/cwt	1.18-1.22	44%
SRA	1.5 gal/yd^3	0.935	--

3.2 CONCRETE MIXTURE DESIGNS EVALUATED

Under TxDOT 6332 and IAC-FA, forty-two separate mixtures, and twenty-three different mixture designs were evaluated to determine their performance under simulated temperature profiles. The mixture designs were chosen to reflect those used in Texas bridge deck construction.

3.2.1 Identification of Mixture Designs

To delineate the many mixtures performed under this research project, a naming scheme was developed to identify if SCMs were used, if low of high alkalinity cement was used, what percentage of replacement was used for the SCMs, what type of coarse aggregate was used, and whether that specific mixture was being tested under hot, cold, or isothermal temperature simulations. For this report, ground granulated blast furnace slag is abbreviated as GGBFS, supplementary cementitious materials are abbreviated as SCMs, and ultra-fine fly ash is abbreviated as UFFA. Descriptions of the mixtures tested and the mixture proportions used are presented in Table 3-10 through Table 3-19.

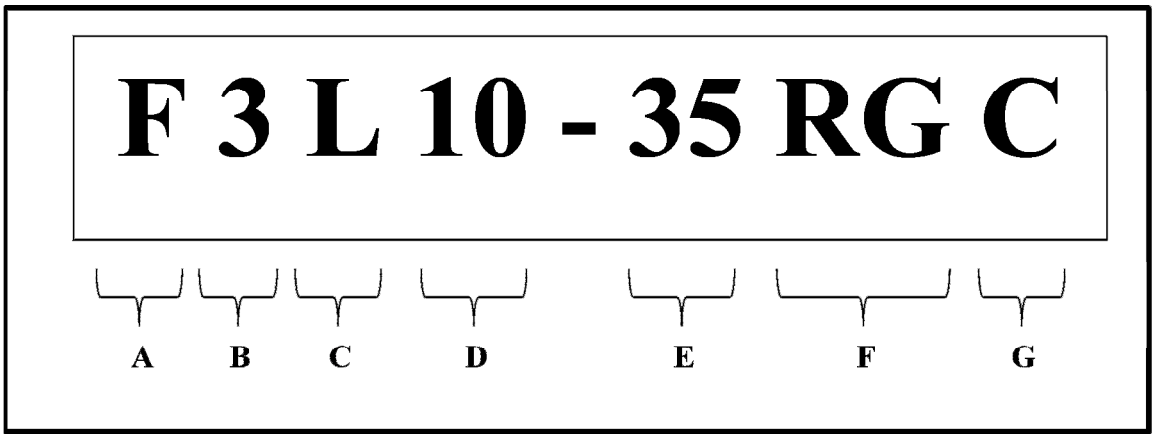

A. Mixture Type: Identifies the type, if any, of SCM or special admixture used.
   - C: Control Mixture- No SCMs or special admixtures used.
   - F: Fly Ash Mixture- Fly ash is used to replace a portion of the cement.
   - G: GGBFS Mixture- GGBFS is used to replace a portion of the cement.
   - O: Optimized- A straight cement mixture, with an optimized aggregate gradation.
   - U: UFFA Mixture- UFFA replaces 10% of the cement. Additional cement replacement from fly ash as well.

- S: Shrinkage Reducing- A control mixture, with a shrinkage reducing admixture used.

B. Fly Ash Type: Identifies the specific fly ash, if any, that was used.
   - No Number: No fly ash used in the mixture.
   - 1: Class F- FA-1 (CaO = 1.2%)
   - 2: Class F- FA-2 (CaO = 12.1%)
   - 3: Class C- FA-3 (CaO = 22.8%)
   - 4: Class C- FA-4 (CaO = 24.6%)

C. Cement Alkalinity: Identifies the type of cement used.
   - H: High Alkalinity- CEM-2 (Na_2Oeq= .756%)
   - L: Low Alkalinity- CEM-1 (Na_2Oeq= .467%)

D. Paste Reduction: Identifies the percentage of paste volume, if any, that was replaced with optimized aggregate fractions.

E. SCM Replacement: Identifies the percentage of cement, if any, that was replaced with SCMs.

F. Aggregate Type: Identifies the type of coarse aggregate that was used.
   - RG: River gravel used as the coarse aggregate.
   - LS: Limestone used as the coarse aggregate.

G. Temperature Profile: Identifies the type of temperature profile used for that particular mixture.
   - No final letter: Hot weather temperature profile used.
   - C: Cold weather temperature profile used.
   - I: Isothermal temperature profile used.

3.2.1.1 Control Mixtures Tested

Under the two research projects, seven 'control' mixtures were evaluated. These mixtures, which contained no SCMs, allowed the research team to isolate the effects of fly ash replacement in bridge deck concrete mixtures. Low and high alkali cements, river gravel and limestone coarse aggregate, and hot and cold temperature profiles were used in the evaluation of the control mixtures. In addition, an isothermal temperature profile was used on one of the control mixtures to isolate the benefits of using shrinkage reducing admixture with regard to autogenous shrinkage.

Table 3-10: Control mixtures.

	Cement	SCM Source	SCM CaO Content	SCM Replacement
CL-RG	CEM-1	None	--	--
CL-RGC	CEM-1	None	--	--
CL-RGI	CEM-1	None	--	--
CH-RG	CEM-2	None	--	--
CH-RGC	CEM-2	None	--	--
CL-LS	CEM-1	None	--	--
CL-LSC	CEM-1	None	--	--

* Denotes a mixture that was completed under IAC-FA

Table 3-11: Mixture proportions for control mixtures

Mix ID	Cement lb/yd^3	SCM lb/yd^3	Water lb/yd^3	Coarse Agg. lb/yd^3	Fine Agg. lb/yd^3	WR oz. / cwt
CL-RG	564	--	254	1940	1231	3
CL-RGC	564	--	254	1940	1231	3
CL-RGI	564	--	254	1940	1231	3
CH-RG	564	--	254	1941	1232	3
CH-RGC	564	--	254	1941	1232	3
CL-LS	564	--	254	1922	1220	3
CL-LSC	564	--	254	1922	1220	3

* Denotes a mixture that was completed under IAC-FA

3.2.1.2 Class C Fly Ash Mixtures

Ten mixtures were tested that utilized Class C fly ash (CaO greater than 20%). Class C fly ashes included FA-3, from San Antonio, Texas, and FA-4 from Thompsons, Texas. Under the IAC-FA project, a higher CaO Type C fly ash was used (FA-C), but had to be abandoned due to limited resources. The IAC-FA project was finished with FA-4 as the highest CaO fly ash, and TxDOT Project 6332 used FA-4 exclusively for the high CaO fly ash. Mixtures that used the FA-C fly ash will not be included in this thesis.

Table 3-12: Class C fly ash mixtures.

	Cement	SCM Source	SCM CaO Content	SCM Replacement
F3L-25RG*	CEM-1	FA-3	22.8%	25%
F3L-35RG*	CEM-1	FA-3	22.8%	35%
F3L-35RGC	CEM-1	FA-3	22.8%	35%
F3L-35LS	CEM-1	FA-3	22.8%	35%
F3L-35LSC	CEM-1	FA-3	22.8%	35%
F4L-25RG*	CEM-1	FA-4	24.6%	25%
F4L-35RGC	CEM-1	FA-4	24.6%	35%
F4H-25RG*	CEM-2	FA-4	24.6%	35%
F4H-35RG	CEM-2	FA-4	24.6%	35%
F4H-35RGC	CEM-2	FA-4	24.6%	35%

* Denotes a mixture that was completed under IAC-FA

Table 3-13: Mixture proportions for Class C fly ash mixtures.

Mix ID	Cement lb/yd^3	SCM lb/yd^3	Water lb/yd^3	Coarse Agg. lb/yd^3	Fine Agg. lb/yd^3	WR oz. / cwt
F3L-25RG*	423	141	254	1929	1224	3
F3L-35RG*	367	197	254	1924	1221	3
F3L-35RGC	367	197	254	1923	1220	3
F3L-35LS	367	197	254	1905	1209	3
F3L-35LSC	367	197	254	1905	1209	3
F4L-25RG*	423	141	254	1929	1223	3
F4L-35RGC	367	197	254	1954	1240	3
F4H-25RG*	423	141	254	1927	1223	3
F4H-35RG	367	197	254	1921	1219	3
F4H-35RGC	367	197	254	1920	1219	3

* Denotes a mixture that was completed under IAC-FA

3.2.1.3 Class F Fly Ash Mixtures

Ten mixtures were tested that utilized Class F fly ash (CaO less than 20%). Class F fly ashes included FA-1, from Stokes County, North Carolina, and FA-2 from Rockdale, Texas.

Table 3-14: Class F fly ash mixtures.

	Cement	SCM Source	SCM CaO Content	SCM Replacement
F1L-25RG*	CEM-1	FA-1	1.2%	25%
F1L-25RGC	CEM-1	FA-1	1.2%	25%
F1H-25RG*	CEM-2	FA-1	1.2%	25%
F1H-25RGC	CEM-2	FA-1	1.2%	25%
F2L-25RG*	CEM-1	FA-2	15.9%	25%
F2L-25RGC	CEM-1	FA-2	15.9%	25%
F2L-35RG*	CEM-1	FA-2	15.9%	35%
F2L-35RGC	CEM-1	FA-2	15.9%	35%
F2H-25RG	CEM-2	FA-2	15.9%	25%
F2H-25RGC	CEM-2	FA-2	15.9%	25%

* Denotes a mixture that was completed under IAC-FA

Table 3-15: Mixture proportions for Class F fly ash mixtures.

Mix ID	Cement lb/yd^3	SCM lb/yd^3	Water lb/yd^3	Coarse Agg. lb/yd^3	Fine Agg. lb/yd^3	WR oz. / cwt
F1L-25RG*	423	141	254	1916	1216	3
F1L-25RGC	423	141	254	1906	1209	3
F1H-25RG*	423	141	254	1916	1216	3
F1H-25RGC	423	141	254	1914	1215	3
F2L-25RG*	423	141	254	1917	1216	3
F2L-25RGC	423	141	254	1916	1216	3
F2L-35RG*	367	197	254	1907	1210	3
F2L-35RGC	367	197	254	1906	1209	3
F2H-25RG	423	141	254	1917	1216	3
F2H-25RGC	423	141	254	1916	1216	3

* Denotes a mixture that was completed under IAC-FA

3.2.1.4 GGBFS Mixtures

Eight mixtures were tested that utilized SLG120 GGBFS, from Chicago, Illinois.

Table 3-16: GGBFS mixtures.

	Cement	SCM Source	SCM CaO Content	SCM Replacement
GL-35RG	CEM-1	SLG120	43.10%	35%
GL-35RGC	CEM-1	SLG120	43.10%	35%
GL-50RG	CEM-1	SLG120	43.10%	50%
GL-50RGC	CEM-1	SLG120	43.10%	50%
GH-50RG	CEM-2	SLG120	43.10%	50%
GH-50RGC	CEM-2	SLG120	43.10%	50%
GL-50LS	CEM-1	SLG120	43.10%	50%
GL-50LSC	CEM-1	SLG120	43.10%	50%

* Denotes a mixture that was completed under IAC-FA

Table 3-17: Mixture proportions for GGBFS mixtures.

Mix ID	Cement lb/yd^3	SCM lb/yd^3	Water lb/yd^3	Coarse Agg. lb/yd^3	Fine Agg. lb/yd^3	WR oz. / cwt
GL-35RG	367	197	254	1932	1226	3
GL-35RGC	367	197	254	1931	1225	3
GL-50RG	282	282	254	1928	1223	3
GL-50RGC	282	282	254	1926	1222	3
GH-50RG	282	282	254	1928	1223	3
GH-50RGC	282	282	254	1926	1222	3
GL-50LS	282	282	254	1908	1211	3
GL-50LSC	282	282	254	1908	1211	3

* Denotes a mixture that was completed under IAC-FA

3.2.1.4 Other Mixtures

In addition to the previous mixtures, seven 'other' mixtures were evaluated that examined the effects of a ternary blend, use of shrinkage reducing admixtures, and of the use of optimized aggregate gradations. Two mixtures were evaluated that used a ternary blend of 10% UFFA with 35% FA-4 fly ash. Three mixtures were evaluated that were composed of the low alkali, river gravel control mixture, but with a shrinkage reducing admixture, SRA, used in addition to the mid-range water-reducer, WR, used in all of the mixtures evaluated. Finally, two mixtures were evaluated that utilized an optimized aggregate gradation. One of these mixtures, OL10-RG, utilized a 10% volume reduction in paste to study a more economical mixture design. This was conducted by increasing the optimized aggregate gradation fractions by 10%.

Table 3-18: Other mixtures.

	Cement	SCM Source	SCM CaO Content	SCM Replacement
U4L-35RG*	CEM-1	FA-4 and UFFA	24.6% and 12.1%	35% and 10%
U4L-35RGC	CEM-1	FA-4 and UFFA	24.6% and 12.1%	35% and 10%
SL-RG	CEM-1	None	--	--
SL-RGC	CEM-1	None	--	--
SL-RGI	CEM-1	None	--	--
OL-RG	CEM-1	None	--	--
OL10-RG	CEM-1	None	--	--

* Denotes a mixture that was completed under IAC-FA

Table 3-19: Mixture proportions for other mixtures.

Mix ID	Cement lb/yd^3	SCM lb/yd^3	Water lb/yd^3	Coarse Agg. lb/yd^3	Fine Agg. lb/yd^3	WR oz. / cwt	SRA gal / yd.
U4L-35RG*	367	197 & 56	254	1890	1199	3	--
U4L-35RGC	310	197 & 56	254	1914	1214	3	--
SL-RG	564	--	254	1940	1231	3	1.5
SL-RGC	564	--	254	1940	1231	3	1.5
SL-RGI	564	--	254	1940	1231	3	1.5
OL-RG	564	--	254	1893	1343	3	--
OL10-RG	508	--	229	1959	1390	3	--

* Denotes a mixture that was completed under IAC-FA

3.3 EXPERIMENTAL PROCEDURES

This section outlines the experimental procedures that were taken for each mixture tested. Descriptions of the batching process, the mixing process, and of the fresh and hardened concrete tests that were performed are presented in this section.

3.3.1 Batching

At least 24 hours prior to mixing, the research team batched the materials that were to be used for that week's mixture. Coarse and fine aggregate were taken from outdoor storage bins. Inside the mixing room, the coarse and fine aggregate were placed, at separate times, inside the mixer, and allowed to blend with a small amount of water. The blending with water allowed the dry aggregate to achieve a condition closer to saturated surface dry (SSD) prior to mixing. After being allowed to blend for 1-2 minutes, the aggregate was emptied into 5-gallon buckets and weighed. Samples were collected to evaluate the moisture content of the aggregate. Cement and SCMs were collected from 55-gallon drums that were located inside closed storage containers outside. Cement and SCMs were placed into 5-gallon buckets, weighed, and placed inside.

For mixtures that were to undergo hot weather temperature simulation or isothermal testing, the batched materials were left inside the mixing room. Mixing room conditions were typically kept at 73°F ± 3°F. If a mixture was to undergo cold weather temperature simulation, the materials, as well as buckets of pre-batched mix water, was stored in an environmental chamber that was kept at 45°F. This allowed for a RCF placement temperature of approximately 65°F.

3.3.2 Mixing Procedures

On the mixing day, moisture content samples were reweighed, and the moisture content of the coarse and fine aggregate was calculated. Corrections to the coarse and fine aggregate batch weights, and to the quantity of mixing water, were made. Mixing water and chemical admixtures were then weighed out, and the chemical admixtures were added to and blended with the mixing water. The concrete mixer, wheelbarrows, and fresh concrete testing materials were then lightly wetted just prior to mixing.

Mixing began by adding all of the coarse and fine aggregate into the mixer, starting the mixer, and then adding approximately 1/3 of the mixing water. The aggregate and water were then allowed to mix for approximately one minute, at which time the mixer was stopped, and the cement and SCMs were added to the mixer. The time was marked at this point as the start of mixing. A lid was then placed on the mixer, the mixer was started, and the mixture was allowed to blend for approximately 30 seconds. The lid was then removed from the mixer, and while still mixing, the remaining 2/3 of the mixing water was slowly added to the mixture. The mixture was then allowed to mix for three minutes. If any caking in the back of the mixer was seen, the mixer was momentarily stopped, the caked material was broken up and pulled back into the bulk of the mixture, and the mixer was started again. After three minutes of mixing, the mixer was stopped, the lid was placed on the mixer, and the mixture was allowed to sit still for three minutes. After the three minute rest, the mixer was turned back on, and the mixture was mixed for a final two minutes. At the end of two minutes, concrete that was to be used for the rigid cracking frame and free shrinkage frame was placed in one wheel barrow, and taken to the building where the frames were located. The remaining concrete was poured into another wheelbarrow, and fresh concrete tests were performed. After fresh concrete testing was completed, concrete was wet sieved through a No. 4 sieve on a vibrating table to generate the mortar for the time of set specimens. When the time of set specimens were completed, the specimens and the remaining concrete were taken to the building where the frames were located. The remaining concrete was then placed into twenty-six 4”x8” cylinders, twenty-four of which were then placed inside the match-cure water bath. The remaining two 4”x8” cylinders were allowed to cure at air-temperature, and were evaluated for coefficient of thermal expansion at a later date.

3.3.3 Fresh Concrete Testing

For each concrete mixture that was tested, slump, unit weight, and air content were recorded. These tests followed the following ASTM standards:

- Slump: ASTM C 143 (2010)
- Unit Weight: ASTM C 138 (2010)
- Air Content: ASTM C 231 (2010)

3.3.4 Hardened Concrete Testing

For each mixture, twenty-four 4”x8” cylinder were cast for mechanical testing, two 4x8” cylinder were cast for evaluation of the mixtures coefficient of thermal expansion, and nine 3”x3”x11.25” prisms were cast for drying shrinkage evaluation. Hardened concrete testing followed the following ASTM standards:

- Compressive strength: ASTM C 39 (2010)
- Splitting Tensile strength: ASTM C 496 (2004)
- Static Modulus of Elasticity: ASTM C 469 (2010)
- Drying Shrinkage: ASTM C 157 (2008)

3.4 EXPERIMENTAL TESTING PROGRAM

To evaluate each mixture design for cracking potential, a testing program was initiated to evaluate the stress development of a concrete mixture due to early-age volume changes under simulated environmental conditions. For each mixture, semi-adiabatic calorimetry, rigid cracking frame, free shrinkage frame, setting time and match-cured cylinder testing was performed. Figure 3-11 shows the order in which these tests were completed.

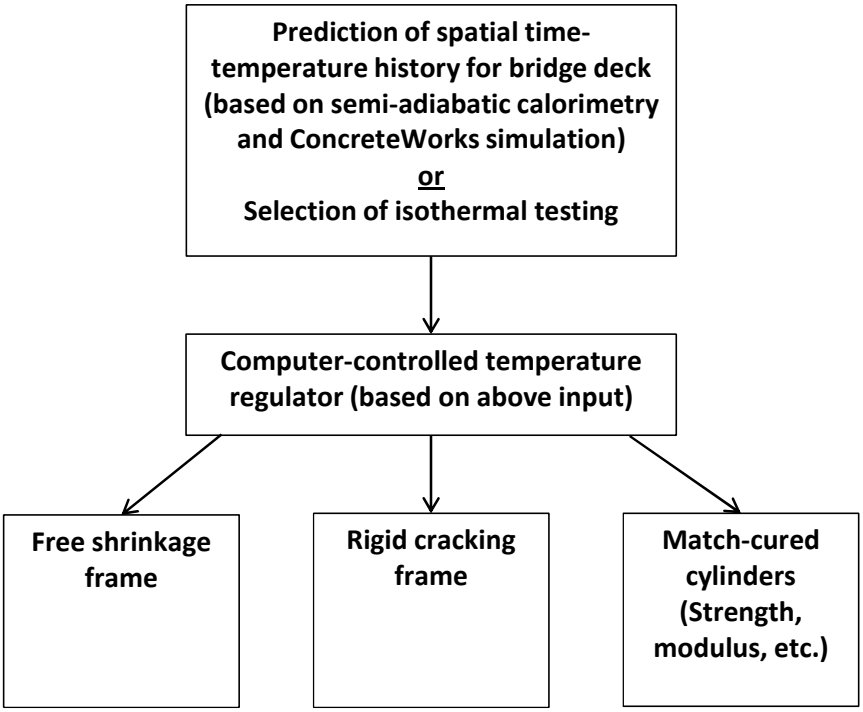

Figure 3-11: Testing process for rigid cracking frame.

3.4.1 Semi-adiabatic Calorimetry

Before a rigid cracking frame test can be started for a mixture, the hydration parameters for that mixture must be calculated so that the simulated temperature development may be determined from ConcreteWorks. At least seven days before the rigid cracking frame testing began, a 2 ft^3 concrete mixture was made to create one 6"x12" cylinder and 12 ASTM C157 (2008) drying shrinkage prisms. The 2 ft^3 mixture size was determined based on the smallest allowable size mixture that was allowed by the concrete mixer. The 6"x12" cylinder was made in three lifts, with rodding and tapping of the sides between each lift. The cylinder was then weighed, and placed in the Q-drum, marking how long after mixing had begun before the cylinder was placed in the Q-drum. The temperature of the concrete was measured using a Type K thermocouple inserted

into the top of the concrete, and the heat flux through the insulated Q-drum was measured at the location of the logging box. After 120 hours had passed, the 6"x12" cylinder was removed from the Q-drum, and the data were collected and processed.

Figure 3-12: Quadrel Q-drum

3.4.2 Estimation of Bridge Deck Temperatures

Before the temperature profile could be created, several hydration parameters had to be determined for each mixture. The activation energy of the mixture (E_a) was determined using an empirical formula from Poole (2007) in Eq. 3-29:

$$E_a = 41{,}230 + 1{,}416{,}000 * [(C_3A + C_4AF) * p_{Cement} * SO_3 * p_{Cement}] - 347{,}000 * Na_2O_{eq} - 19.8 * Blaine + 29{,}600 * p_{Flyash} * p_{CaO-Flyash} + 16{,}200 * p_{GGBFS} - 51{,}600 * p_{SF} - 3{,}090{,}000 * WRRET - 345{,}000 * ACCL$$

Eq. 3-29

The ultimate heat of hydration then had to be determined for the concrete mixture. This was done within the ConcreteWorks program, after inputting the concrete mixture design. Eq. 3-30, found in Riding (2007) was used in the ConcreteWorks program to determine the ultimate heat of hydration.

$$H_u = H_{cem} * p_{Cem} + 461 * p_{GGBF-100} + 550 * p_{GGBF-120} + 1800 * p_{FA-CaO} * p_{FA} + 330 * p_{S.F.}$$

Eq. 3-30

With the calculated activation energy and ultimate heat of hydration, the hydration parameters for the mixture could then be determined. Using the data gathered from the semi-adiabatic calorimetry testing, hydration parameters α, β, and τ for the concrete mixture were curve fit to match the values calculated from Eq. 2-7 with those measured from the Q-drum. This process is described further in Riding (2007), Poole (2007), and Schindler and Folliard (2005)

With the hydration parameters calculated, a temperature profile could then be created in ConcreteWorks. Inputs for the ConcreteWorks program were the following:

- General Parameters
    - Placement Time = 10 A.M.
    - Placement Date:
- Summer Pour = August 15, 2008
- Winter Pour = February 17, 2008
    - Placement Location: Lubbock, TX
    - 8" thick bridge deck with metal pan formwork
- Mixture proportions and aggregate types
- Cement Bogue values (determined with XRF testing)
- Hydration parameters: Ea, Hu, α, β, and τ
- Construction Inputs:
    - Summer Pour: 73^{o} placement temperature, blanket with 2.91 R-value
    - Winter Pour: 65^{o} placement temperature, blanket with 5.67 R-value

Inputs not specified were taken as the default values provided by ConcreteWorks. A sample report, which contains many of the inputs used, is provided in Appendix A.

After the ConcreteWorks temperature profile was created, the temperatures at approximately 4" below the concrete surface (mid-depth on the simulated bridge deck) were selected from the ConcreteWorks output as the temperature profile input for the rigid cracking frame mixture. Figure 3-13 shows sample summer and winter temperature profiles for a straight cement mixture (CH-RG) and a 35% Type C fly-ash replacement mixture (F4H-35RG).

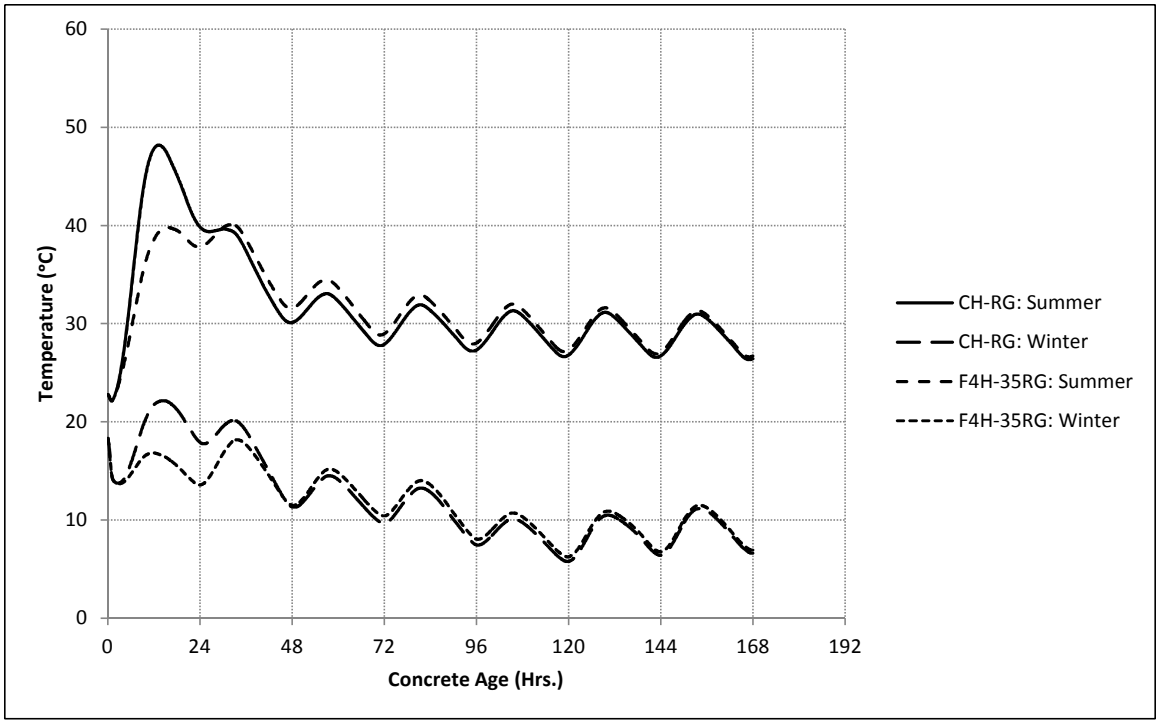

Figure 3-13: Simulated temperature profiles for summer and winter pours.

3.4.3 Rigid Cracking Frame

After the one week in which the semi-adiabatic calorimetry and drying shrinkage prisms were cast, a 5 ft^3 concrete mixture was made to supply concrete to the rigid cracking frame, free shrinkage frame, setting time specimens, and the match cured concrete cylinders.

Before being set into place on the cracking frame, the bottom and two side pieces of the formwork were covered with tight fitting plastic sheeting, which was taped into place using waterproof HVAC aluminum foil tape. The bottom and side pieces of formwork were then fit into place against the bottom of the cracking frame. After aligning the formwork, a combination of 'plumber's putty' and silicone were used to smooth and seal the gaps between the bottom crossbars, crossheads, and the gaps between the bottom and sides of the formwork.

Concrete was placed in two lifts in the rigid cracking frame, with a mechanical vibrator used after each lift to consolidate the concrete. Special attention was paid to the concrete placed inside the crossheads, to ensure that a good bond formed between the concrete and the teeth in the crosshead. Once the second lift was completed, a wooden trowel was used to smooth the concrete surface. The concrete was then covered with a plastic sheet and sealed with HVAC tape. The top crossbars were installed and torqued to specification, and then then top formwork was placed on top of the frame. Thermocouples were then inserted into the concrete through the top of the top formwork, and the hoses that connect the circulator, crossheads, and the formwork were connected. Finally, strain and temperature gauges were attached to the Invar side bars. A diagram of the rigid cracking frame is provided in Figure 3-14, and thorough discussion on the details of the rigid cracking frame can be found in Whigham (2005).

Six days after mixing, the concrete from the previous week's mixture was jackhammered out of the rigid cracking frame, and the crossheads were cleaned with a wire brush. The bottom and two sides of formwork pieces had the previously used plastic and silicone removed, and were then cleaned with a wire brush and oiled.

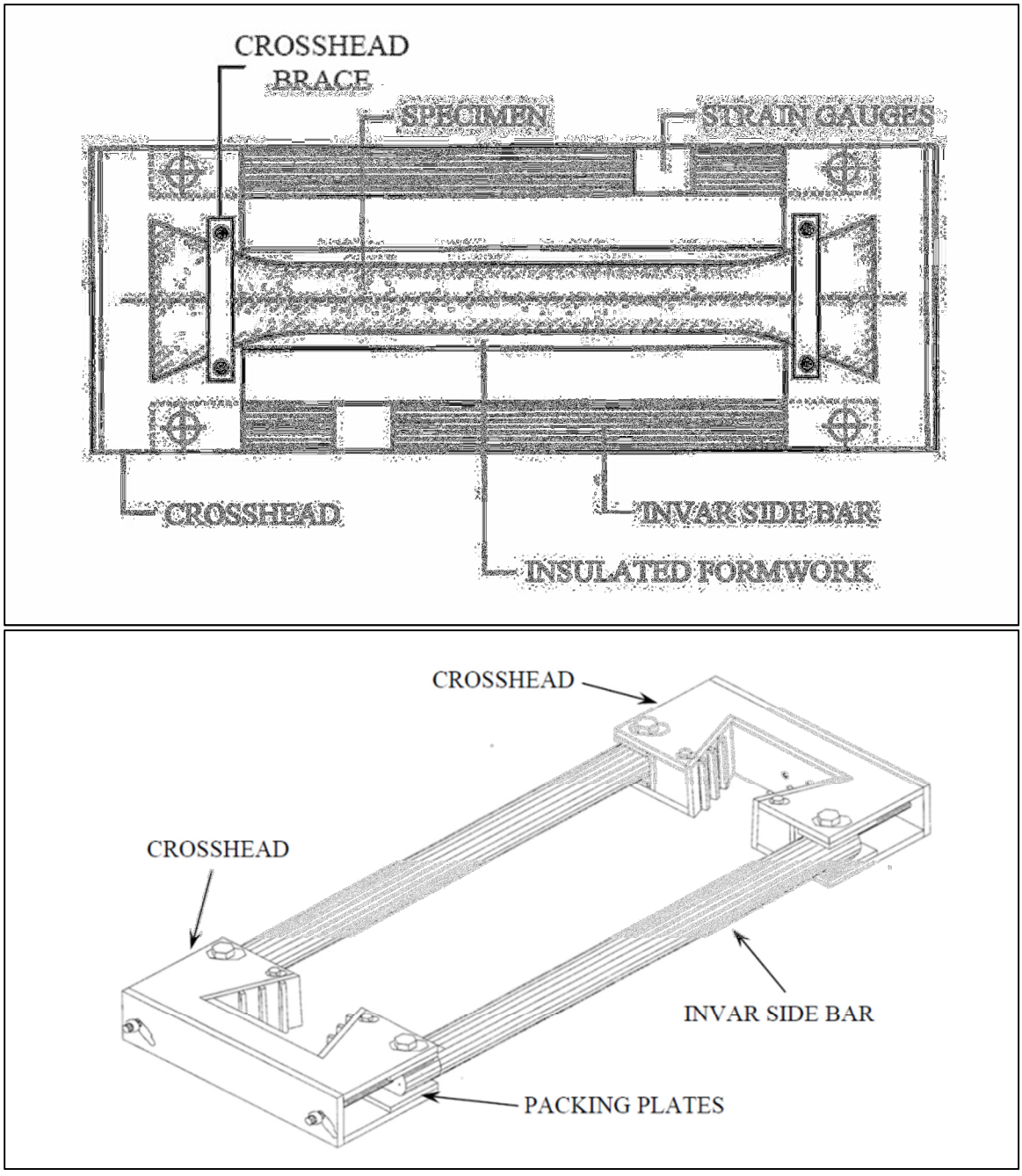

Figure 3-14: Rigid cracking frame drawings (Whigham, 2005; Meadows, 2007)

When simulating the summer and winter concrete pours, concrete in the rigid cracking frame, free shrinkage frame, and match cured cylinder bath were subjected to

the ConcreteWorks-generated temperature profile for 96 hours. After this period, the concrete was cooled artificially at a rate of 1.8 1°F / hr. (1°C / hr.) to force cracking to occur. If cracking did not occur by 120 hours after mixing (24 hours of artificial cooling), the test was stopped. This time limit of 120 hours was chosen because past that time, the frame had usually reached the limit of its ability to lower the concrete temperature (due to the insulative properties of the frame, and temperature control in the testing room). If a concrete mixture was being tested isothermally, the rigid cracking frame, free shrinkage frame, and match cured cylinder bath were all kept at a temperature of 26.8°F (20°C) for 240 hours, after which the mixture was artificially cooled at 1.8 1°F / hr. Artificial cooling was allowed to run until approximately 260-300 hours after the start of mixing.

When the first test runs for the cold weather temperature profiles were placed in the cracking frame, it was found that the one water circulator that was used to control the rigid cracking frame and the free shrinkage frame had difficulty keeping the temperature on track during the first eight hours, and had trouble reaching low temperatures during the artificial cooling phase of the test. This was due to the inadequate temperature control in the room used for testing during the summer months. To remedy the issue, cotton rags were wrapped around the brass fittings of the circulator hoses, and foam panels were taped against the sides of the crosshead that were exposed. The increased insulation proved to be effective in keeping a tighter tolerance between the concrete temperature and the temperature profile, and has also allowed the concrete to reach a lower temperature during the artificial cooling stage. Application of the additional insulation can be seen in Figure 3-15.

Figure 3-15: Rigid cracking frame with added insulation

Before testing began on TxDOT Project 6332, the formwork that had been previously used for rigid cracking frame testing, shown in Figure 3-16, was replaced with formwork built by the author, shown in Figure 3-17. After many mixtures and years of testing, the previous wooden formwork had considerable distress, as shown in Figure 3-16, including rotting wood, separation of copper flashing, and fatiguing of the walls of the formwork. Fatigue of the sides of the formwork led to the sides shifting during concrete placement in the formwork, which later caused stress concentrations at the formwork-crosshead interface. The new formwork was built with a steel frame, and consists of three separate pieces. The new design was constructed to provide a greater ease of use, and to create formwork that would withstand the rigors of the set-up and removal procedure for many years. The new formwork is shown in Figure 3-17, with further construction pictures and information presented in Appendix C.

Figure 3-16: Old formwork for rigid cracking frame

Figure 3-17: Rigid cracking frame with new formwork

3.4.4 Free Shrinkage Frame

For each rigid cracking frame test, a free shrinkage frame test specimen was also cast. This specimen evaluates the unrestrained volume changes in the concrete under the same temperature conditions as the rigid cracking frame, such that creep parameters can be back calculated from the measured restrained stresses in the rigid cracking frame.

Before a mixture, the previous mixture was removed from the free shrinkage frame, and the frame and end plates were wiped clean. The endplates were bolted back onto the free shrinkage frame, and the inside of the frame was wiped down with oil. A layer of plastic was then set inside the frame and taped with painter's tape at the tops of the sides. Another layer of oil was then applied to the free shrinkage frame to decrease the resistance to concrete movement, and then another layer of plastic was placed in the frame, and secured at the top of the sides. Special care was taken to insure that the plastic fit completely into the frame, such that it did not reduce the specimen cross section. Two plastic sheet squares were then placed in front of the end plates, and threaded Invar rods were pushed through this sheet of plastic. On the exterior of the frame, the Invar rods were connected to LVDTs, and on the interior, connected to a 1"x1" aluminum square that was screwed onto the end of the threaded rod. The Invar rod that was on the interior of the frame was then covered with a thick grease, to allow for safe removal of the rod after the test was completed.

On the mixing day, concrete was placed in the free shrinkage frame in two lifts, with mechanical vibration used after each lift to achieve proper consolidation. Special care was taken to insure that concrete was well consolidated between the aluminum squares and the steel end plates. While vibrating the second lift of the free shrinkage frame, the LVDTs were monitored and adjusted so that they were in an optimal location

for measurement during the test, otherwise, inaccurate measurements would be taken if the LVDTs were positioned either too far 'in' or 'out' (National Instruments, 2006).

The end plates of the free shrinkage frame have interior plates that are able to move in and out of the inside of the free shrinkage frame. When fresh concrete is placed in the frame, bolts hold the plates so that they are further inside the frame. During the first few hours after mixing, these plates hold the concrete in place. Upon reaching initial set, as determined by a separate ASTM C403 (2008) test, bolts are tightened on the exterior of the free shrinkage frame that 'back-off' the plates, thereby leaving the concrete specimen free to expand and contract within the free shrinkage frame. The free shrinkage frame is shown in Figure 3-18 and Figure 3-19 The initial set time was recorded, and is presented on the individual graphs related to rigid cracking frame and free shrinkage frame testing in Appendix A. A table of setting time values is also presented in Section 4.9.

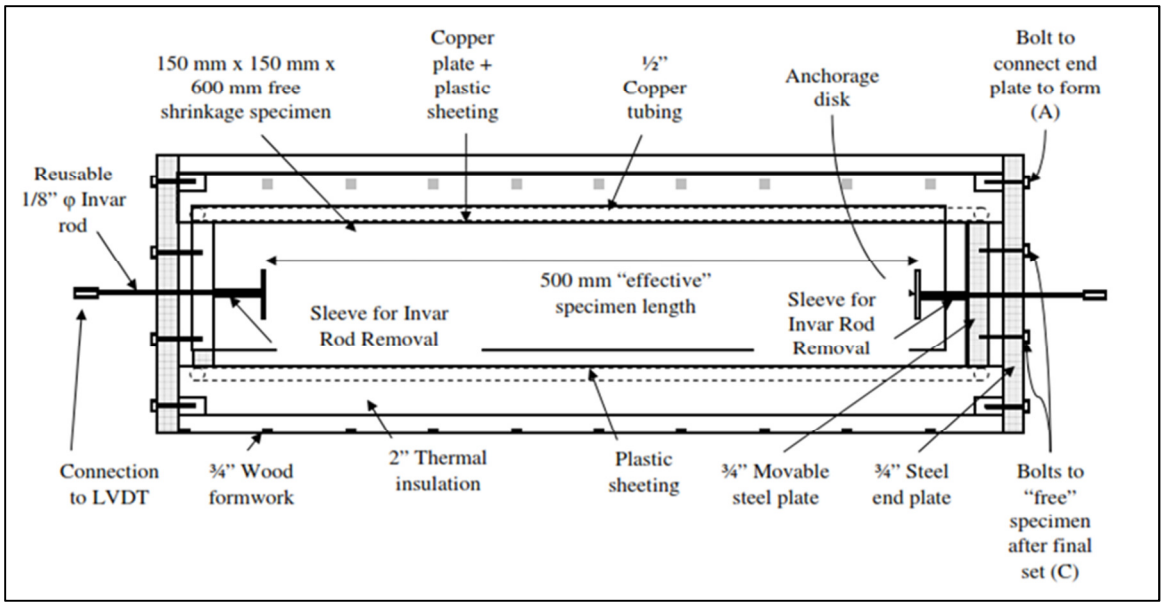

Figure 3-18: Plan view of free shrinkage frame (Meadows, 2007).

Figure 3-19: Free shrinkage frame after mix preparation.

3.4.5 Setting time and Equivalent Age

For each concrete mixture, three time of set specimens were made in accordance with ASTM C 403 (2008). The specimens were cast in ink cans that measured 5" in height and a 6" diameter. Approximately halfway through the testing for TxDOT 6332, the research team began including an iButton temperature measuring devices in the time of set cans (Maxim, 2011). The time of set can with an iButton installed is shown in Figure 3-20. With that time-temperature and penetration resistance information, a substantial database of maturity and time of set data was created.

Figure 3-20: Temperature collection inside time of set can.

In addition to the two time of set cans that were cast and placed in a match-cured water bath under previous studies involving the free shrinkage frame (Riding, 2007; Rao, 2008; Whigham, 2005), another time of set specimen was cast with an iButton sensor, and allowed to cure in a room that was kept at 73°F and 50% RH (for use in drying shrinkage and length change measurements). This separate can, and separate temperature development, allowed the research team to further evaluate the prediction model proposed by Schindler (2004) for a given mixture design under different time-temperature histories. This temperature measurement, placed at the center of the time of set specimen, allowed the researcher to generate time-temperature histories for each time of set test that was performed.

3.4.6 Cylinder Match Curing System

For each rigid cracking frame that was tested, twenty-six 4”x8” concrete cylinders were cast. Twenty-four of these cylinders were placed in a water bath that was driven by a circulator, and programmed to match the temperature of the middle of the rigid cracking frame. A Type K thermocouple was placed inside one of the cylinders at the beginning of the test to provide a feedback loop for the program that controlled the match-cure water bath. The match curing system is shown in Figure 3-21.

Figure 3-21: Cylinder match curing system.

For concrete mixtures undergoing hot weather simulations, cylinders were tested at 12 hours, 1 day, 2 day, 3 day, 7 day, and 28 days after mixing. Mixtures that were undergoing cold weather simulation were tested at 1 day, 2 day, 3 day, 4 day, 7 day, and 28 days after mixing. For each testing day, four cylinders were removed from the match

cured water bath, and replaced with 'dummy' concrete cylinders. On the first set of testing (12 hour for hot simulations and 1 day for cold simulations), two cylinders were tested for splitting tensile strength, then one cylinder tested to determine compressive strength, then the last cylinder was tested for modulus of elasticity, using 0.4 x f'c from the previous test as an upper bound, then broken to obtain the compressive strength. On subsequent testing days, two cylinders were broken in splitting tension, and then the following two cylinders underwent both modulus and compression testing. The first cylinder that was tested for modulus of elasticity used an approximation for the 0.4 x f'c upper bound that was obtained from the percent load increase obtained from the splitting tensile cylinder tests. The second cylinder that was tested used an upper bound value that was calculated from the first cylinders compressive strength. This method of estimation for estimating the upper bound of the elastic modulus test was found to be quite accurate over the course of the project, and allowed the research team to conduct a greater number of modulus tests with the cylinders that were available for testing. Compression, splitting tension, and modulus of elasticity tests were performed according to ASTM standards (ASTM C39, 2010; ASTM C496, 2004; ASTM C469, 2010). The mechanical properties of the mixtures tested are presented in Chapter 4.

3.4.7 Drying Shrinkage Testing

As part of the 2 ft^3 concrete mix that was prepared for semi-adiabatic calorimetry, nine 3"x3"x11.25" concrete prisms were prepared in accordance with ASTM C 157 (2008). Measurement of the drying shrinkage specimens followed a process similar to that presented in ASTM C 157, but with modifications to allow the research team to evaluate the effects of extended curing and hydration on drying shrinkage performance. After allowing the nine prisms to cure for 24 hours, the prisms were demolded, and then

placed in 73°F lime-saturated water for approximately 1 hour. At the end of the hour, three of the prisms were removed from the lime-saturated water, gently dried of surface moisture, and measured and weighed. The remaining six prisms were allowed to continue curing in the lime-saturated water. At seven days after mixing, three more of the prisms were removed and measured, and at ten days after mixing, the last three prisms were removed, dried, and measured. Seven and ten days were selected, as these are they typical number of days after mixing that curing blankets are removed from bridge decks in the field. For each set, the measurement that was taken immediately after the prisms were removed from the lime-saturated water was considered the initial measurement for the shrinkage calculations. For all prisms, after they were removed from the lime-saturated water, future measurements were taken at 4, 7, 14, 28, 56, 112, and 180 days after the removal from the lime-saturated water. Drying shrinkage prisms stored in the drying shrinkage room can be seen in Figure 3-22.

Figure 3-22: Drying shrinkage prisms.

Chapter 4: Laboratory Testing Program Results

The results obtained from the laboratory testing program are presented in this chapter. The fresh concrete properties and hydration parameters are presented first, followed by the mechanical strength development and drying shrinkage strains that were recorded for each mixture. In Section 4.3, models are also evaluated against the measured strength development and drying shrinkage strains. The remainder of the chapter involves the presentation and comparison of the temperature profiles, rigid cracking frame stresses, and free shrinkage frame strains for the mixtures evaluated. At the end of the chapter, a modified B3 creep model is evaluated for the mixtures tested. In post–processing of the results, the research team noted that erroneous hydration parameters were used in the generation of the temperature profiles for F1H-25RG, F4H-25RG, and U4L-RG. Ultimate degree of hydration, α_u, values were taken higher than 100% for these mixtures. While the results from these tests cannot be compared to the other mixtures, the mixtures have been included in this thesis for completeness.

4.1 Fresh Concrete Properties

Table 4-20 provides the fresh concrete properties measured by the research team, in accordance with the standards provided in Section 3.3.3.

Table 4-20: Fresh concrete properties.

Mixture Type	Mixture Name	Slump in.	Unit Weight lb/yd^3	Air %
Control Mixtures	CL-RG	5.00	149.6	3.4
	CL-RGC	5.50	148.0	3.3
	CL-RGI	3.25	148.8	2.3
	CH-RG	5.00	146.4	5.8
	CH-RGC	5.00	144.8	3.5
	CL-LS	3.25	146.8	2.4
	CL-LSC	6.75	147.2	2.5
Class-C Fly Ash Mixtures	*F3L-25RG	7.25	146.4	1.0
	*F3L-35RG	6.50	144.9	1.6
	F3L-35RGC	9.00	148.0	1.0
	F3L-35LS	9.00	145.6	1.0
	F3L-35LSC	8.50	146.4	2.2
	*F4L-25RG	8.50	147.6	1.5
	F4L-35RGC	9.25	146.0	1.6
	*F4H-25RG	3.50	146.4	2.1
	F4H-35RG	9.00	152.0	3.2
	F4H-35RGC	8.00	143.6	3.0
Other Mixtures	*U4L-35RG	9.00	147.3	0.7
	U4L-35RGC	10.50	146.8	1.0
	SL-RG	5.00	149.6	3.5
	SL-RGC	6.00	148.0	2.4
	SL-RGI	4.50	147.2	2.5
	OL-RG	1.50	148.4	2.0
	OL10-RG	0.50	147.7	2.0

Mixture Type	Mixture Name	Slump in.	Unit Weight lb/yd^3	Air %
Class-F Fly Ash Mixtures	*F1L-25RG	4.00	143.1	2.0
	F1L-25RGC	7.00	146	1.0
	*F1H-25RG	3.50	142.4	1.9
	F1H-25RGC	6.00	146.4	2.8
	*F2L-25RG	6.00	147.1	1.0
	F2L-25RGC	9.00	144.8	3.2
	*F2L-35RG	4.75	144.2	1.4
	F2L-35RGC	9.50	146	5.5
	F2H-25RG	8.50	146	3.8
	F2H-25RGC	8.25	142	4.1
GGBFS Mixtures	GL-35RG	3.50	146.4	4.0
	GL-35RGC	6.50	147.2	2.4
	GL-50RG	4.50	147.2	2.9
	GL-50RGC	7.00	147.2	2.0
	GH-50RG	4.00	147.6	3.9
	GH-50RGC	6.00	145.2	3.8
	GL-50LS	5.00	144	3.0
	GL-50LSC	9.25	146.8	2.5

* Denotes a mixture that was completed under IAC-FA

4.2 SEMI-ADIABATIC CALORIMETRY

Table 4-21through Table 4-25 provide the semi-adiabatic calorimetry results for the concrete mixtures tested. E_a, the activation energy, is calculated as shown in Eq. 3-29; H_u, the ultimate heat of hydration, is calculated as shown in Eq. 3-30; and α, β, and τ are curve fit using Excel S+olver to match Eq. 2-7 with the measured heat release from the Q-drum.

Table 4-21: Semi-adiabatic results for control mixtures.

Mixture Type	Mixture Name	E_a J/mol	H_u J/kg	α_u %	β	τ hrs.
Control Mixtures	CL-RG	32,119	468,839	0.747	1.011	14.44
	CL-RGC	32,119	468,838	0.747	1.011	14.44
	CL-RGI	32,119	468,839	0.747	1.011	14.44
	CH-RG	32,252	475,170	0.837	0.959	14.60
	CH-RGC	32,049	475,170	0.836	0.962	14.55
	CL-LS	32,129	468,839	0.774	1.103	15.55
	CL-LSC	32,129	468,839	0.774	1.103	15.55

* Denotes a mixture that was completed under IAC-FA

Table 4-22: Semi-adiabatic calorimetry results for Class C fly ash mixtures.

Mixture Type	Mixture Name	E_a J/mol	H_u J/kg	α_u %	β	τ hrs.
Class-C Fly Ash Mixtures	F3L-25RG*	26,499	410,919	0.828	0.729	25.66
	F3L-35RG*	26,650	410,168	0.817	0.914	20.71
	F3L-35RGC	30,339	448,133	1.000	0.718	34.75
	F3L-35LS	30,339	448,152	0.759	0.839	33.11
	F3L-35LSC	30,339	448,152	0.759	0.839	33.11
	F4L-25RG*	25,461	347,919	0.953	0.973	19.68
	F4L-35RGC	30,529	459,725	0.690	1.178	27.57
	F4H-25RG*	25,461	347,919	1.284	1.014	18.47
	F4H-35RG	29,886	468,757	0.904	0.789	26.93
	F4H-35RGC	29,846	468,286	0.904	0.790	26.91

* Denotes a mixture that was completed under IAC-FA

Table 4-23: Semi-adiabatic calorimetry results for Class F fly ash mixtures.

Mixture Type	Mixture Name	E_a J/mol	H_u J/kg	α_u %	β	τ hrs.
Class-F Fly Ash Mixtures	F1L-25RG*	25,000	309,368	0.896	0.934	14.67
	F1L-25RGC	29,119	356,975	0.862	0.974	15.75
	F1H-25RG*	25,461	347,919	1.074	0.796	14.42
	F1H-25RGC	28,588	369,091	0.941	0.907	16.25
	F2L-25RG*	27,102	447,461	2.773	2.769	28.22
	F2L-25RGC	30,163	423,193	0.702	1.091	17.92
	F2L-35RG*	25,461	347,919	0.787	1.028	16.86
	F2L-35RGC	29,631	404,934	0.570	1.242	19.87
	F2H-25RG	29,453	415,328	0.857	0.893	17.34
	F2H-25RGC	29,626	444,403	0.801	0.892	17.36

* Denotes a mixture that was completed under IAC-FA

Table 4-24: Semi-adiabatic calorimetry results for GGBFS mixtures.

Mixture Type	Mixture Name	E_a J/mol	H_u J/kg	α_u %	β	τ hrs.
GGBFS Mixtures	GL-35RG	33,651	497,245	0.812	0.713	24.53
	GL-35RGC	33,651	497,245	0.812	0.713	24.53
	GL-50RG	34,841	509,419	0.901	0.601	36.94
	GL-50RGC	34,841	509,419	0.901	0.601	36.94
	GH-50RG	33,871	512,585	0.831	0.709	28.72
	GH-50RGC	33,978	517,497	0.823	0.708	28.78
	GL-50LS	34,841	509,419	0.735	0.595	36.16
	GL-50LSC	34,841	509,419	0.735	0.595	36.16

* Denotes a mixture that was completed under IAC-FA

Table 4-25: Semi-adiabatic calorimetry results for other mixtures.

Mixture Type	Mixture Name	E_a J/mol	H_u J/kg	α_u %	β	τ hrs.
Other Mixtures	*U4L-35RG	27080	436268	1.436	0.668	32.84
	U4L-35RGC	30239	412841	0.675	1.284	30.76
	SL-RG	32129	468838	0.749	1.082	17.42
	SL-RGC	32129	468839	0.749	1.082	17.42
	SL-RGI	32129	468839	0.749	1.082	17.42
	OL-RG	32129	468839	0.782	1.087	15.60
	OL10-RG	32129	468838	0.795	1.023	14.83

* Denotes a mixture that was completed under IAC-FA

4.3 HARDENED CONCRETE PROPERTIES

As previously discussed, mechanical testing was performed at various times throughout the course of a mixture. Additionally, a set of drying shrinkage specimens were cast for each mixture design and evaluated to obtain the drying shrinkage for that mixture with various curing times. The results of these tests are presented, and compared with existing prediction models.

4.3.1 Mechanical Properties

Table 4-26 through Table 4-30 provide the mechanical testing results for the mixtures tested. For conciseness, f'c is used to abbreviate the compressive strength, f'st is used to abbreviate the splitting tensile strength, and E is used to abbreviate the elastic modulus of elasticity. Mixtures tested under IAC-FA are denoted with an asterisk before their name. Mixtures OL-RG and OL10-RG do not have the mechanical testing listed. The testing for these mixtures is still ongoing during the time that this thesis was completed. However, the results from these two mixtures will be included in the final report for TxDOT Project 6332. All values are rounded and reported as specified by their respective ASTM specification.

Table 4-26: Mechanical properties for control mixtures.

CL-RG				
Time of Test	hrs.	f'c psi	f'st psi	E psi
12 Hr.	12.9	2,140	315	3,800,000
1 Day	24.7	3,670	445	4,500,000
2 Day	49.7	4,480	540	4,700,000
3 Day	73.0	4,790	540	5,250,000
7 Day	168.1	5,450	560	5,150,000
28 Day	677.0	6,120	590	5,850,000

CL-RGI				
Time of Test	hrs.	f'c psi	f'st psi	E psi
24 Hr.	20.7	1,620	260	3,050,000
2 Day	49.1	3,630	490	4,500,000
3 Day	73.6	4,390	575	4,500,000
4 Day	97.9	4,580	600	4,900,000
7 Day	171.0	5,400	635	5,050,000
28 Day	675.9	6,140	660	5,450,000

CH-RGC				
Time of Test	hrs.	f'c psi	f'st psi	E psi
24 Hr.	22.5	1,740	270	3,500,000
2 Day	48.1	2,970	425	4,500,000
3 Day	75.0	3,380	415	4,500,000
4 Day	100.3	3,690	505	4,550,000
7 Day	167.4	4,240	510	4,600,000
28 Day	679.2	5,550	590	5,200,000

CL-LSC				
Time of Test	hrs.	f'c psi	f'st psi	E psi
24 Hr.	26.6	1,890	270	2,600,000
2 Day	48.8	3,530	445	3,350,000
3 Day	73.6	4,070	510	3,500,000
4 Day	99.5	4,360	545	4,000,000
7 Day	173.8	4,980	610	4,150,000
28 Day	679.9	6,240	675	5,100,000

CL-RGC				
Time of Test	hrs.	f'c psi	f'st psi	E psi
12 Hr.	14.8	680	100	1,800,000
1 Day	26.0	2,240	350	3,750,000
2 Day	52.4	3,830	555	4,450,000
3 Day	74.5	4,290	555	4,750,000
7 Day	166.3	5,580	560	5,050,000
28 Day	678.7	6,900	710	5,350,000

CH-RG				
Time of Test	hrs.	f'c psi	f'st psi	E psi
12 Hr.	10.9	1,380	210	3,350,000
1 Day	25.2	2,840	380	4,550,000
2 Day	49.0	3,450	445	4,600,000
3 Day	73.5	3,560	480	4,650,000
7 Day	166.9	3,940	480	5,150,000
28 Day	669.7	4,480	520	5,300,000

CL-LS				
Time of Test	hrs.	f'c psi	f'st psi	E psi
12 Hr.	12.4	1,210	180	2,600,000
1 Day	29.4	3,800	470	4,100,000
2 Day	51.6	5,080	515	4,550,000
3 Day	80.3	5,080	565	4,600,000
7 Day	172.6	5,410	605	4,700,000
28 Day	674.3	6,420	700	4,850,000

* Denotes a mixture that was completed under IAC-FA

Table 4-27: Mechanical properties for Class C fly ash mixtures.

*F3L-25RG				
Time of Test	hrs.	f'c psi	f'st psi	E psi
12 Hr.	10.5	280	35	1,450,000
1 Day	26.5	2,260	395	3,700,000
2 Day	52.0	3,460	520	4,650,000
3 Day	70.0	3,800	570	4,650,000
7 Day	171.0	3,850	645	5,350,000
28 Day	675.0	4,920	750	5,150,000

F3L-35RGC				
Time of Test	hrs.	f'c psi	f'st psi	E psi
24 Hr.	30.9	600	90	2,200,000
2 Day	59.3	1,520	250	3,300,000
3 Day	77.1	2,000	325	3,550,000
4 Day	100.1	2,370	375	3,950,000
7 Day	176.7	3,930	465	4,500,000
28 Day	679.9	6,220	695	5,350,000

F3L-35LSC				
Time of Test	hrs.	f'c psi	f'st psi	E psi
24 Hr.	30.7	350	40	1,450,000
2 Day	57.5	1,330	185	2,850,000
3 Day	80.3	1,850	260	2,950,000
4 Day	99.9	2,210	330	3,050,000
7 Day	201.7	4,140	490	4,050,000
28 Day	682.6	5,970	670	4,800,000

F4L-35RGC				
Time of Test	hrs.	f'c psi	f'st psi	E psi
24 Hr.	37.3	680	80	2,350,000
2 Day	63.8	1,830	295	3,700,000
3 Day	84.1	2,390	340	4,050,000
4 Day	109.3	2,740	405	4,350,000
7 Day	174.1	4,030	525	4,800,000
28 Day	677.9	6,960	680	4,850,000

F4H-35RG				
Time of Test	hrs.	f'c psi	f'st psi	E psi
12 Hr.	13.3	580	80	2,500,000
1 Day	25.0	1,830	290	3,750,000
2 Day	49.4	3,070	415	4,150,000
3 Day	73.4	3,840	465	4,700,000
7 Day	170.4	4,370	515	4,900,000
28 Day	671.9	5,510	565	5,250,000

*F3L-35RG				
Time of Test	hrs.	f'c psi	f'st psi	E psi
12 Hr.	11.0	210	30	1,400,000
1 Day	25.5	1,290	270	3,350,000
2 Day	48.0	2,570	430	4,050,000
3 Day	71.0	3,060	525	4,100,000
7 Day	170.8	3,670	600	4,200,000
28 Day	675.0	5,250	760	5,250,000

F3L-35LS				
Time of Test	hrs.	f'c psi	f'st psi	E psi
12 Hr.	14.0	420	55	1,500,000
1 Day	28.9	1,770	250	3,100,000
2 Day	51.0	2,840	385	3,550,000
3 Day	77.4	3,660	450	4,100,000
7 Day	176.6	4,720	535	4,500,000
28 Day	677.8	6,020	635	4,850,000

*F4L-25RG				
Time of Test	hrs.	f'c psi	f'st psi	E psi
12 Hr.	10.0	290	65	950,000
1 Day	25.8	2,330	430	4,350,000
2 Day	49.8	3,370	530	5,000,000
3 Day	70.0	3,960	625	4,700,000
7 Day	171.5	4,500	670	4,850,000
28 Day	676.0	5,910	740	5,900,000

*F4H-25RG				
Time of Test	hrs.	f'c psi	f'st psi	E psi
12 Hr.	12.0	940	145	2,550,000
1 Day	28.0	2,500	390	4,050,000
2 Day	52.8	3,300	510	4,450,000
3 Day	81.8	3,550	555	4,750,000
7 Day	173.5	3,880	555	4,950,000
28 Day	679.7	5,040	690	5,350,000

F4H-35RGC				
Time of Test	hrs.	f'c psi	f'st psi	E psi
24 Hr.	23.3	530	75	2,200,000
2 Day	48.9	1,570	255	3,350,000
3 Day	75.6	2,270	325	3,650,000
4 Day	97.3	2,660	370	3,850,000
7 Day	172.8	4,160	495	4,500,000
28 Day	677.3	6,270	610	5,400,000

* Denotes a mixture that was completed under IAC-FA

Table 4-28: Mechanical properties for Class F fly ash mixtures.

*F1L-25RG				
Time of Test	hrs.	f'c psi	f'st psi	E psi
12 Hr.	9.0	160	25	850,000
1 Day	25.3	2,160	395	3,900,000
2 Day	51.0	2,990	480	4,400,000
3 Day	71.0	3,160	505	4,550,000
7 Day	171.0	3,670	600	4,200,000
28 Day	676.5	4,880	680	5,300,000

F1L-25RGC				
Time of Test	hrs.	f'c psi	f'st psi	E psi
24 Hr.	26.7	1,100	175	2,400,000
2 Day	49.6	2,020	295	3,600,000
3 Day	70.9	2,480	370	4,050,000
4 Day	98.4	3,010	425	4,100,000
7 Day	170.3	3,810	480	4,600,000
28 Day	680.9	5,460	660	5,200,000

*F1H-25RG				
Time of Test	hrs.	f'c psi	f'st psi	E psi
12 Hr.	11.1	1,010	175	3,250,000
1 Day	29.3	1,980	325	3,450,000
2 Day	52.8	2,340	385	4,400,000
3 Day	76.3	2,630	385	4,400,000
7 Day	173.6	2,990	455	4,500,000
28 Day	678.4	3,800	625	4,950,000

F1H-25RGC				
Time of Test	hrs.	f'c psi	f'st psi	E psi
24 Hr.	22.0	1,100	180	2,700,000
2 Day	49.2	2,310	340	3,850,000
3 Day	71.7	2,750	380	4,000,000
4 Day	98.4	3,080	450	4,250,000
7 Day	170.0	3,840	480	4,750,000
28 Day	676.2	5,180	610	5,150,000

*F2L-25RG				
Time of Test	hrs.	f'c psi	f'st psi	E psi
12 Hr.	9.0	180	25	700,000
1 Day	25.3	2,000	415	1,000,000
2 Day	50.5	2,790	485	4,550,000
3 Day	69.5	3,270	535	4,300,000
7 Day	171.0	3,960	670	4,400,000
28 Day	671.5	5,520	730	6,450,000

F2L-25RGC				
Time of Test	hrs.	f'c psi	f'st psi	E psi
24 Hr.	23.7	530	70	1,900,000
2 Day	48.0	1,670	265	3,500,000
3 Day	70.2	2,300	325	3,950,000
4 Day	97.3	2,580	390	4,100,000
7 Day	164.3	3,250	465	4,400,000
28 Day	681.8	5,660	665	5,200,000

*F2L-35RG				
Time of Test	hrs.	f'c psi	f'st psi	E psi
12 Hr.	11.0	230	35	1,000,000
1 Day	25.8	1,720	310	3,300,000
2 Day	49.3	2,500	435	4,100,000
3 Day	69.0	2,720	475	4,200,000
7 Day	168.0	3,320	655	4,450,000
28 Day	673.7	4,560	710	5,400,000

F2L-35RGC				
Time of Test	hrs.	f'c psi	f'st psi	E psi
24 Hr.	32.9	480	65	1,300,000
2 Day	48.1	1,080	150	2,950,000
3 Day	76.8	1,870	250	3,800,000
4 Day	100.8	1,960	315	3,750,000
7 Day	171.9	2,800	420	4,550,000
28 Day	678.9	5,120	605	5,100,000

F2H-25RG				
Time of Test	hrs.	f'c psi	f'st psi	E psi
12 Hr.	11.3	820	125	1,400,000
1 Day	25.4	2,370	325	4,000,000
2 Day	49.9	2,890	415	4,500,000
3 Day	73.4	3,190	385	4,550,000
7 Day	166.6	3,370	445	4,700,000
28 Day	669.9	4,840	555	4,950,000

F2H-25RGC				
Time of Test	hrs.	f'c psi	f'st psi	E psi
24 Hr.	27.0	1,090	160	2,750,000
2 Day	50.3	2,060	305	3,400,000
3 Day	74.8	2,390	365	3,500,000
4 Day	101.4	2,680	415	3,600,000
7 Day	170.1	3,510	440	3,900,000
28 Day	670.4	5,090	565	4,350,000

*Denotes a mixture that was completed under IAC-FA

Table 4-29: Mechanical properties for GGBFS mixtures.

GL-35RG				
Time of Test	hrs.	f'c psi	f'st psi	E psi
12 Hr.	13.5	1,250	180	2,900,000
1 Day	24.2	2,660	370	4,150,000
2 Day	50.9	4,110	475	4,700,000
3 Day	72.6	4,650	525	4,800,000
7 Day	166.3	5,170	525	5,000,000
28 Day	669.2	6,340	710	5,700,000

GL-35RGC				
Time of Test	hrs.	f'c psi	f'st psi	E psi
24 Hr.	30.3	900	135	2,350,000
2 Day	48.0	1,500	245	3,250,000
3 Day	79.2	2,080	320	3,700,000
4 Day	96.1	2,270	365	4,000,000
7 Day	172.4	3,450	460	4,500,000
28 Day	672.4	6,540	690	4,700,000

GL-50RG				
Time of Test	hrs.	f'c psi	f'st psi	E psi
12 Hr.	14.0	870	120	2,500,000
1 Day	24.7	1,980	315	3,300,000
2 Day	51.5	3,440	455	4,850,000
3 Day	73.4	4,240	510	5,350,000
7 Day	169.7	5,070	535	5,400,000
28 Day	674.2	6,000	600	5,500,000

GL-50RGC				
Time of Test	hrs.	f'c psi	f'st psi	E psi
24 Hr.	26.8	390	55	1,600,000
2 Day	46.3	840	135	2,350,000
3 Day	80.6	1,300	220	3,250,000
4 Day	100.2	1,450	235	3,300,000
7 Day	176.8	2,810	440	4,250,000
28 Day	676.6	6,880	740	5,850,000

GH-50RG				
Time of Test	hrs.	f'c psi	f'st psi	E psi
12 Hr.	11.6	570	75	2,800,000
1 Day	25.0	2,180	295	3,900,000
2 Day	48.2	3,440	450	4,600,000
3 Day	72.9	4,060	470	4,900,000
7 Day	166.9	4,510	545	5,050,000
28 Day	669.9	5,380	575	5,650,000

GH-50RGC				
Time of Test	hrs.	f'c psi	f'st psi	E psi
24 Hr.	28.5	510	65	1,700,000
2 Day	52.5	1,090	185	2,550,000
3 Day	73.5	1,390	230	2,800,000
4 Day	97.2	1,760	305	3,050,000
7 Day	168.9	3,410	500	3,650,000
28 Day	676.3	5,480	660	4,650,000

GL-50LS				
Time of Test	hrs.	f'c psi	f'st psi	E psi
12 Hr.	12.6	460	50	1,700,000
1 Day	28.8	1,640	235	3,250,000
2 Day	53.2	1,570	375	3,950,000
3 Day	79.1	3,820	475	4,200,000
7 Day	176.5	5,120	565	4,700,000
28 Day	681.0	6,760	730	4,950,000

Gl-50LSC				
Time of Test	hrs.	f'c psi	f'st psi	E psi
24 Hr.	30.7	660	95	1,850,000
2 Day	56.4	1,260	185	2,650,000
3 Day	74.6	1,440	215	2,700,000
4 Day	98.8	1,840	265	3,250,000
7 Day	177.6	3,080	425	4,000,000
28 Day	675.6	7,160	730	5,150,000

* Denotes a mixtures that was completed under IAC-FA

Table 4-30: Mechanical properties for other mixtures.

*U4L-35RG				
Time of Test	hrs.	f'c psi	f'st psi	E psi
12 Hr.	11.9	490	70	1,750,000
1 Day	29.9	2,130	350	3,850,000
2 Day	52.3	3,200	500	4,500,000
3 Day	76.1	3,640	520	5,150,000
7 Day	171.9	4,510	615	5,050,000
28 Day	678.4	5,480	685	5,750,000

SL-RG				
Time of Test	hrs.	f'c psi	f'st psi	E psi
12 Hr.	13.1	1,390	195	3,100,000
1 Day	26.3	3,340	435	4,650,000
2 Day	51.0	4,010	490	4,800,000
3 Day	74.7	4,390	545	5,250,000
7 Day	172.4	4,550	540	5,450,000
28 Day	676.7	6,050	635	5,500,000

SL-RGI				
Time of Test	hrs.	f'c psi	f'st psi	E psi
24 Hr.	26.2	1,530	245	3,100,000
2 Day	47.9	2,980	430	4,250,000
3 Day	73.8	3,940	515	4,600,000
4 Day	97.9	4,330	550	4,800,000
7 Day	169.2	4,730	585	5,000,000
28 Day	674.8	6,480	655	5,450,000

U4L-35RGC				
Time of Test	hrs.	f'c psi	f'st psi	E psi
24 Hr.	35.3	140	20	450,000
2 Day	60.8	1,010	145	2,800,000
3 Day	82.1	1,360	210	3,350,000
4 Day	102.0	1,780	260	3,900,000
7 Day	173.0	3,360	430	3,950,000
28 Day	680.3	5,220	605	4,500,000

SL-RGC				
Time of Test	hrs.	f'c psi	f'st psi	E psi
24 Hr.	30.7	1,420	230	2,600,000
2 Day	56.2	2,990	425	3,650,000
3 Day	76.8	3,490	455	3,900,000
4 Day	103.2	3,930	530	3,950,000
7 Day	177.7	4,920	585	4,500,000
28 Day	679.8	5,860	685	5,350,000

* Denotes a mixture that was completed under IAC-FA

4.3.1.1 Mechanical Property Parameters

As discussed in Chapter 2, equations in the literature have shown an acceptable ability to capture the strength development profile for concrete mixtures. These formulations, coupled with equivalent age calculations, allow the research team to know the stress / strength throughout the course of a rigid cracking frame test. For the purposes of curve fitting the strength equations, Eq. 2-15 is rewritten as Eq. 4-31. The parameters for compressive strength, modulus of elasticity, and splitting tensile strength are presented in Table 4-31 through Table 4-35.

$$E_c = {w_c}^{1.5} * A * {f'_c}^{B}$$

Eq. 4-31

Table 4-31: Strength development parameters- Control mixtures.

Mixture	Compressive Strength			Elastic Modulus		Splitting Tensile Strength	
	fcult	τ_s	β_s	A	B	l	m
CL-RG	6,653	24.970	0.729	86.080	0.410	3.535	0.591
CL-RGC	7,155	26.135	0.963	63.704	0.441	1.665	0.689
CL-RGI	6,395	25.268	0.982	73.427	0.425	1.941	0.674
CH-RG	4,806	23.024	0.738	112.102	0.390	0.892	0.761
CH-RGC	6,266	27.217	0.654	201.410	0.313	2.422	0.641
CL-LS	6,611	28.820	0.927	98.073	0.382	0.513	0.821
CL-LSC	6,471	24.636	0.924	11.643	0.626	0.825	0.772

*Denotes a mixture that was completed under IAC-FA

Table 4-32: Strength development parameters- Class C fly ash mixtures.

Mixture	Compressive Strength			Elastic Modulus		Splitting Tensile Strength	
	fcult	τ_s	β_s	A	B	l	m
*F3L-25RG	4,969	35.029	1.028	49.749	0.488	0.244	0.946
*F3L-35RG	6,422	75.923	0.683	100.718	0.394	0.861	0.795
F3L-35RGC	7,701	79.238	0.745	133.956	0.355	1.151	0.733
F3L-35LS	7,729	77.939	0.705	67.941	0.428	0.779	0.772
F3L-35LSC	7,064	72.269	0.829	84.099	0.399	0.527	0.823
*F4L-25RG	6,440	57.952	0.657	75.815	0.429	0.511	0.850
F4L-35RGC	8,892	85.543	0.704	235.692	0.288	1.451	0.702
*F4H-25RG	6,123	50.318	0.581	68.055	0.448	0.490	0.854
F4H-35RG	6,169	53.779	0.817	166.403	0.328	1.280	0.713
F4H-35RGC	7,625	68.631	0.739	136.848	0.356	1.646	0.681

*Denotes a mixture that was completed under IAC-FA

Table 4-33: Strength development parameters- Class F fly ash mixtures.

Mixture	Compressive Strength			Elastic Modulus		Splitting Tensile Strength	
	fcult	τ_s	β_s	A	B	l	m
*F1L-25RG	5,423	44.373	0.726	33.103	0.538	0.788	0.802
F1L-25RGC	6,476	46.440	0.669	70.780	0.437	0.723	0.792
*F1H-25RG	5,292	58.559	0.435	152.762	0.357	0.153	1.005
F1H-25RGC	5,874	36.452	0.713	85.782	0.414	1.030	0.748
*F2L-25RG	7,234	73.927	0.555	0.404	1.065	1.600	0.720
F2L-25RGC	7,559	75.994	0.577	92.696	0.408	0.685	0.800
*F2L-35RG	5,389	57.045	0.668	25.048	0.576	0.394	0.899
F2L-35RGC	7,727	106.800	0.578	60.018	0.466	0.487	0.839
F2H-25RG	6,251	53.752	0.493	19.643	0.600	0.673	0.795
F2H-25RGC	6,415	51.287	0.583	208.132	0.295	1.481	0.701

*Denotes a mixture that was completed under IAC-FA

Table 4-34: Strength development parameters- GGBFS mixtures.

Mixture	Compressive Strength			Elastic Modulus		Splitting Tensile Strength	
	fcult	τ_s	β_s	A	B	l	m
GL-35RG	6,947	39.446	0.789	102.207	0.391	0.623	0.799
GL-35RGC	14,467	335.354	0.367	196.166	0.305	1.377	0.710
GL-50RG	6,708	49.190	0.838	75.081	0.434	1.749	0.675
GL-50RGC	57,576	15406.876	0.235	80.870	0.422	0.952	0.757
GH-50RG	5,714	39.504	0.920	192.339	0.321	0.599	0.805
GH-50RGC	6,763	82.051	0.798	119.124	0.358	0.929	0.766
GL-50LS	9,086	117.977	0.752	312.952	0.252	2.801	0.627
GL-50LSC	10,000	135.778	0.651	128.112	0.352	0.997	0.745

*Denotes a mixture that was completed under IAC-FA

Table 4-35: Strength development parameters- Other mixtures.

Mixture	Compressive Strength			Elastic Modulus		Splitting Tensile Strength	
	fcult	τ_s	β_s	A	B	l	m
*U4L-35RG	6,884	75.082	0.720	66.860	0.451	1.042	0.757
U4L-35RGC	5,776	71.185	1.069	94.489	0.398	0.573	0.814
SL-RG	6,743	34.937	0.658	88.974	0.410	0.839	0.767
SL-RGC	6,063	31.259	1.105	33.191	0.512	0.997	0.753
SL-RGI	7,114	37.535	0.791	105.703	0.386	2.394	0.646

*Denotes a mixture that was completed under IAC-FA

4.3.2 Drying Shrinkage

As discussed in Chapter 3, drying shrinkage specimens were cast, cured, and measured to judge the effect of various curing regimes on the final drying shrinkage strain. As discussed in Chapter 2, many tests and models have been developed that attempt to capture drying shrinkage. Figure 4-23 shows what the input parameters are for some of the most commonly used drying shrinkage models. With the assistance of an undergraduate working on an independent study, the research team was able to evaluate the drying shrinkage strains that were recorded for the mixtures tested, against those that are predicted by the ACI 209, CEB 90, and B3 models (ACI Committee 209, 2008; CEB-FIP Model Code '90, 1993; Bazant, 1995). Figure 4-24 displays the total drying shrinkage values for all the mixtures tested under TxDOT Project 6332. Inputs that are required for the drying shrinkage modeling are labeled with an “S”, and inputs needed for creep modeling are labeled with a “C”. While many more mixtures were conducted, temperature effects were not considered in the drying shrinkage modeling, so only the unique mixture designs were evaluated.

	ACI 209	CEB 90	B3	GL 2000
Relative humidity	*S, C*	*S, C*	*S, C*	*S*
Specimen size	*S, C*	*S, C*	*S*	*S, C*
Specimen shape	—	—	*S*	—
Compressive strength at 28 days after casting (f_{cm28})	*C*	*S, C*	*S, C*	*S, C*
Compressive strength at age of loading (f_{cmto})	*C*	—	—	*C*
Modulus of elasticity 28 days after casting (E_{cm28})	*C*	*C*	*C*	*C*
Modulus of elasticity at age of loading (E_{cmto})	*C*	*C*	—	*C*
Cement types	*C*	*C*	*S, C*	*S*
Water-cement ratio (w/c)	—	—	*C*	—
Aggregate-cement ratio (a/c)	—	—	*C*	—
Curing types	*S, C*	—	*S, C*	—
Age at end of curing (t_c)	*S*	*S*	*S*	*S*
Age at loading (t_o)	*C*	*C*	*C*	*C*
Total parameters required for shrinkage (*S*)	4	4	7	4
Total parameters required for creep (*C*)	9	7	8	6

Figure 4-23: Input factors for predicting shrinkage and creep (Al-Manseer & Lam, 2005)

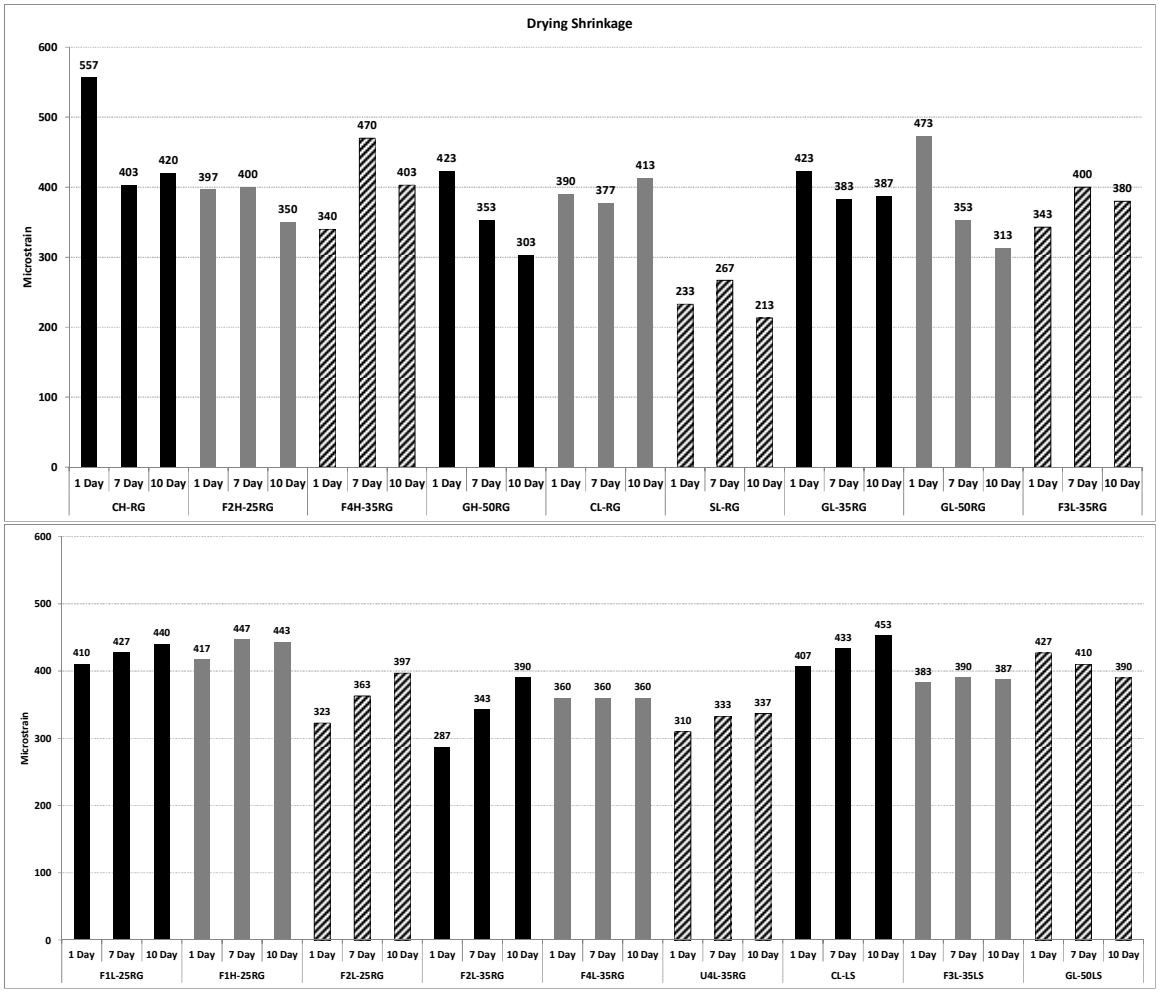

Figure 4-24: 180-day drying shrinkage strains.

Table 4-36 presents the measured versus the predicted 180-day drying shrinkage strains for the specimens that underwent the seven day curing regime. The research team was able to determine, using the measured values, that the effects of initial curing on the specimens tested was minimal on the final drying shrinkage strains. In addition, using the data set generated under TxDOT Project 6332, the B3 model was chosen as the best for predicting drying shrinkage strains, and will be used in the future for the purposes of computer modeling of bridge deck systems. A more thorough discussion of the models

evaluated and of the results obtained from testing the models against the values recorded by the research team is in progress, and will be included in the final report for this project.

Table 4-36: Measured vs. predicted drying shrinkage values for 7 day cure.

Mix ID		ACI 209R-92	B3 Bazant	CEB MC90-99	Measured Microstrain
CH-RG	Microstrain	666.8	466.0	560.9	-403.3
	% Error	65.3	15.5	39.1	
F2H-25RG	Microstrain	750.3	462.2	544.6	-400.0
	% Error	87.6	15.5	36.2	
F4H-35RG	Microstrain	766.6	455.8	515.2	-470.0
	% Error	63.1	-3.0	9.6	
GH-50RG	Microstrain	641.7	457.0	520.9	-353.3
	% Error	81.6	29.3	47.4	
CL-RG	Microstrain	666.8	450.8	489.8	-376.7
	% Error	77.0	19.7	30.0	
GL-35RG	Microstrain	629.4	449.1	480.9	-383.3
	% Error	64.2	17.2	25.4	
GL-50RG	Microstrain	654.3	451.7	494.5	-353.3
	% Error	85.2	27.8	39.9	
SL-RG	Microstrain	666.8	451.3	492.5	-256.7
	% Error	159.8	75.8	91.9	
F3L-35RG	Microstrain	766.5	450.0	485.8	-400.0
	% Error	91.6	12.5	21.5	
F1L-25RG	Microstrain	716.8	456.2	517.3	-426.7
	% Error	68.0	6.9	21.2	
F1H-25RG	Microstrain	691.8	458.8	529.5	-446.7
	% Error	54.9	2.7	18.5	
F2L-25RG	Microstrain	766.6	454.5	508.8	-363.3
	% Error	111.0	25.1	40.0	
F2L-35RG	Microstrain	779.0	459.4	532.0	-343.3
	% Error	126.9	33.8	54.9	
F4L-35RG	Microstrain	773.0	444.8	456.7	-360.0
	% Error	114.7	23.5	26.9	
U4L-35RG	Microstrain	803.9	458.4	527.6	-333.3
	% Error	141.2	37.5	58.3	
CL-LS	Microstrain	623.1	449.9	485.1	-433.3
	% Error	43.8	3.8	11.9	
F3L-35LS	Microstrain	766.6	451.9	495.7	-390.0
	% Error	96.6	15.9	27.1	
GL-50LS	Microstrain	666.8	443.5	449.3	-410.0
	% Error	62.6	8.2	9.6	
Average % Error		88.6	20.4	33.9	

4.4 SIMULATED TEMPERATURE PROFILES

This section provides the simulated temperature profiles for the concrete mixtures tested. Figure 4-25 through Figure 4-30 provide the simulated temperature profiles for the concrete mixture types, with individual temperature profiles presented in Appendix A. While the temperatures in the following graphs has been converted to °F, the individual temperature profiles Appendix A are presented in °C, as this was the convention used throughout the rigid cracking frame data processing programs. Semi-adiabatic calorimetry parameters, cement chemistry, mixture design, and location and specimen geometries were input into ConcreteWorks to generate the profiles presented. All profiles presented represent mid-depth on an 8" thick concrete bridge deck. Figure 4-30, at the end of the section, displays the temperature profiles across various mixture types.

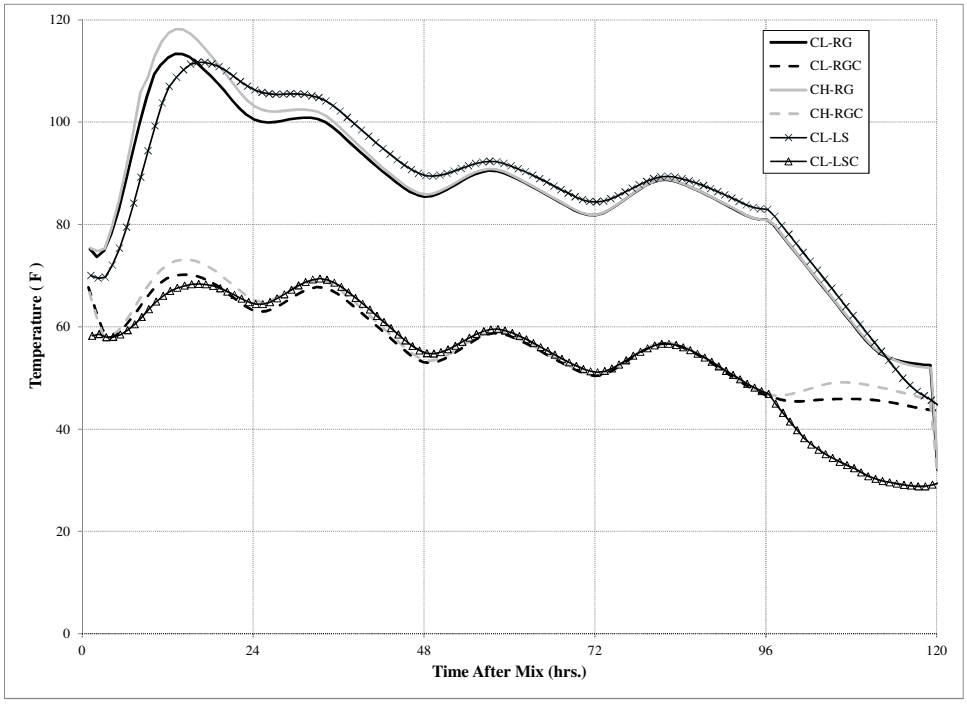

Figure 4-25: Temperature profiles for Control mixtures.

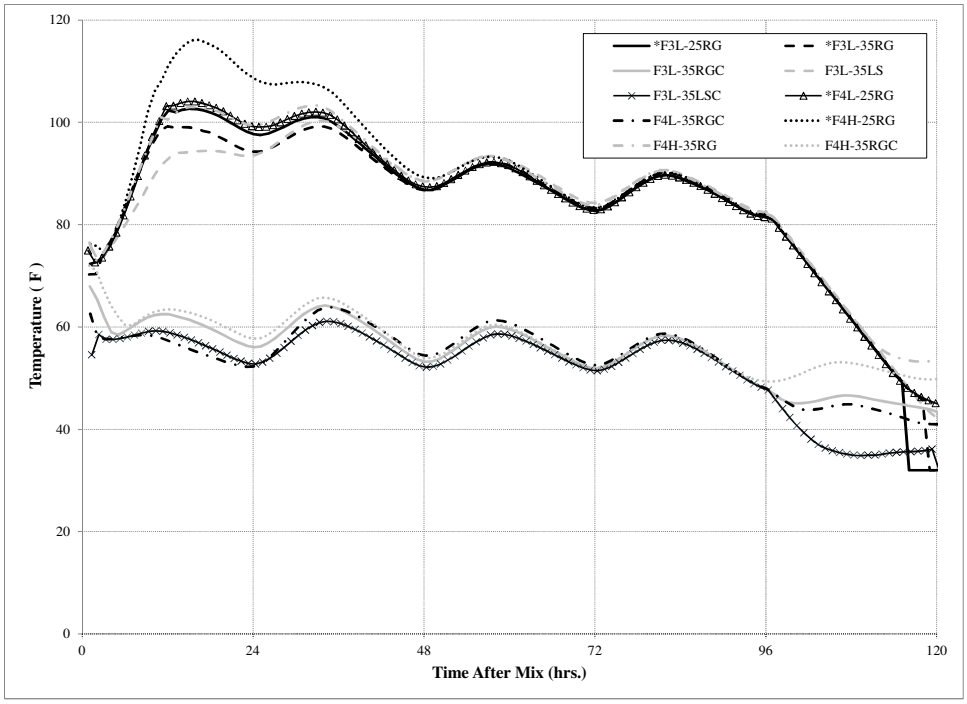

Figure 4-26: Temperature profiles for Class C fly ash mixtures.

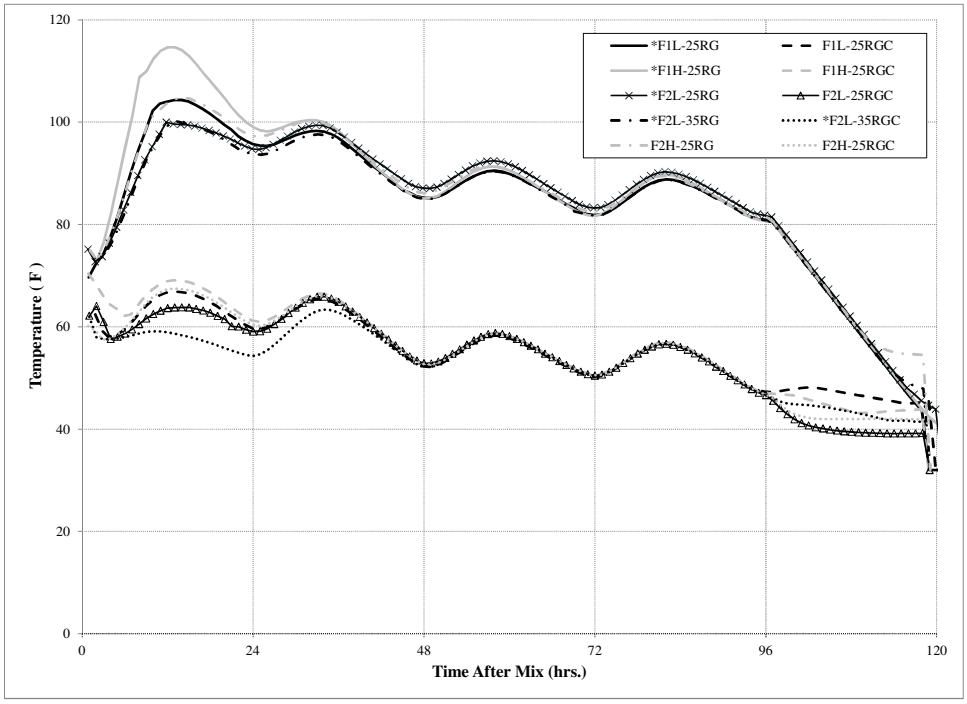

Figure 4-27: Temperature profiles for Class F fly ash mixtures.

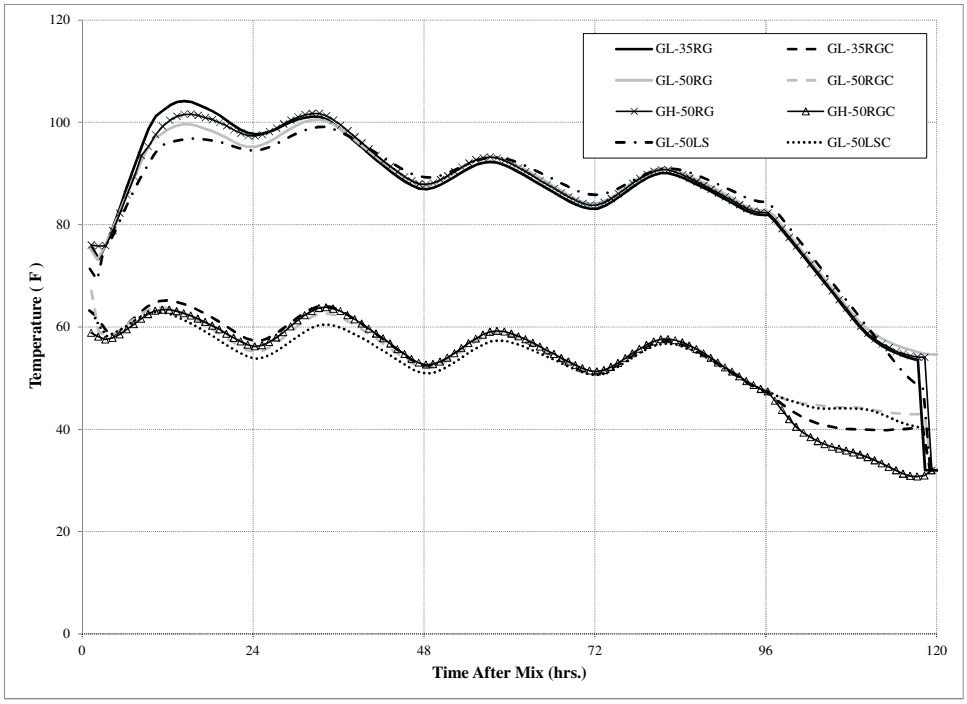

Figure 4-28: Temperature profiles for GGBFS mixtures.

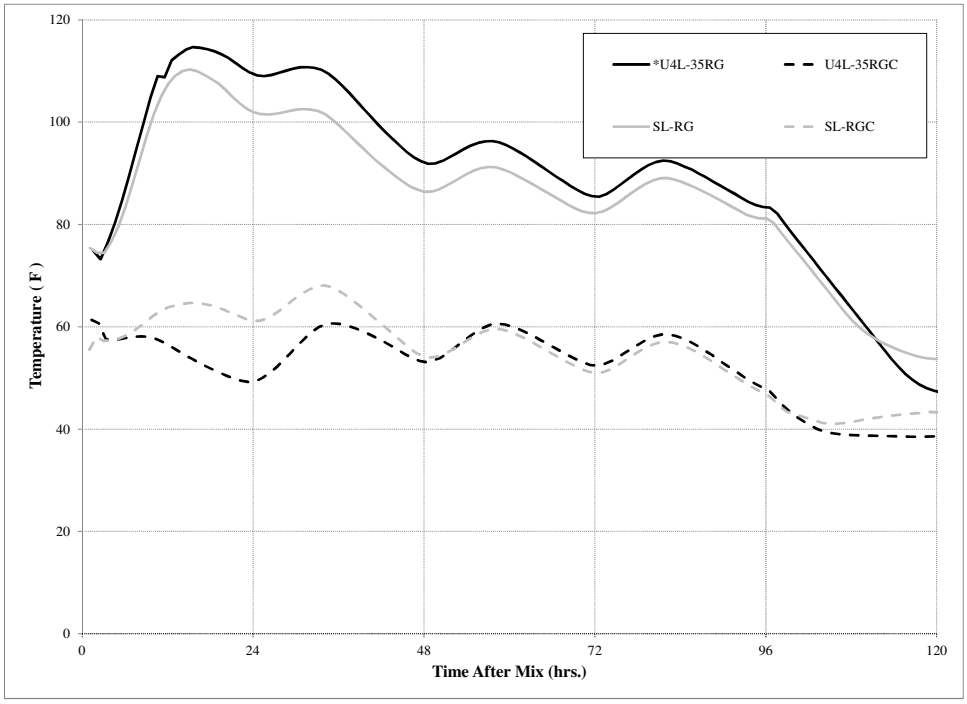

Figure 4-29: Temperature profile for Other mixtures.

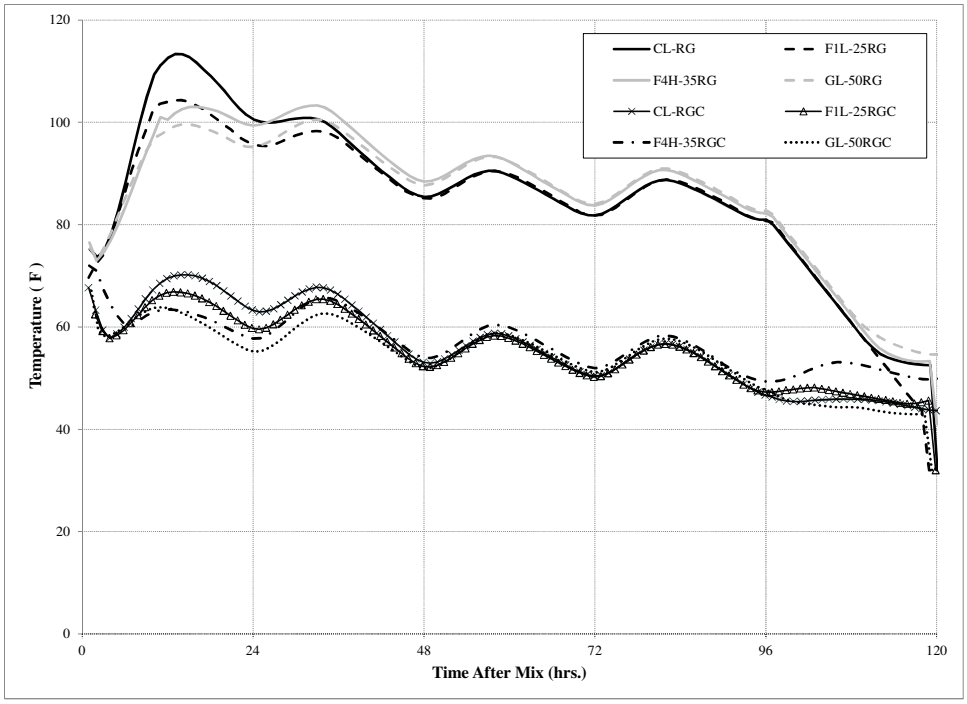

Figure 4-30: Temperature profile comparison across various mixture types.

4.5 RESTRAINED STRESS DEVELOPMENT UNDER SIMULATED TEMPERATURES

This section provides the recorded stresses in the rigid cracking frame for the mixtures tested. The individual sections also provide some of the key points from each mixture. In the summaries, the 'Δ Temp' refers to the difference between the temperature at initial set and the temperature at the respective event. Under time of cracking, mixtures that cracked display the hour after mixing at which cracking occurred, while 'NC' denotes mixtures that did not crack. The various 'ratios' presented represent the stress in the rigid cracking frame divided by the curve-fit splitting tensile strength at the equivalent age corresponding to the respective event. The 'Reserve' ratio is the difference between the stress / strength at 96 hours after mixing compared to the ratio at the time of cracking. Section 4.5.6 compares some of the key points across all of the

mixture types. The restrained stress development for individual mixtures can be found in Appendix A.

4.5.1 Control Mixtures

Figure 4-31 and Table 4-37 show the results of the rigid cracking frame testing for the control mixtures. Unlike most of the hot temperature profile mixtures, the CL-LS mixture did not crack, and had a considerably lower maximum stress during the 96 hour simulation. The high and low alkali mixtures were seen to perform quite similarly.

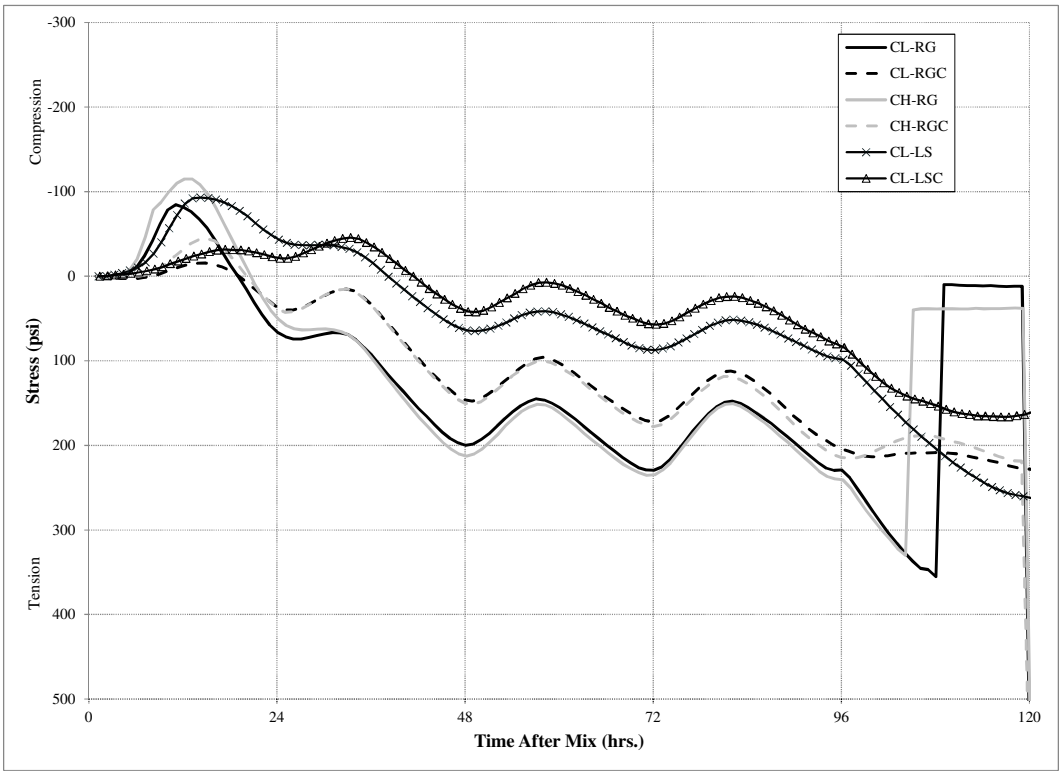

Figure 4-31: Rigid cracking frame stresses- Control Mixtures

Table 4-37: Summary of rigid cracking frame results- Control mixtures.

Mix Name	CL-RG	CL-RGC	CH-RG	CH-RGC	CL-LS	CL-LSC	Averages
Time of Cracking	108.5	NC	105.0	NC	NC	NC	
Cracking Stress	354	--	334	--	--	--	344
Temperature at Initial Set	81.1	61.7	80.4	64.5	75.7	60.4	70.6
Cracking Temperature	60.0	--	66.2	--	--	--	63.1
ΔTemp at Cracking	21.1	--	14.2	--	--	--	17.6
Cracking Ratio	0.639	--	0.702	--	--	--	0.670
Reserve	0.219	--	0.192	--	--	--	0.205
ΔTemp at 96hr. Max Stress	0.1	15.0	-0.5	17.6	-7.3	13.2	6.4
Max 96hr Stress	231	70	241	214	98	82	156
Ratio at 96hr Max	0.421	0.177	0.510	0.463	0.165	0.154	0.315
Temperature at t_{max}	--	43.6	--	45.9	41.1	29.9	40.1
ΔTemp at t_{max}	--	18.1	--	18.6	34.6	30.5	25.4
Stress at t_{max}	--	228	--	219	266	159	218
Ratio at t_{max}	--	0.442	--	0.457	0.441	0.290	0.407

All stresses are in psi, all temperatures in •F

* Denotes a mixture that was tested under IAC-FA

4.5.2 Class C Fly Ash Mixtures

Figure 4-32 and Table 4-38 show the results of the rigid cracking frame testing for Class C fly ash mixtures. While the table was split between FA-3 and FA-4, the average column at the end of the bottom table is still an average of all Class C fly ash mixtures. In the results, FA-4 mixtures were seen to have slightly higher stresses and stress /strength ratios at the end of the 96 hour temperature simulation. Class C fly ash mixtures that utilized limestone coarse aggregate developed approximately half the stress at 96 hours that the respective river gravel mixture developed.

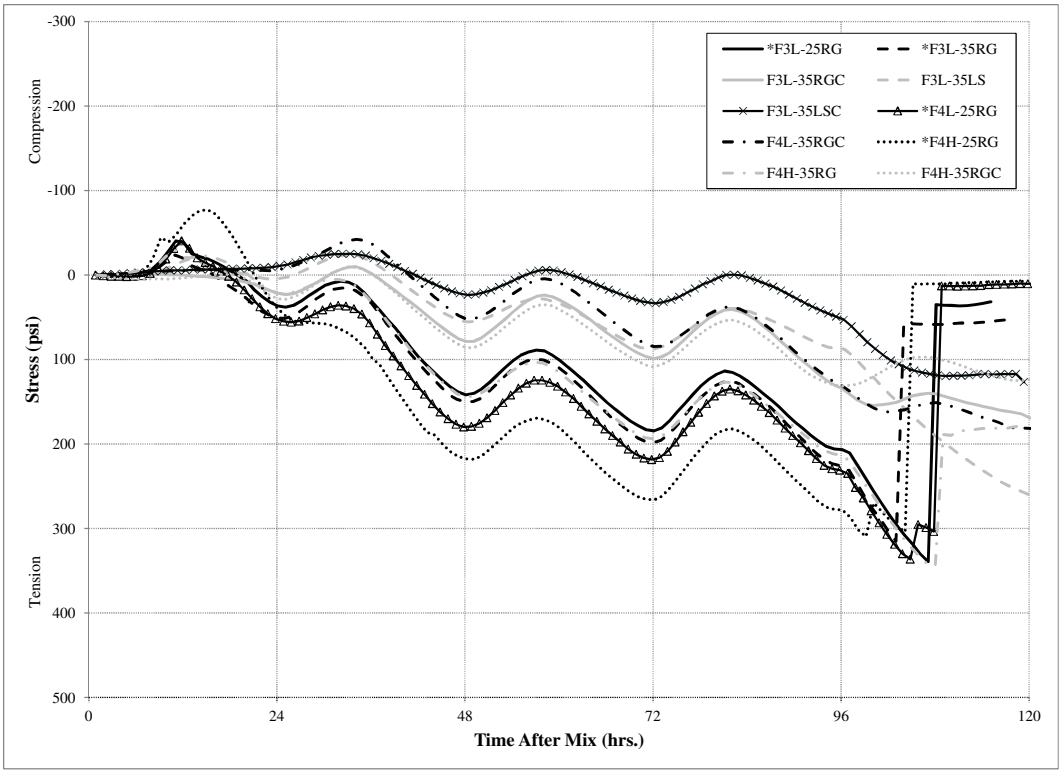

Figure 4-32: Rigid cracking frame stresses- Class C fly ash mixtures.

Table 4-38: Summary of rigid cracking frame results- Class C fly ash mixtures.

Mixture Name	*F3L-25RG	*F3L-35RG	F3L-35RGC	F3L-35LS	F3L-35LSC
Time of Cracking	107.4	103.7	NC	NC	NC
Cracking Stress	341	315	--	--	--
Temperature at Initial Set	87.3	89.0	62.0	87.6	57.4
Cracking Temperature	62.5	69.5	--	--	--
ΔTemp at Cracking	24.7	19.6	--	--	--
Cracking Ratio	0.541	0.562	--	--	--
Reserve	0.207	0.150	--	--	--
ΔTemp at 96hr. Max Stress	5.8	7.1	14.1	5.2	9.5
Max 96hr Stress	207	226	134	88	51
Ratio at 96hr Max	0.334	0.411	0.387	0.205	0.170
Temperature at t_{max}	--	--	43.2	39.5	36.1
ΔTemp at t_{max}	--	--	18.8	48.1	21.3
Stress at t_{max}	--	--	171	279	127
Ratio at t_{max}	--	--	0.447	0.552	0.382

Mixture name	*F4L-25RG	F4L-35RGC	*F4H-25RG	F4H-35RG	F4H-35RGC	Averages
Time of Cracking	108.8	NC	104.3	108.2	NC	5
Cracking Stress	303	--	304	344	--	321
Temperature at Initial Set	89.8	53.2	89.9	93.1	63.5	77
Cracking Temperature	60.0	--	68.1	61.9	--	64
ΔTemp at Cracking	29.8	--	21.8	31.1	--	25
Cracking Ratio	0.530	--	0.548	0.708	--	0.578
Reserve	0.116	--	0.040	0.261	--	0.155
ΔTemp at 96hr. Max Stress	8.3	5.2	8.2	10.9	14.1	9
Max 96hr Stress	231	130	278	213	132	169
Ratio at 96hr Max	0.414	0.365	0.508	0.447	0.368	0.361
Temperature at t_{max}	--	42.6	--	--	50.5	42
ΔTemp at t_{max}	--	10.6	--	--	13.0	22
Stress at t_{max}	--	160	--	--	116	170
Ratio at t_{max}	--	0.399	--	--	0.294	0.415

All stresses are in psi, all temperatures in •F

* Denotes a mixture that was completed under IAC-FA

4.5.3 Class F Fly Ash Mixtures

Figure 4-33 and Table 4-39 show the results of the rigid cracking frame testing for Class F fly ash mixtures. While the table was split between FA-1 and FA-2, the average column at the end of the bottom table is still an average of all Class F fly ash mixtures. The research team included F1H-25RGC only for completeness in this section. The abnormal results from this rigid cracking frame are likely an error with the connection of the strain gauges before the test equipment began recording. F1H-25RGC will be redone

at a future date, and included in the final report for the project. No significant trends were seen in this mixture series.

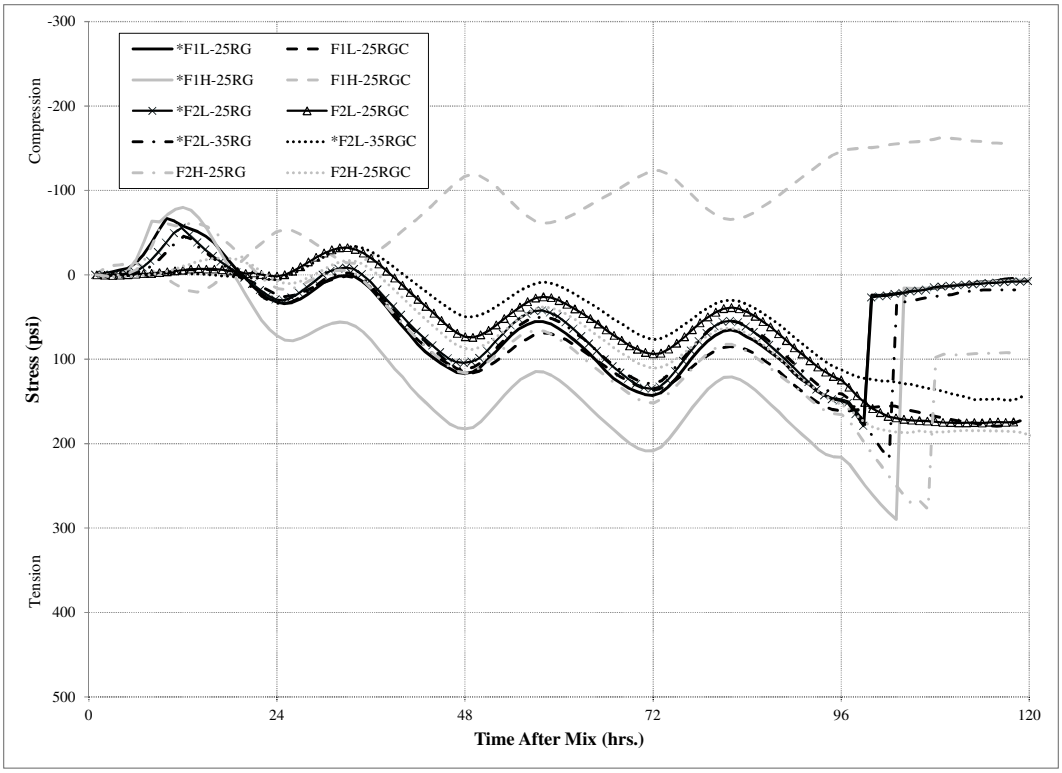

Figure 4-33: Rigid cracking frame stresses- Class F fly ash mixtures.

Table 4-39: Summary of rigid cracking frame results- Class F fly ash mixtures.

Mixture Name	*F2L-25RG	F2L-25RGC	*F2L-35RG	F2L-35RGC	F2H-25RG	F2H-25RGC
Time of Cracking	99.7	NC	102.2	NC	108.0	NC
Cracking Stress	185	--	214	--	274	--
Temperature at Initial Set	81.4	62.5	83.2	58.6	93.6	65.2
Cracking Temperature	76.5	--	71.2	--	61.4	--
ΔTemp at Cracking	4.9	--	12.1	--	32.2	--
Cracking Ratio	0.314	--	0.386	--	0.620	--
Reserve	0.059	--	0.126	--	0.238	--
ΔTemp at 96hr. Max Stress	-0.3	15.8	2.4	12.0	12.2	18.5
Max 96hr Stress	149	125	142	112	166	153
Ratio at 96hr Max	0.255	0.349	0.260	0.401	0.382	0.410
Temperature at t_{max}	--	39.2	--	41.9	--	41.2
ΔTemp at t_{max}	--	23.3	--	16.7	--	24.0
Stress at t_{max}	--	174	--	143	--	192
Ratio at t_{max}	--	0.457	--	0.430	--	0.487

Mixture name	*F1L-25RG	F1L-25RGC	*F1H-25RG	F1H-25RGC	Averages
Time of Cracking	99.1	NC	103.1	NC	5
Cracking Stress	152	--	289	--	223
Temperature at Initial Set	91.4	63.3	87.3	61.6	75
Cracking Temperature	76.6	--	69.9	--	71
ΔTemp at Cracking	14.8	--	17.5	--	16
Cracking Ratio	0.272	--	0.649	--	0.448
Reserve	0.005	--	0.155	--	0.117
ΔTemp at 96hr. Max Stress	10.6	16.0	6.6	14.5	11
Max 96hr Stress	148	162	217	-146	123
Ratio at 96hr Max	0.267	0.404	0.494	-0.351	0.287
Temperature at t_{max}	--	45.7	--	43.9	42
ΔTemp at t_{max}	--	17.6	--	17.7	20
Stress at t_{max}	--	172	--	-155	105
Ratio at t_{max}	--	0.403	--	-0.355	0.285

All stresses are in psi, all temperatures in •F

* Denotes a mixture that was completed under IAC-FA

4.5.4 GGBFS Mixtures

Figure 4-34 and Table 4-40 show the results of the rigid cracking frame testing for Class F fly ash mixtures. As seen in previous mixture series, the limestone coarse aggregate mixtures had considerably lower maximum 96 hours stresses than did their respective river gravel mixtures.

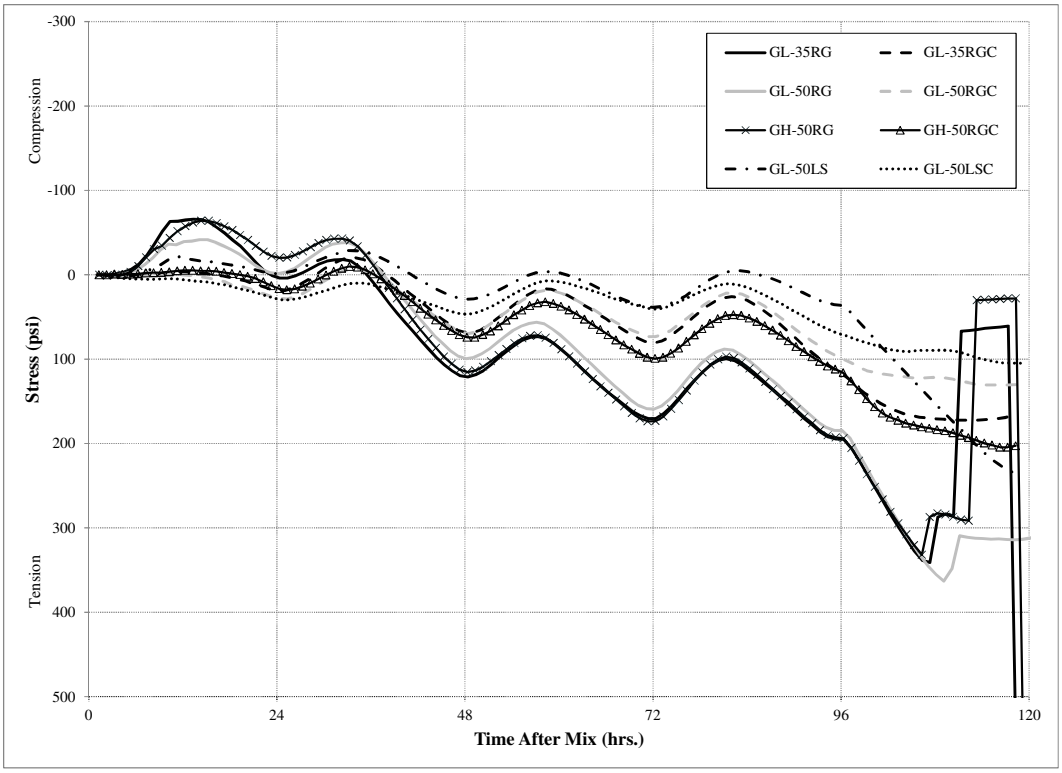

Figure 4-34: Rigid cracking frame stresses- GGBFS mixes.

Table 4-40: Summary of rigid cracking frame results- GGBFS Mixtures.

Mix Name	GL-35RG	GL-35RGC	GL-50RG	GL-50RGC	GH-50RG	GH-50RGC	GL-50LS	GL-50LSC	Averages
Time of Cracking	110.8	NC	110.0	NC	112.8	NC	NC	NC	3
Cracking Stress	284	--	368	--	290	--	--	--	314
Temperature at Initial Set	80.2	63.2	81.2	63.8	79.9	62.9	85.8	62.1	72
Cracking Temperature	57.8	--	59.9	--	56.3	--	--	--	58
ΔTemp at Cracking	22.4	--	21.3	--	23.6	--	--	--	22
Cracking Ratio	0.502	--	0.706	--	0.567	--	--	--	0.592
Reserve	0.151	--	0.344	--	0.181	--	--	--	0.225
ΔTemp at 96hr. Max Stress	-1.7	15.9	-1.5	16.1	-2.4	15.4	1.3	14.5	7
Max 96hr Stress	195	116	185	99	193	114	39	70	126
Ratio at 96hr Max	0.352	0.346	0.362	0.407	0.386	0.369	0.087	0.259	0.321
Temperature at t_{max}	--	40.5	--	43.3	--	30.8	46.2	39.5	40
ΔTemp at t_{max}	--	22.8	--	20.5	--	32.1	39.6	22.6	27
Stress at t_{max}	--	167	--	127	--	201	242	104	168
Ratio at t_{max}	--	0.467	--	0.472	--	0.585	0.460	0.337	0.464

All stresses are in psi, all temperatures in •F

* Denotes a mixture that was tested under IAC-FA

4.5.5 Other Mixtures

Figure 4-35 and Table 4-41 show the results of the rigid cracking frame testing for the Other mixtures. The shrinkage reducing admixture mixtures were shown to have lower stress / strength ratios and lower maximum stresses after 96 hours, most likely due to reduced contributions from chemical shrinkage.

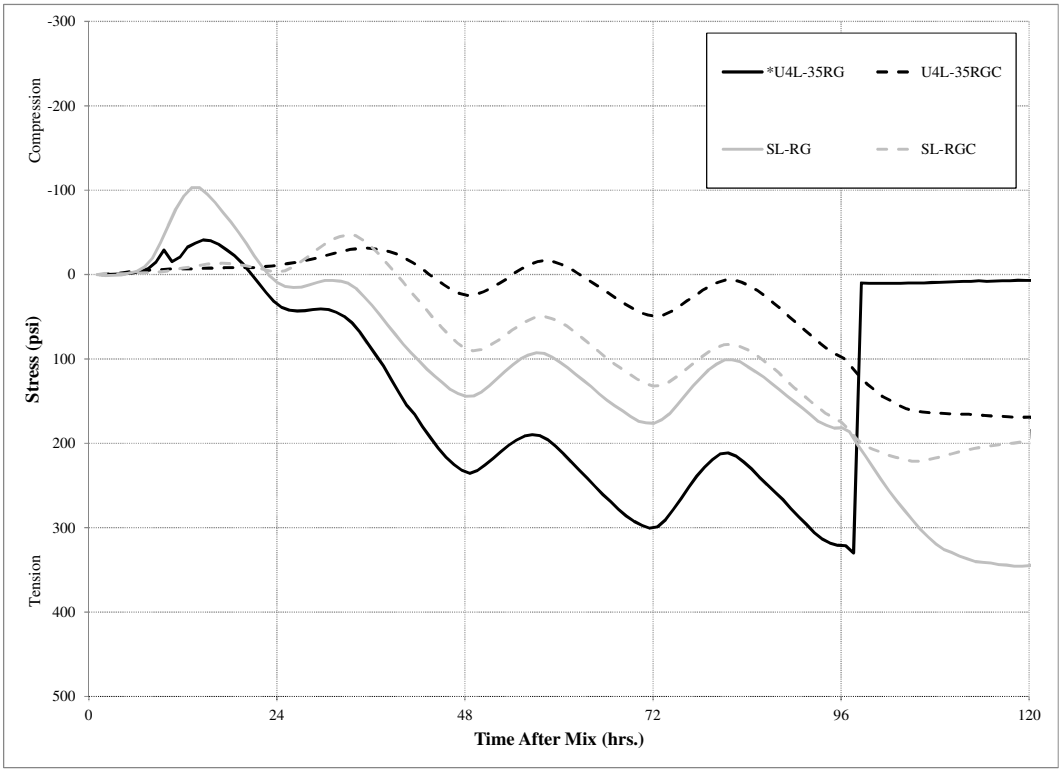

Figure 4-35: Rigid cracking frame stresses- Other mixtures.

Table 4-41: Summary of rigid cracking frame results- Other mixtures.

Mix Name	*U4L-35RG	U4L-35RGC	SL-RG	SL-RGC	Averages
Time of Cracking	98.3	NC	NC	NC	1
Cracking Stress	338	--	--	--	338
Temperature at Initial Set	96.3	50.8	87.3	61.6	74
Cracking Temperature	80.7	--	--	--	81
ΔTemp at Cracking	15.6	--	--	--	16
Cracking Ratio	0.607	--	--	--	0.607
Reserve	0.028	--	--	--	0.028
ΔTemp at 96hr. Max Stress	12.9	2.9	6.1	14.6	9
Max 96hr Stress	321	97	184	175	194
Ratio at 96hr Max	0.579	0.386	0.339	0.346	0.413
Temperature at t_{max}	--	38.6	51.7	43.6	45
ΔTemp at t_{max}	--	12.2	35.6	18.0	22
Stress at t_{max}	--	168	331	196	232
Ratio at t_{max}	--	0.576	0.595	0.367	0.513

All stresses are in psi, all temperatures in •F

* Denotes a mixture that was tested under IAC-FA

4.5.6 Comparison of All Mixture Types

Figure 4-36, Figure 4-37, and Table 4-42 show a comparison of selected rigid cracking results from various mixture types. Table 4-42 was created by taking the average of all the values in a mixture category for the given criteria. Due to the fewer number of mixtures performed within the Other mixtures category, they are only intermittently presented in the following figures, however, the results from the Other mixtures are presented in Table 4-42 for comparison with the other mixture types. Evaluation of these graphs show that, generally, the control mixtures generate the highest early stress peaks, with GGBFS generating the lowest; and control mixtures and shrinkage-reducing admixture mixtures generate the highest 96 hours stresses, with GGBFS and Class F fly ash mixtures producing the lowest maximum 96 hour stresses. It is believed that the shrinkage reducing admixture mixture generated stresses similar to the control mixture due to the lack of autogenous and drying shrinkage. Figure 4-38 through Figure 4-40 further compare aspects of average cracking and maximum 96 hours

stresses, stress / strength ratios, reserve strength ratios, 96 hours maximum stress ratios, and temperatures and temperature differences at cracking. 'D Temp' denotes the difference between the temperature at cracking and that at initial set.

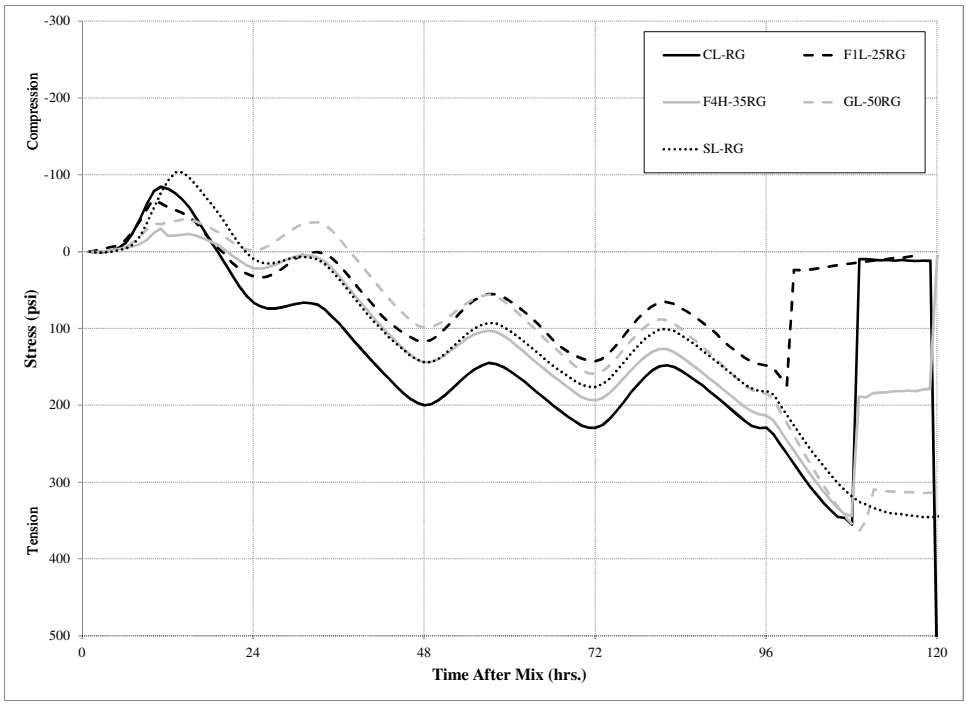

Figure 4-36: Hot weather rigid cracking frame stresses- All mixture types.

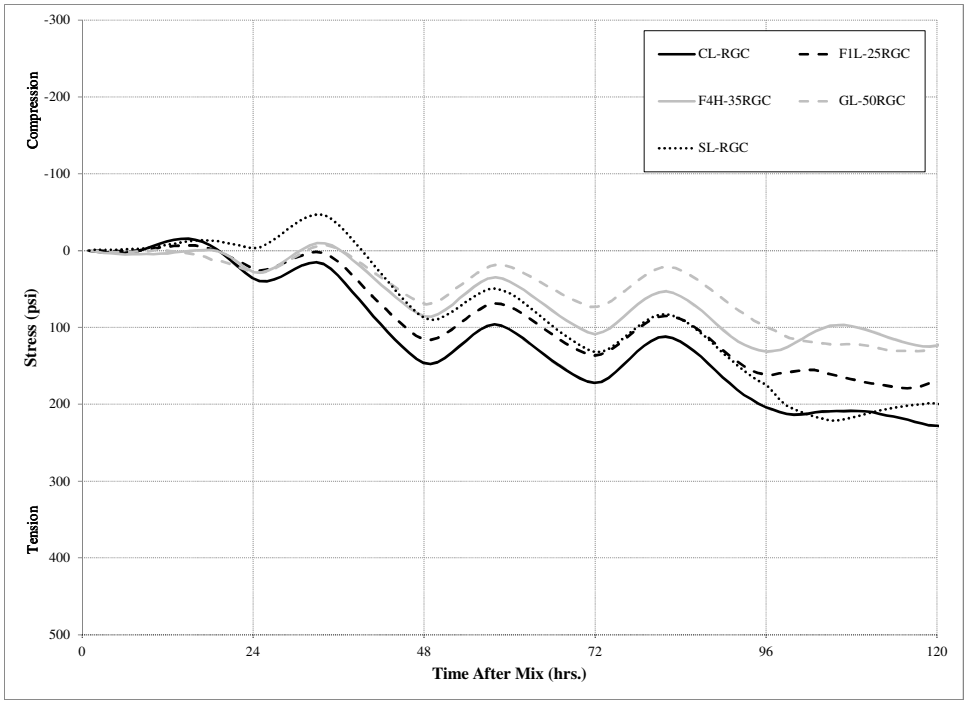

Figure 4-37: Cold weather rigid cracking frame stresses- All mixture types.

Table 4-42: Summary of rigid cracking frame results- All mixture types.

Mixtures	Control Mixtures	Class C Fly Ash	Class F Fly Ash	GGBFS Mixtures	Other Mixtures
Number of Mixes Cracked	2	5	5	4	1
Cracking Stress	344	321	223	260	338
Temperature at Initial Set	70.6	77	75	72	74
Cracking Temperature	63.1	64	71	55	81
ΔTemp at Cracking	17.6	25	16	21	16
Cracking Ratio	0.670	0.578	0.448	0.545	0.607
Reserve	0.205	0.155	0.117	0.168	0.028
ΔTemp at 96hr. Max Stress	6.4	9	11	7	9
Max 96hr Stress	156	169	123	126	194
Ratio at 96hr Max	0.315	0.361	0.287	0.321	0.413
Temperature at t_{max}	40.1	42	42	39	45
ΔTemp at t_{max}	25.4	22	20	29	22
Stress at t_{max}	218	170	105	178	232
Ratio at t_{max}	0.407	0.415	0.285	0.462	0.513

All stresses are in psi, all temperatures in • F

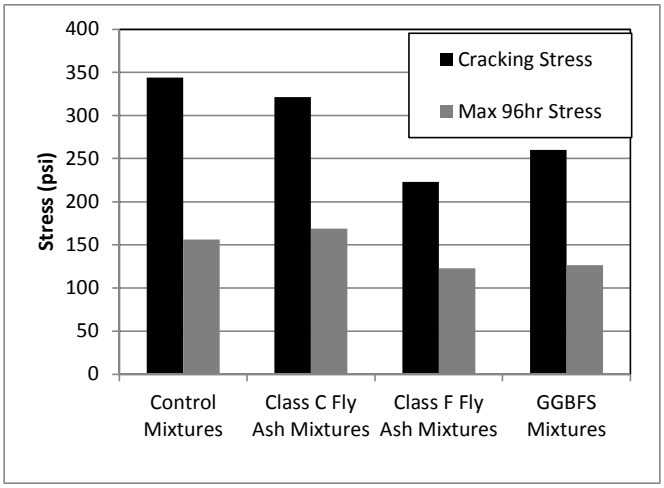

Figure 4-38: Comparison of stresses for mixture types.

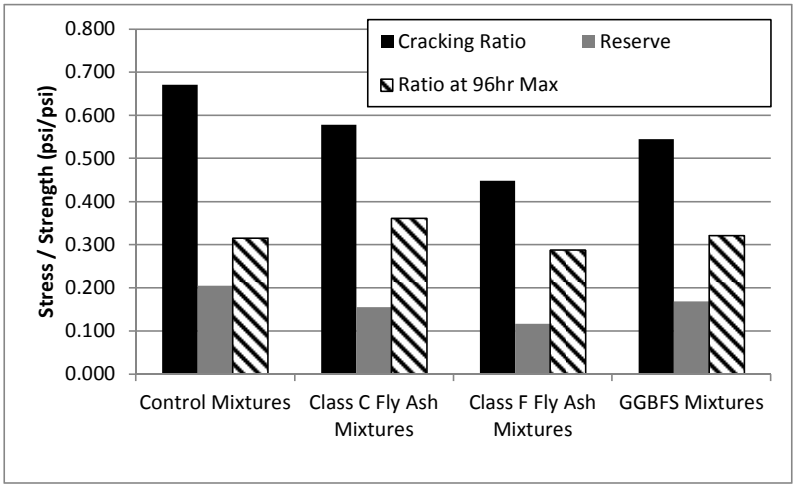

Figure 4-39: Comparison of stress / strength ratios for mixture types.

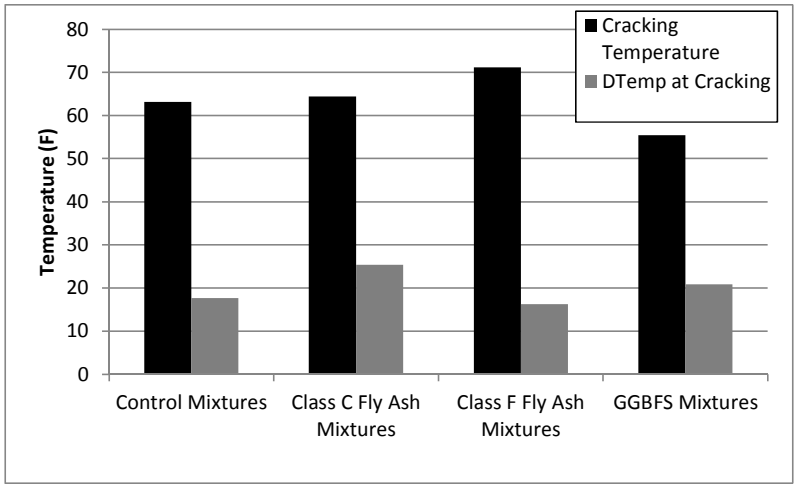

Figure 4-40: Comparison of temperatures for mixture types.

4.6 FREE DEFORMATION UNDER SIMULATED TEMPERATURES

This section presents the results of the free shrinkage frame testing performed under this project. It should be noted that twelve of the thirty-two mixtures performed under TxDOT Project 6332 did not produce satisfactory free shrinkage frame data. This problem was usually caused by one of the LVDTs not measuring throughout the test due to the rod being hung up in the hole in the end plates. This typically resulted in only one of the two LVDTs recording quality data over the course of the test. The research team was able to re-run four of these bad free shrinkage frame mixtures before the completion of this thesis, and those corrected data are what have been presented in this report. The poorly performing mixtures are still presented throughout this report, for completeness, and will be corrected in the final report. To the best of the research team's knowledge, the following mixtures have poor free shrinkage frame data: CL-RGC, F4L-35RGC, F4H-35RGC, GL-35RG, GL-50RG, GH-50RGC, GL-50LSC.

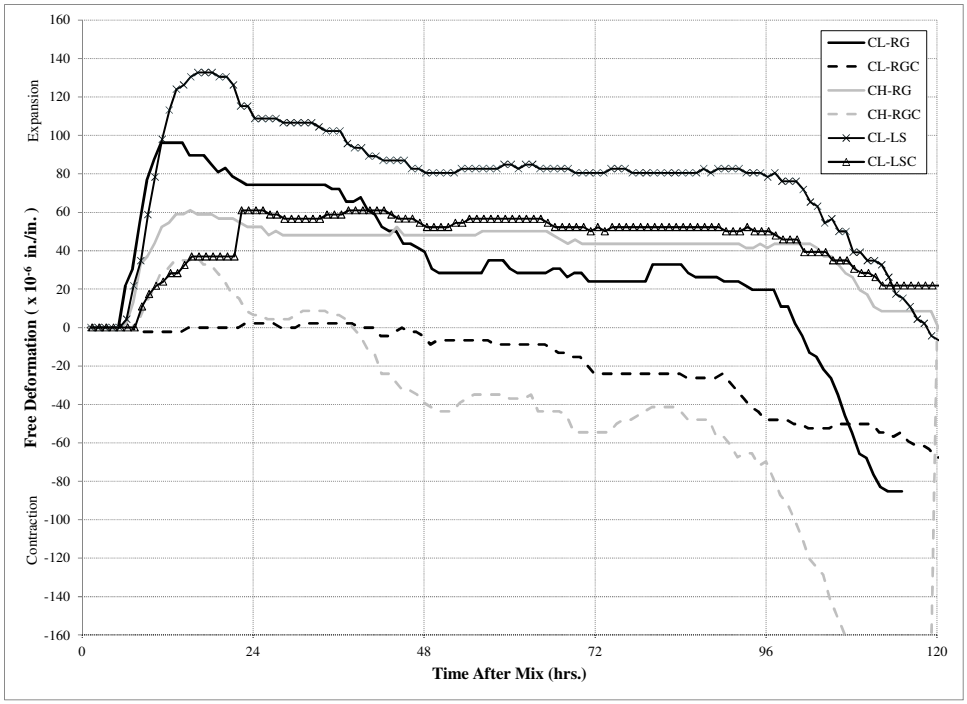

Figure 4-41: Free shrinkage frame strains- Control mixtures.

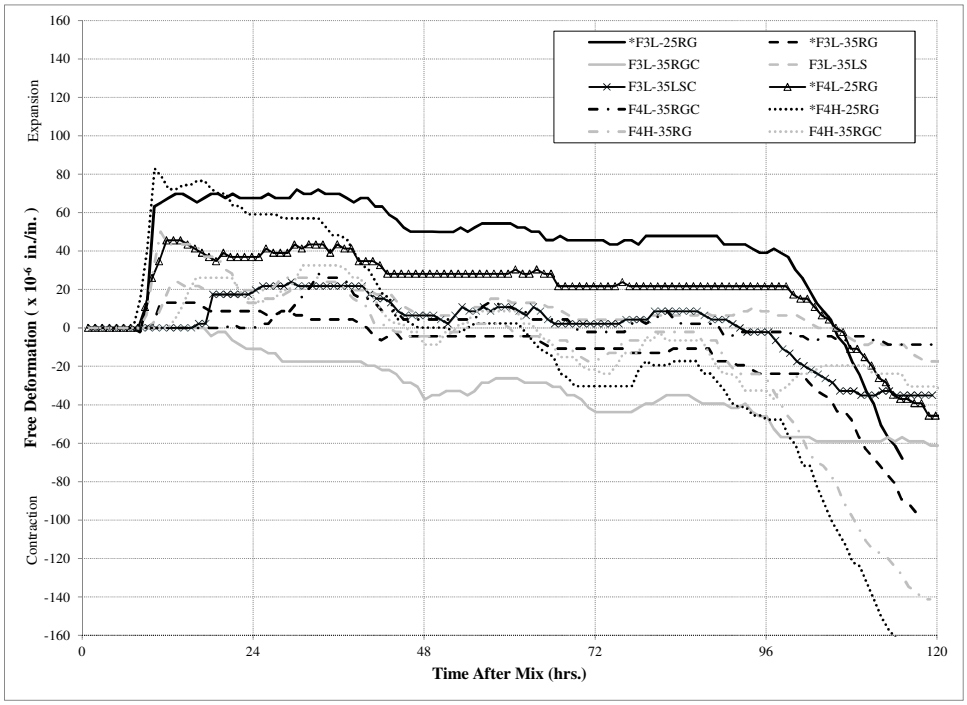

Figure 4-42: Free shrinkage frame strains- Class C fly ash mixtures.

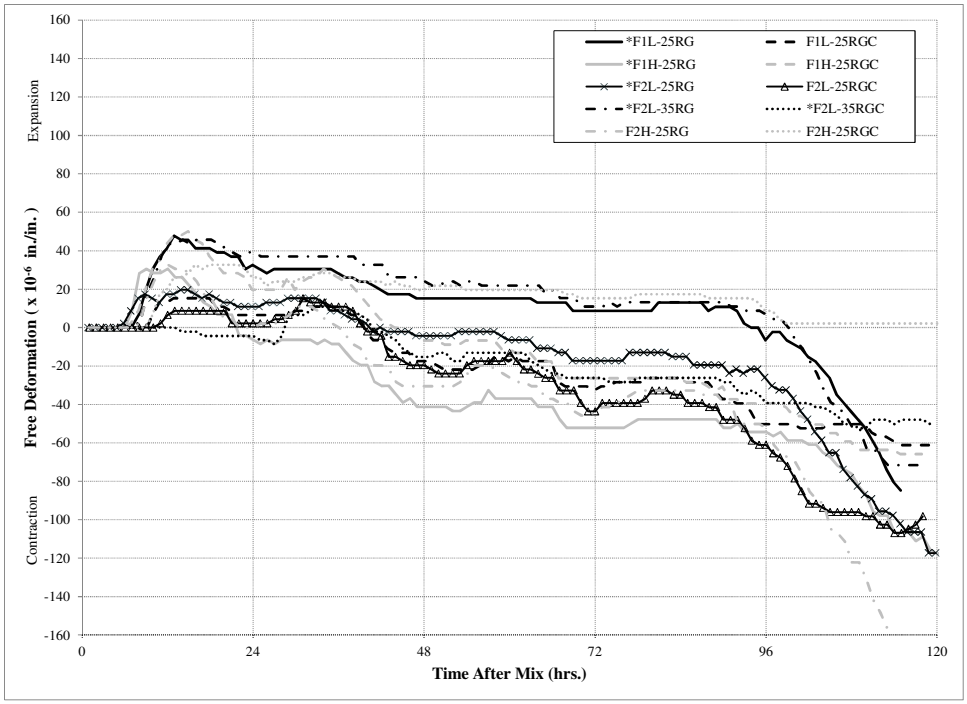

Figure 4-43: Free shrinkage frame strains- Class F fly ash mixtures.

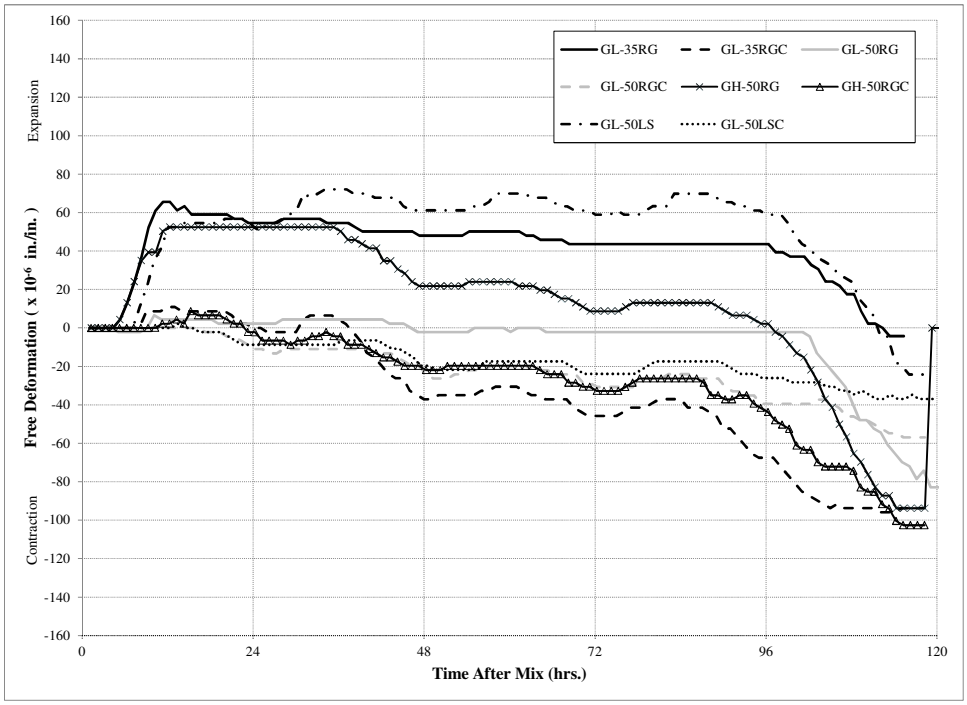

Figure 4-44: Free shrinkage frame strains- GGBFS mixes.

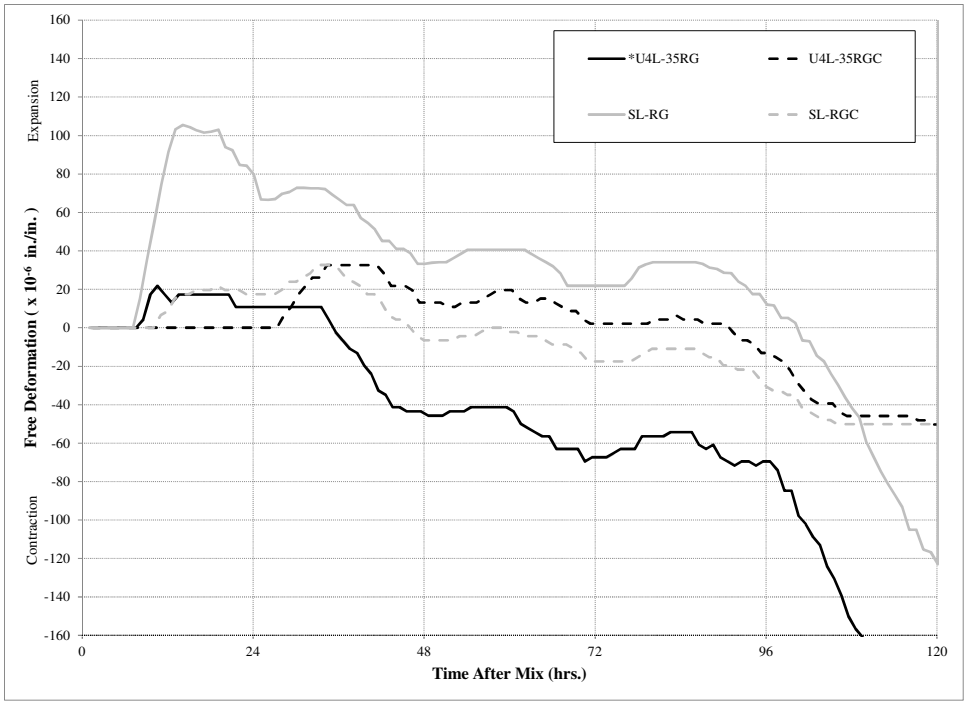

Figure 4-45: Free shrinkage frame strains- Other mixtures.

4.7 RESTRAINED STRESS DEVELOPMENT UNDER ISOTHERMAL CONDITIONS

Figure 4-46 provides the results from the rigid cracking frame for the isothermally cured mixtures. While the shrinkage-reducing admixture appears to lower the stresses in the cracking frame at earlier ages, by the end of the test (10 days), the mixtures appear to have the same level of stress.

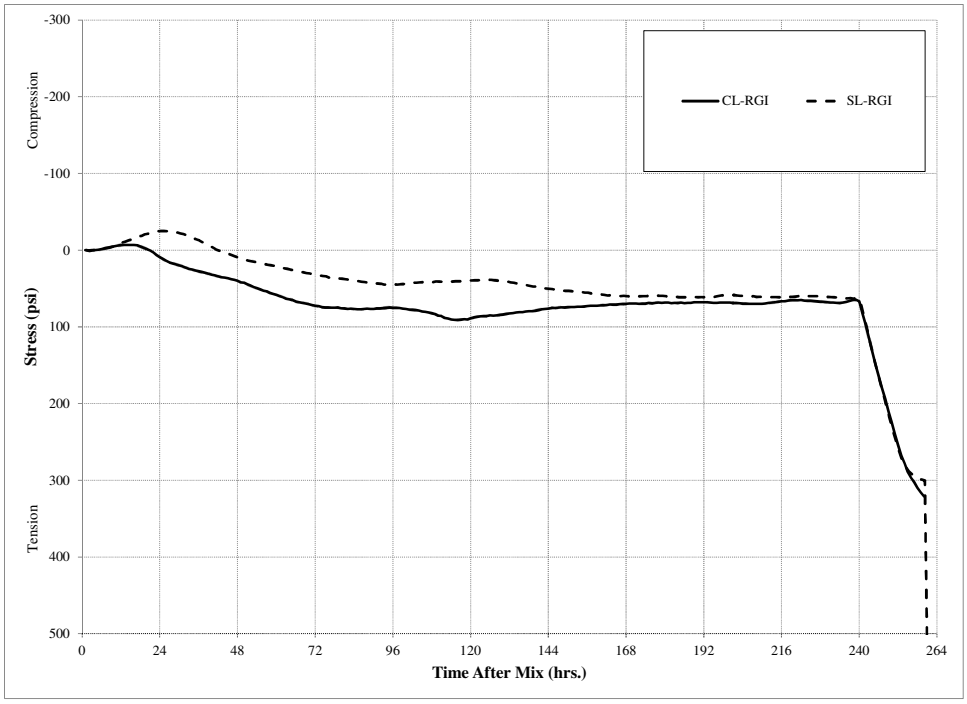

Figure 4-46: Rigid cracking frame stresses- Isothermal mixtures.

4.8 FREE DEFORMATION UNDER ISOTHERMAL CONDITIONS

Figure 4-47 displays the free shrinkage frame results for the isothermally cured mixtures. As is apparent in the graph, the shrinkage reducing admixture was effective in minimizing the shrinkage strains in the concrete. Strains in SL-RGI were approximately zero at the end of the 10-day test.

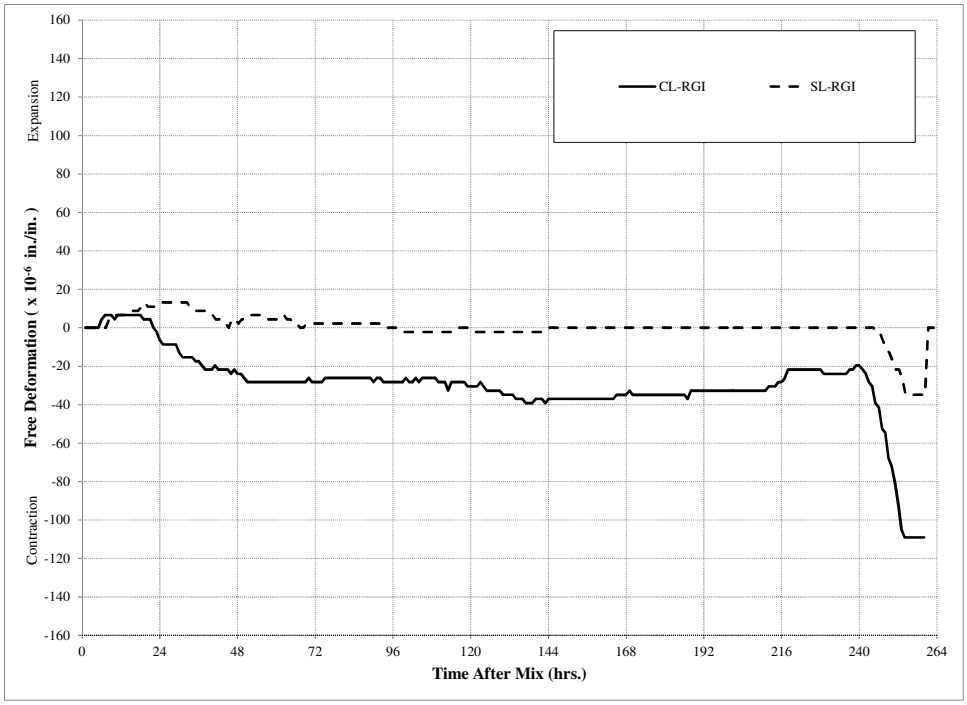

Figure 4-47: Free shrinkage frame strains- Isothermal mixtures.

4.9 SETTING TIMES

Table 4-43 presents the setting times for the concrete mixtures evaluated. The research team, approximately halfway through the TxDOT 6332 test matrix, began instrumenting time of set specimens with iButton temperature data loggers, and for each mixture tested, placed time of set cans in a temperature controlled room, in a room that had a high air temperature, and in the match cured water bath. In Table 4-43, Hot Air Cure specifies that a time of set specimen was left inside a testing room where the ambient air temperature was approximately 90 °F. Hot and Cold Mix Profile are time of set specimens that were kept inside the match cured water bath that matched the temperature of the rigid cracking frame for that mixture under either hot or cold temperature simulation. DS Room Cure specimens were placed inside the same room that was used in evaluating concrete drying shrinkage. The DS Room was kept at 73 °F.

As noted in the table, in the mixtures marked with an asterisk, the time of set data for the Hot Mix Profile was obtained from the hot weather rigid cracking frame test performed under IAC-FA.

The research team, in collaboration with Auburn University, is attempting to use the data collected in Table 4-43, along with the time-temperature history for each of the tests, to generate equivalent age setting times for the different mixture designs. When the equivalent age of initial and final set is found for the mixtures, the degree of hydration at initial and final set may also be determined. The research team, in doing this, hopes to use the data collected under this project, as well as previous TxDOT funded projects, to generate general degrees of hydration that can be associated with initial and final set for any mixture. Previous work by Schindler (2004) and Edson (2007) have shown that this is possible for mixtures with a variety of SCMs, admixtures, and time-temperature histories.

Table 4-43: Setting times of concrete mixtures.

Mixture Name		Hot Air Cure		Hot Mix Profile		Cold Mix Profile		DS Room Cure	
		Initial Set	Final Set	Initial Set	Final Set	Initial Set	Final Set	Initial Set	Final Set
Control Mixtures	CL-RG	--	--	4.6	6.0	6.5	9.1	--	--
	CH-RG	4.7	5.8	4.3	5.5	6.7	9.4	--	--
	CL-LS	--	--	5.0	6.7	7.0	9.9	5.5	7.4
Class C Fly Ash Mixtures	F3L-35RG*	8.1	9.5	7.5	8.8	13.3	16.0	10.1	13.0
	F3L-35LS	--	--	9.1	11.3	14.9	19.2	9.2	11.4
	F4L-35RG	--	--	--	--	20.7	34.7	12.0	14.6
	F4H-35RG	7.1	8.2	7.9	9.7	12.3	14.0	--	--
Class F Fly Ash Mixtures	F1L-25RG*	5.5	7.5	4.9	6.3	8.5	11.5	6.5	8.3
	F1H-25RG*	4.6	5.8	4.6	5.8	6.4	8.4	5.9	7.3
	F2L-25RG*	--	--	5.4	7.0	10.0	13.6	8.0	9.8
	F2L-35RG*	--	--	6.4	7.9	13.6	19.0	9.5	11.7
	F2H-25RG	--	--	5.2	6.5	9.1	11.5	6.6	8.3
GGBFS Mixtures	GL-35RG	--	--	4.5	5.9	8.3	10.8	6.7	8.9
	GL-50RG	--	--	4.7	6.4	10.1	13.0	--	--
	GH-50RG	--	--	4.5	6.1	9.1	11.8	7.0	9.1
	GL-50LS	--	--	5.3	7.0	8.0	11.1	6.1	8.4
Other Mixtures	U4L-35RG*	--	--	7.7	10.0	25.4	31.6	15.5	18.1
	SL-RG	--	--	5.9	7.2	9.0	12.8	6.5	8.6
	OL-RG	--	--	5.0	6.7	--	--	5.0	7.0

* Denotes a mixture whose Hot Profile was a mixture completed under IAC-FA
All values presented are in hours after start of mix.

4.10 EVALUATION OF MODIFIED B3 CREEP MODEL

In collaboration with Auburn University, a modified version of the B3 model developed by Byard (2011) has been evaluated against the results of the rigid cracking frame testing conducted under TxDOT 6332. The modified B3 model aims to better capture the early-age behavior of the concrete by modifying the ageing viscoelastic term and the elastic modulus to obtain a closer approximation of early-age concrete behavior. The modification to the q_2 term is seen in Eq. 4-32, with the addition of the term including q_5. q_5 is intended to be an equivalent age 'modified set time' at which the concrete begins to gain strength.

$$q_2 = \left[86.814 * 10^{-6} * c^{0.5} * {f_{cm}}^{-0.9}\right] * \frac{t_o}{t_o - q_5}$$

Eq. 4-32

While Bazant recommended the use of the 28-day elastic modulus in the calculation of q_1, it is well known that the modulus of elasticity rapidly increases at early ages. The use of a hyperbolic modulus curve captures this early-age change. In the hyperbolic modulus curve, S_u, k_T, and t_0 are curve fit to match values from cylinder testing. The modified B3 model further adjusts the early-age modulus to better characterize the instantaneous strain at early ages. In Eq. 4-34, t_e and q_6 are in units of equivalent age days.

$$Hyperbolic\ Modulus = S_u * k_T * \frac{t - t_0}{(1 + k_T * [t - t_0])}$$

Eq. 4-33

$$Modified\ Modulus = \left[S_u * k_T * \frac{t - t_0}{(1 + k_T * [t - t_0])}\right] * \frac{t_e - q_6}{t_e}$$

Eq. 4-34

In evaluating this creep model against the mixtures tested under TxDOT 6332, the research team evaluated the R^2 of the models prediction against a default 0.2 for both q_5 and q_6. The values of q5 and q6 were then curve fit to maximize the R^2 value for that specific mixture using Excel Solver. For each set of mixtures evaluated, only the mixtures that provide R^2 values greater than 70% will be used in the final model to be implemented into ConcreteWorks. Mixtures that perform below this standard will be highlighted in the following tables. As discussed previously, some of the free shrinkage frame tests failed to record desirably. While these mixes were included in the following tables for completeness, only the mixtures that are NOT highlighted will be used in averaging R^2 values and q_5 and q_6 terms. Mixtures with '—' did not have the required data analysis done in time for this report, but will be included in the final report.

Table 4-44: Modified B3 model performance- Control mixtures.

Mixture	Original Terms R^2	New Terms R^2	New q_5	New q_6
CL-RG	0.741	0.880	0.334	0.200
CL-RGC	0.659	0.537	1.052	0.127
CL-RGI	0.959	0.966	0.003	0.134
CH-RG	0.355	0.463	0.287	0.200
CH-RGC	0.961	0.964	0.939	0.156
CL-LS	0.702	0.818	0.294	0.001
CL-LSC	-0.686	0.500	0.513	0.001
Average	0.841	0.907	0.393	0.123

*Denotes a mixture that was completed under IAC-FA

Table 4-45: Modified B3 model performance- Class C fly ash mixtures.

Mixture	Original Terms R^2	New Terms R^2	New q_5	New q_6
*F3L-25RG	-0.439	0.714	0.925	0.146
*F3L-35RG	0.387	0.402	0.001	0.001
F3L-35RGC	0.927	0.928	0.138	0.144
F3L-35LS	0.604	0.784	0.672	0.201
F3L-35LSC	0.806	0.876	0.404	0.145
*F4L-25RG	0.118	0.817	1.332	0.202
F4L-35RGC	0.608	0.622	0.272	0.200
*F4H-25RG	0.193	0.828	0.864	0.182
F4H-35RG	0.751	0.883	0.692	0.202
F4H-35RGC	0.847	0.944	0.593	0.086
Average	0.476	0.847	0.703	0.163

*Denotes a mixture that was completed under IAC-FA

Table 4-46: Modified B3 model performance- Class F fly ash mixtures.

Mixture	Original Terms R^2	New Terms R^2	New q_5	New q_6
*F1L-25RG	0.202	0.736	0.696	0.199
F1L-25RGC	0.908	0.981	0.001	0.452
*F1H-25RG	0.593	0.632	0.331	0.200
F1H-25RGC	-1.324	-1.041	0.001	0.136
*F2L-25RG	0.410	0.742	1.031	0.198
F2L-25RGC	0.898	0.940	0.504	0.177
*F2L-35RG	-0.222	0.779	0.974	0.199
F2L-35RGC	0.927	0.933	0.368	0.149
F2H-25RG	0.955	0.974	0.001	0.001
F2H-25RGC	0.423	0.823	0.748	0.219
Average	0.563	0.864	0.540	0.199

*Denotes a mixture that was completed under IAC-FA

Table 4-47: Modified B3 model performance- GGBFS mixtures.

Mixture	Original Terms R^2	New Terms R^2	New q_5	New q_6
GL-35RG	0.490	0.632	0.287	0.200
GL-35RGC	0.723	0.864	0.497	0.174
GL-50RG	0.546	0.862	0.001	0.414
GL-50RGC	0.911	0.919	0.056	0.216
GH-50RG	0.847	0.873	0.284	0.200
GH-50RGC	0.952	0.968	0.001	0.001
GL-50LS	-3.587	0.293	0.458	0.160
GL-50LSC	0.813	0.826	0.104	0.437
Average	0.799	0.885	0.157	0.240

*Denotes a mixture that was completed under IAC-FA

Table 4-48: Modified B3 model performance- Other mixtures.

Mixture	Original Terms R^2	New Terms R^2	New q_5	New q_6
*U4L-35RG	0.437	0.446	0.276	0.001
U4L-35RGC	0.559	0.778	0.570	0.110
SL-RG	0.802	0.902	0.397	0.203
SL-RGC	0.883	0.907	0.650	0.200
SL-RGI	0.783	0.791	0.216	0.001
OL-RG	--	--	--	--
OL10-RG	--	--	--	--
Average	0.757	0.845	0.458	0.129

*Denotes a mixture that was completed under IAC-FA

A relatively good fit was found for the majority of the mixtures that were evaluated against this model. The mixtures that were found to not have a good fit typically had poor free shrinkage frame data, a key input in the modified B3 model. While a good fit is shown for the mixes under TxDOT 6332, the model is still undergoing changes at Auburn University. The research team will continue collaboration with Auburn University, and will present the final results of the modified B3 model's performance against the measured rigid cracking frame stresses. The final version of the modified B3 model will be published as a PhD thesis at a later date.

Chapter 5: Field Testing Program

Chapter 5 covers the four bridge decks that the research team instrumented. At each pour, multiple temperature sensors were placed in the concrete, semi-adiabatic testing was conducted on the field concrete, and mechanical testing specimens were collected. After the pours were completed, the research team evaluated the performance of their testing procedures, and made adjustments to ensure better data collection in the future.

5.1 SAN ANTONIO BRIDGE DECK

The first bridge deck that the research team instrumented was in San Antonio, Texas, at Ingram Road and Interstate 410. The bridge deck consisted of 8" of cast-in-place concrete on metal pan formwork, supported by steel beams. The pour began on July 19, 2009 at 9:40PM, and ended on July 20, 2009 at 1:40 AM. Information gained from this field instrumentation included temperature data from July 19th to July 31st, two sets of semi-adiabatic calorimetry data, and mechanical testing results.

5.1.1 Structural Plans for San Antonio Bridge Deck

The San Antonio bridge deck was an 8" cast-in-place concrete bridge deck, formed with steel pans, and supported by steel beams. A typical cross section and the elevation of the bridge deck are presented in Figure 5-48 and Figure 5-49. Additional structural plans, specifically those that detail the span lengths and widths can be found in Appendix B.

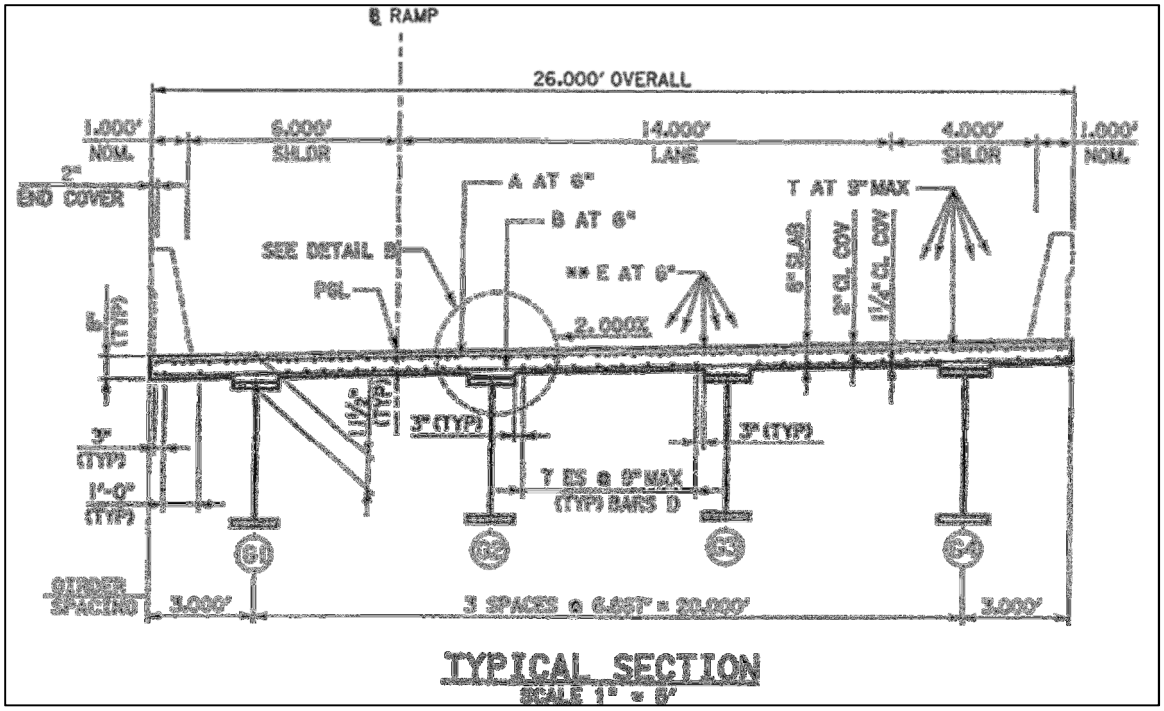

Figure 5-48: San Antonio bridge deck typical section.

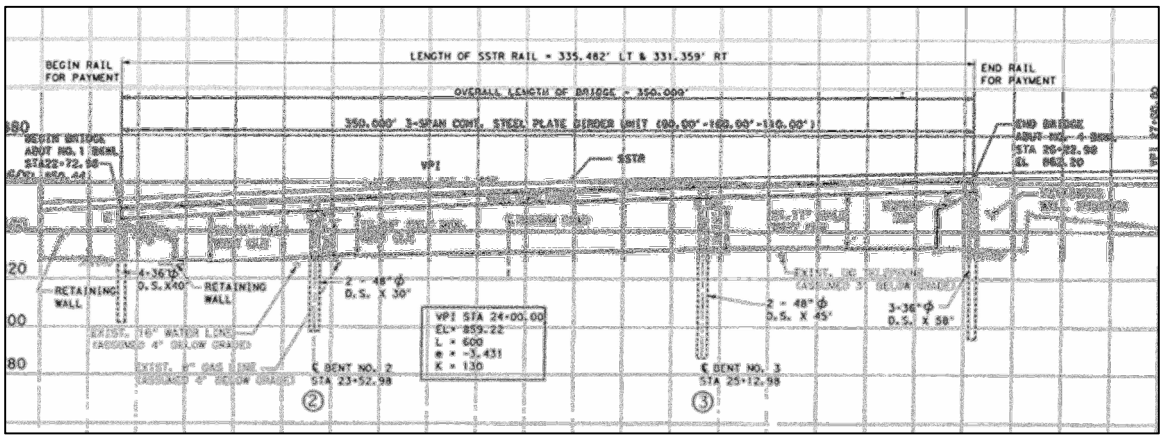

Figure 5-49: Elevation of San Antonio bridge deck.

5.1.2 Materials and Mixture Design of San Antonio Bridge Deck

The mixture design for the San Antonio bridge deck is presented in Table 5-49. The mixture designs were acquired from the batch tickets that were collected throughout the pour. Information was not collected on the cement or fly ash type. The San Antonio

bridge deck pour used approximately 1" maximum-size-aggregate (MSA) limestone. Information from the batch ticket indicates that this was most likely a TxDOT Gr. 4 coarse aggregate. River sand was used as the fine aggregate.

Table 5-49: Mixture design for San Antonio bridge deck.

	Cement lb/yd^3	Fly Ash lb/yd^3	Water lb/yd^3	Ice lb/yd^3	Coarse lb/yd^3	Fine lb/yd^3	WR2 oz/yd^3
First Truck	489	122	188	80	1822	1330	23
Mid Mix	489	122	188	100	1822	1330	19
End of Mix	489	122	188	100	1822	1330	15

5.1.3 Instrumentation and Testing of San Antonio Bridge Deck

The layout of the iButton instrumentation is provided in Figure 5-50 and Figure 5-51. Strands A and D were used to evaluate the difference in temperature development at the beginning of the pour with that at the end of the pour. Strands B and C had buttons strings that were located in the middle of width of the deck, on the deck overhang, and over the girders on the bridge deck. Further information on the iButton locations and depths can be found in Appendix B.

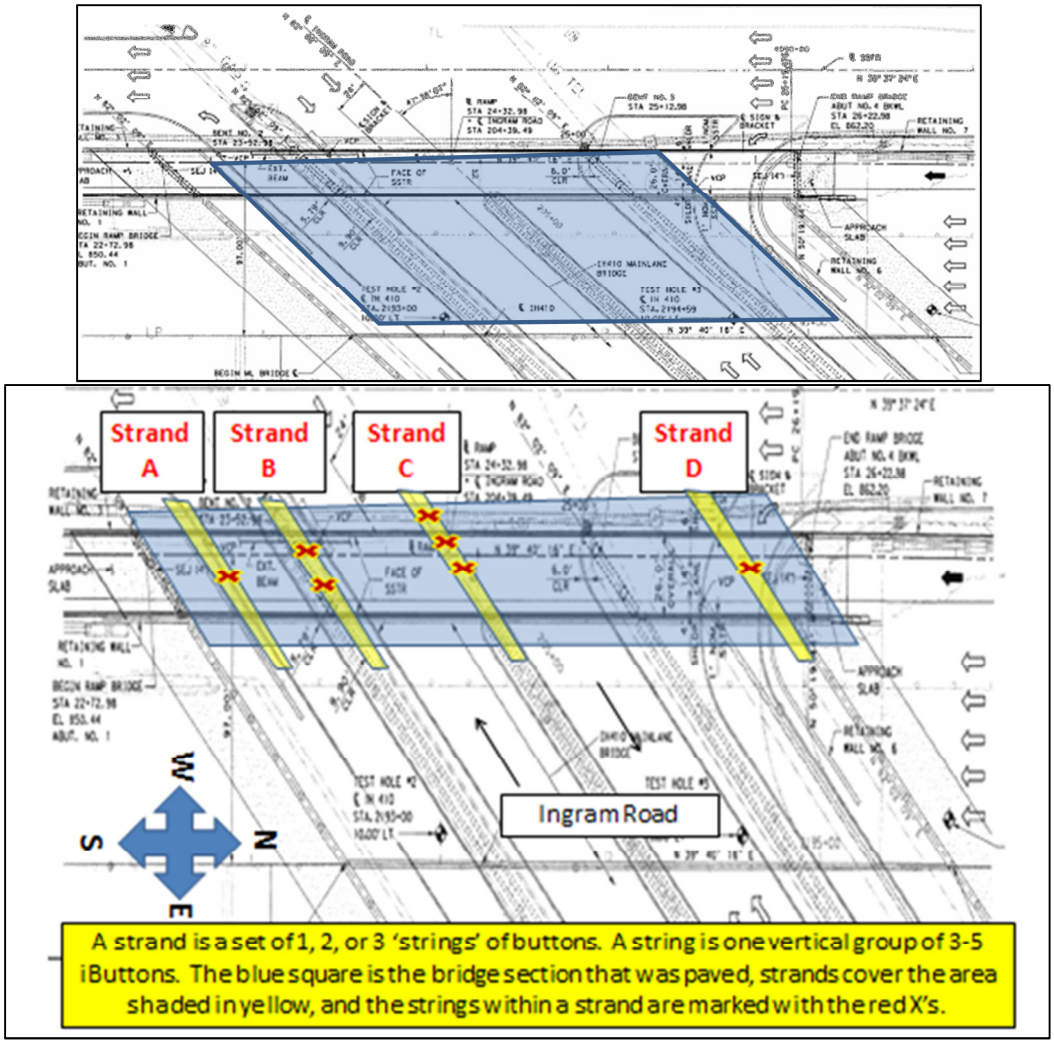

Figure 5-50: iButton string layout for San Antonio bridge deck.

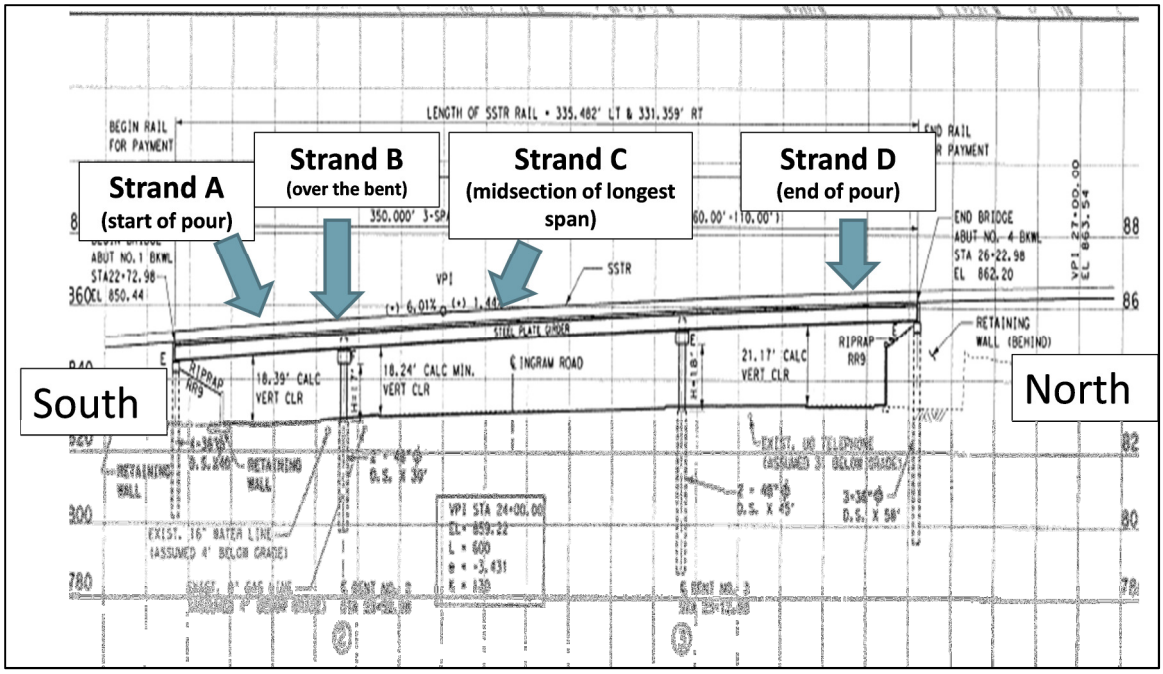

Figure 5-51: iButton strand layout for San Antonio bridge deck.

The San Antonio bridge deck provided the research team with their first experience at instrumentation using iButtons embedded in concrete for extended periods of time. To ensure that the iButtons would not be corrupted, they had to be sealed before they could be embedded in concrete. This was accomplished by covering the iButtons in a two-part epoxy before they were attached with plastic ties to the plastic rod. In addition, to reduce the number of wires that would be required to collect data from the iButtons, a single two-conductor wire was soldered to each iButton, connecting all the iButtons on a given string. The wires were then run transversely across the deck, and labeled for later data collection. A typical four-button iButton string for the San Antonio bridge deck is shown in Figure 5-52.

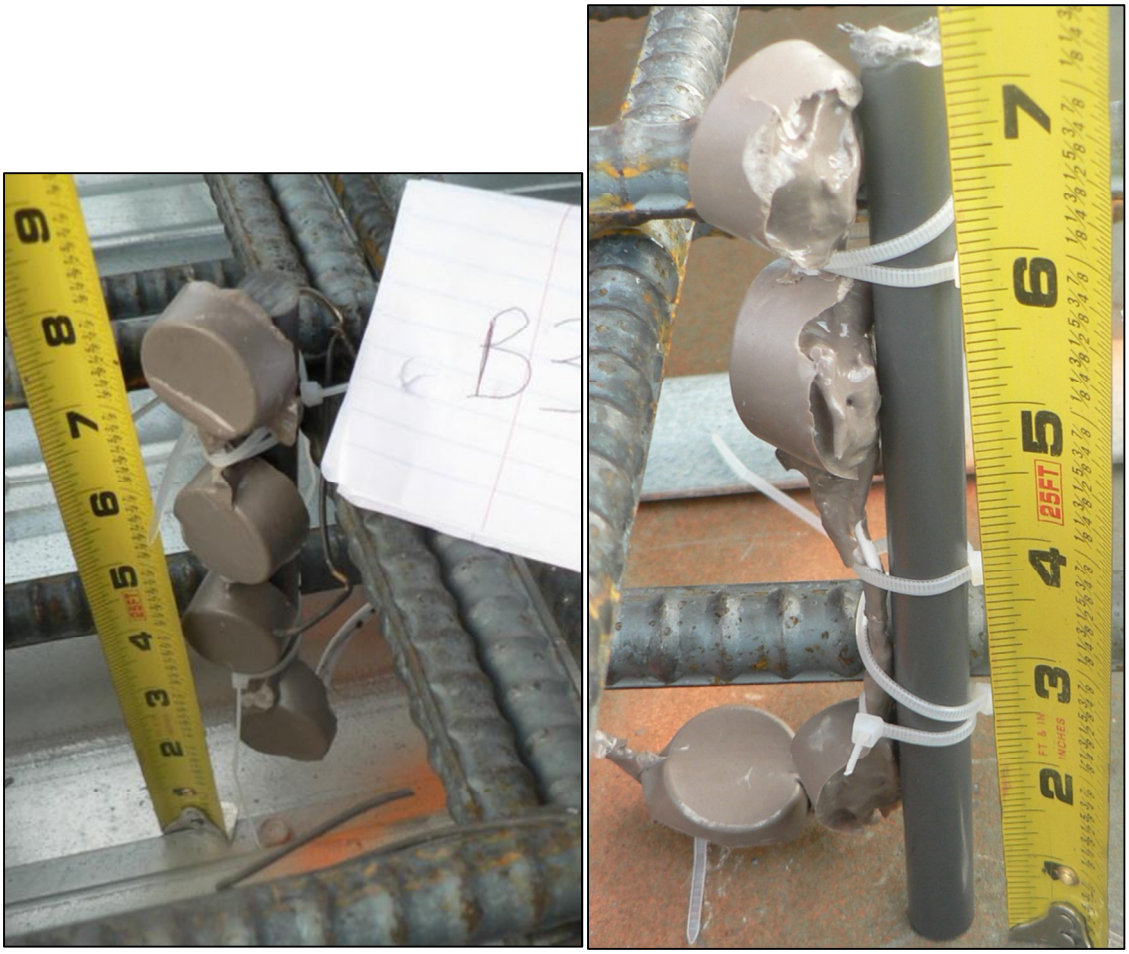

Figure 5-52: iButton strings for San Antonio bridge deck.

Approximately 12 hours after the pour began, the research team returned to the bridge deck for the first set of data collection. At this point, the iButtons were reset to have a longer time interval between measurements, and the buttons were left to continue recording. It was noted at this point that the curing method that was in place was black plastic sheeting directly on top of the concrete, as shown in Figure 5-53. In later discussions, TxDOT reported that the practice of using black plastic was no longer allowed, but that due to the early date at which the construction contract was granted, the construction firm was not forbidden from using black plastic. The use of black plastic

during the summer, combined with the placement time of the concrete, led to substantially high temperatures in the first temperature peak. This can be seen further in the temperature data in Chapter 6.

Figure 5-53: Curing method for San Antonio bridge deck.

Two more trips were made to the bridge deck to collect data at later dates. On the last data collection trip, the research team inspected the bridge deck to see if any early-age cracking could be found. While some 'crack-like' lines were found at regularly spaced intervals running transversely across the bridge deck between tining grooves, shown in Figure 5-54 , it could not be concluded that they were in fact early-age cracking. The research team reasoned that these 'cracks' were more likely an effect of twisted or broken tine on the tining rake.

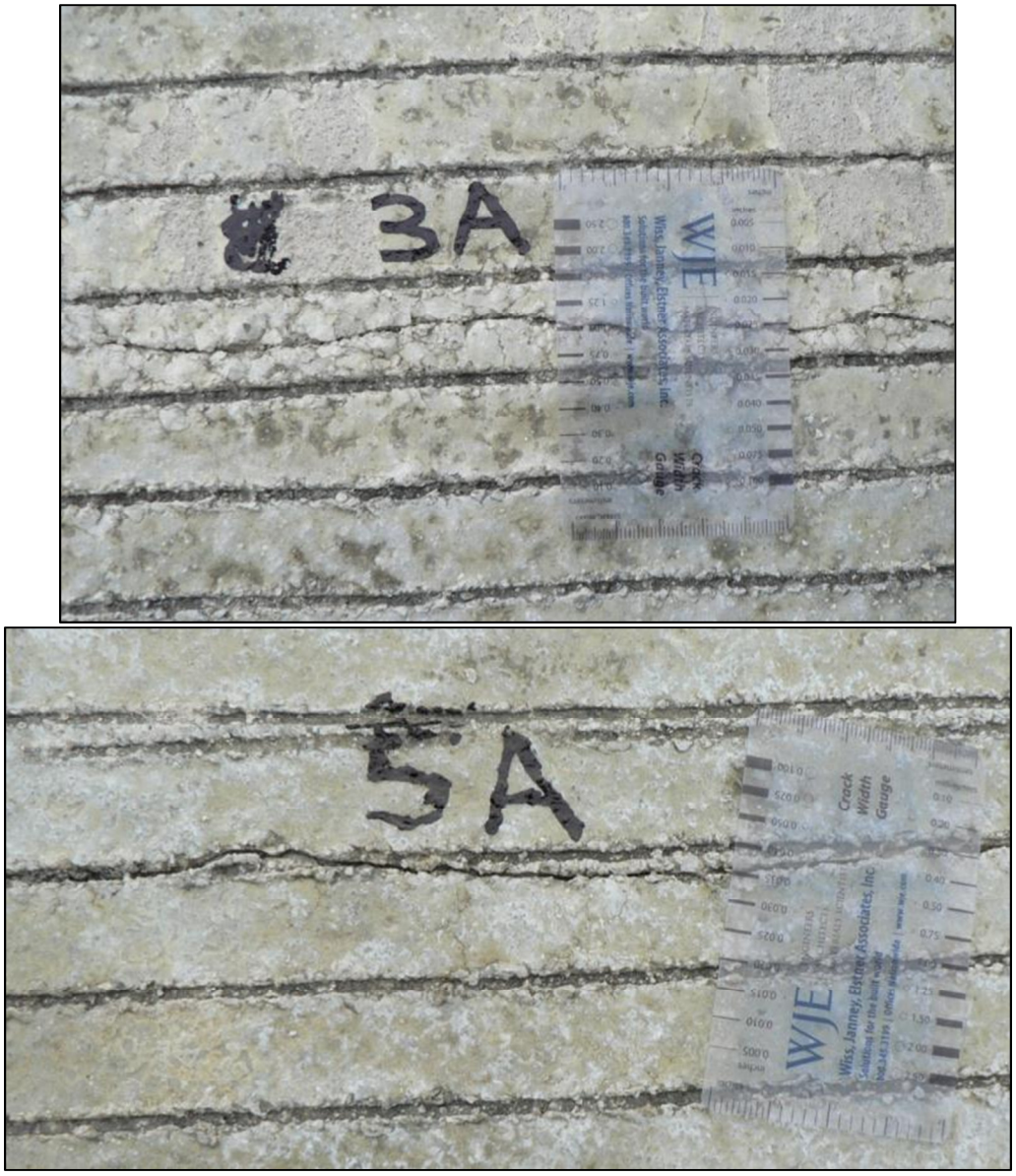

Figure 5-54: Crack-like lines on San Antonio bridge deck.

5.2 GEORGETOWN BRIDGE DECK : SUMMER POUR

The research team's second bridge deck instrumentation was located in Georgetown, Texas, at College Street over the San Gabriel River. The bridge deck consisted of 4" cast-in-place concrete on top of 4" precast, prestressed concrete panels,

supported by precast, prestressed concrete girders. The pour began on August 19, 2009 at 4:00 AM, and concluded at approximately August 19th at 7:00 AM. Information gathered from this instrumentation included temperature data from August 19th to either August 25th or September 2nd, depending on when the contractor cut the iButton collection lines, two sets of semi-adiabatic calorimetry data, and mechanical testing results.

5.2.1 Structural Plans for Georgetown Bridge Deck

The Georgetown bridge deck was a 4" cast-in-place concrete bridge deck, with 4" precast, prestressed concrete panels supported by precast, prestressed concrete girders. A typical cross section and the elevation of the bridge deck can be seen in Figure 5-55 and Figure 5-56. Additional structural plans, specifically those that detail the span lengths and widths can be found in Appendix B.

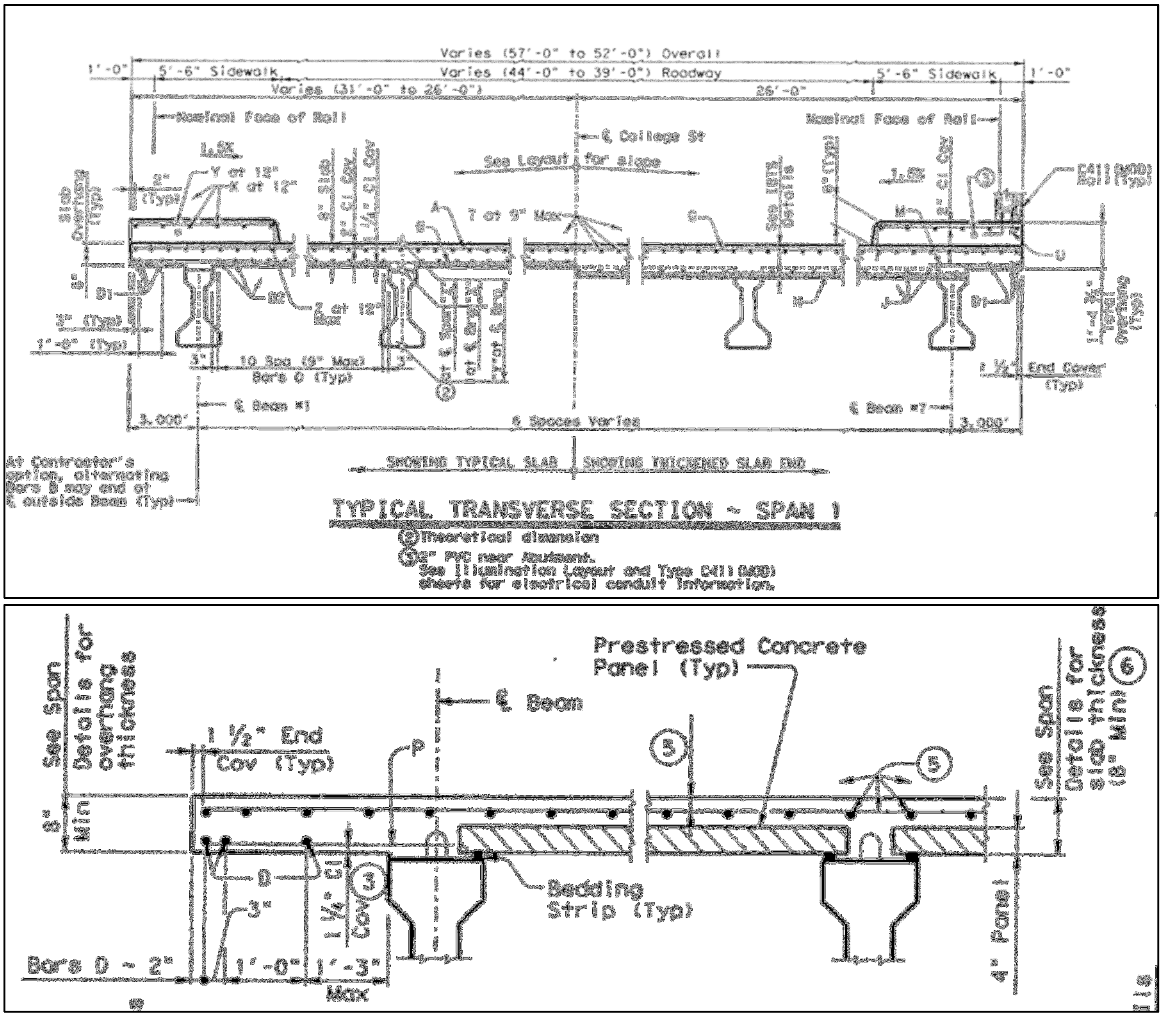

Figure 5-55: Cross section of Georgetown bridge deck: Summer Pour.

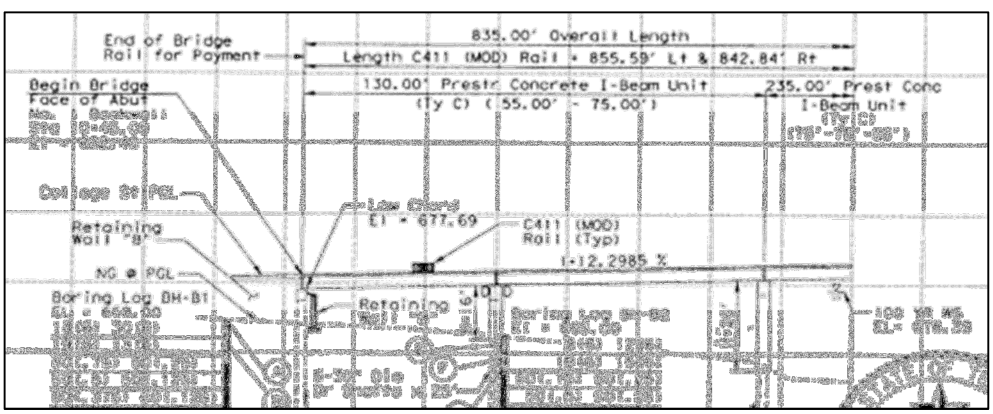

Figure 5-56: Elevation of Georgetown bridge deck: Summer Pour

5.2.2 Materials and Mixture Design of Georgetown Bridge Deck

The mixture design, acquired from the batching tickets, for the Georgetown bridge deck summer pour is shown in Table 5-50. A low-alkali cement, ASTM C 618 Class C fly ash, approximately 1" MSA limestone coarse aggregate, and river sand were used for this mixture design. The research team also noted that approximately halfway through the pour, the use of 70 lb/yd^3 of ice was used (replacing mixture water). It is unknown whether the ice was used at the beginning of the pour as well, or only during the second half. In Table 5-50, only one mixture design is shown, as there were no changes made to the mixture design throughout the pour.

Table 5-50: Mixture design for Georgetown bridge deck summer pour.

Cement lb/yd^3	Fly Ash lb/yd^3	Water lb/yd^3	Coarse lb/yd^3	Fine lb/yd^3	AE oz/yd^3	WR3 oz/yd^3
430	143	257	1758	1267	2.2	22

5.2.3 Instrumentation and Testing of Georgetown Bridge Deck

The layout of the iButton instrumentation is provided in Figure 5-57 and Figure 5-58. Once again, Strands A and D were used to capture changes between the first trucks to arrive to the site, and the last trucks to arrive. Strand B was used to capture temperature data on the middle and East side of the bridge deck, and Strand C was used to capture data on the middle and West side of the bridge deck. In order to better understand the heat transfer between the bridge deck and the underside of the bridge deck, the research team decided to place iButtons underneath the precast panels, and at the middle of the precast panel. iButtons were placed in the middle of the panel by drilling a hole at a 45° into the precast panel, placing the iButton in the middle, then epoxying the hole shut. Both Strand B and C had iButtons located under the bridge deck panels, inside the bridge deck panels, above the panels, above the girders, and above the

falsework on the edge of the deck. Further information on the iButton locations and depths can be found in Appendix B.

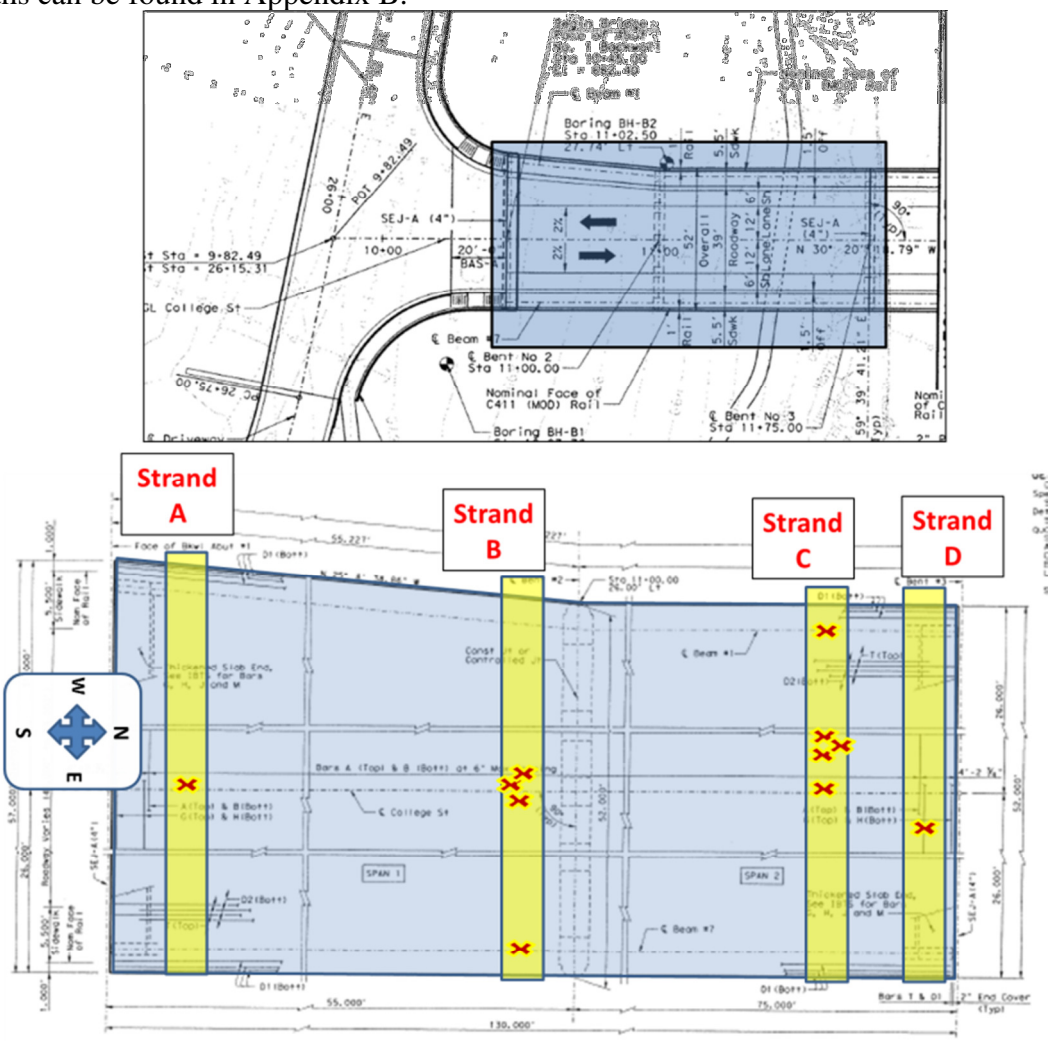

Figure 5-57: iButton string layout for Georgetown bridge deck summer pour.

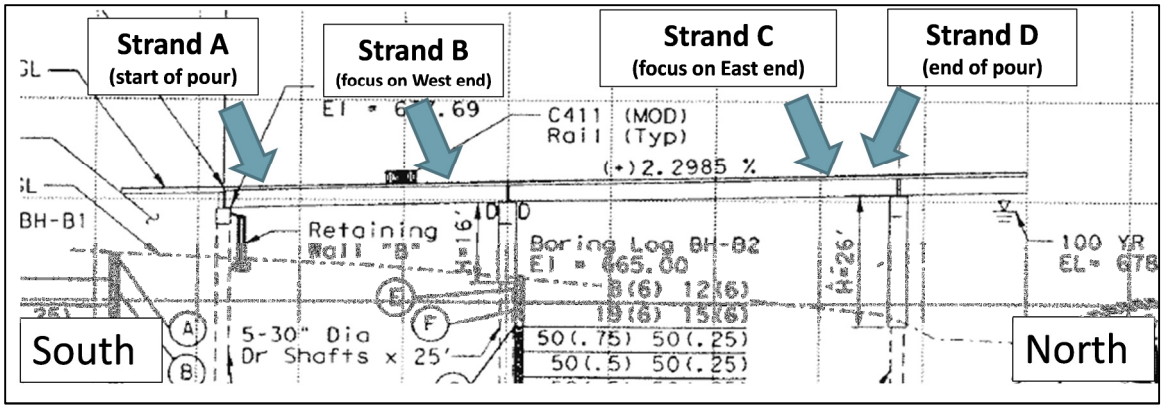

Figure 5-58: iButton strand layout for Georgetown bridge deck summer pour.

On the Georgetown bridge deck summer pour, the research team made some slight modifications to their iButton preparation procedures. As before, a single two-conductor wire was soldered to a string of iButtons, allowing multiple iButtons to be read from one string. A hollow plastic rod had a space cut into it, and then the iButtons were placed into the rod, and held in place with a plastic tie. Two part epoxy was then used to waterproof and protect the iButtons, and to seal the hole at the top of the plastic rod. Rather than floating the iButton plastic rod in the reinforcement cage, as was done in San Antonio, a ¾" hole was drilled into the precast panels, and the bottom of the plastic rod was epoxied into this hole. This method was to prevent the iButton string from twisting out of a vertical orientation, and to provide a more accurate knowledge of the depth of the iButtons after concrete was placed around them. The wires for the iButtons were run transversely across the deck, and over the top of the side formwork. iButton strings from the Georgetown bridge deck summer pour are shown in Figure 5-59.

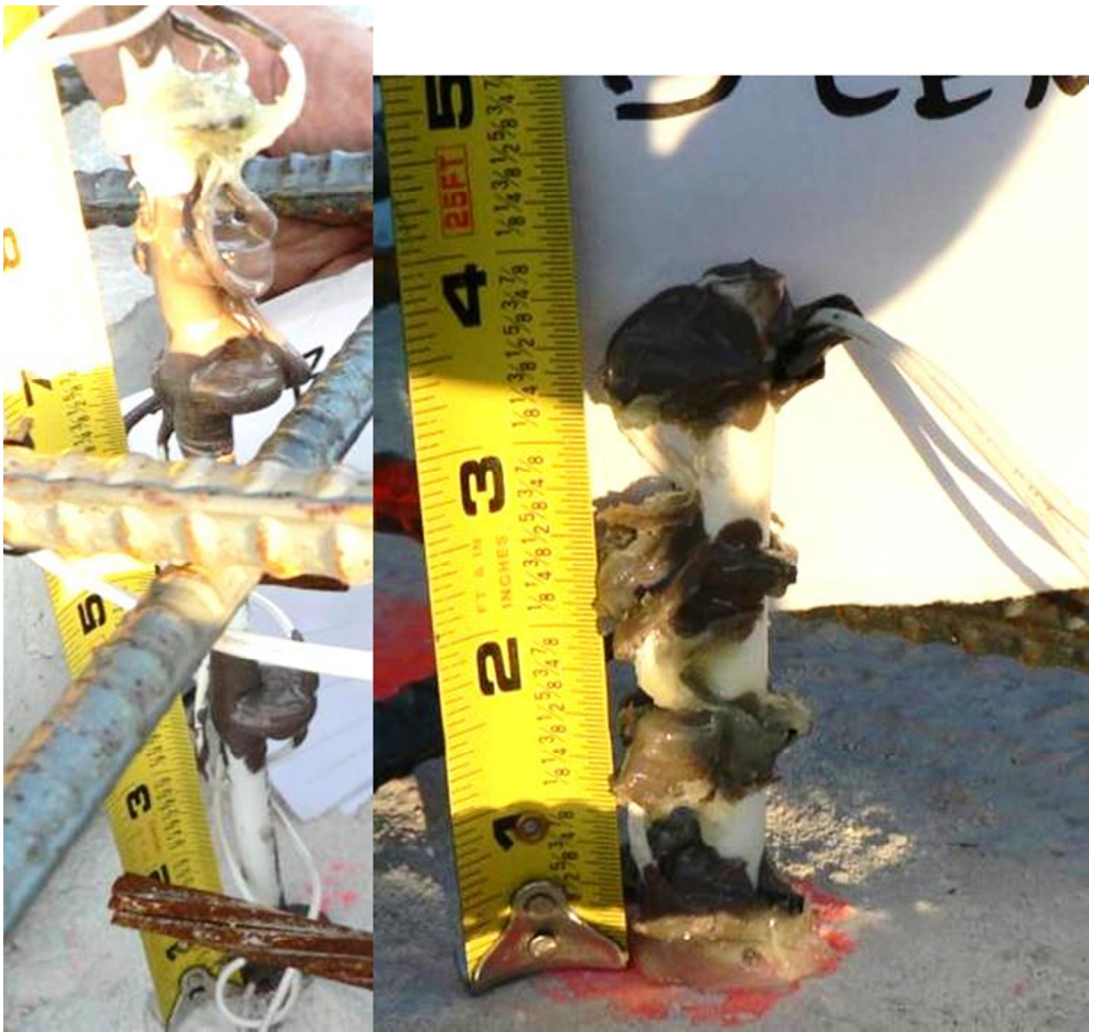

Figure 5-59: iButton strings on Georgetown bridge deck summer pour.

Two days after the pour, the research team returned to the bridge deck for the first data collection. The research team downloaded the data from the last two days, and reset the iButtons with a longer time interval between recordings. The research team also discovered that three of their eight iButton strings, including both of the six-button strings that were placed in the deeper sections over the girder, had been corrupted and could not be read. The research team, after considering various options, deemed that the use of a single two-conductor wire, coupled with having a button wedged against the precast

panels was the culprit in the iButton failures. The bottom button, more than likely, was damaged during the pour. Due to the fact that the iButtons were connected in series, the failure of one iButton resulted in the inability to collect data from any of the iButtons on that string. The research team decided, for future pours, that a parallel wiring scheme would be used. Each iButton was wired with an independent jumper that went to the common ground wire, and with a separate, individual wire. Using this method, if one iButton were corrupted, either by moisture intrusion or damaging of the solder connection, the rest of the iButton data on the string could still be acquired. The research team also used a naming scheme on all the wiring, such that specific colors were always placed in the same order (silver for ground, red on bottom button, brown on the button above…etc.) to reduce confusion when downloading data from the iButtons. The wiring scheme and examples of the iButton strings can be seen in Figure 5-60 and Figure 5-61.

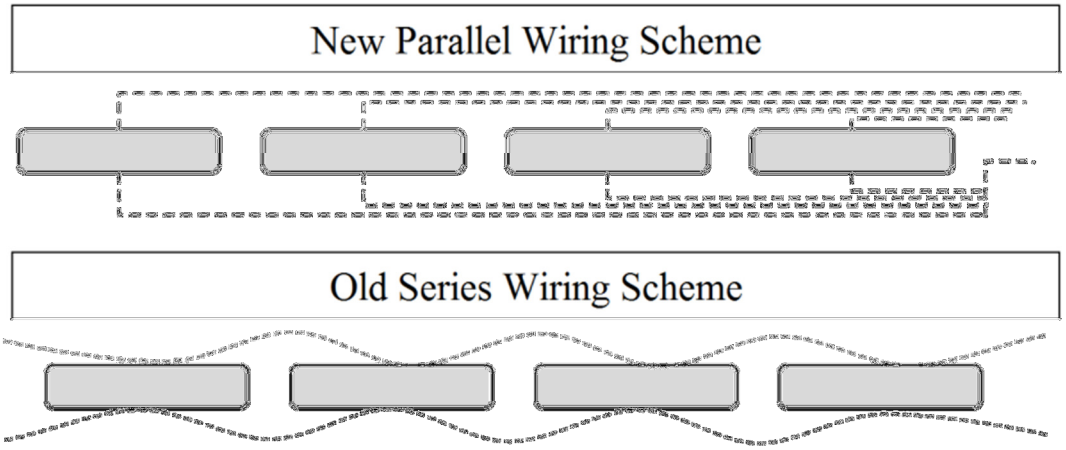

Figure 5-60: New and old iButton wiring schemes.

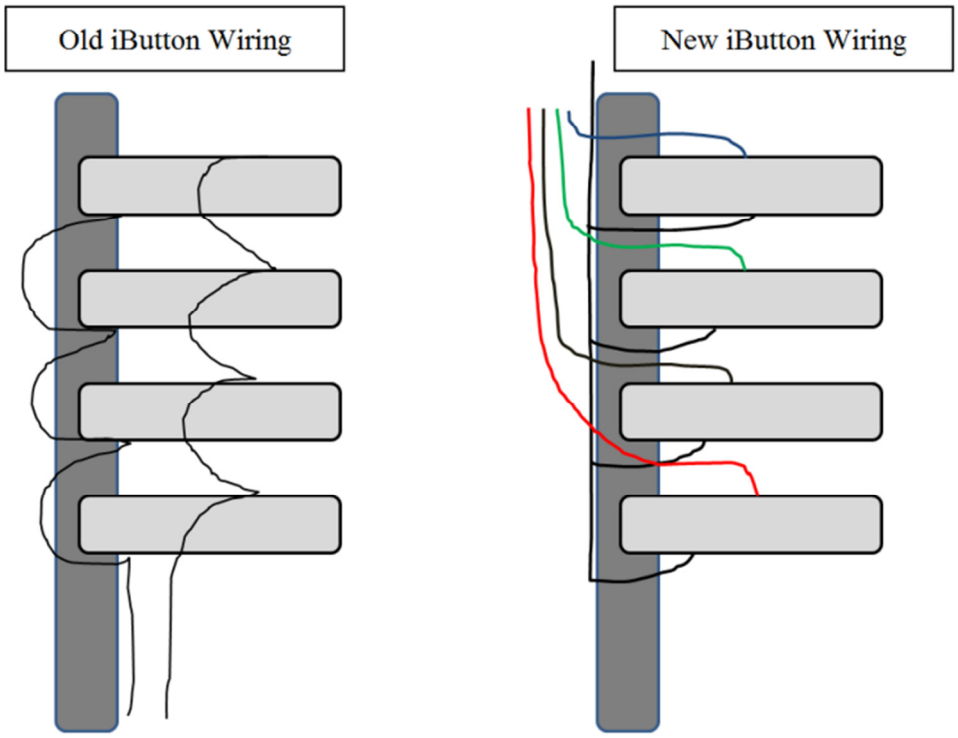

Figure 5-61: iButton string wiring configurations.

On the first return trip, and the following two data collection trips, the research team took note of the curing method that was used by the contractors. For this pour, moist cotton curing blankets were placed on top of the concrete, and were covered by a sheet of black plastic. The plastic was in place to prevent evaporation from the curing blankets below. While having the plastic separated from the concrete by a curing blanket, it was reasoned that the use of black plastic, rather than white or clear, was probably a poor choice in the summer time, and contributed to a higher daily peak temperature in the concrete than would have been seen with a white or clear plastic. Unfortunately, the research team did not take any pictures of the curing methods that were used on the Georgetown bridge deck for the summer pour.

On the last of the return trips to the Georgetown bridge deck summer pour, the research team inspected the bridge deck in an attempt to find early-age cracking. In the section that was available for the research team to inspect, no early-age cracking could be found.

5.3 GEORGETOWN BRIDGE DECK: WINTER POUR

In November of 2009, the research team returned to the Georgetown bridge deck to instrument the last span of the bridge. Prior to this instrumentation, and following the first span that was poured, contractors had completed two separate pours to cross the midspan of the bridge. As before, the bridge deck consisted of 4" of cast-in-place concrete on top of 4" precast, prestressed concrete panels, that were supported by precast, prestressed concrete girders. The pour began on November 19, 2009 at 8:00 AM, and concluded on November 19, 2009 at approximately 12:00 PM. Information gained from this field instrumentation included temperature data from November 19th to either December 10th or January 8th, depending on when the contractors cut the remaining iButton collection lines, two sets of semi-adiabatic calorimetry data, and mechanical testing results.

5.3.1 Structural Plans for Georgetown Bridge Deck

The Georgetown bridge deck winter pour consisted of 4" cast-in-place concrete over 4" precast, prestressed concrete panels, supported by precast, prestressed concrete girders. A typical cross section is shown in Figure 5-48, and the elevation for the winter pour can be seen in Figure 5-62.

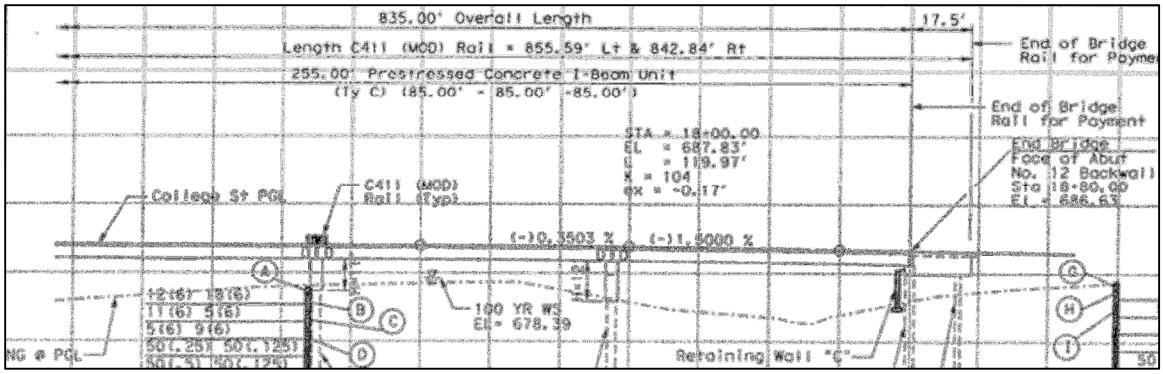

Figure 5-62: Elevation of Georgetown bridge deck winter pour.

5.3.2 Materials and Mixture Design of Georgetown Bridge Deck

The mixture design for the Georgetown bridge deck winter pour is presented in Table 5-51. A low-alkali cement, ASTM C 618 Class C fly ash, approximately 1" MSA limestone coarse aggregate, and river sand were used for this mixture design. The mixture design information was acquired from batch tickets that were collected throughout the pour. The mixture design was not seen to change over the course of the Georgetown bridge deck winter pour.

Table 5-51: Mixture design for Georgetown bridge deck winter pour.

Cement lb/yd^3	Fly Ash lb/yd^3	Water lb/yd^3	Coarse lb/yd^3	Fine lb/yd^3	AE oz/yd^3	WR3 oz/yd^3
430	143	252	1776	1254	2.2	22

5.3.3 Instrumentation and Testing of Georgetown Bridge Deck

The layout for the Georgetown bridge deck winter pour is provided in Figure 5-63 and Figure 5-64. Strands A and D were used to capture the changes between the beginning and end of the pour, and Strands B and C were used to capture data throughout the middle of the pour. As before, iButtons were placed both under and inside the precast panels on Strings B and C. On this pour, due to results seen from previous

instrumentation, no procedures were taken to evaluate one side of the deck relative to the other (i.e. Ease vs. West). Further information on the layout and position of the iButtons can be found in Appendix B.

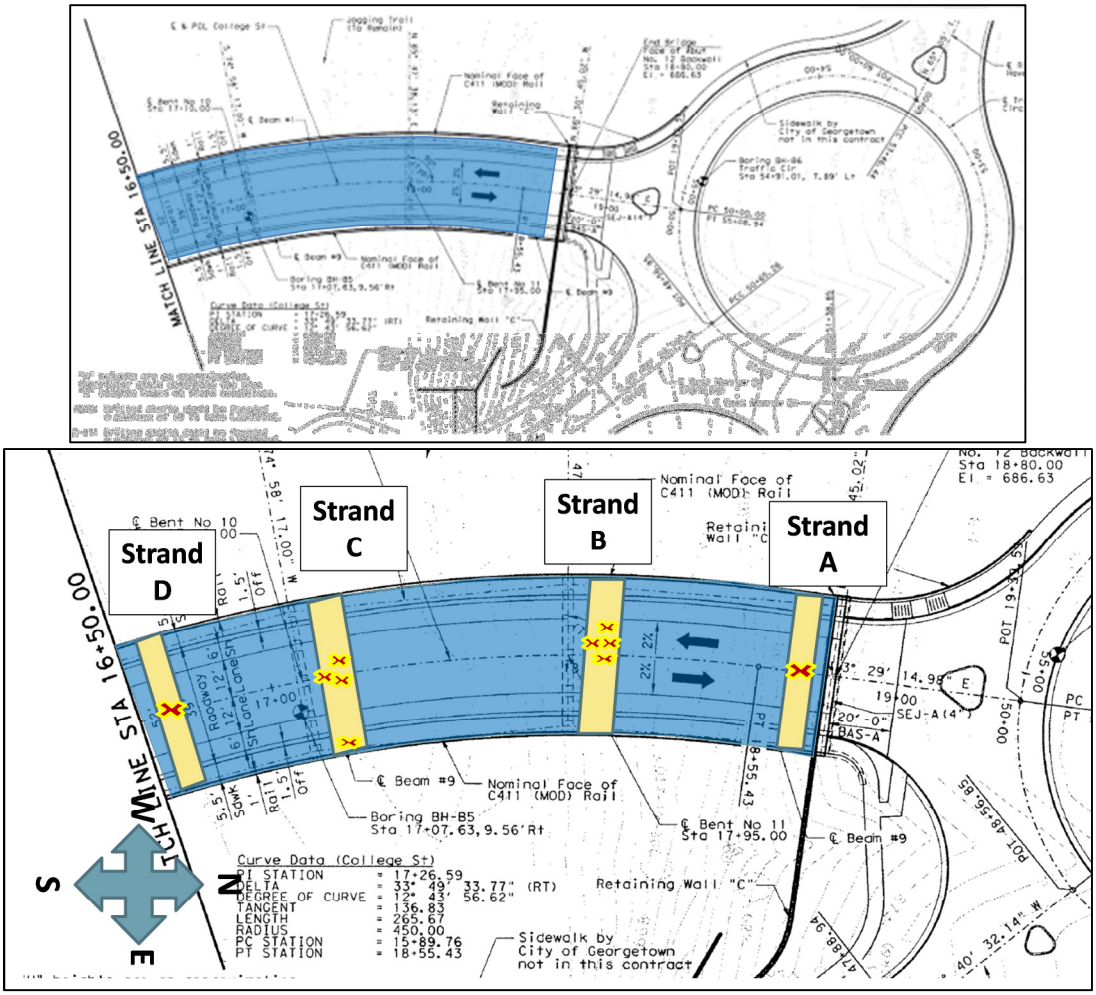

Figure 5-63: iButton string layout for Georgetown bridge deck winter pour.

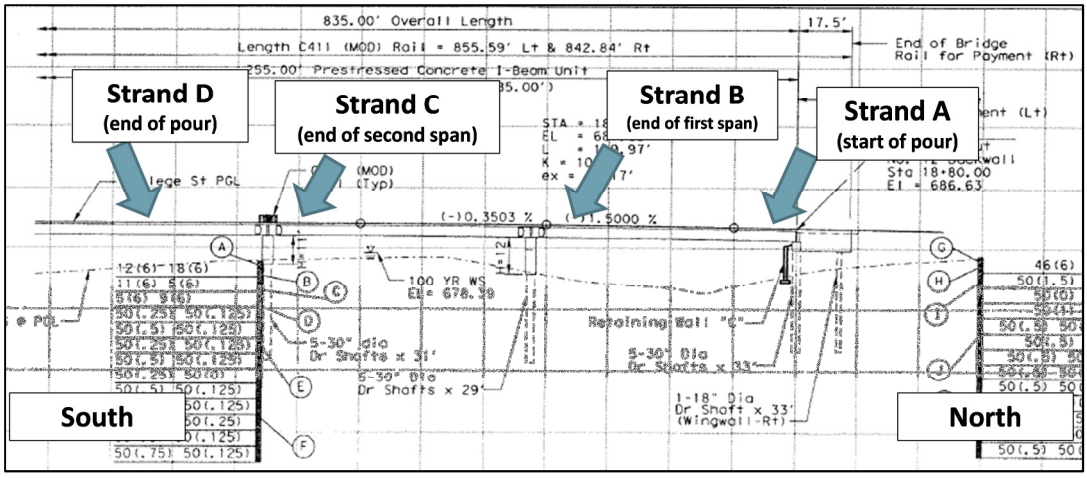

Figure 5-64: iButton strand layout for Georgetown bridge deck winter pour.

On their third bridge deck, the research team made modifications to their iButton preparation from lessons that had been learned from failures in previous bridge decks. The iButton strings now consisted of a solid, slightly flexible piece of plastic rod that had gaps cut out for iButtons. iButtons were soldered to six-conductor wire, this time in parallel, and then connected to the plastic rod with plastic ties. Two part epoxy was then used to cover the iButtons. Once again, a hole was drilled into the precast panel, and the bottom of the plastic rod was epoxied into this hole. The wires for the iButtons were run transversely across the deck, and with the foreman's permission, were run through a small hole that was drilled into the side formwork for the deck. It should be noted that the long duration of temperature measurements that the research team collected was due largely in part to the cooperation of the foreman of the contracting crew. By the time the winter pour was completed, the research team had built a good communication system with the foreman, and he worked to keep the iButton wires in readable condition in the months following the pour. Data collection ended with the pouring of the sidewalks on the bridge deck, which covered the remaining iButton collection wires. iButton strings from the Georgetown bridge deck winter pour can be seen in Figure 5-65.

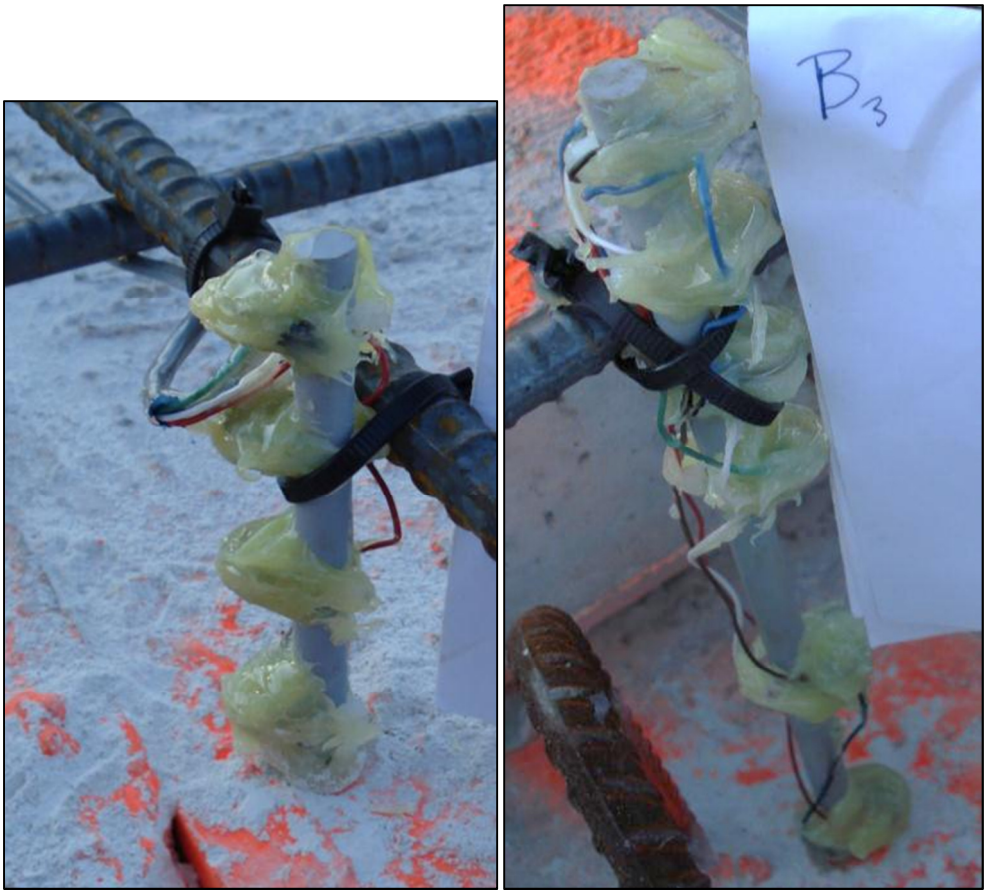

Figure 5-65: iButton strings for Georgetown bridge deck winter pour.

The research team returned to the bridge deck for the first data collection three days after the day of the pour. The iButtons were reset at this point for a longer collection interval, and data from the first three days was downloaded. The research team noted that for curing, the contractors had placed black plastic on top of the concrete, and then covered the black plastic with curing blankets. Later conversations with the contractor and TxDOT employees revealed that this method, in the freezing temperatures that prevailed in the days after the pour, helped protect the concrete from frost damage during the first days after casting. The curing method can be seen in Figure 5-66 and Figure 5-67.

Figure 5-66: Curing method for Georgetown bridge deck winter pour.

Figure 5-67: Black plastic under curing blanket at Georgetown winter pour.

Two more trips were made to the bridge deck to collect data from the iButtons, and to inspect the deck for early-age cracking. While no true early-age cracking was found, there were minor cracks located above the plastic 'zip strip'. The cracking above the plastic strips is shown in Figure 5-68.

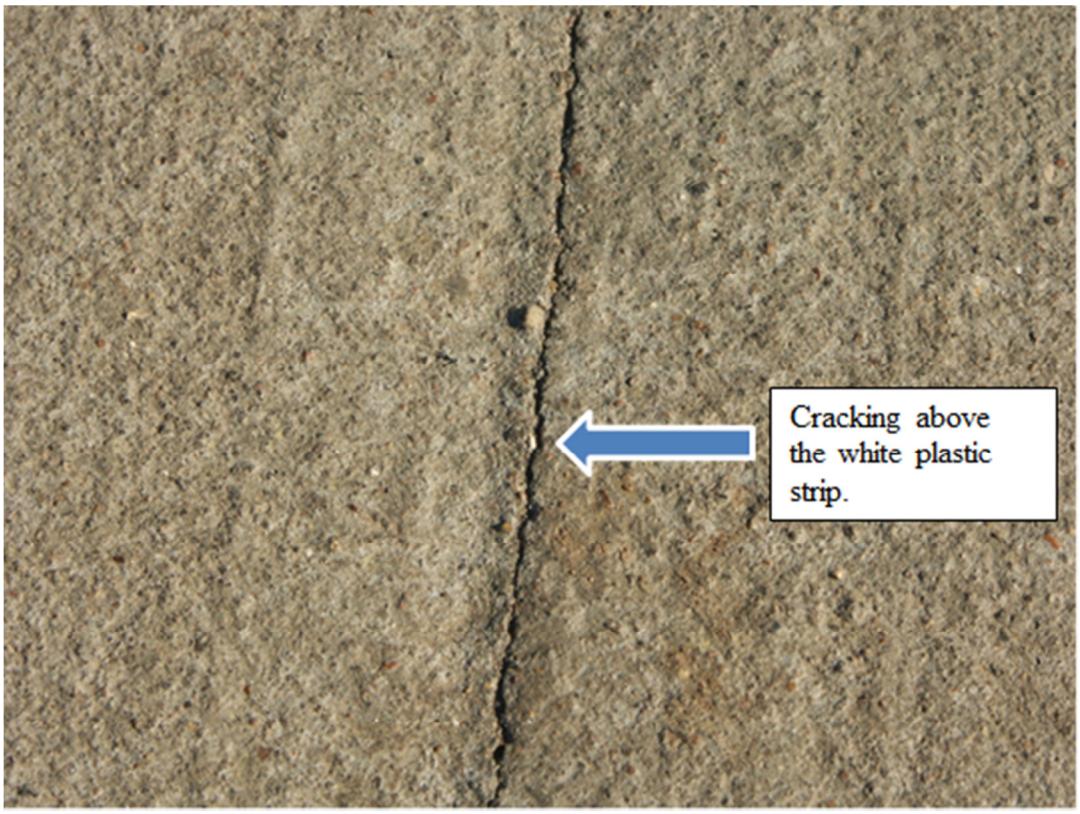

Figure 5-68: Cracking above plastic strip on bridge deck.

Cracking was also seen longitudinally between the sidewalk-bridge deck interface and in the transversely in the sidewalk at the line where the plastic strip was located in the bridge deck. The sidewalks were cast several months after the casting of the bridge deck. Cracks in the sidewalk can be seen in Figure 5-69 and Figure 5-70.

Figure 5-69: Cracking between bridge deck and sidewalk concrete.

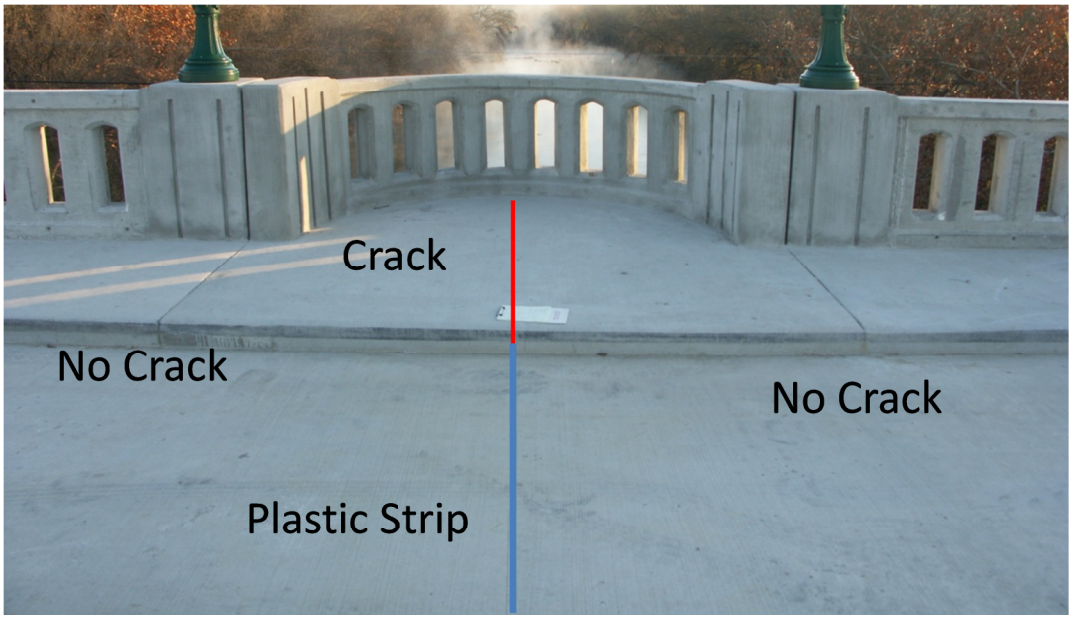

Figure 5-70: Transverse cracking in sidewalk concrete.

5.4 LUBBOCK BRIDGE DECK

The final bridge deck that the research team instrumented was in Lubbock, Texas, at Loop 289 and Slide Road. The bridge deck had two separate pours for the northbound and southbound lanes. The research team only instrumented the southbound lane pour. The bridge deck consisted of 4" of cast-in-place concrete over 4" precast, prestressed concrete panels, supported by precast, prestressed concrete girders. The pour began on July 15, 2010 at 11:00 PM and concluded on July 16, 2010 at 5:30 AM. Information gained from this field instrumentation included temperature data from July 15th to August 5th, semi-adiabatic calorimetry data, and mechanical testing results.

5.4.1 Structural Plans for Lubbock Bridge Deck

The Lubbock bridge deck consisted of 4" of cast-in-place concrete, 4" precast, prestressed concrete panels, and was supported by precast, prestressed concrete girders. This bridge deck also utilized epoxy coated reinforcement, where none of the previously instrumented bridge decks had done so. Elevation and cross sections of the bridge are provided in Figure 5-71, Figure 5-72, and Figure 5-73.

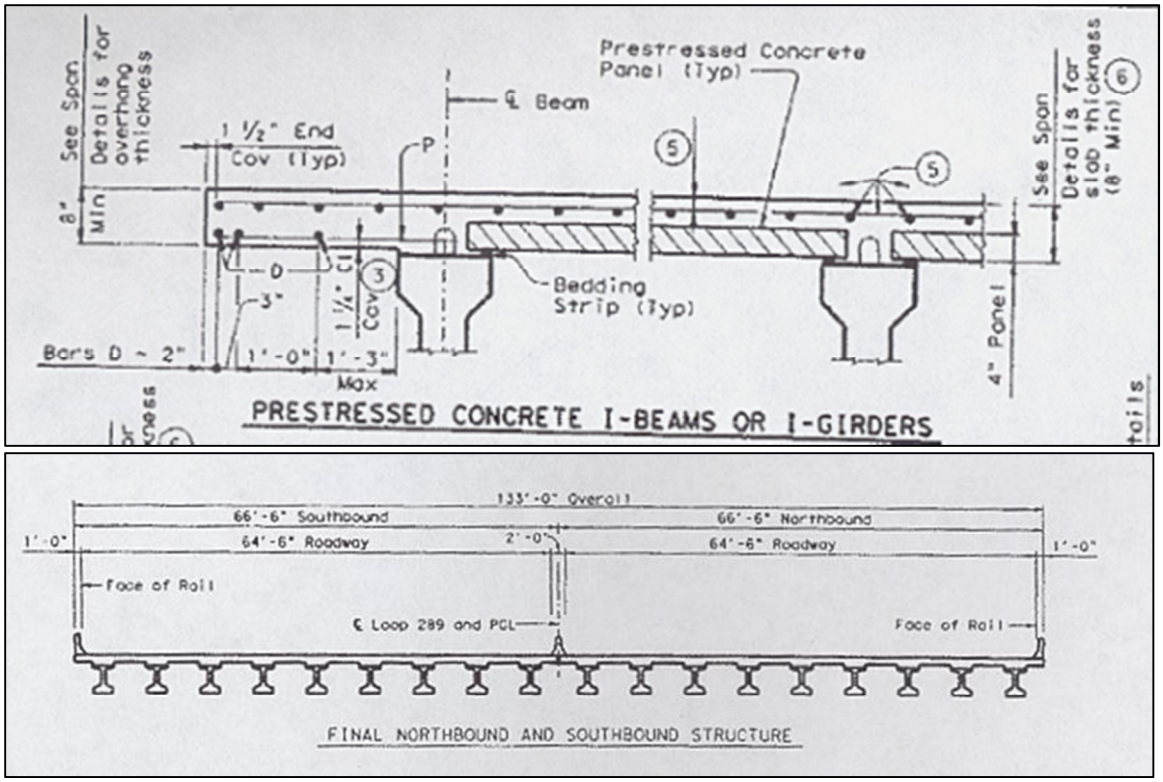

Figure 5-71: Cross section for Lubbock bridge deck.

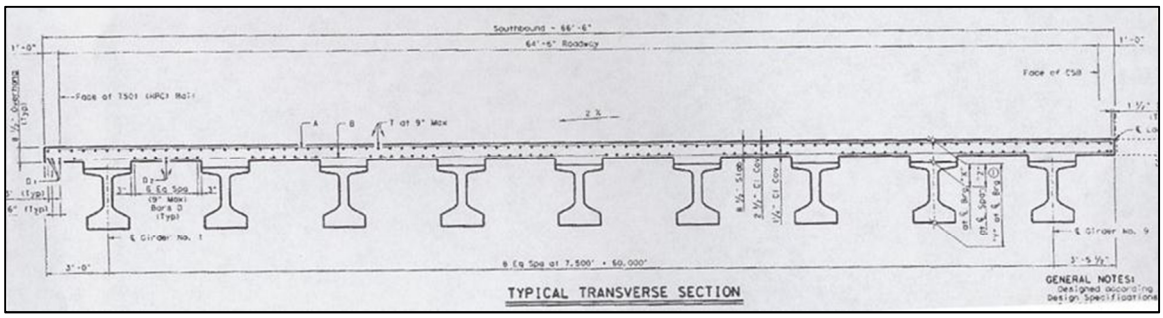

Figure 5-72: Cross section of Lubbock bridge deck southbound lane.

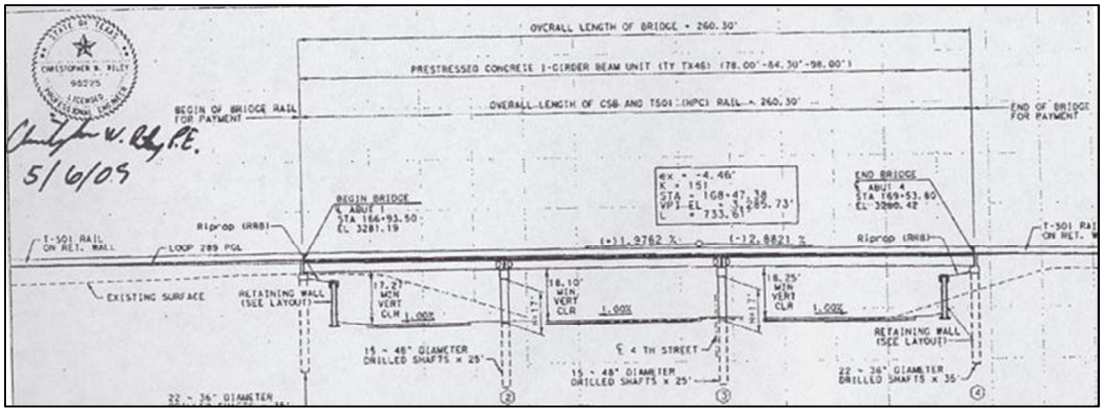

Figure 5-73: Elevation of Lubbock bridge deck.

5.4.2 Mixture Design of Lubbock Bridge Deck

The mixture design for the Lubbock bridge deck is provided in Table 5-52. The cement used was a low-alkali cement, with an ASTM C 618 Class C fly ash used as a 35% replacement for cement. The primary gradation of coarse aggregate was an approximately 1" MSA siliceous river gravel, while the secondary gradation of coarse aggregate was a TxDOT Gr. 5 siliceous coarse aggregate. River sand was used for the fine aggregate. Only one batch ticket, from the middle of the pour, was collected for this pour. However, discussions with TxDOT during the pour informed the research team that the mixture design was not changing throughout the pour. The Lubbock bridge deck was also the only bridge deck that the research team instrumented that utilized fibrillated polypropylene fibers in the mixture. These fibers provide an easier pathway for bleed water to reach the concrete surface, and help prevent plastic shrinkage cracking. The Lubbock area, with high winds and typically low relative humidity, is well-known for being a 'high-risk' for plastic shrinkage cracking if precautions are not taken.

Table 5-52: Mixture design for Lubbock bridge deck.

Cement lb/yd^3	Fly Ash lb/yd^3	Water lb/yd^3	Coarse1 lb/yd^3	Coarse2 lb/yd^3	Fine lb/yd^3	AE2 oz/yd^3	WR4 oz/yd^3	Fibers lb/yd^3
380	204	263	1506	475	996	7.5	58.4	1.5

5.4.3 Instrumentation and Testing of Lubbock Bridge Deck

The iButton layout for the Lubbock bridge deck is provided in Figure 5-74 and Figure 5-75. Strands A and D were used to capture the changes between the beginning and end of the bridge deck pour. Strands B and C captured the middle of the pour, with strand B consisting of 4-button strings located on the panels, and strand C of 6-button strings located above the girders. Further information on the iButton locations and depths can be found in Appendix B.

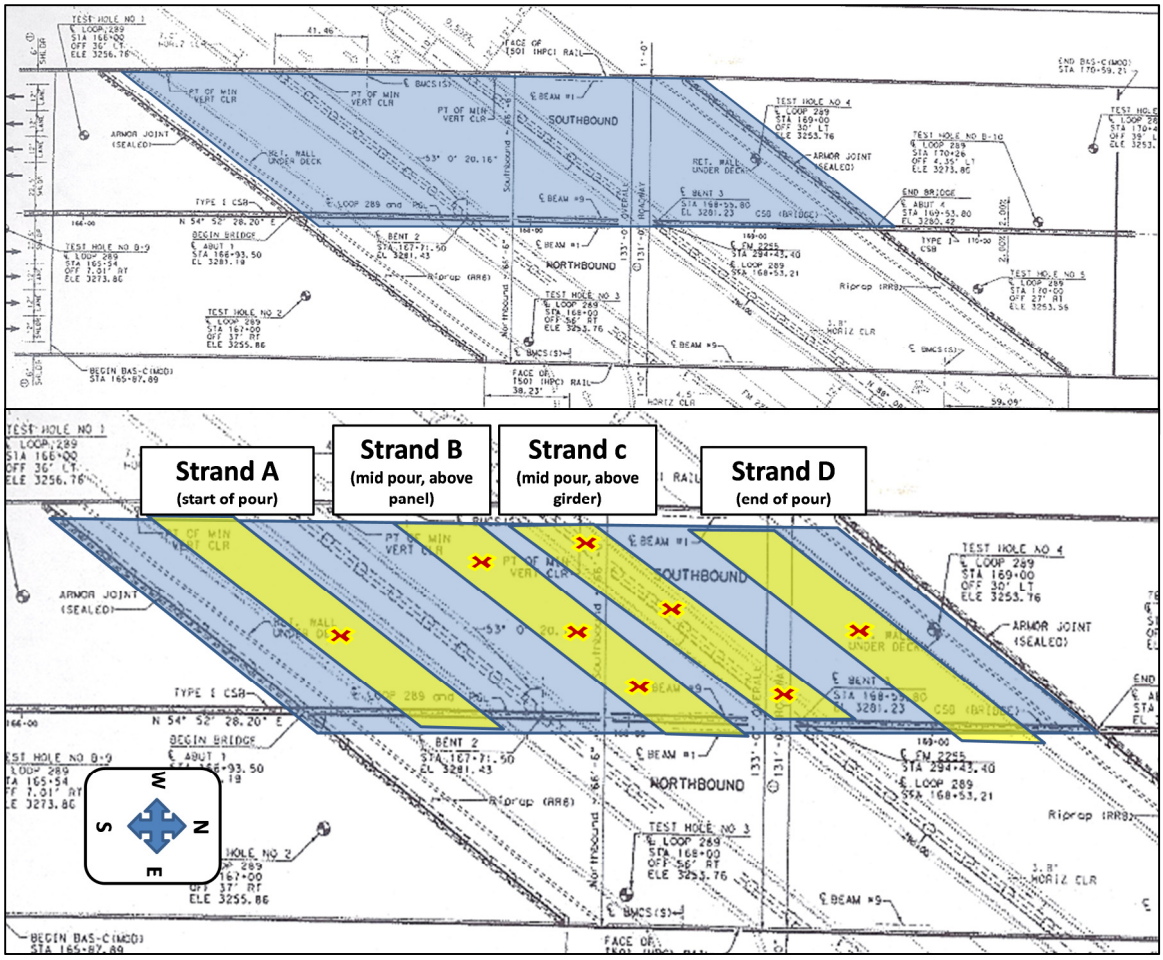

Figure 5-74: iButton string layout for Lubbock bridge deck.

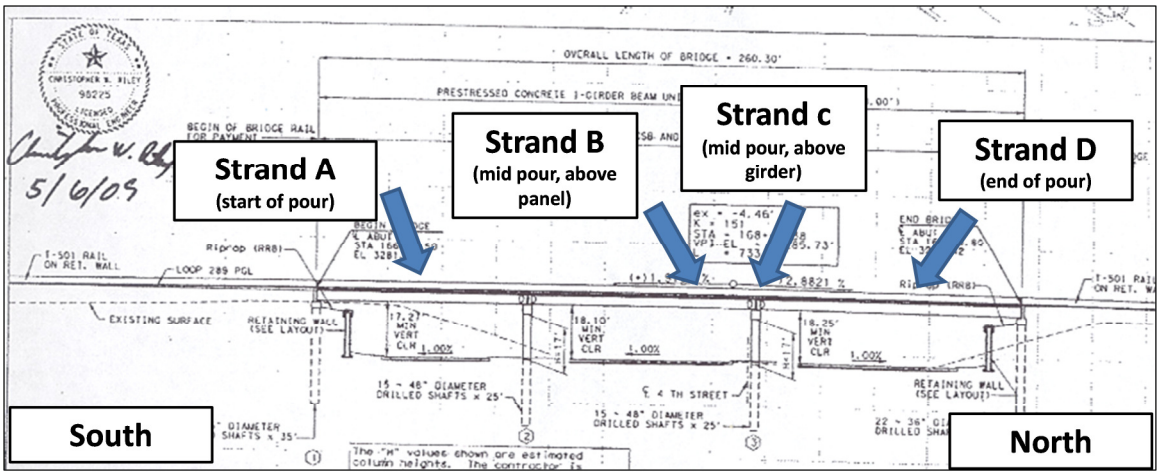

Figure 5-75: iButton strand layout for Lubbock bridge deck.

Due to the success that the research team found with the iButton preparation process used in the Georgetown bridge deck winter pour, the team implemented the same methods for the iButtons to be used in the Lubbock bridge deck. The only modification that was made was to have the wires connect to the string at the bottom of the plastic rod, between the bottom and second iButton, rather than the top. This was chosen to give the team greater flexibility in placing the iButton strings. If a plastic rod was too long at the bottom or too tall at the top, with the new preparation method, modifications could be made at the job site. At the Lubbock site, the research team was asked by the contractor to remove the top iButton from their taller, 6-button strings, for fear that they would interfere with the finishing crew on the bridge deck. Due to the use of parallel wiring, and the bottom-fed collection wire, the research team was able to meet this request in the field. Figure 5-65 shows the previous top-fed iButton string, and Figure 5-76 shows the bottom-fed iButton strings that were used in the Lubbock bridge deck pour.

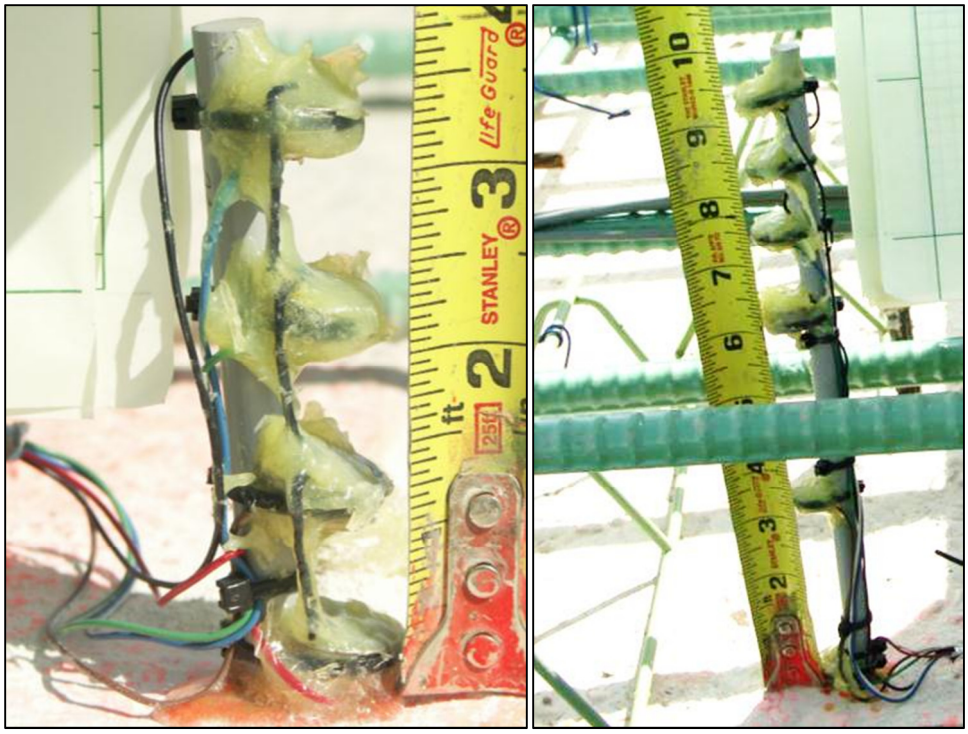

Figure 5-76: iButton strings for Lubbock bridge deck.

Two days after the pour, the research team returned to the bridge deck to collect data and reset the iButton recording interval. In addition to the curing compound that had been applied immediately after the pour, the contractors used wet cotton blankets, with opaque white plastic covering the blankets to cure the concrete, as shown in Figure 5-77.

Figure 5-77: Curing method for Lubbock bridge deck.

No early-age cracking was found when the research team returned to the bridge deck in August 2010.

Chapter 6: Field Testing Program Results

Chapter 6 provides the results from the field testing program. The chapter first presents the fresh concrete properties, chemical compositions and information on the cements and admixtures, mechanical strength development, and the hydration parameters determined from semi-adiabatic calorimetry. Chapter 6 concludes with a presentation of the temperatures and temperature gradients that were recorded in the field testing program.

6.1 Fresh Concrete Properties

Table 6-53 through Table 6-56 provide the fresh concrete properties that were measured by the research team during casting at the field instrumentations. All values were confirmed by tests conducted concurrently by a certified TxDOT inspector.

Table 6-53: Fresh concrete properties- San Antonio bridge deck.

Strand	Slump in.	Air Content %
A	2.5	2.4
B	5.5	1.7

Table 6-54: Fresh concrete properties- Georgetown summer pour.

Strand	Time	Slump in.	Air %	Temperature ° F
A	4:31 AM	5.0	4.6	86
B	5:22 AM	5.0	4.9	82
C	6:40 AM	4.3	4.7	83
D	7:19 AM	4.5	4.7	82

Table 6-55: Fresh concrete properties- Georgetown winter pour.

Strand	Time	Slump in.	Air %	Temperature ° F
A	7:54 AM	5.5	5.4	65
B	8:14 AM	5.4	--	66
C	9:40 AM	5.5	5.0	71
D	10:05 AM	3.5	5.1	73

Table 6-56: Fresh concrete properties- Lubbock bridge deck.

Strand	Time	Slump in.	Air %	Temperature ° F
B/C	1:50 AM	5.5	5.0	83

6.2 CHEMICAL ANALYSES OF FIELD TESTING MATERIALS

Cement, fly ash, and admixtures were acquired from the ready mix producers for the Georgetown and Lubbock bridge decks. Due to safety concerns from the producer, cement, fly ash, admixture, and aggregates were unable to be collected from the San Antonio pour. XRF and Bogue calculation results are presented for the cements and SCMs. Dosages from the batch tickets and physical properties from producer information sheets are provided for the concrete admixtures.

6.2.1 Cements and SCMs

Table 6-57 presents the results of XRF and Bogue calculated cement phases. GTBD denotes for Georgetown bridge deck, and LBD denotes Lubbock bridge deck.

Table 6-57: XRF and Bogue results for field materials.

		GTBD Cement	GTBD Fly Ash	LBD Cement	LBD Fly Ash
XRF Results	SiO_2	20.5	47.1	20.7	33.1
	Al_2O_3	4.3	15.4	4.4	18.7
	Fe_2O_3	3.0	5.2	5.0	6.3
	CaO	63.4	28.7	62.8	25.0
	MgO	1.6	2.4	0.8	4.6
	SO_3	2.8	0.9	2.9	1.2
	Na_2O	0.18	0.31	0.24	1.21
	K_2O	0.46	1.05	0.24	0.27
	Na_2Oe	0.48	1.00	0.39	1.39
Cement Phases	C_3S	61.3	--	53.9	--
	C_2S	12.4	--	18.6	--
	C_3A	6.4	--	3.3	--
	C_4AF	9.2	--	15.1	--

All values are in % by weight.

* Na_2Oe equivalent alkali content

6.2.2 Admixtures

The properties of the admixtures used at the Georgetown and Lubbock bridge deck pours are provided in Table 6-58. AE and WR3 refer to the air-entraining and water reducing admixtures used at both the Georgetown summer and winter pours. AE2, WR4, and Fibers refer to the admixtures and fibrilliated polypropylene fibers used in the Lubbock pour.

Table 6-58: Concrete admixtures for Georgetown and Lubbock pours.

Admixture	Dosage	Specific Gravity	% Solids
AE	0.38 oz./cwt	1.01	6%
WR3	3.8 oz./cwt	1.2	41%
AE2	1.28 oz./cwt	1.01	13%
WR4	10 oz./cwt	1.27	43%
Fibers	1.5 lb./yd^3	0.91	--

6.3 MECHANICAL STRENGTH DEVELOPMENT

Table 6-59 through Table 6-62 give the mechanical strength development for the bridge deck mixtures. The choice as to where and when to take cylinders from the field site varied for each site due to decisions made from previous pours, limitations from the contractor, and limitations on what could be transported back to the laboratory.

Table 6-59: Mechanical properties for San Antonio bridge deck.

Test		Strand A	Strand B
12 Hr.	f'c	1,152	1,225
	f'st	--	--
	E	--	--
24Hr.	f'c	2,887	2,887
	f'st	403	403
	E	--	--
2 Day	f'c	3,621	3,375
	f'st	507	506
	E	--	--
3 Day	f'c	--	4,730
	f'st	--	593
	E	--	--
7 Day	f'c	5,968	5,599
	f'st	--	721
	E	--	--
28 day	f'c	7,463	7,676
	f'st	816	843
	E	--	5,025,873
1 Year	f'c	--	8,035
	f'st	--	807
	E	--	5,744,161

All values in psi.

Table 6-60: Mechanical Properties for Georgetown summer pour.

Test	(psi)	String A	String B	String D
12Hr.	f'c	1,243	1,101	1,176
	f'st	--	179	--
	E	--	--	--
24Hr.	f'c	2,023	1,922	1,924
	f'st	339	295	298
	E	--	2,728,880	--
2 Day	f'c	2,811	2,646	2,800
	f'st	395	415	410
	E	--	3,165,204	--
3 Day	f'c	--	2,986	--
	f'st	--	424	--
	E	--	3,349,360	--
7 Day	f'c	--	3,828	--
	f'st	--	516	--
	E	--	3,538,608	--
14 Day	f'c	--	4,227	--
	f'st	--	526	--
	E	--	3,830,903	--
28 day	f'c	5,112	5,175	5,529
	f'st	574	564	582
	E	4,350,670	4,093,487	4,187,861
1 Year	f'c	--	5,792	--
	f'st	--	608	--
	E	--	--	--

All values in psi.

Table 6-61: Mechanical Testing for Georgetown winter pour.

Test		String A	String B	String C	String D
12Hr.	f'c	397	585	319	636
	f'st	58	83	68	87
	E	--	2,171,721	1,671,058	--
24Hr.	f'c	1,475	1,395	1,418	1,713
	f'st	211	211	185	219
	E	--	2,457,722	2,213,622	--
2 Day	f'c	2,546	2,404	2,291	2,693
	f'st	351	351	331	399
	E	--	2,986,560	2,928,232	--
8 Day	f'c	--	3,956	3,762	--
	f'st	--	488	497	--
	E	--	3,660,785	3,705,279	--
14 Day	f'c	--	4,478	4,133	--
	f'st	--	544	516	--
	E	--	4,117,225	3,801,262	--
28 Day	f'c	4,848	5,125	4,869	5,219
	f'st	581	563	523	570
	E	--	3,940,209	3,873,570	--

All values in psi.

Table 6-62: Mechanical properties for Lubbock bridge deck.

Test		Strand B
12 Hr.	f'c	310
	f'st	--
	E	--
24 Hr.	f'c	1,411
	f'st	209
	E	3,040,221
2 Day	f'c	1,872
	f'st	257
	E	3,389,402
7 Day	f'c	2,837
	f'st	364
	E	3,544,319
28 day	f'c	4,286
	f'st	500
	E	4,490,021

All values in psi.

6.4 SEMI-ADIABATIC CALORIMETRY

Table 6-63 presents the semi-adiabatic calorimetry results from the field pours. In this table, GTBDS represents the summer Georgetown bridge deck pour, GTBDW represents the winter Georgetown bridge deck pour, and LBD represents the Lubbock bridge deck pour. While the research team was able to collect Q-drum data from the San Antonio pour, the inability to acquire a sample of the cement and fly ash resulted in an inability to determine the activation energy and ultimate heat of hydration; parameters that are required in the semi-adiabatic calorimetry data analysis for determining the hydration parameters α, β, and τ. As described before in Chapter 3, activation energy, Ea, and ultimate heat of hydration, Hu, are calculated using empirical equations from previous work done by members of the research team. The hydration parameters α, β, and τ are found using curve fitting to match the heat generated within the Q-drum with that predicted by Eq. 2-7.

Table 6-63: Semi-adiabatic calorimetry results for field pours.

Qdrum Recording	E_a J/mol	H_u J/kg	α_u %	β	τ hrs.
GTBDS-Strand A	34,771	484,154	0.801	0.561	22.81
GTBDS-Strand B	34,771	484,154	0.788	0.569	23.07
GTBDW-Strand B	34,771	484,154	0.754	0.678	17.49
GTBDW-Strand C	34,771	484,154	0.863	0.792	16.19
LBD- Strand B	35,023	446,253	0.795	0.657	30.57

6.5 RECORDED BRIDGE DECK TEMPERATURES

This section presents temperature data from the middle of the pour, in the middle of the bridge deck, for the bridge decks that were instrumented. In the following sections, as well as in Appendix B, the graphs are titled with the bridge deck that was

instrumented, the button string being displayed, and the duration of data being presented. Bridge decks are denoted as follows:

- SABD: San Antonio Bridge Deck
- GTBDS: Georgetown Bridge Deck: Summer Pour
- GTBDW: Georgetown Bridge Deck Winter Pour
- LBD: Lubbock Bridge Deck

The complete sets of recorded bridge deck temperatures can be found in Appendix B.

Over the course of four sets of field instrumentation, a very large database of bridge deck temperatures for hot and cold weather conditions was collected. The research team will use this information to calibrate, validate, and improve upon the temperature prediction models used in ConcreteWorks. The final results of this recalibration will be presented in the final report for this project, and available in a future version of ConcreteWorks.

6.5.1 San Antonio Bridge Deck

Figure 6-78 and Figure 6-79 display the recorded bridge deck temperatures in the middle of the San Antonio bridge deck. The San Antonio bridge deck had the highest first peak temperatures of all the mixtures evaluated, likely due to the time of placement and the use of black plastic for curing. The research team was not able to clearly determine, through the data or through communication with the contractor, when the curing plastic was removed from the bridge deck. However, a best guess based on correspondence between the ambient air temperature and the top iButton temperature led to the assumption that the curing plastic was removed on July 29, 2009.

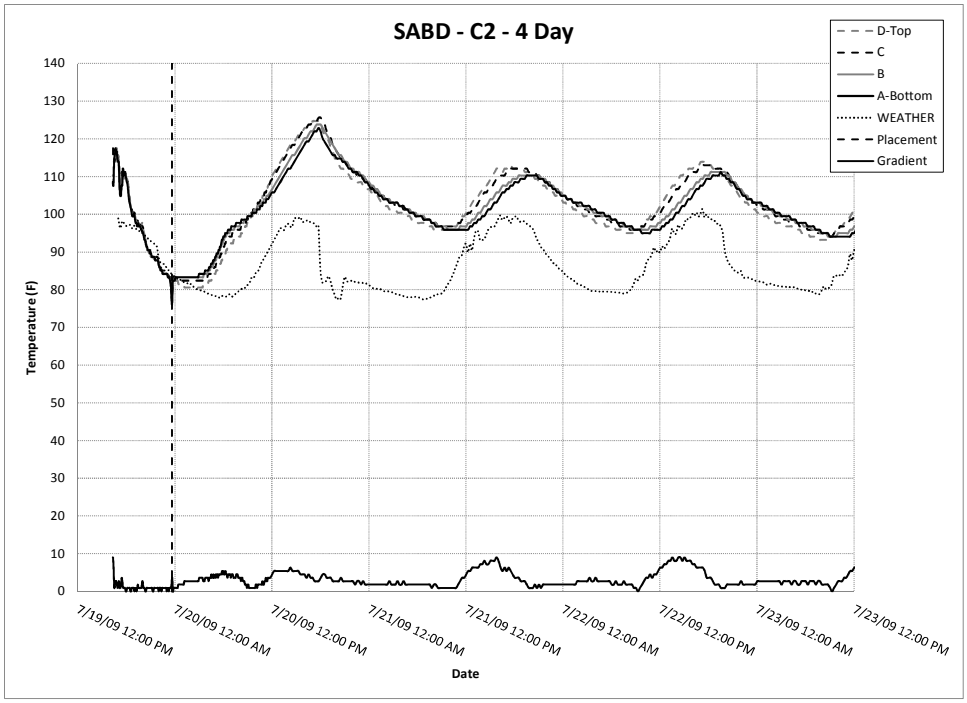

Figure 6-78: Four day temperature data: SABD - C1

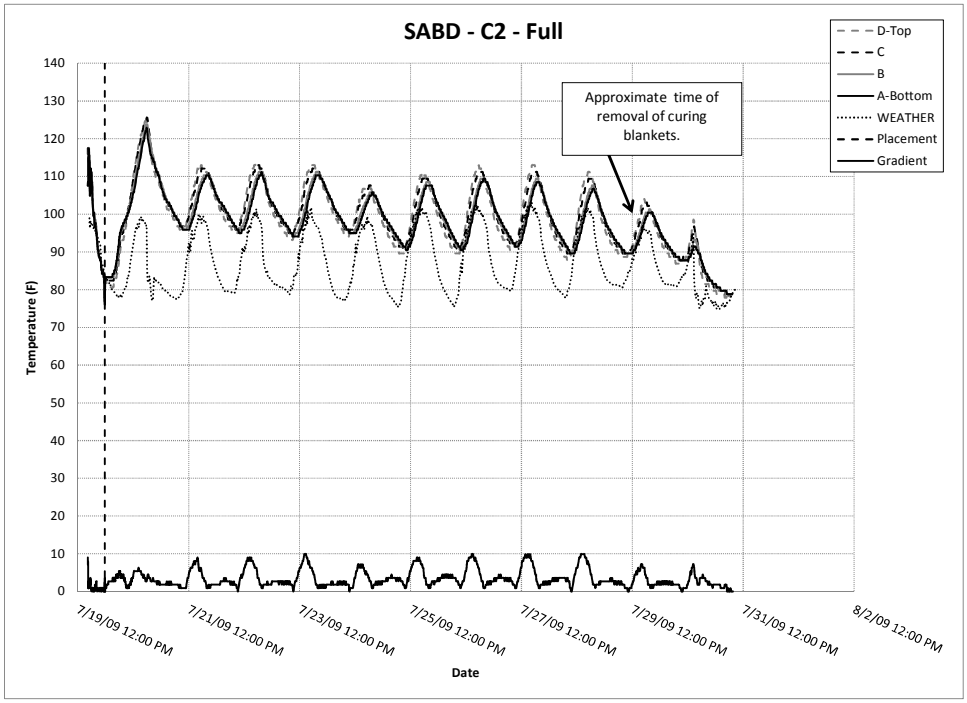

Figure 6-79: Full temperature data: SABD - C1

6.5.2 Georgetown Bridge Deck: Summer Pour

Figure 6-80 and Figure 6-81 display the temperature data for the middle of the bridge deck cast in the Georgetown summer pour. In this bridge deck, as well as in the winter pour, the research team was able to place iButtons underneath the bridge deck panels, as well as inside the middle of bridge deck panels. This provided the team with a better understanding of the heat transfer occurring between the existing superstructure and the newly cast bridge deck concrete. While not as high as those seen in San Antonio, the Georgetown summer pour did have some high temperatures in the first few temperature peaks, partially due to the use of black plastic on top of the curing blankets during very high summer time temperatures. The research team was able to determine the cause for the high temperatures by examining the temperatures in the bridge deck following the removal of the curing blankets and plastic on August 8, 2009.

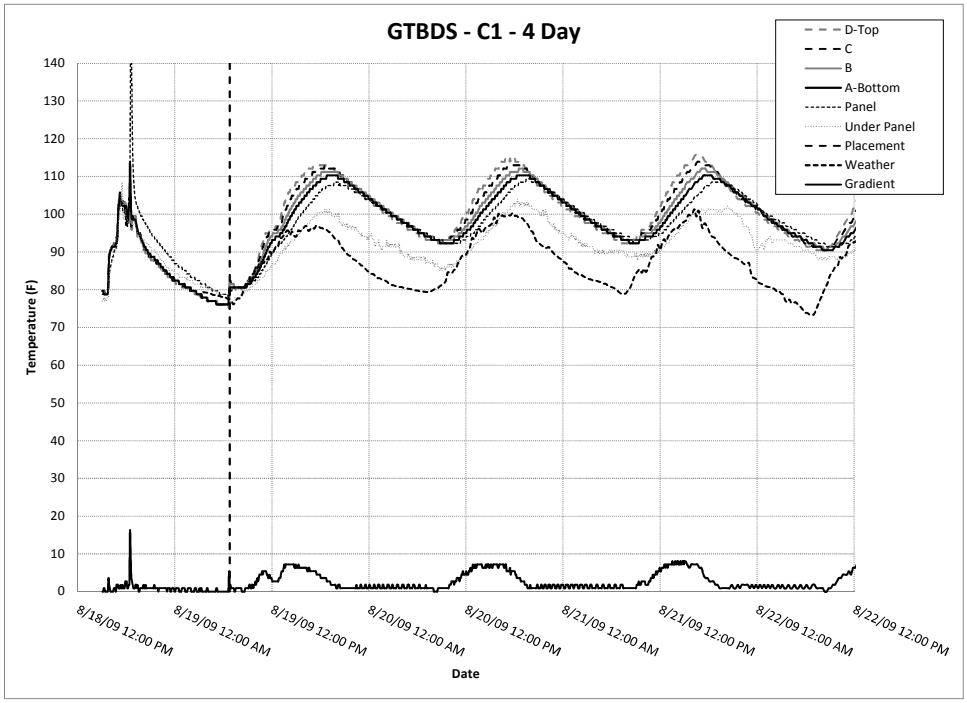

Figure 6-80: Four day temperature data: GTBDS – C1

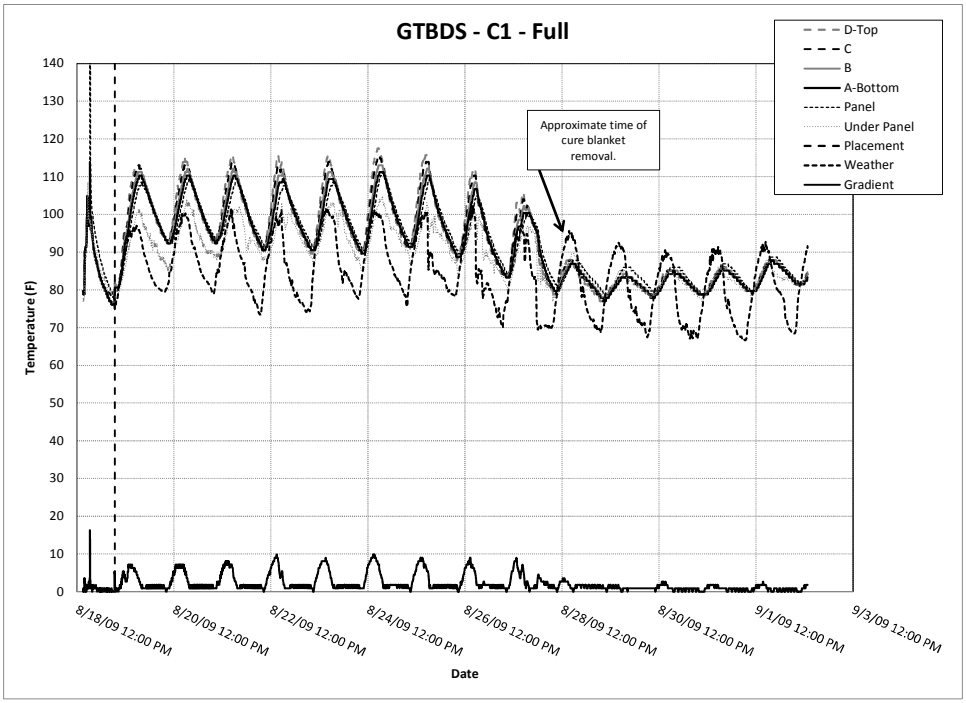

Figure 6-81: Full temperature data: GTBDS – C1

6.5.3 Georgetown Bridge Deck: Winter Pour

Figure 6-82 and Figure 6-83 display the temperature data for the middle of the bridge deck cast in the Georgetown winter pour. As with the Georgetown summer pour, the research team was able to instrument the middle and underside of the bridge deck panels, in addition to the measurements taken inside the bridge deck. For this pour, the research team was able to capture much more data than had been available in previous instrumentations. Due to the extended data, the graphs presented in this section span seven and twenty-eight days. Full plots of the bridge deck temperatures are presented in Appendix B. The research team was informed by the contractor that curing blankets for the Georgetown bridge deck winter pour were removed ten days after casting, on November 29, 2009 at approximately 12:00 PM.

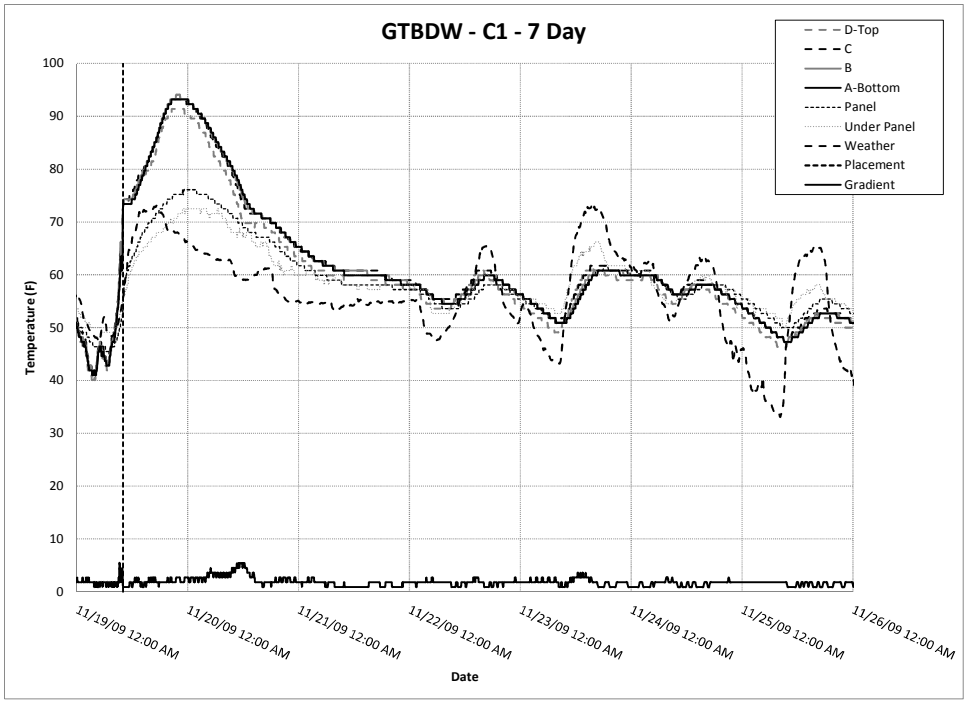

Figure 6-82: Seven day temperature data: GTBDW – C1

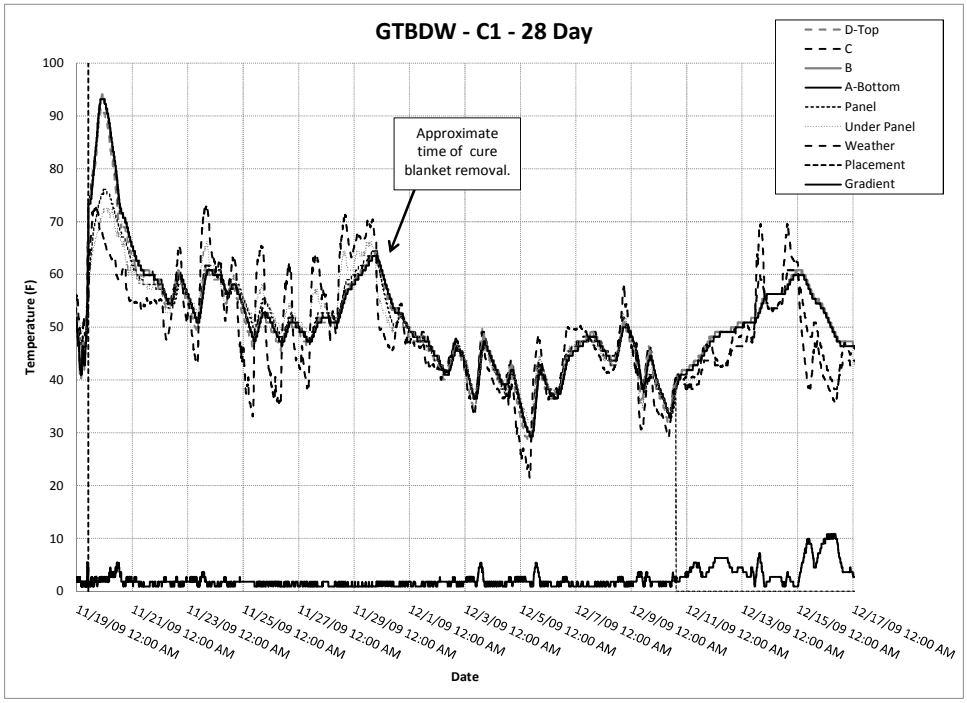

Figure 6-83: Twenty-eight day temperature data: GTBDW – C1

6.5.3 Lubbock Bridge Deck

Figure 6-84 and Figure 6-85 display the temperature data from the middle of the bridge deck cast in the Lubbock bridge deck pour. As opposed to previous instrumentations, the research team was required to instrument the Lubbock bridge deck with a smaller team and with a smaller time window. As such, the research team was unable to place iButtons under and inside the precast prestressed concrete panels. Through examination of the temperature data, the research team determined that the curing blankets and plastic were removed on July 29, 2010.

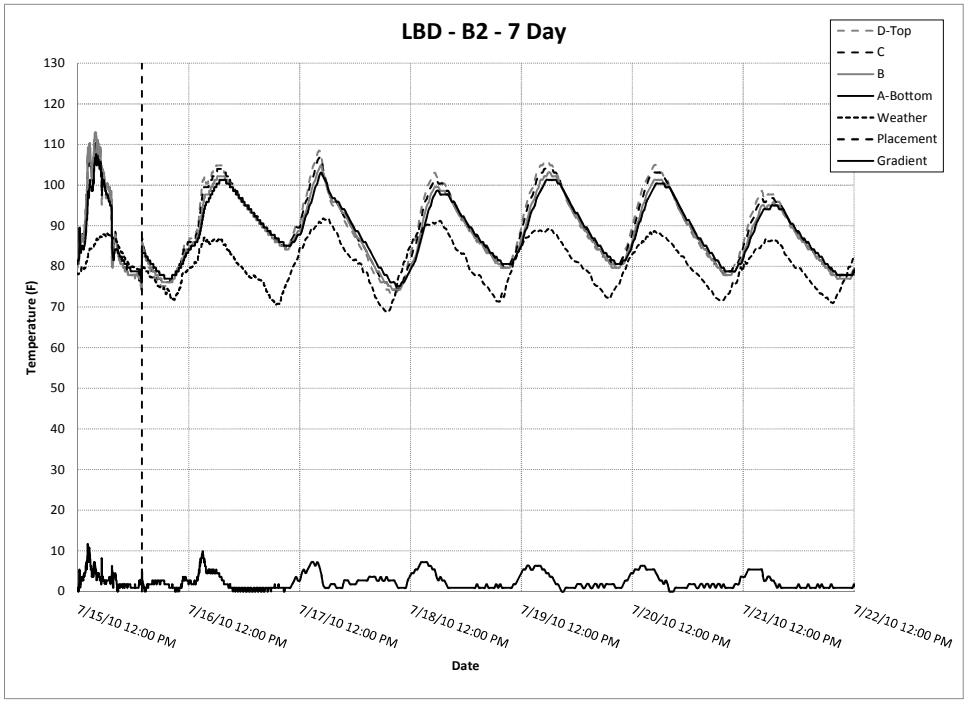

Figure 6-84: Seven day temperature data: LBD – B2

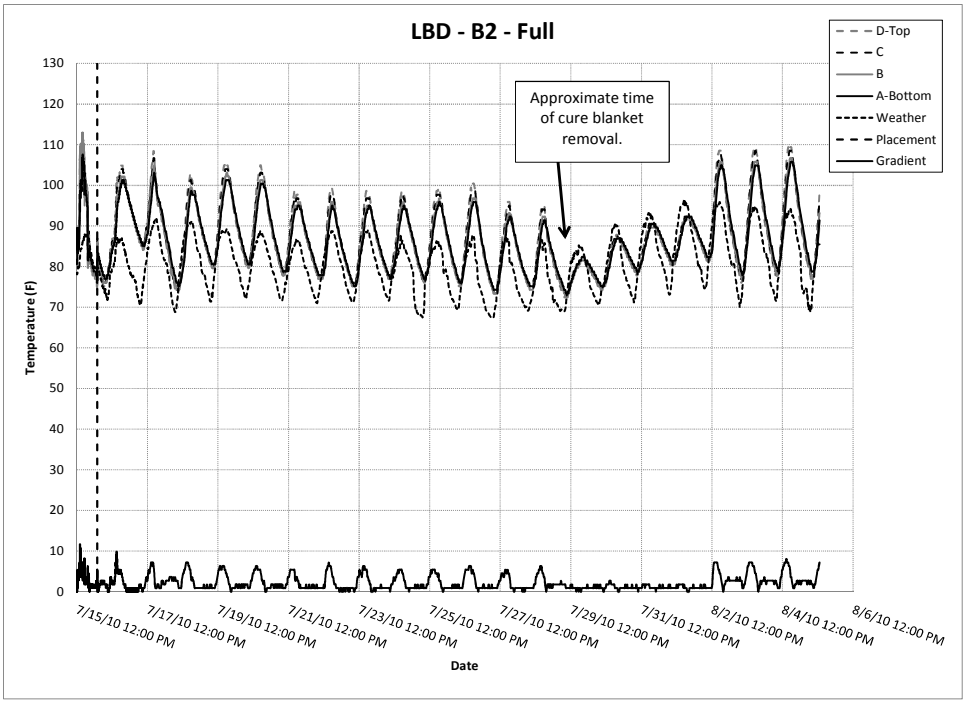

Figure 6-85: Full temperature data: LBD – B2

Chapter 7: Conclusions and Recommendations

7.1 CONCLUSIONS

Some of the more relevant and important conclusions from this study are as follows:

- Straight cement mixtures generate more heat during hydration than mixtures that contain SCMs, and therefore have higher peak temperatures. High-alkali cements generate more heat and have higher peak temperatures than do low-alkali cements.
- Mixtures incorporating ground granulated blast furnace slag have the lowest peak temperatures. Higher replacements of GGBFS result in lower temperatures than do lower replacements.
- After 96 hours of hot weather simulation, GGBFS and Class F fly ash mixtures had generated the lowest maximum stress. However, when inducing cracking, the stress at cracking and the stress / strength ratio at cracking for the Class F fly ash mixtures was also the lowest. The reserve stress / strength ratio was also the lowest for the Class F fly ash mixtures. Class F fly ash mixtures appeared to be more susceptible to early age cracking.
- After 96 hours of hot weather simulation, Class C fly ash and Control mixtures had the highest maximum stresses. However, the Class C fly ash and Control mixtures also had the highest cracking stresses and therefore high reserve stress / strength ratios.
- Under hot weather simulation, slag-containing mixtures had the lowest maximum stress over the course of 96 hours, and the highest stresses at cracking. This resulted in the largest reserve stress / strength ratio of the

mixtures evaluated. Slag-containing mixtures were determined to be the least susceptible to early-age cracking.

- Under cold weather simulations, cracking could not be induced in any of the mixtures evaluated, due to the inability to generate a great enough differential between the concrete temperature and the temperature at initial set. However, after 96 hours of simulation, Control mixtures had generated the highest maximum stress, and Class F fly ash mixtures had generated the lowest maximum stresses.
- The research team was unable to induce cracking in any of the mixtures containing limestone coarse aggregate. Maximum 96 hour stresses under hot and cold weather simulations were lower for the limestone mixtures than for any other mixtures. Limestone mixtures, during artificial cooling, were able to withstand temperature differentials between the concrete temperature and the temperature at initial set in excess of 35°F. In the river gravel mixtures that cracked, cracking usually occurred at a temperature differential less than 20°F. The reduced coefficient of thermal expansion of limestone results in a considerable decrease in early-age cracking risk.
- Reduction in pore water surface tension through the use of shrinkage reducing admixtures is effective at minimizing the effects of chemical and autogenous shrinkage.
- The choice of curing method can have a large impact on the peak concrete temperature. Black plastic exposed to direct sunlight should be avoided during the summer months. In winter months, black plastic may be

effective in increasing the rate of mechanical strength development by transferring heat to the concrete through solar radiation.

- Predictive equations/models were evaluated for the key volume change mechanisms active in bridge decks, and an improved creep model developed by Byard (2011) was successfully applied to the cracking frame data generated under this project.

7.2 RECOMMENDATIONS

At the conclusion of this project, the following research is recommended to further understand early-age concrete behavior:

- Further testing within the rigid cracking frame to capture the stresses generated during the temperature drop that is typical when curing blankets and/or plastic is removed.
- Further testing within the rigid cracking frame to evaluate the stresses developed under temperature profiles generated from field instrumentation.
- Further testing within the rigid cracking frame to evaluate the performance of mixtures with no admixtures, and with higher range water reducers and retarders.
- Further evaluation of setting time under simulated temperature profiles with varying concrete placement temperatures.
- Further instrumentation of field and possibly laboratory specimens to better understand the effects of different curing methods on the temperature development of concrete during summer and winter months.

- Further instrumentation of field and possibly laboratory specimens to better understand the interplay between localized environmental conditions underneath concrete bridge decks, and their effects on early-age concrete temperature development.

Appendix A: Rigid Cracking Frame Mixture Information

A.1 Sample Report from ConcreteWorks for Mixture CL-RG

Parameter	Value	Units
Results		
TxDOT 2004 Specifications Used		
Max Temperature	115	℉
This mix is not ASR susceptable as defined by:	TxDOT	
Original Concrete Materials CO2 emissions	10	lb/yd^3
Steel Corrosion Results		
Time to Top steel Corrosion	19	Years
Time to Concrete Damage From Top Mat Steel Corrosion	25	Years
Time to Bottom Steel Corrosion	> 20	Years
Time to Concrete Damage From Bottom Mat Steel Corrosion	> 26	Years
General Inputs		
Project Location	Lubbock	
Unit System	English	
Chloride Units	Percent of Concrete	
Life Cycle Analysis Duration	20	Years
Analysis Duration	7	days
Concrete placement time	10	am
Concrete placement date	8/15/2008	
Member Inputs		
Shape Choice	Permanent Metal Decking Deck	

Parameter	Value	Units
Deck Thickness	8	inches
Top Mat Cover	2	inches
Bottom Mat Cover	5.75	inches
Mixture Proportions		
Cement Content	564	lb/yd^3
Water Content	254	lb/yd^3
Coarse Aggregate Content	1941	lb/yd^3
Fine Aggregate Content	1232	lb/yd^3
Air Content	2	%
Chemical Admixture ASTM C494	Type A, NRWR	
Chemical Admixture ASTM C494	Type B, Retarder	
Material Properties		
Cement Type	I/II	
C3S content	62.398	%
C2S content	10.525	%
C3A content	5.448	%
C4AF content	11.077	%
Free CaO content	0.9	%
SO3 content	3.07	%
MgO content	0.7	%
Alkali content	0.47	%

Parameter	Value	Units
Deck Thickness	8	inches
Top Mat Cover	2	inches
Bottom Mat Cover	5.75	inches
Mixture Proportions		
Cement Content	564	lb/yd^3
Water Content	254	lb/yd^3
Coarse Aggregate Content	1941	lb/yd^3
Fine Aggregate Content	1232	lb/yd^3
Air Content	2	%
Chemical Admixture ASTM C494	Type A, NRWR	
Chemical Admixture ASTM C494	Type B, Retarder	
Material Properties		
Cement Type	I/II	
C3S content	62.398	%
C2S content	10.525	%
C3A content	5.448	%
C4AF content	11.077	%
Free CaO content	0.9	%
SO3 content	3.07	%
MgO content	0.7	%
Alkali content	0.47	%

Parameter	Value	Units
Concrete Fresh Temperature	73	℉
Blanket R-Value	2.91	℉
Cure Method Application Age	1	hrs
Cure Method Application Age	1	hrs
White Cure Plastic Used		
Corrosion Inputs		
Top Steel Type	Black Steel	
Bottom Steel Type	Black Steel	
Cast-In-Place Dref	108.9	x 10^-13 (m^2/s)
Cast-In-Place m	0.26	
No Barrier Method Selected		
Exposure Class	Urban Road	

A.2 SAMPLE REPORT FROM CONCRETEWORKS FOR MIXTURE F3L-35RGC

Parameter	Value	Units
Results		
TxDOT 2004 Specifications Used		
Max Temperature	64	℉
This mix is ASR susceptable as defined by:	TxDOT	
Original Concrete Materials CO2 emissions	10	lb/yd^3
Steel Corrosion Results		
Time to Top steel Corrosion	> 20	Years
Time to Concrete Damage From Top Mat Steel Corrosion	> 26	Years
Time to Bottom Steel Corrosion	> 20	Years
Time to Concrete Damage From Bottom Mat Steel Corrosion	> 26	Years
General Inputs		
Project Location	Lubbock	
Unit System	English	
Chloride Units	Percent of Concrete	
Life Cycle Analysis Duration	20	Years
Analysis Duration	7	days
Concrete placement time	10	am
Concrete placement date	2/17/2008	
Member Inputs		
Shape Choice	Permanent Metal Decking Deck	

Parameter	Value	Units
Deck Thickness	8	inches
Top Mat Cover	2	inches
Bottom Mat Cover	5.75	inches
Mixture Proportions		
Cement Content	366.6	lb/yd^3
C Fly Ash Content	197.4	lb/yd^3
Water Content	254	lb/yd^3
Coarse Aggregate Content	1923	lb/yd^3
Fine Aggregate Content	1220	lb/yd^3
Air Content	2	%
Chemical Admixture ASTM C494	Type A, NRWR	
Chemical Admixture ASTM C494	Type B, Retarder	
Material Properties		
Cement Type	I/II	
C3S content	62.398	%
C2S content	10.525	%
C3A content	5.448	%
C4AF content	11.077	%
Free CaO content	0.9	%
SO3 content	3.07	%
MgO content	0.7	%

Parameter	Value	Units
Alkali content	0.47	%
Blaine Fineness	371.5	m^2/kg
Activation Energy	25593.502	J/mol
Alpha	1	
Tau	34.748	hrs
Beta	0.718	
Hu	448133.272	
Coarse Agg. type	Siliceous River Gravel	
Fine Agg. type	Siliceous River Sand	
Coarse Agg. type	Siliceous River Gravel	
Fine Agg. type	Siliceous River Sand	
Mechanical Properties		
Maturity Method	Nurse-Saul	
Environment Inputs Summary		
Ave. Daily Max Temp.	55.4	℉
Ave. Daily Min Temp.	33.1	℉
Ave. Max Daily Solar Radiation	630.1	W/m^2
Ave. Max Daily Wind Speed	17.9	m/s
Ave. Max Relative Humidity	71.5	%
Ave. Min Relative Humidity	39	%

Parameter	Value	Units
Construction Inputs		
Concrete Fresh Temperature	65	℉
Blanket R-Value	5.67	℉
Cure Method Application Age	1	hrs
Cure Method Application Age	1	hrs
White Cure Plastic Used		
Corrosion Inputs		
Top Steel Type	Black Steel	
Bottom Steel Type	Black Steel	
Cast-In-Place Dref	108.9	x 10^-13 (m^2/s)
Cast-In-Place m	0.54	
No Barrier Method Selected		
Exposure Class	Urban Road	

A.3 RIGID CRACKING FRAME RESULTS

A.3.1 Control Mixtures

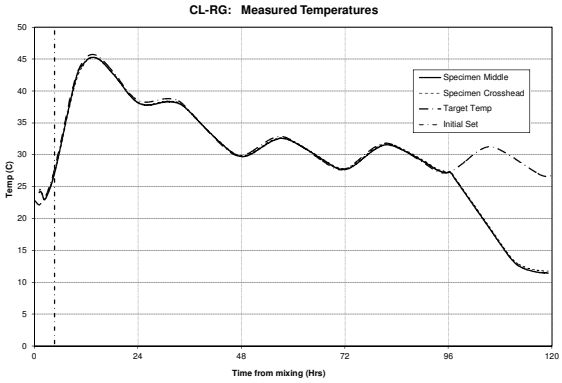

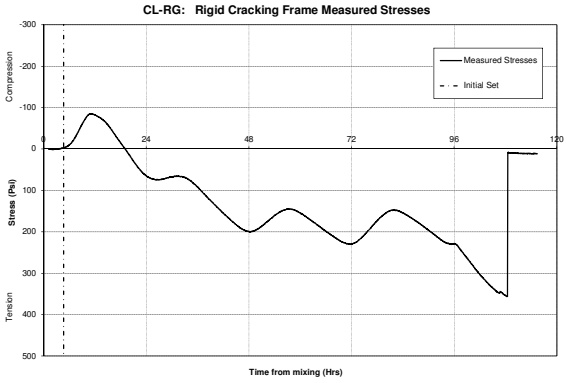

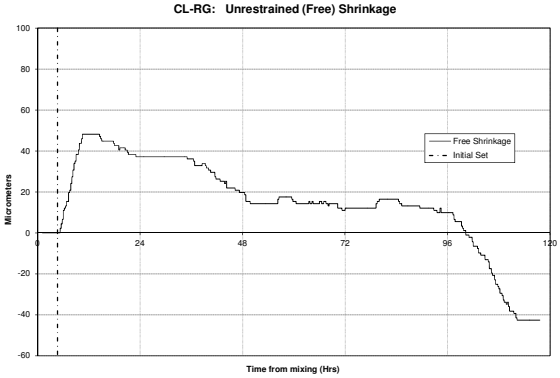

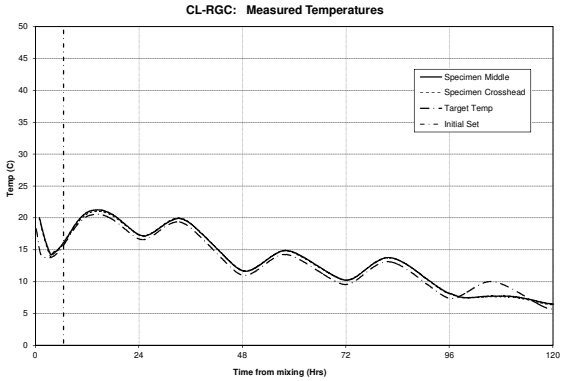
CL-RGC: Measured Temperatures
Specimen Middle
Specimen Crosshead
Target Temp
Initial Set
Temp (C)
Time from mixing (Hrs)

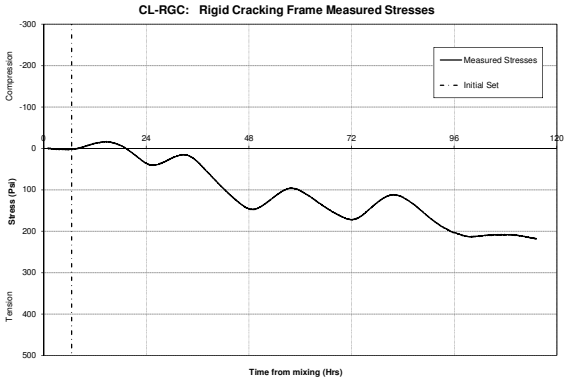
CL-RGC: Rigid Cracking Frame Measured Stresses
Measured Stresses
Initial Set
Compression
Tension
Stress (Psi)
Time from mixing (Hrs)

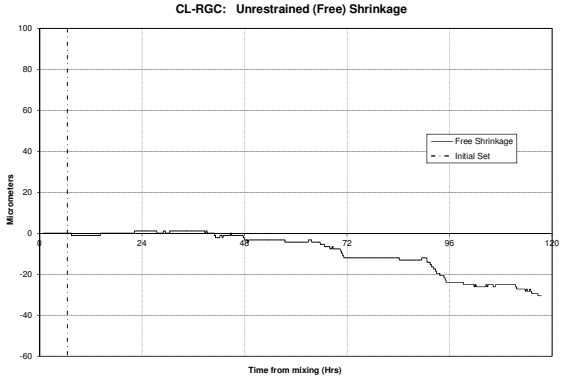
CL-RGC: Unrestrained (Free) Shrinkage
Free Shrinkage
Initial Set
Micrometers
Time from mixing (Hrs)

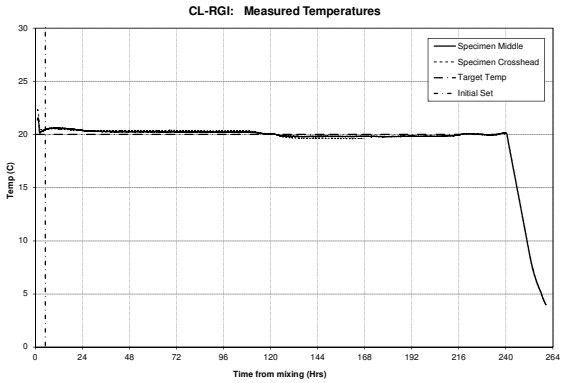
CL-RGI: Measured Temperatures
Specimen Middle
Specimen Crosshead
Target Temp
Initial Set
Temp (C)
Time from mixing (Hrs)

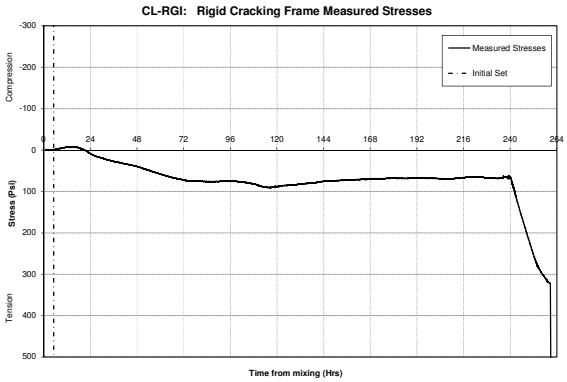
CL-RGI: Rigid Cracking Frame Measured Stresses
Measured Stresses
Initial Set
Compression
Tension
Stress (Psi)
Time from mixing (Hrs)

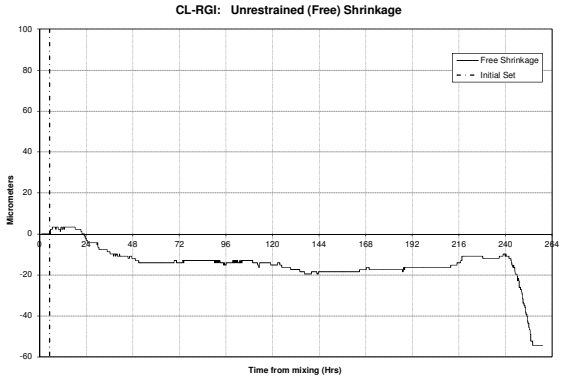
CL-RGI: Unrestrained (Free) Shrinkage
Free Shrinkage
Initial Set
Micrometers
Time from mixing (Hrs)

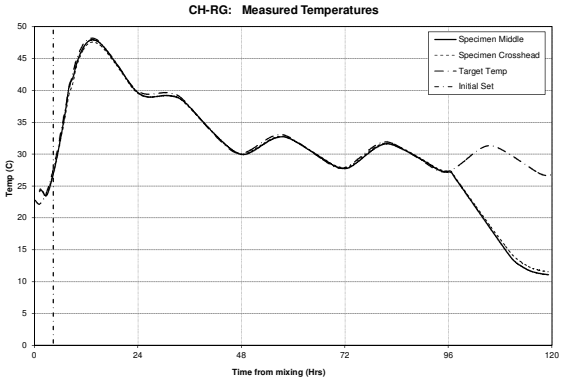
CH-RG: Measured Temperatures
Specimen Middle
Specimen Crosshead
Target Temp
Initial Set
Temp (C)
Time from mixing (Hrs)

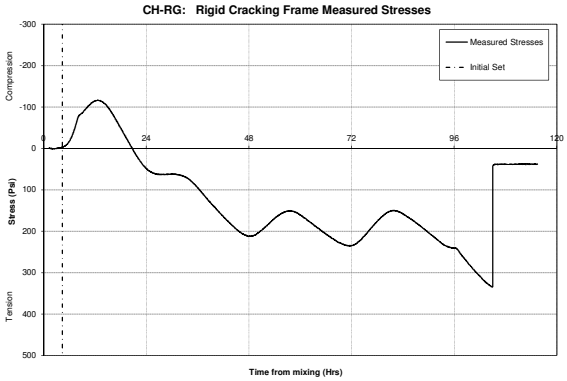
CH-RG: Rigid Cracking Frame Measured Stresses
Measured Stresses
Initial Set
Compression
Tension
Stress (Psi)
Time from mixing (Hrs)

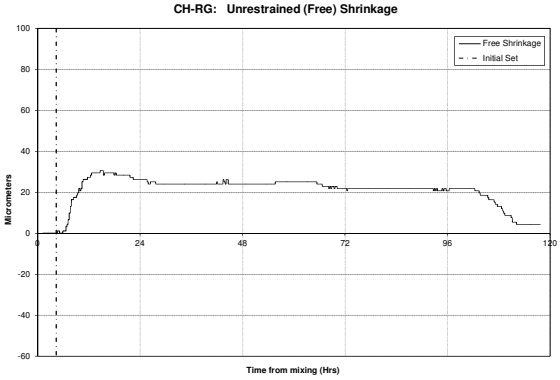
CH-RG: Unrestrained (Free) Shrinkage
Free Shrinkage
Initial Set
Micrometers
Time from mixing (Hrs)

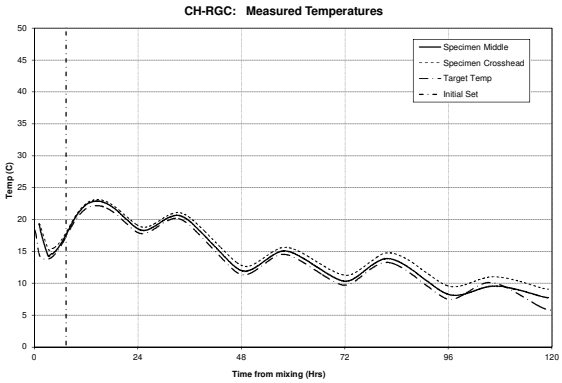
CH-RGC: Measured Temperatures
Specimen Middle
Specimen Crosshead
Target Temp
Initial Set
Temp (C)
Time from mixing (Hrs)

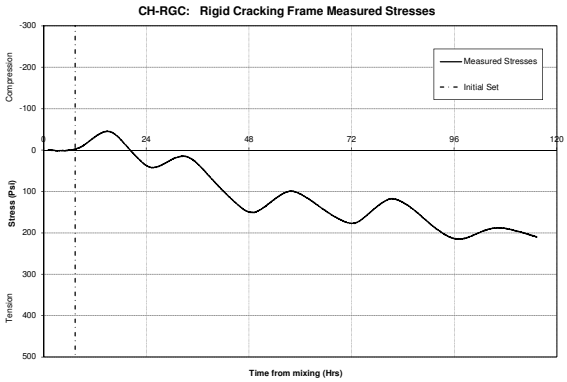
CH-RGC: Rigid Cracking Frame Measured Stresses
Measured Stresses
Initial Set
Compression
Tension
Stress (Psi)
Time from mixing (Hrs)

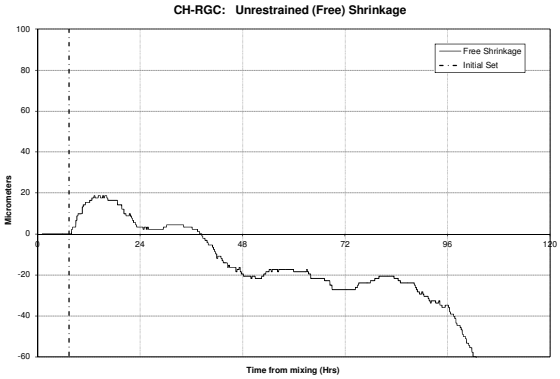
CH-RGC: Unrestrained (Free) Shrinkage
Free Shrinkage
Initial Set
Micrometers
Time from mixing (Hrs)

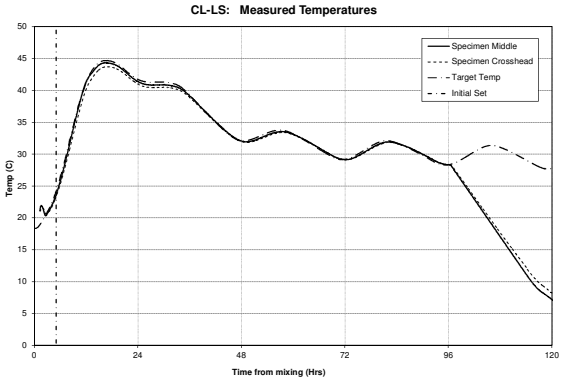
CL-LS: Measured Temperatures
Specimen Middle
Specimen Crosshead
Target Temp
Initial Set
Temp (C)
Time from mixing (Hrs)

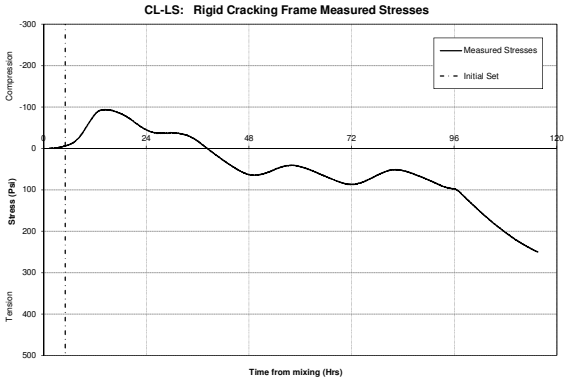
CL-LS: Rigid Cracking Frame Measured Stresses
Measured Stresses
Initial Set
Compression
Tension
Stress (Psi)
Time from mixing (Hrs)

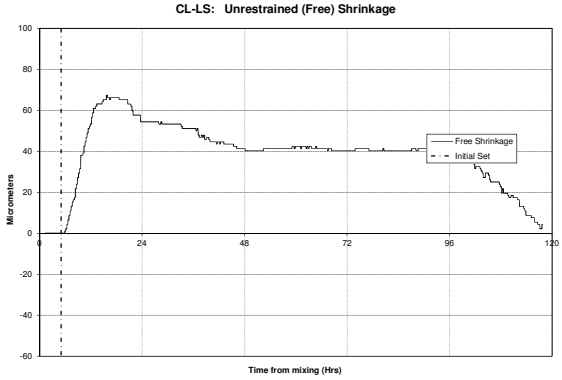
CL-LS: Unrestrained (Free) Shrinkage
Free Shrinkage
Initial Set
Micrometers
Time from mixing (Hrs)

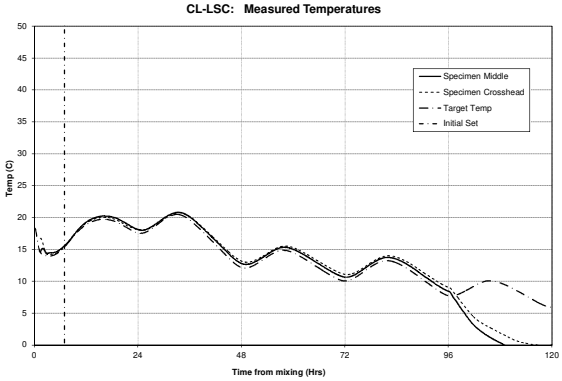
CL-LSC: Measured Temperatures
Specimen Middle
Specimen Crosshead
Target Temp
Initial Set
Temp (C)
Time from mixing (Hrs)

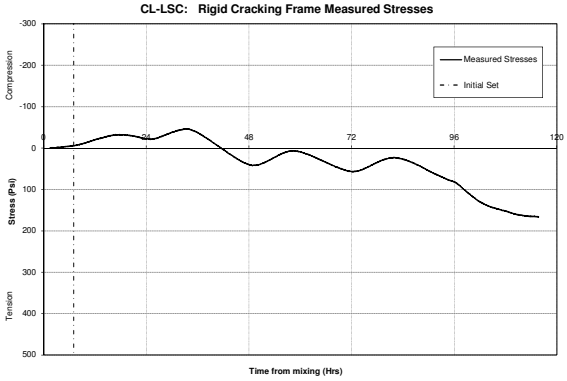
CL-LSC: Rigid Cracking Frame Measured Stresses
Measured Stresses
Initial Set
Compression
Tension
Stress (Psi)
Time from mixing (Hrs)

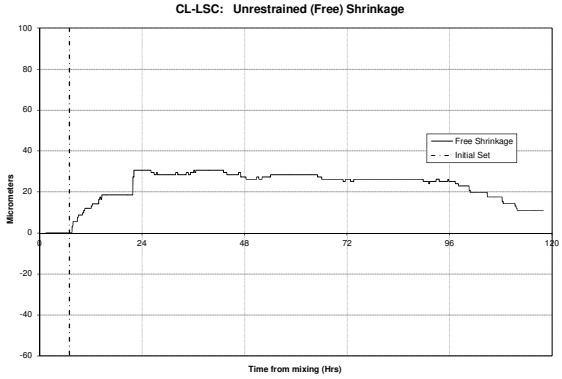
CL-LSC: Unrestrained (Free) Shrinkage
Free Shrinkage
Initial Set
Micrometers
Time from mixing (Hrs)

A.3.2 Class C Fly Ash Mixtures

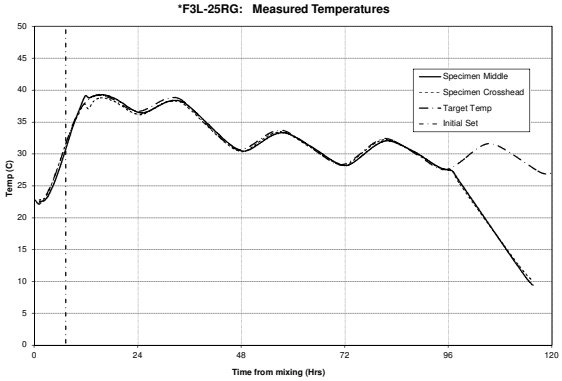

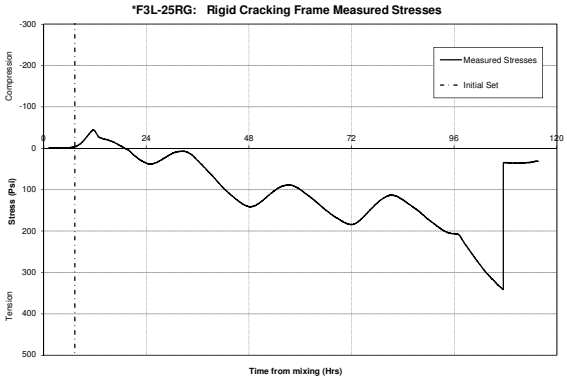

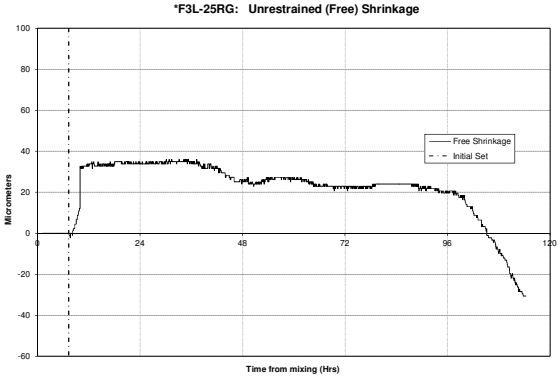

*F3L-35RG: Measured Temperatures

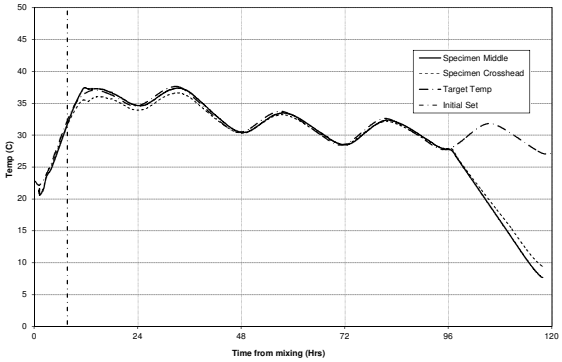

*F3L-35RG: Rigid Cracking Frame Measured Stresses

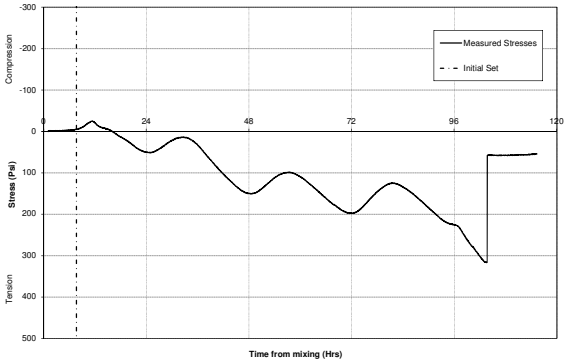

*F3L-35RG: Unrestrained (Free) Shrinkage

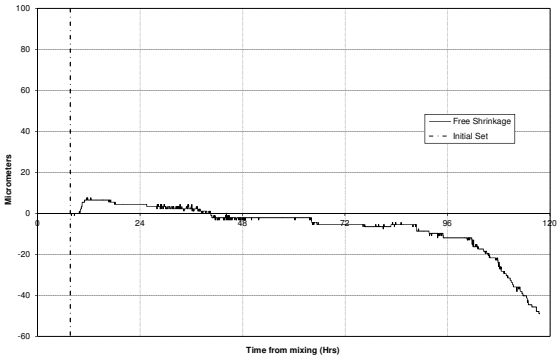

F3L-35RGC: Measured Temperatures

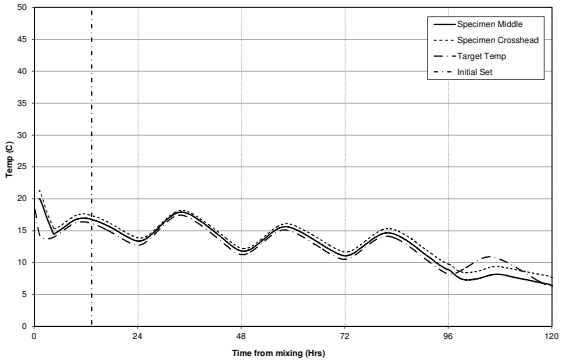

F3L-35RGC: Rigid Cracking Frame Measured Stresses

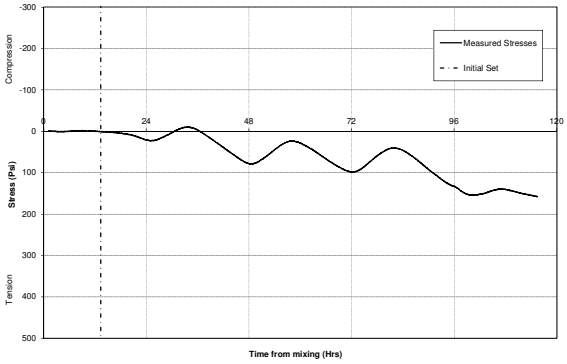

F3L-35RGC: Unrestrained (Free) Shrinkage

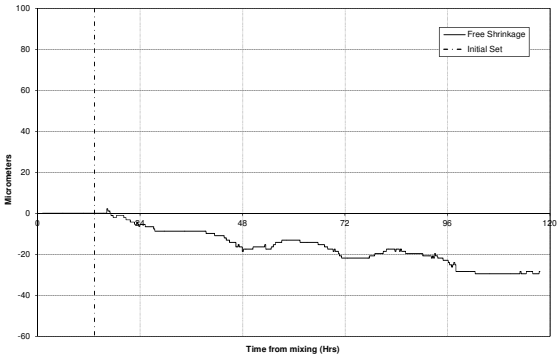

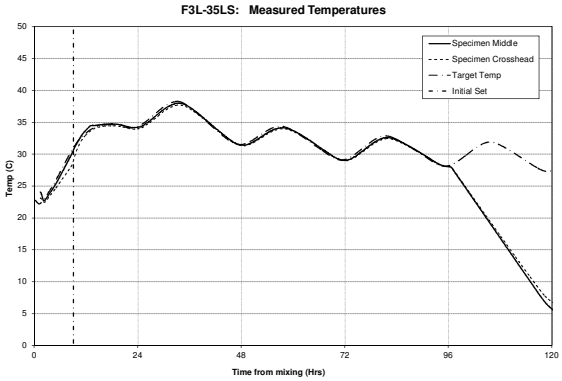
F3L-35LS: Measured Temperatures
Specimen Middle
Specimen Crosshead
Target Temp
Initial Set
Temp (C)
Time from mixing (Hrs)

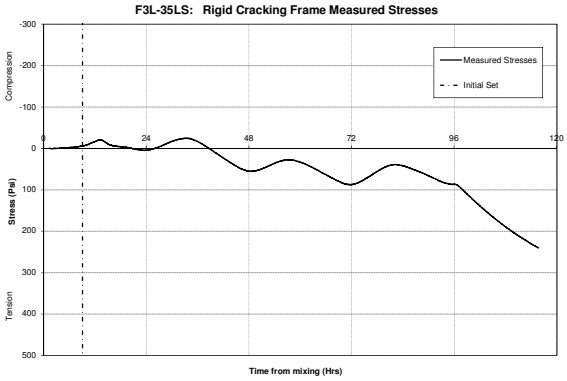
F3L-35LS: Rigid Cracking Frame Measured Stresses
Measured Stresses
Initial Set
Compression
Tension
Stress (Psi)
Time from mixing (Hrs)

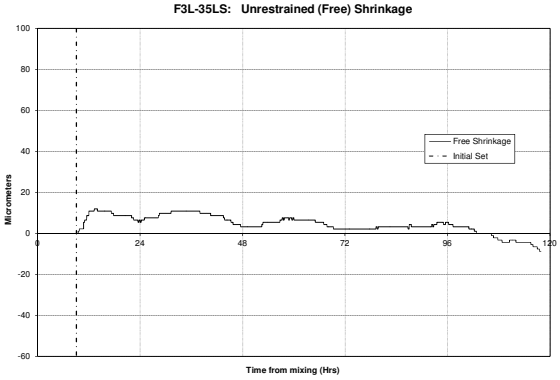
F3L-35LS: Unrestrained (Free) Shrinkage
Free Shrinkage
Initial Set
Micrometers
Time from mixing (Hrs)

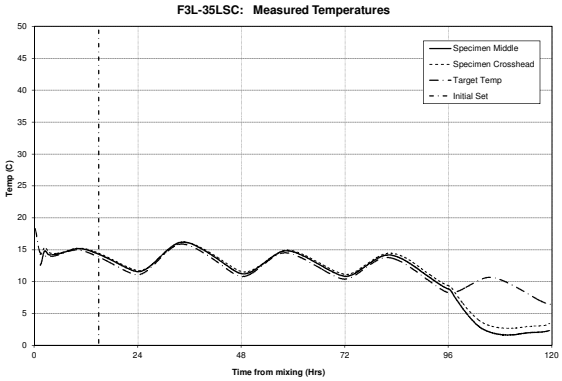
F3L-35LSC: Measured Temperatures
Specimen Middle
Specimen Crosshead
Target Temp
Initial Set
Temp (C)
Time from mixing (Hrs)

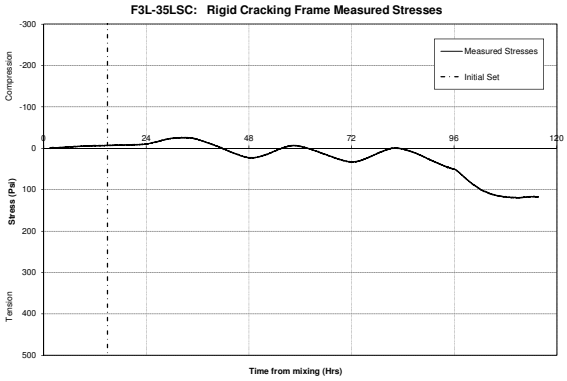
F3L-35LSC: Rigid Cracking Frame Measured Stresses
Measured Stresses
Initial Set
Compression
Tension
Stress (Psi)
Time from mixing (Hrs)

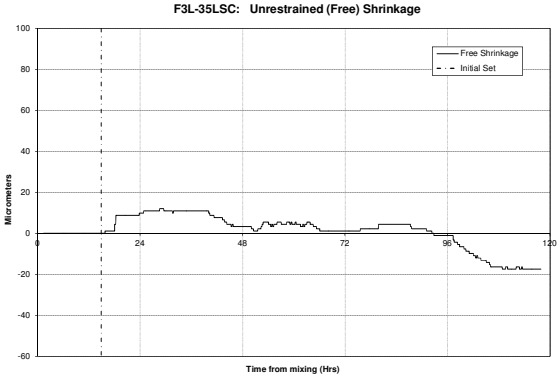
F3L-35LSC: Unrestrained (Free) Shrinkage
Free Shrinkage
Initial Set
Micrometers
Time from mixing (Hrs)

*F4L-25RG: Measured Temperatures

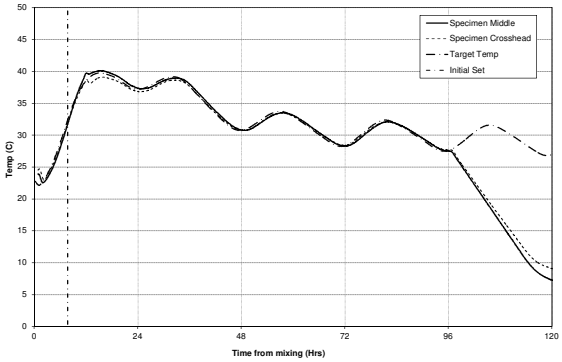

*F4L-25RG: Rigid Cracking Frame Measured Stresses

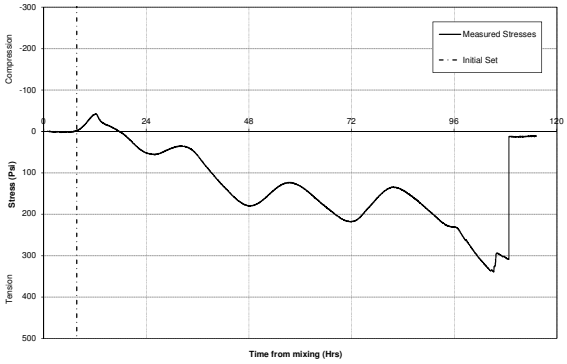

*F4L-25RG: Unrestrained (Free) Shrinkage

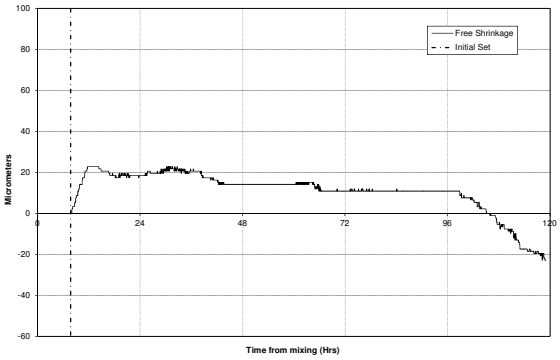

F4L-35RGC: Measured Temperatures

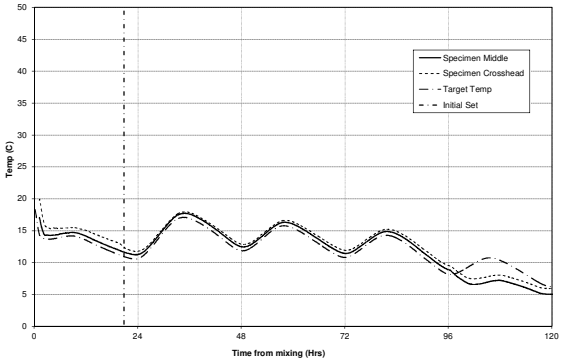

F4L-35RGC: Rigid Cracking Frame Measured Stresses

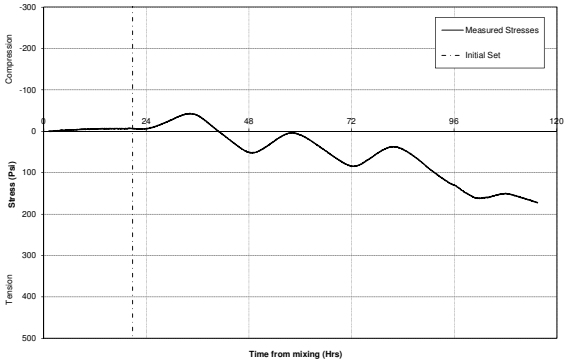

F4L-35RGC: Unrestrained (Free) Shrinkage

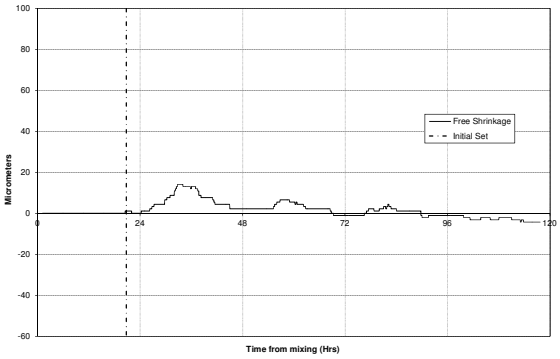

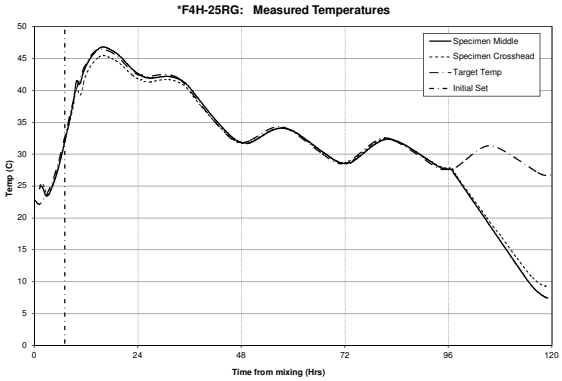
*F4H-25RG: Measured Temperatures
Specimen Middle
Specimen Crosshead
Target Temp
Initial Set
Temp (C)
Time from mixing (Hrs)

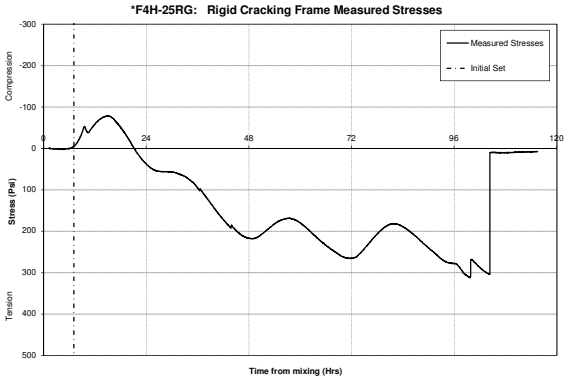
*F4H-25RG: Rigid Cracking Frame Measured Stresses
Measured Stresses
Initial Set
Compression
Tension
Stress (Psi)
Time from mixing (Hrs)

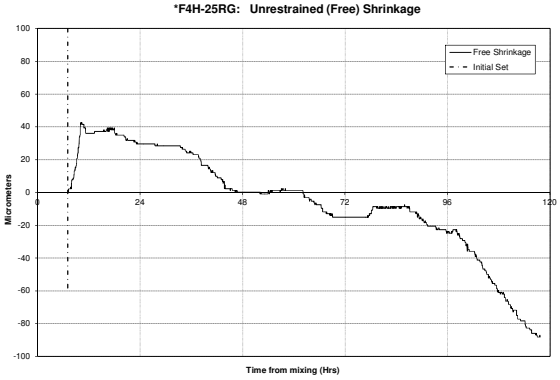
*F4H-25RG: Unrestrained (Free) Shrinkage
Free Shrinkage
Initial Set
Micrometers
Time from mixing (Hrs)

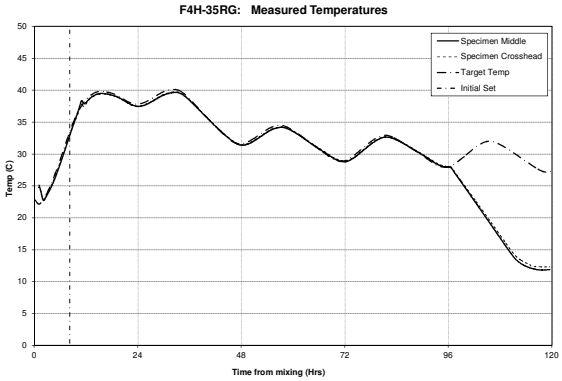
F4H-35RG: Measured Temperatures
Specimen Middle
Specimen Crosshead
Target Temp
Initial Set
Temp (C)
Time from mixing (Hrs)

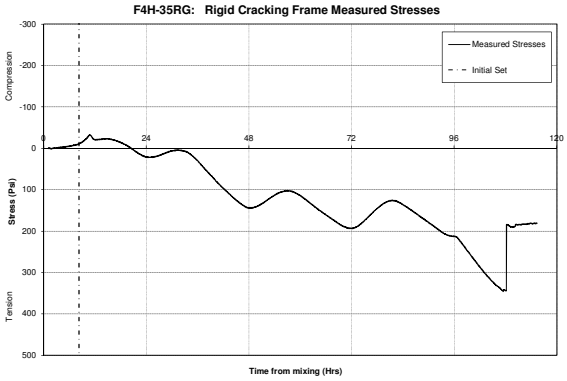
F4H-35RG: Rigid Cracking Frame Measured Stresses
Measured Stresses
Initial Set
Compression
Tension
Stress (Psi)
Time from mixing (Hrs)

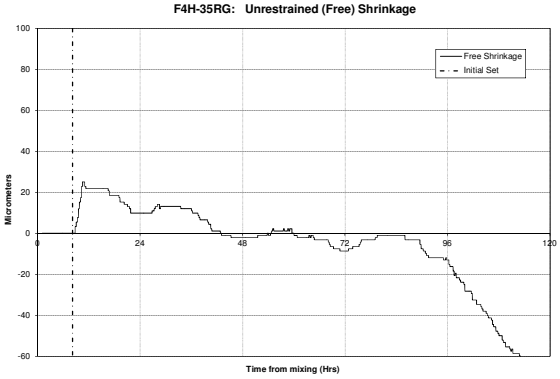
F4H-35RG: Unrestrained (Free) Shrinkage
Free Shrinkage
Initial Set
Micrometers
Time from mixing (Hrs)

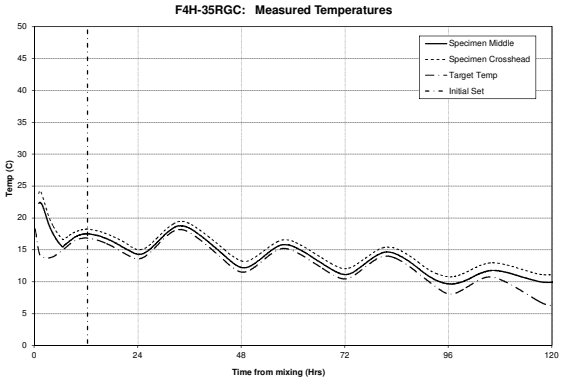
F4H-35RGC: Measured Temperatures
Specimen Middle
Specimen Crosshead
Target Temp
Initial Set
Temp (C)
Time from mixing (Hrs)

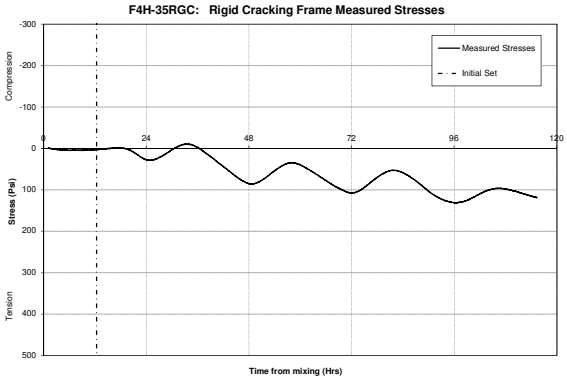
F4H-35RGC: Rigid Cracking Frame Measured Stresses
Measured Stresses
Initial Set
Compression
Tension
Stress (Psi)
Time from mixing (Hrs)

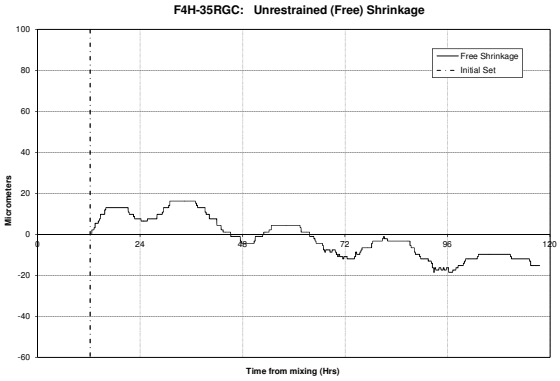
F4H-35RGC: Unrestrained (Free) Shrinkage
Free Shrinkage
Initial Set
Micrometers
Time from mixing (Hrs)

A.3.3 Class F Fly Ash Mixtures

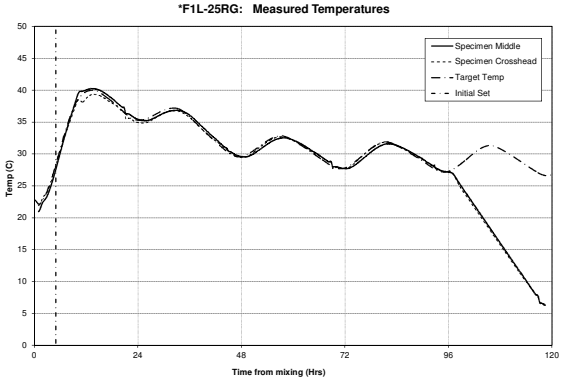

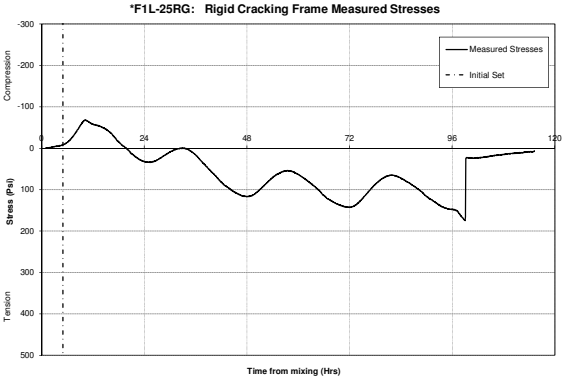

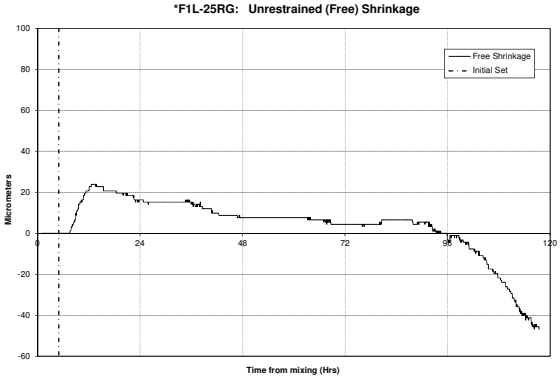

F1L-25RGC: Measured Temperatures

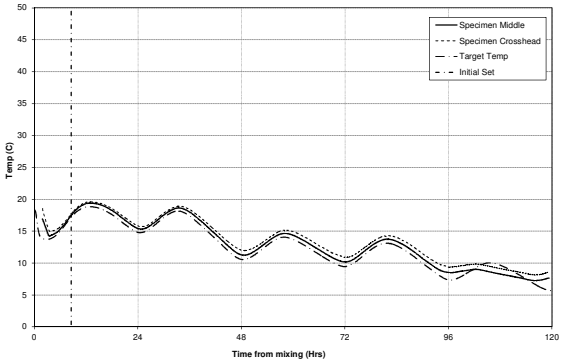

F1L-25RGC: Rigid Cracking Frame Measured Stresses

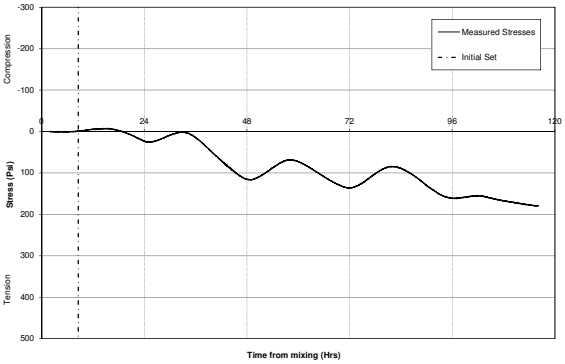

F1L-25RGC: Unrestrained (Free) Shrinkage

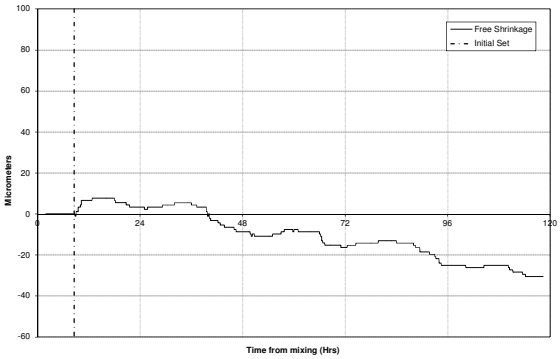

***F1H-25RG: Measured Temperatures**

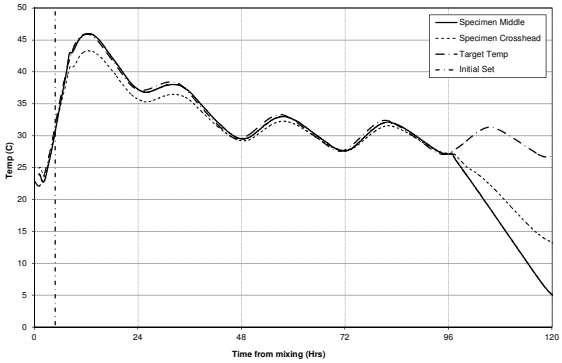

***F1H-25RG: Rigid Cracking Frame Measured Stresses**

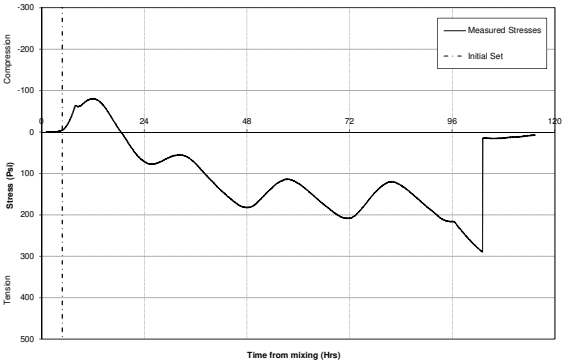

***F1H-25RG: Unrestrained (Free) Shrinkage**

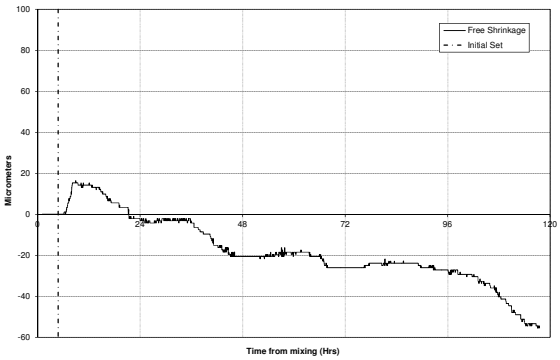

F1H-25RGC: Measured Temperatures

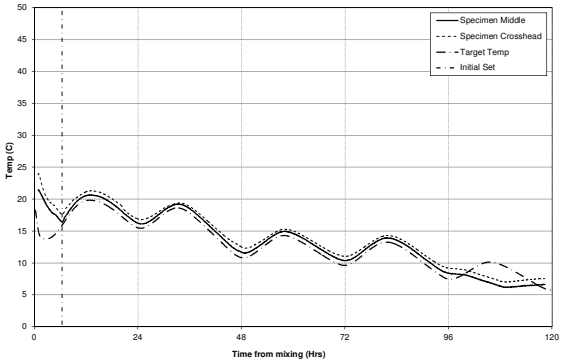

F1H-25RGC: Rigid Cracking Frame Measured Stresses

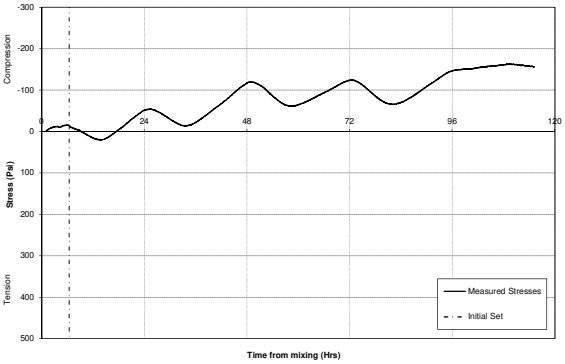

F1H-25RGC: Unrestrained (Free) Shrinkage

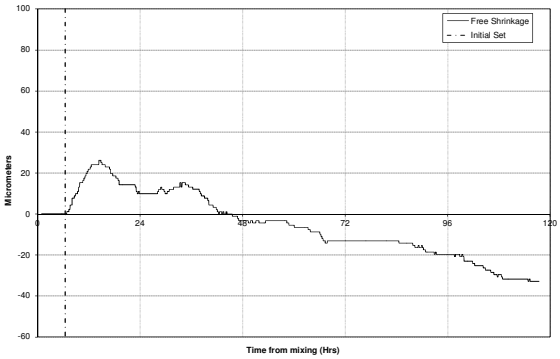

***F2L-25RG: Measured Temperatures**

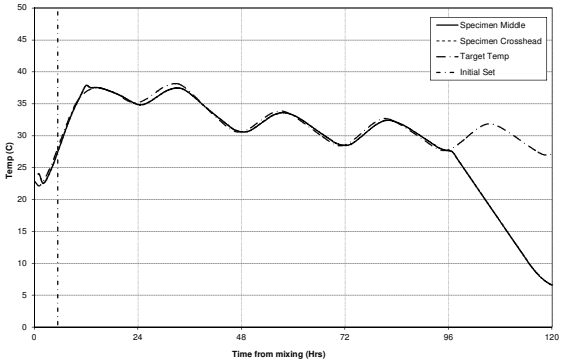

***F2L-25RG: Rigid Cracking Frame Measured Stresses**

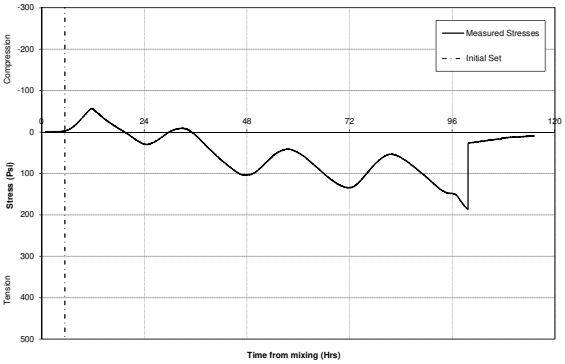

***F2L-25RG: Unrestrained (Free) Shrinkage**

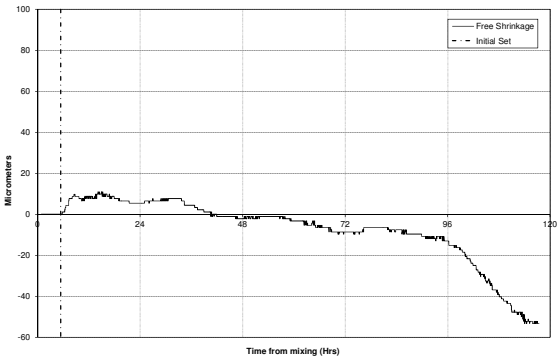

F2L-25RGC: Measured Temperatures

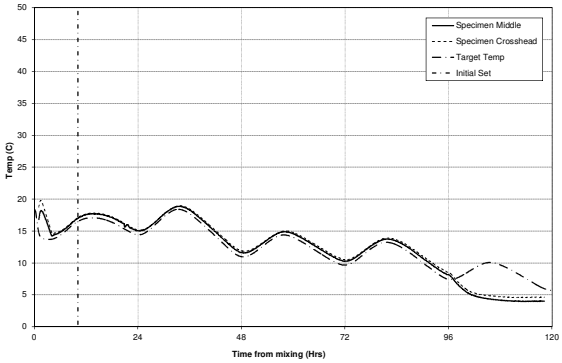

F2L-25RGC: Rigid Cracking Frame Measured Stresses

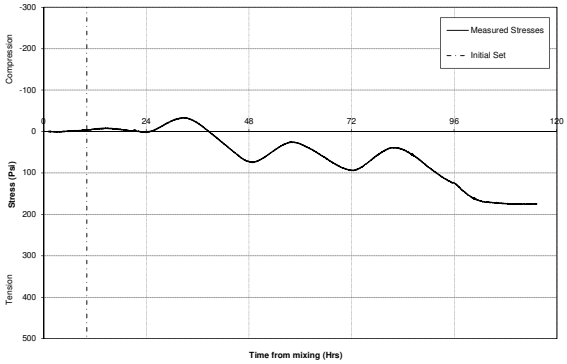

F2L-25RGC: Unrestrained (Free) Shrinkage

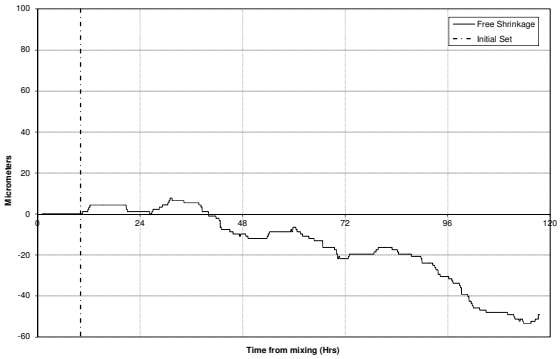

*F2L-35RG: Measured Temperatures

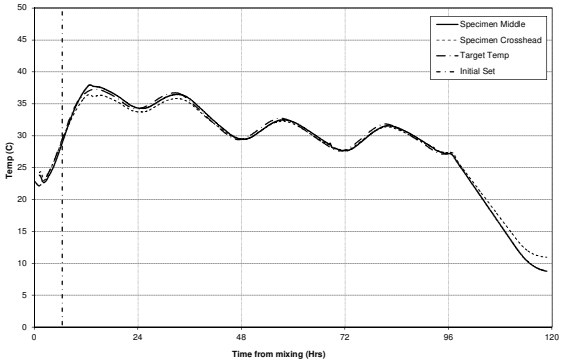

*F2L-35RG: Rigid Cracking Frame Measured Stresses

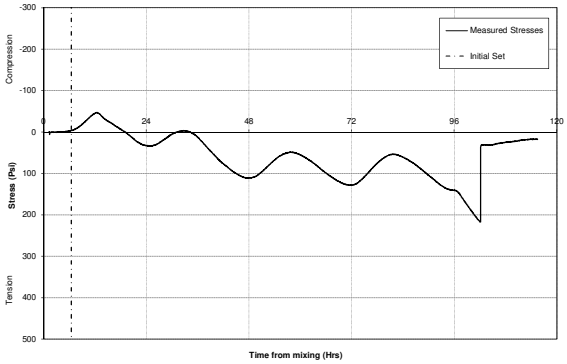

*F2L-35RG: Unrestrained (Free) Shrinkage

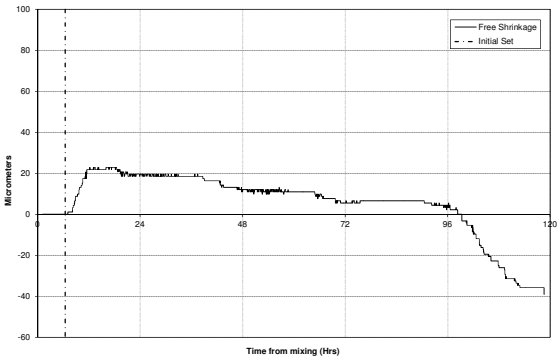

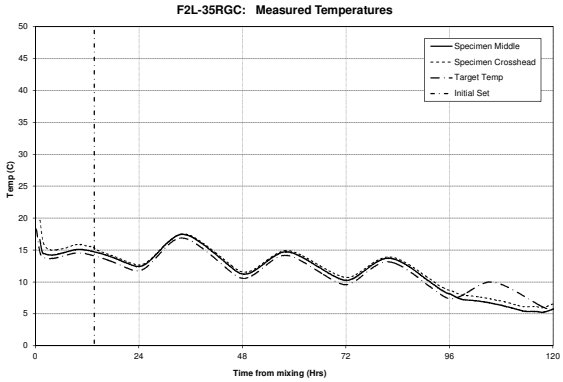
F2L-35RGC: Measured Temperatures
Specimen Middle
Specimen Crosshead
Target Temp
Initial Set
Temp (C)
Time from mixing (Hrs)

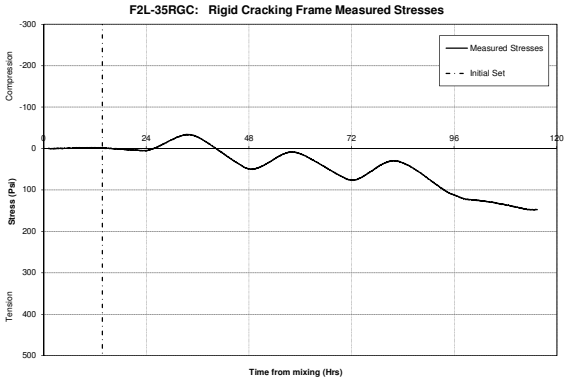
F2L-35RGC: Rigid Cracking Frame Measured Stresses
Measured Stresses
Initial Set
Compression
Tension
Stress (Psi)
Time from mixing (Hrs)

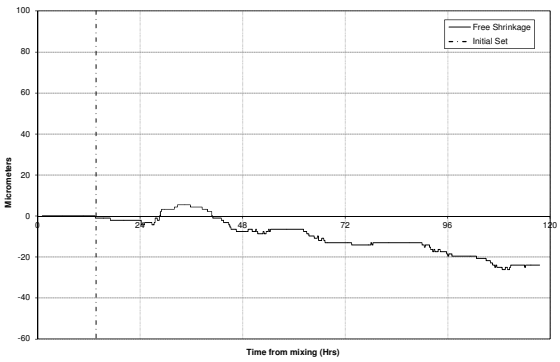
F2L-35RGC: Unrestrained (Free) Shrinkage
Free Shrinkage
Initial Set
Micrometers
Time from mixing (Hrs)

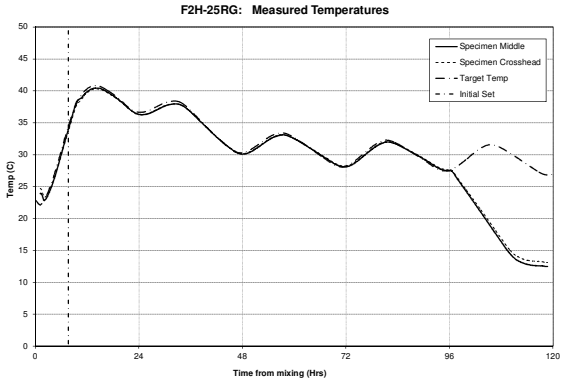
F2H-25RG: Measured Temperatures
Specimen Middle
Specimen Crosshead
Target Temp
Initial Set
Temp (C)
Time from mixing (Hrs)

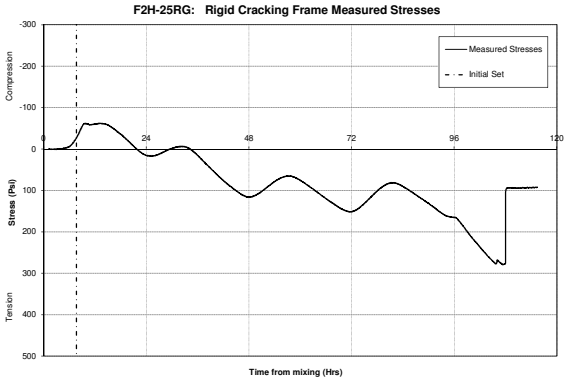
F2H-25RG: Rigid Cracking Frame Measured Stresses
Measured Stresses
Initial Set
Compression
Tension
Stress (Psi)
Time from mixing (Hrs)

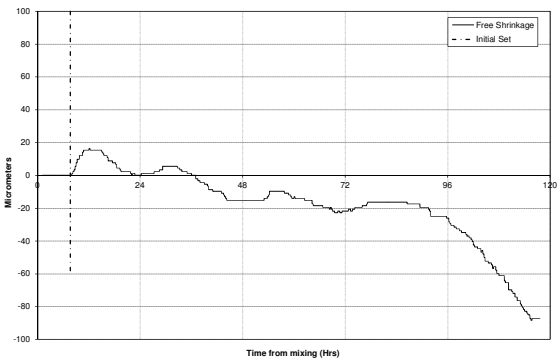
F2H-25RG: Unrestrained (Free) Shrinkage
Free Shrinkage
Initial Set
Micrometers
Time from mixing (Hrs)

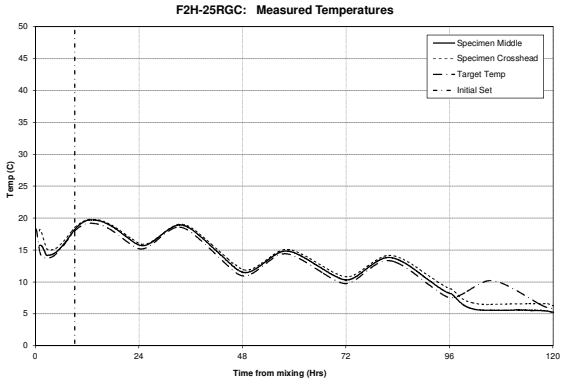
F2H-25RGC: Measured Temperatures
Specimen Middle
Specimen Crosshead
Target Temp
Initial Set
Temp (C)
Time from mixing (Hrs)

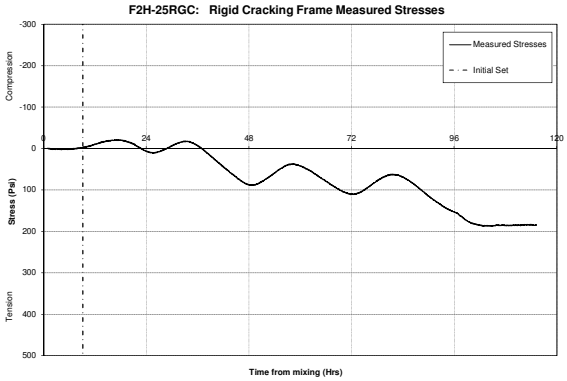
F2H-25RGC: Rigid Cracking Frame Measured Stresses
Measured Stresses
Initial Set
Compression
Tension
Stress (Psi)
Time from mixing (Hrs)

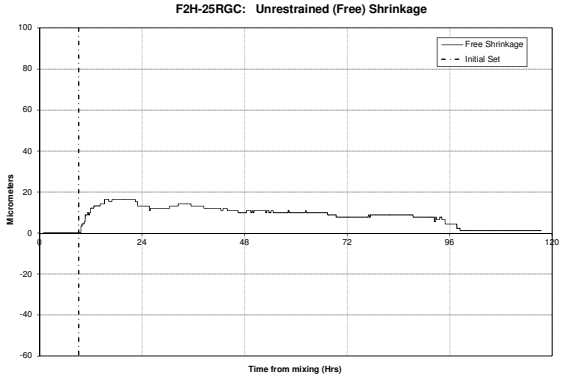
F2H-25RGC: Unrestrained (Free) Shrinkage
Free Shrinkage
Initial Set
Micrometers
Time from mixing (Hrs)

A.3.4 GGBFS Mixtures

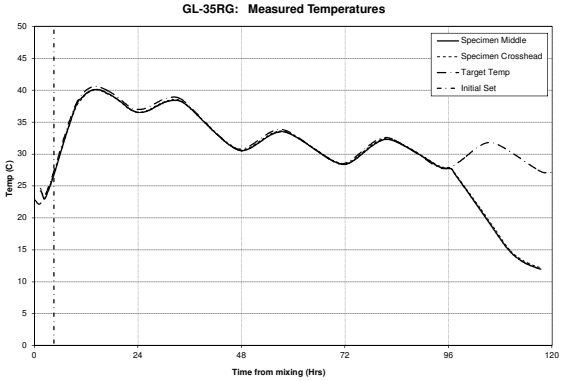

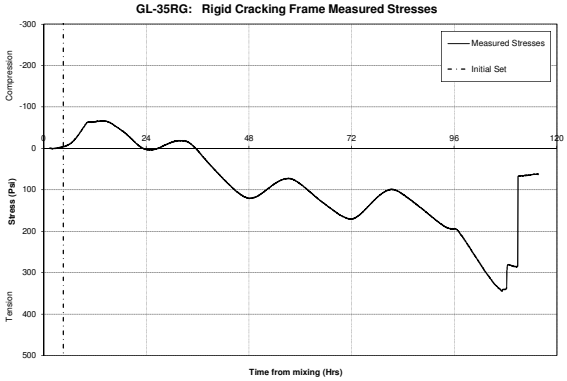

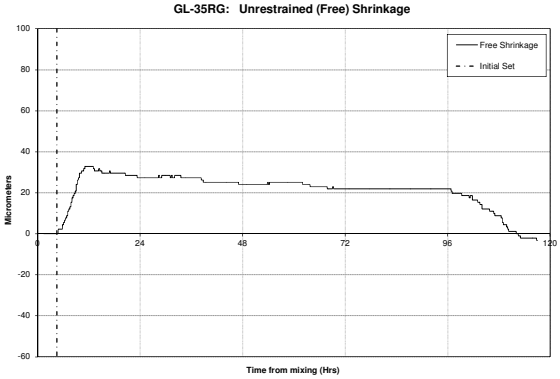

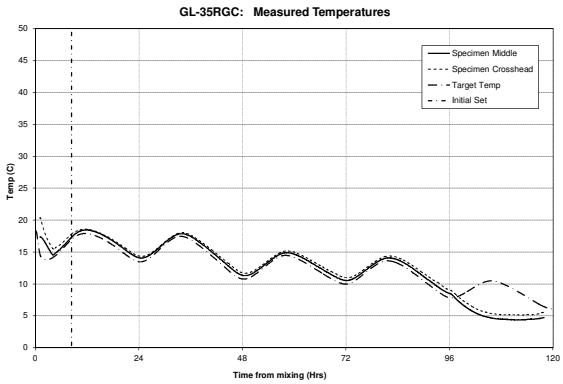
GL-35RGC: Measured Temperatures
Specimen Middle
Specimen Crosshead
Target Temp
Initial Set
Temp (C)
Time from mixing (Hrs)

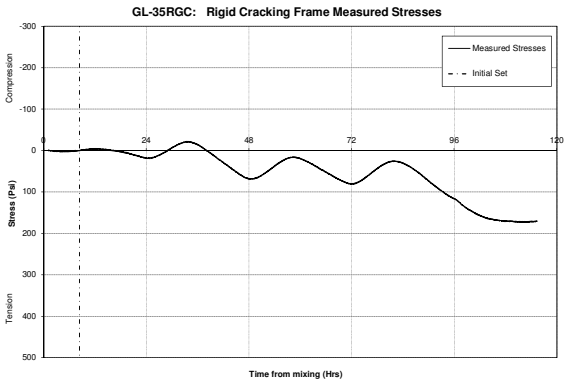
GL-35RGC: Rigid Cracking Frame Measured Stresses
Measured Stresses
Initial Set
Compression
Tension
Stress (Psi)
Time from mixing (Hrs)

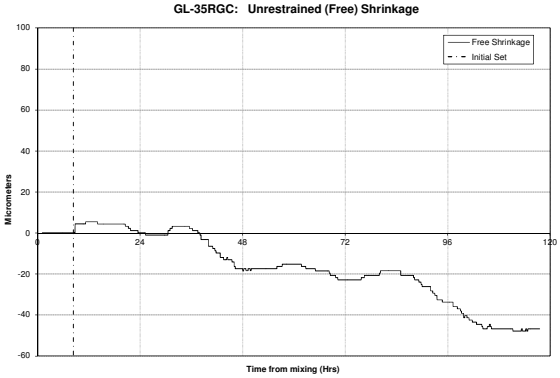
GL-35RGC: Unrestrained (Free) Shrinkage
Free Shrinkage
Initial Set
Micrometers
Time from mixing (Hrs)

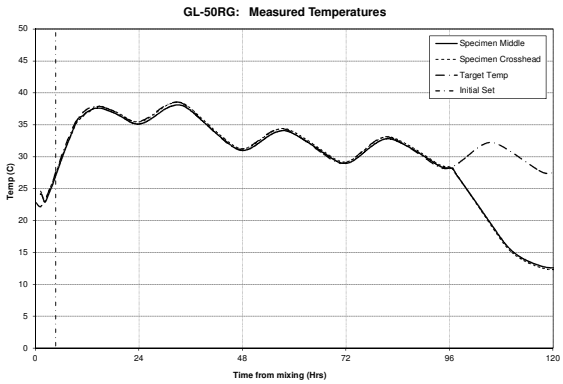
GL-50RG: Measured Temperatures
Specimen Middle
Specimen Crosshead
Target Temp
Initial Set
Temp (C)
Time from mixing (Hrs)

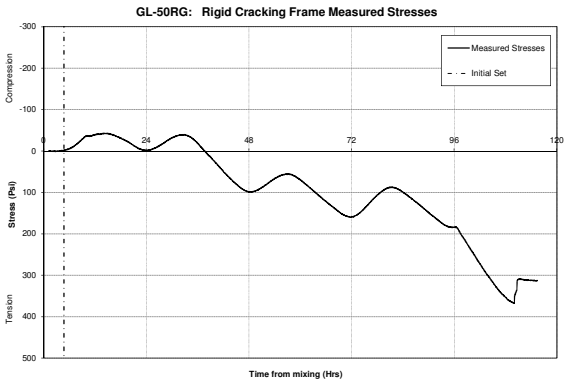
GL-50RG: Rigid Cracking Frame Measured Stresses
Measured Stresses
Initial Set
Compression
Tension
Stress (Psi)
Time from mixing (Hrs)

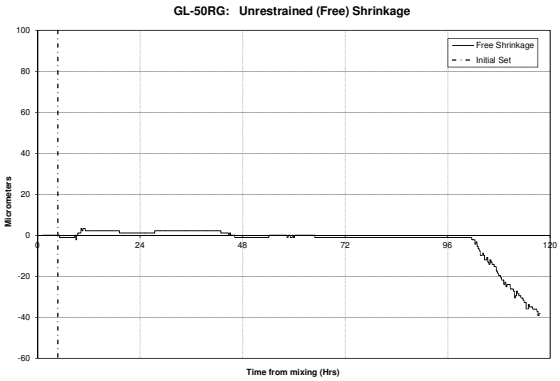
GL-50RG: Unrestrained (Free) Shrinkage
Free Shrinkage
Initial Set
Micrometers
Time from mixing (Hrs)

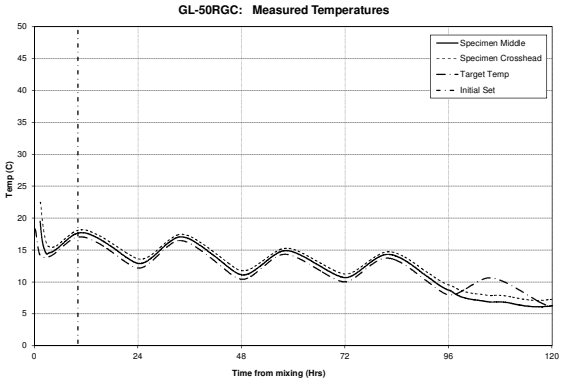
GL-50RGC: Measured Temperatures
Specimen Middle
Specimen Crosshead
Target Temp
Initial Set
Temp (C)
Time from mixing (Hrs)

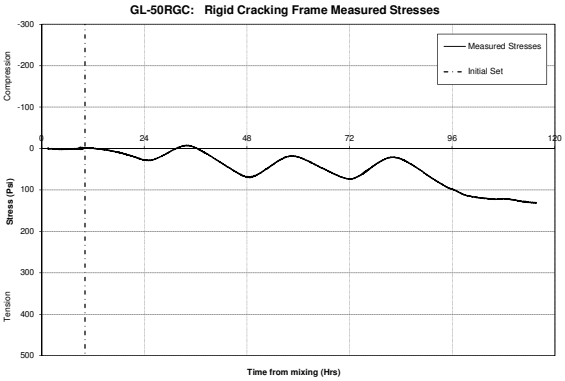
GL-50RGC: Rigid Cracking Frame Measured Stresses
Measured Stresses
Initial Set
Compression
Tension
Stress (Psi)
Time from mixing (Hrs)

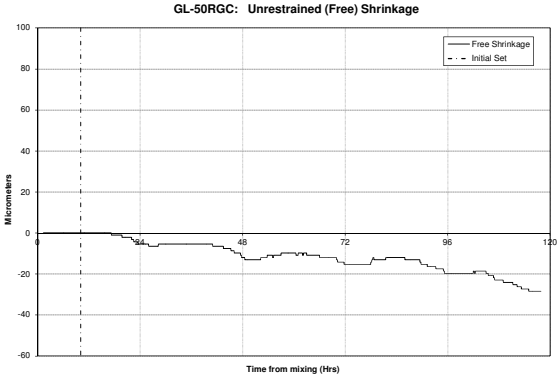
GL-50RGC: Unrestrained (Free) Shrinkage
Free Shrinkage
Initial Set
Micrometers
Time from mixing (Hrs)

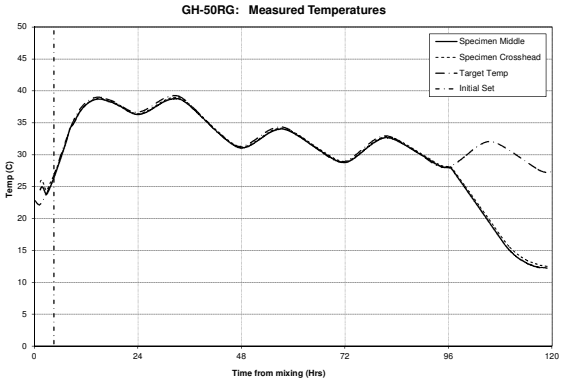
GH-50RG: Measured Temperatures
Specimen Middle
Specimen Crosshead
Target Temp
Initial Set
Temp (C)
Time from mixing (Hrs)

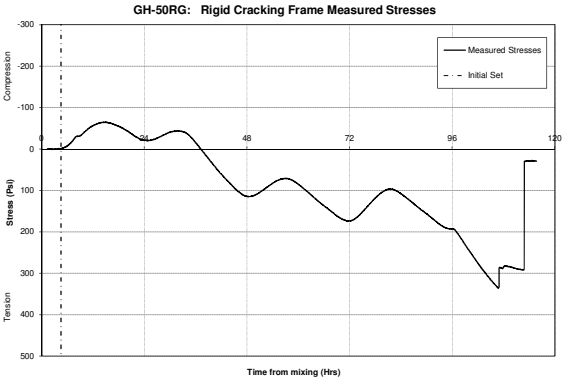
GH-50RG: Rigid Cracking Frame Measured Stresses
Measured Stresses
Initial Set
Compression
Tension
Stress (Psi)
Time from mixing (Hrs)

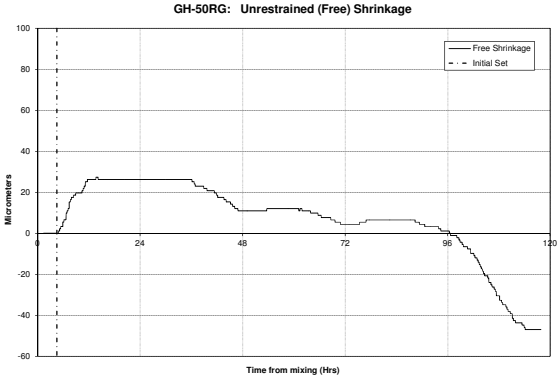
GH-50RG: Unrestrained (Free) Shrinkage
Free Shrinkage
Initial Set
Micrometers
Time from mixing (Hrs)

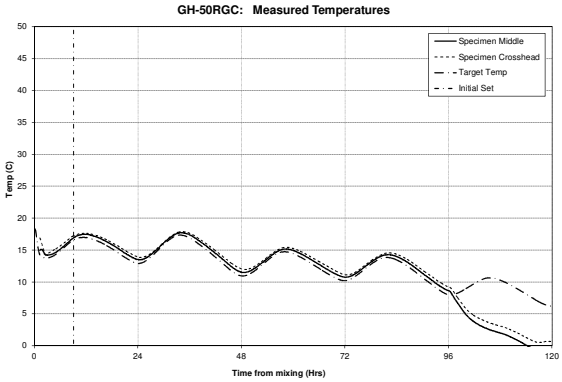
GH-50RGC: Measured Temperatures
Specimen Middle
Specimen Crosshead
Target Temp
Initial Set
Temp (C)
Time from mixing (Hrs)

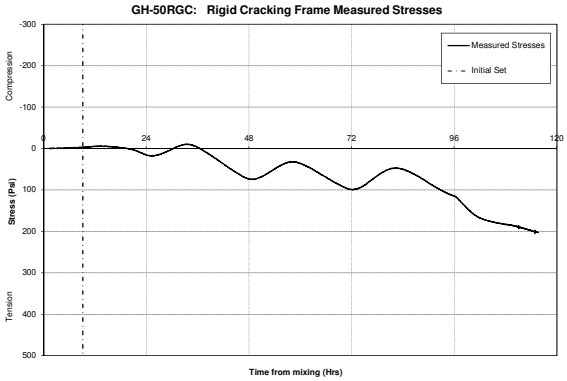
GH-50RGC: Rigid Cracking Frame Measured Stresses
Measured Stresses
Initial Set
Compression
Tension
Stress (Psi)
Time from mixing (Hrs)

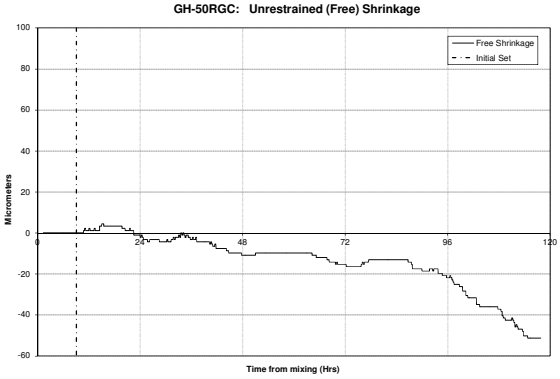
GH-50RGC: Unrestrained (Free) Shrinkage
Free Shrinkage
Initial Set
Micrometers
Time from mixing (Hrs)

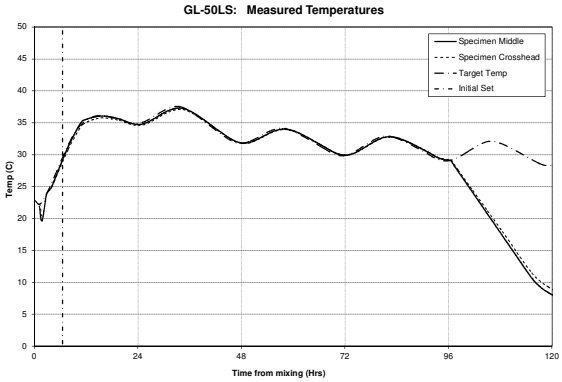
GL-50LS: Measured Temperatures
Specimen Middle
Specimen Crosshead
Target Temp
Initial Set
Temp (C)
Time from mixing (Hrs)

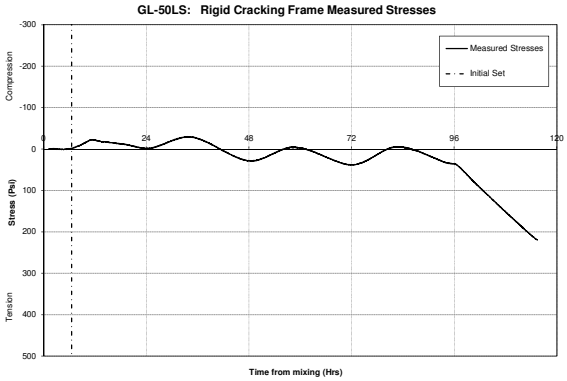
GL-50LS: Rigid Cracking Frame Measured Stresses
Measured Stresses
Initial Set
Compression
Tension
Stress (Psi)
Time from mixing (Hrs)

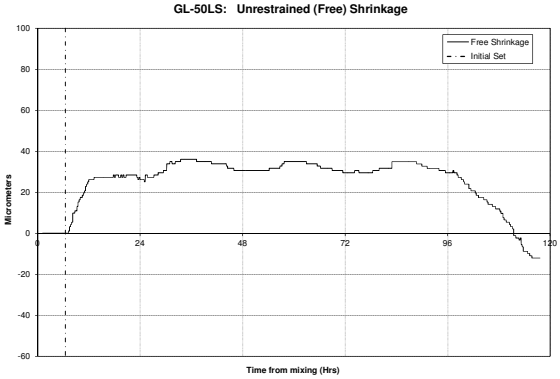
GL-50LS: Unrestrained (Free) Shrinkage
Free Shrinkage
Initial Set
Micrometers
Time from mixing (Hrs)

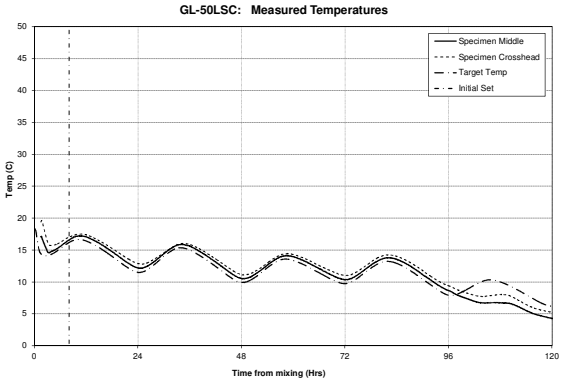
GL-50LSC: Measured Temperatures
Specimen Middle
Specimen Crosshead
Target Temp
Initial Set
Temp (C)
Time from mixing (Hrs)

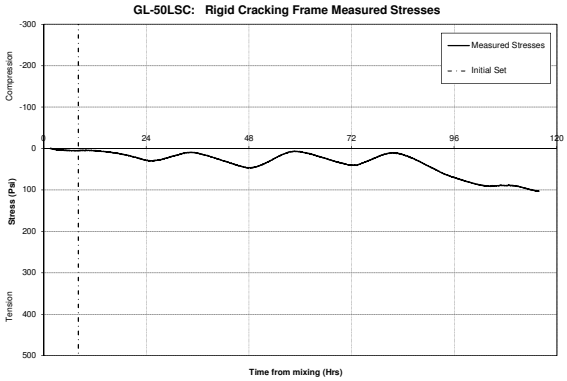
GL-50LSC: Rigid Cracking Frame Measured Stresses
Measured Stresses
Initial Set
Compression
Tension
Stress (Psi)
Time from mixing (Hrs)

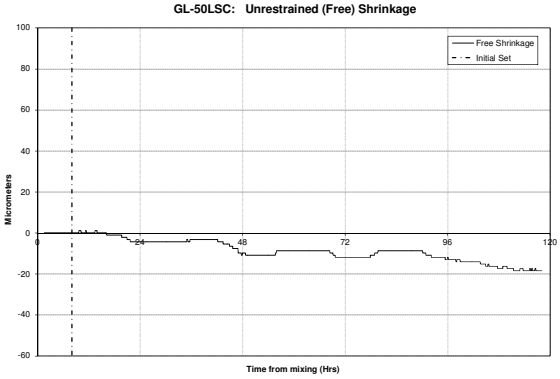
GL-50LSC: Unrestrained (Free) Shrinkage
Free Shrinkage
Initial Set
Micrometers
Time from mixing (Hrs)

A.3.5 Other Mixtures

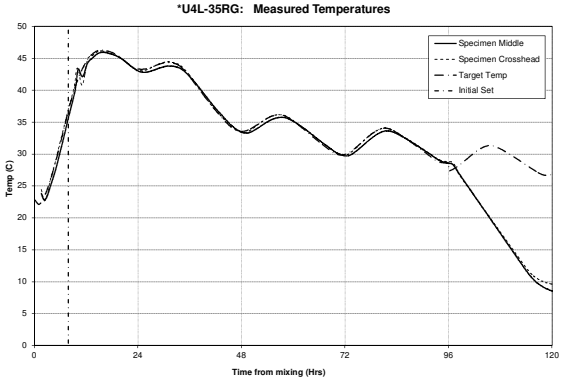

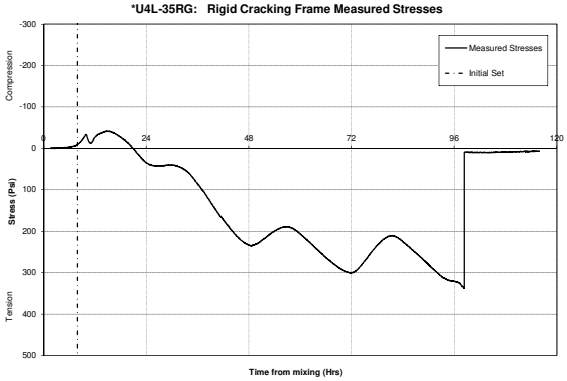

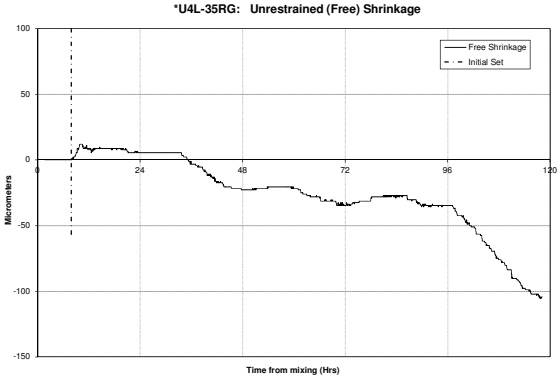

U4L-35RGC: Measured Temperatures

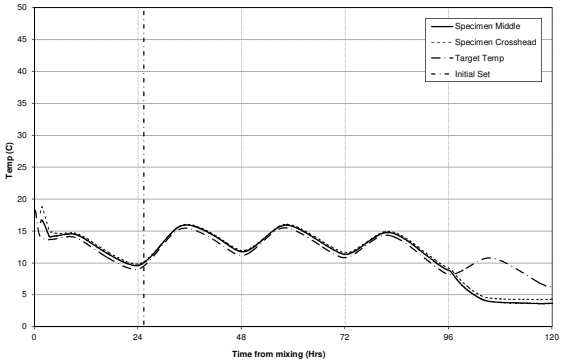

U4L-35RGC: Rigid Cracking Frame Measured Stresses

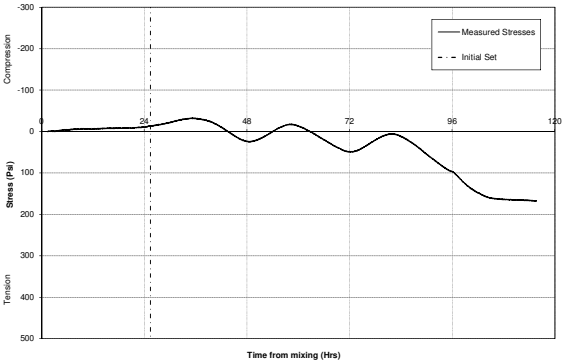

U4L-35RGC: Unrestrained (Free) Shrinkage

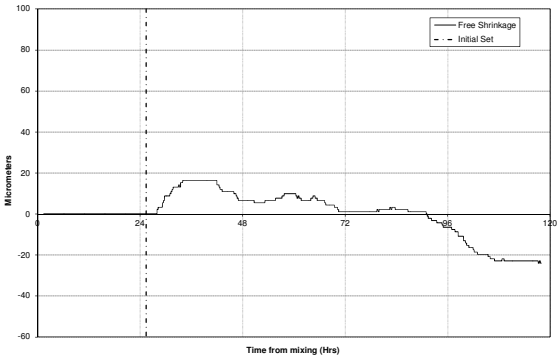

SL-RG: Measured Temperatures

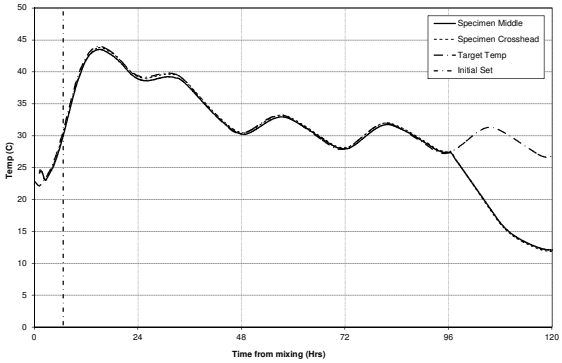

SL-RG: Rigid Cracking Frame Measured Stresses

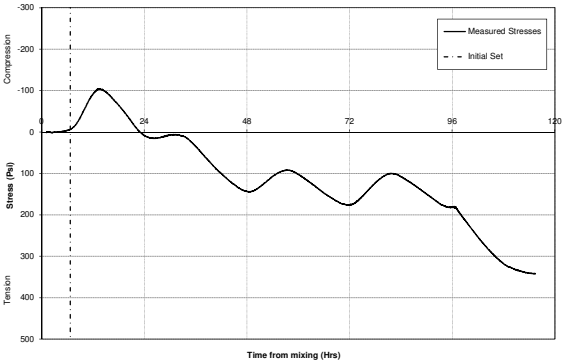

SL-RG: Unrestrained (Free) Shrinkage

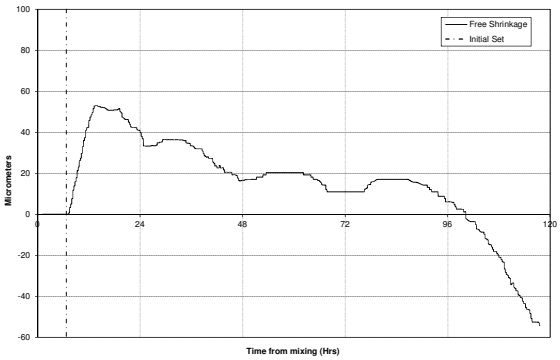

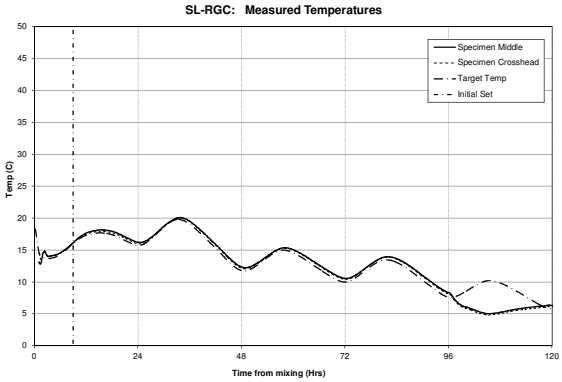
SL-RGC: Measured Temperatures
Specimen Middle
Specimen Crosshead
Target Temp
Initial Set
Temp (C)
Time from mixing (Hrs)

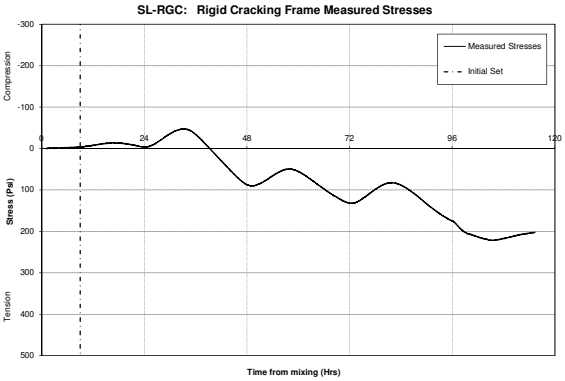
SL-RGC: Rigid Cracking Frame Measured Stresses
Measured Stresses
Initial Set
Compression
Tension
Stress (Psi)
Time from mixing (Hrs)

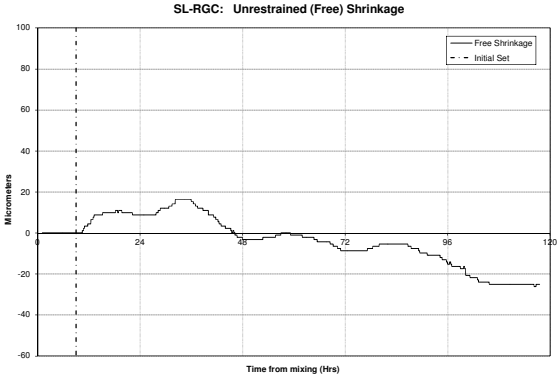
SL-RGC: Unrestrained (Free) Shrinkage
Free Shrinkage
Initial Set
Micrometers
Time from mixing (Hrs)

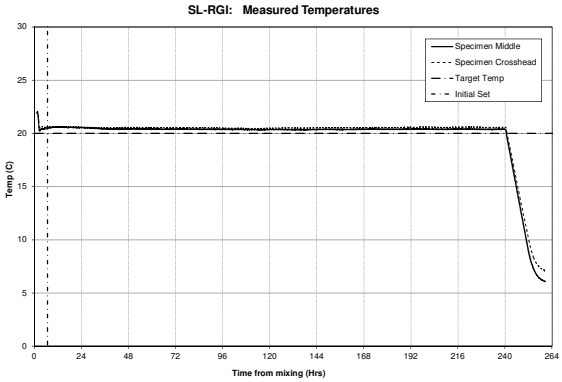
SL-RGI: Measured Temperatures
Specimen Middle
Specimen Crosshead
Target Temp
Initial Set
Temp (C)
Time from mixing (Hrs)

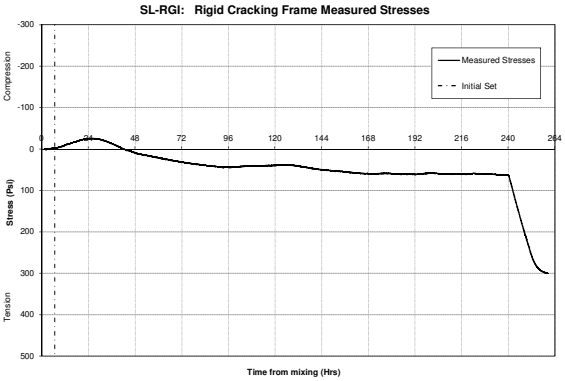
SL-RGI: Rigid Cracking Frame Measured Stresses
Measured Stresses
Initial Set
Compression
Tension
Stress (Psi)
Time from mixing (Hrs)

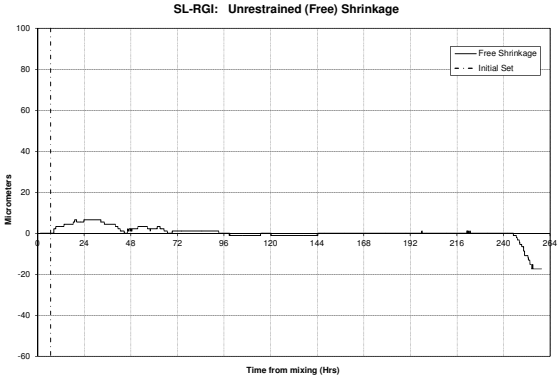
SL-RGI: Unrestrained (Free) Shrinkage
Free Shrinkage
Initial Set
Micrometers
Time from mixing (Hrs)

Appendix B: Bridge Deck Instrumentation

B.1 San Antonio Bridge Deck

B.1.1 iButton String Locations and Placement Times

Locations for this instrumentation, provided in Table B-64, were taken from the West face of the bridge deck. The placement times, as determined from examination of the iButton temperatures, is presented in Table B-65.

Table B-64: iButton string locations- SABD

String	Distance from West face of bridge deck
A1	13.9
B2	16.5
B3	12.9
C1	24.4
C2	13.1
C3	9.6
D1	13.1

All values in feet

Table B-65: Concrete placement times- SABD

Strand	Placement Time
A	7/19/09 9:43 PM
B	7/19/09 10:07 PM
C	7/19/09 11:38 PM
D	7/20/09 1:40 AM

B.1.2 iButton Depths

Table B-66 provides the heights of the iButtons measured from either the steel pan formwork, or the top of the steel girder. While the exact depth of the bridge deck is not known, it is assumed that concrete sections are 8" thick over the steel pan formwork,

and 11.5” thick over the steel girders. Descriptions of the iButton strings are also provided.

Table B-66: iButton depths- SABD

Location	String	Buttons	Height from bottom
Beginning of pour, between girders	A1	C	6.000
		B	4.250
		A	1.500
Over the bent and over the girder	B2	D	7.875
		C	5.875
		B	3.625
		A	2.125
Over the bent and between girders	B3	D	6.625
		C	5.125
		B	1.750
		A	0.500
Middle of long span, middle of deck overhang	C1	C	5.750
		B	3.750
		A	1.500
Mid of long span, Between Girders	C2	D	6.250
		C	4.500
		B	2.500
		A	0.750
Mid of long span, over the girder	C3	E	8.750
		D	6.875
		C	5.375
		B	3.375
		A	1.000
End of pour, between girders	D1	C	6.250
		B	3.875
		A	1.500

All values in inches.

B.1.3 Recorded Temperatures

The following figures present the complete set of temperature data for the San Antonio bridge deck. Figure B-86 presents a comparison of the temperatures recorded for a selected top iButton for each of the strands. The selected iButtons were located in the middle of the bridge deck width, when possible. Figure B-87 presents a comparison of the gradient recorded across the different strands. As before, each strand is represented by the iButton string located in the middle of the bridge deck width, when possible. In the gradient graph, the iButton gradient, in °F, is presented in on the primary vertical axis, while the ambient air temperature, in °F, is presented on the secondary vertical axis. The graphs following Figure B-87 are labeled with the bridge deck pour name, SABD, the iButton string name, and the duration of time presented on that graph. For each string, the first graph presents the 4-day temperature data, such that the first temperature peaks may be examined. The following graph presents the full data set for the iButton string. Due to various factors, some iButton strings may record longer durations than others.

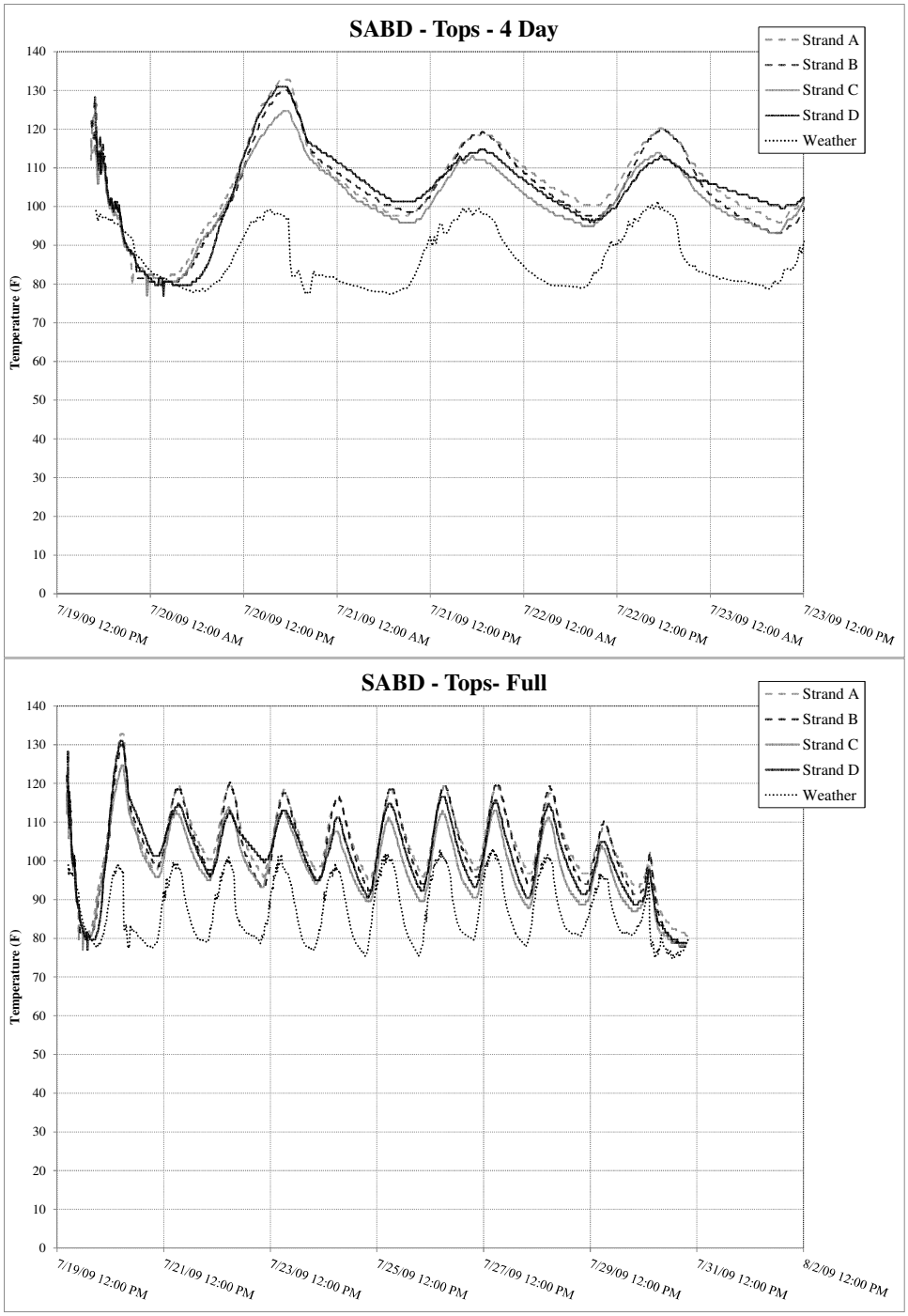

Figure B-86: Comparison of top iButton temperatures- SABD

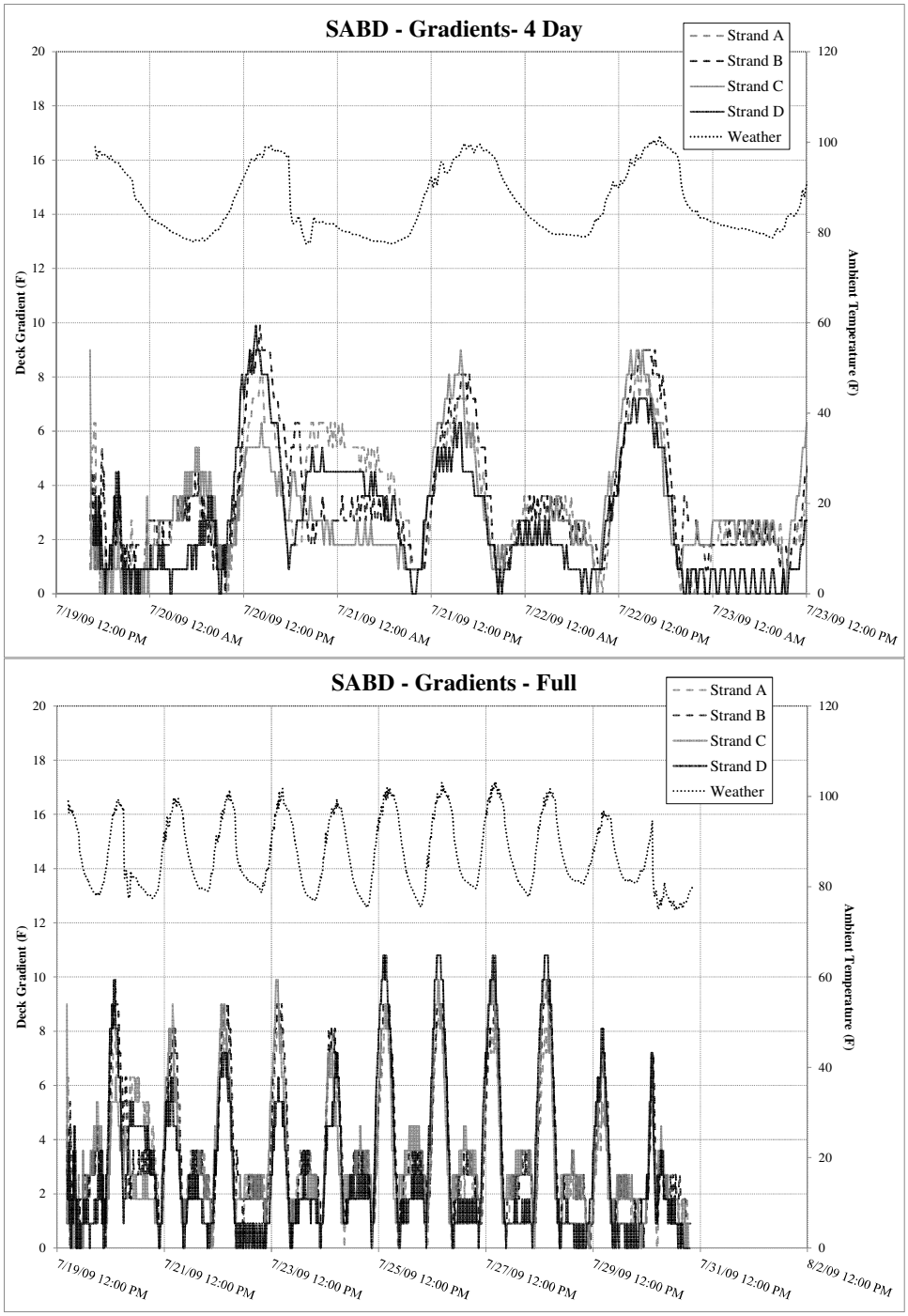

Figure B-87: Comparison of iButton strand gradients- SABD

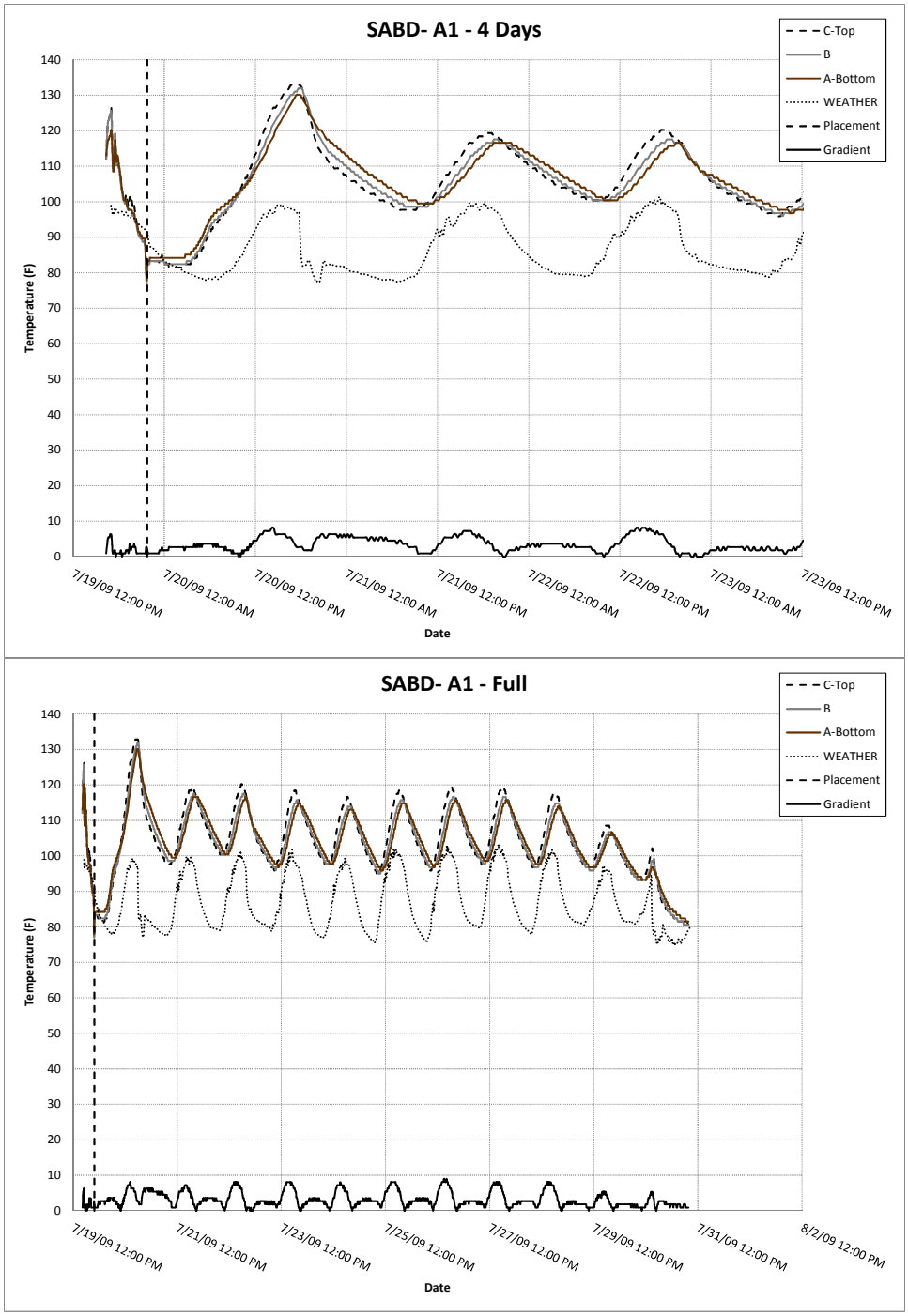
SABD- A1 - 4 Days
C-Top
B
A-Bottom
WEATHER
Placement
Gradient
Temperature (F)
Date
7/19/09 12:00 PM
7/20/09 12:00 AM
7/20/09 12:00 PM
7/21/09 12:00 AM
7/21/09 12:00 PM
7/22/09 12:00 AM
7/22/09 12:00 PM
7/23/09 12:00 AM
7/23/09 12:00 PM
SABD- A1 - Full
C-Top
B
A-Bottom
WEATHER
Placement
Gradient
Temperature (F)
Date
7/19/09 12:00 PM
7/21/09 12:00 PM
7/23/09 12:00 PM
7/25/09 12:00 PM
7/27/09 12:00 PM
7/29/09 12:00 PM
7/31/09 12:00 PM
8/2/09 12:00 PM

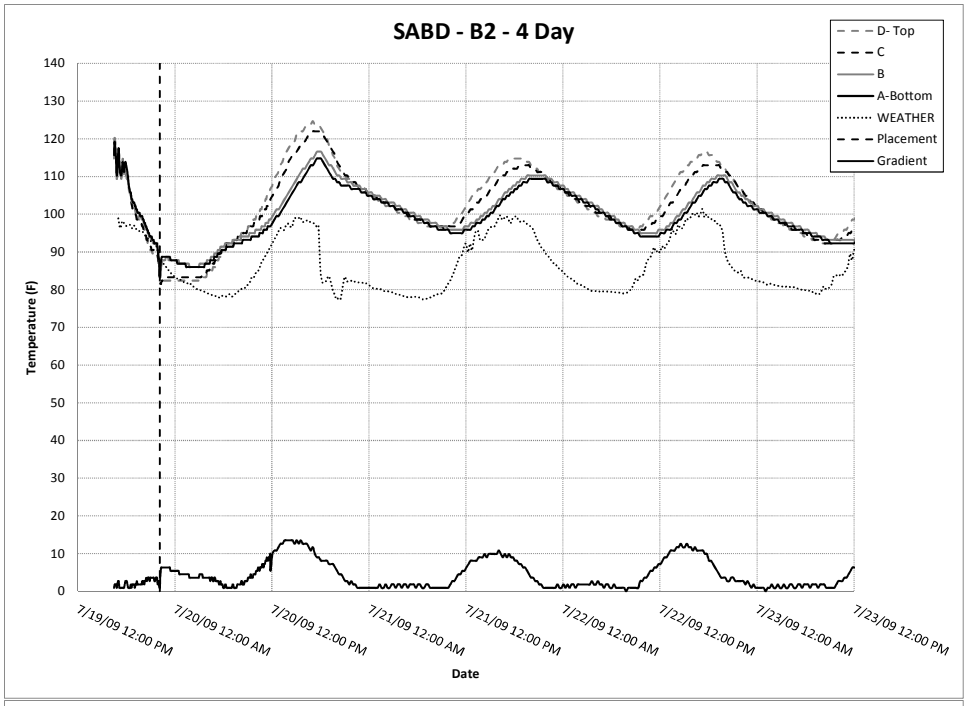
SABD - B2 - 4 Day
D- Top
C
B
A-Bottom
WEATHER
Placement
Gradient
Temperature (F)
140
130
120
110
100
90
80
70
60
50
40
30
20
10
0
7/19/09 12:00 PM
7/20/09 12:00 AM
7/20/09 12:00 PM
7/21/09 12:00 AM
7/21/09 12:00 PM
7/22/09 12:00 AM
7/22/09 12:00 PM
7/23/09 12:00 AM
7/23/09 12:00 PM
Date

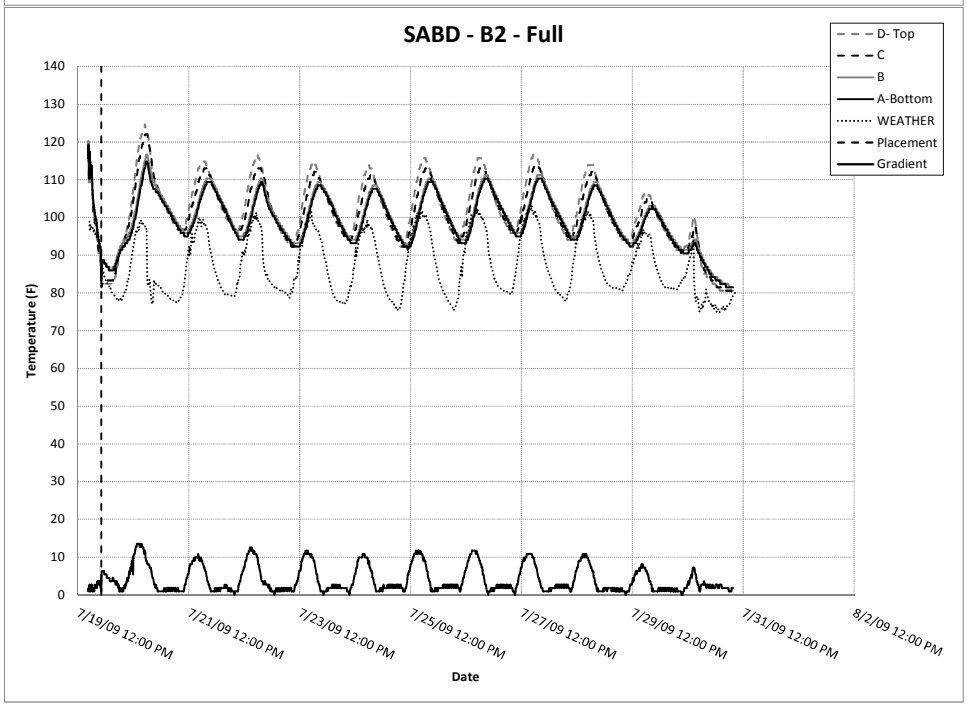
SABD - B2 - Full
D- Top
C
B
A-Bottom
WEATHER
Placement
Gradient
Temperature (F)
140
130
120
110
100
90
80
70
60
50
40
30
20
10
0
7/19/09 12:00 PM
7/21/09 12:00 PM
7/23/09 12:00 PM
7/25/09 12:00 PM
7/27/09 12:00 PM
7/29/09 12:00 PM
7/31/09 12:00 PM
8/2/09 12:00 PM
Date

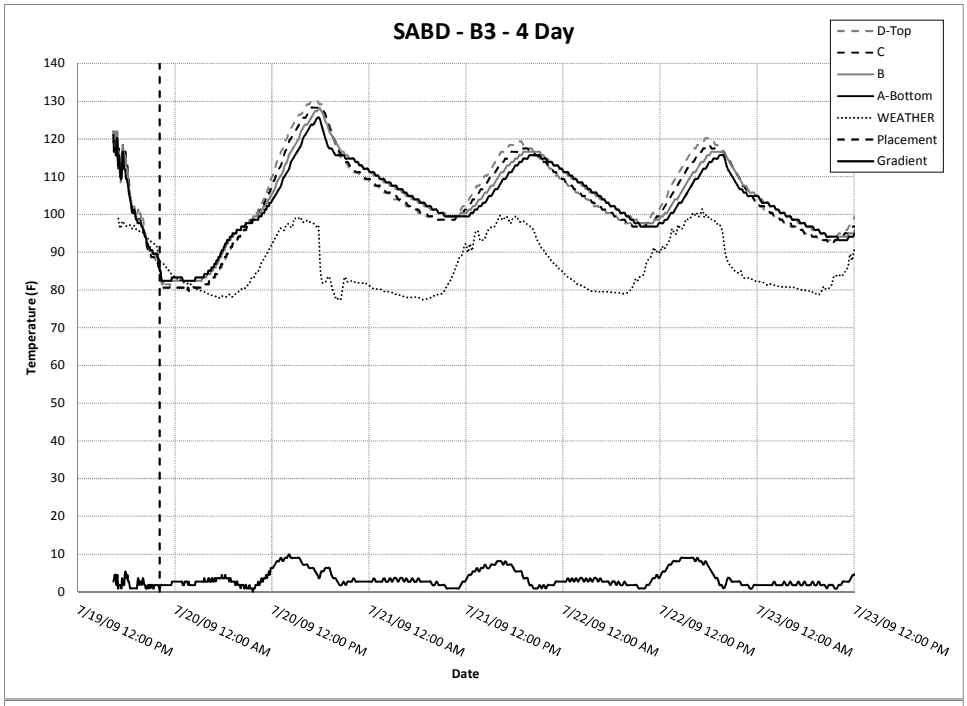
SABD - B3 - 4 Day
D-Top
C
B
A-Bottom
WEATHER
Placement
Gradient
Temperature (F)
Date
7/19/09 12:00 PM
7/20/09 12:00 AM
7/20/09 12:00 PM
7/21/09 12:00 AM
7/21/09 12:00 PM
7/22/09 12:00 AM
7/22/09 12:00 PM
7/23/09 12:00 AM
7/23/09 12:00 PM

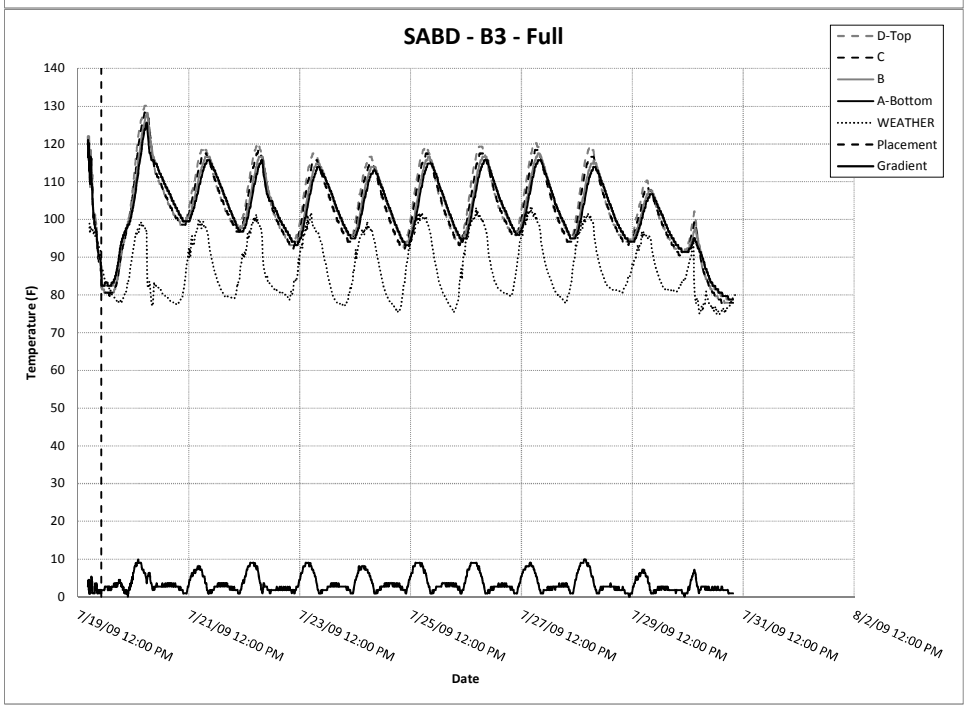
SABD - B3 - Full
D-Top
C
B
A-Bottom
WEATHER
Placement
Gradient
Temperature (F)
Date
7/19/09 12:00 PM
7/21/09 12:00 PM
7/23/09 12:00 PM
7/25/09 12:00 PM
7/27/09 12:00 PM
7/29/09 12:00 PM
7/31/09 12:00 PM
8/2/09 12:00 PM

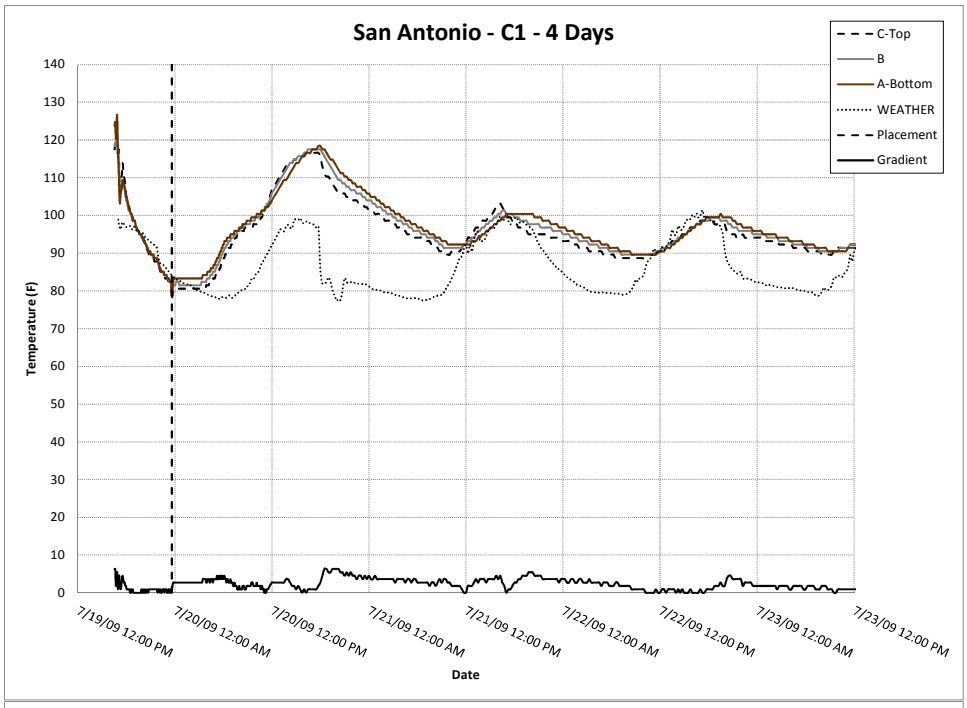
San Antonio - C1 - 4 Days
C-Top
B
A-Bottom
WEATHER
Placement
Gradient
Temperature (F)
140
130
120
110
100
90
80
70
60
50
40
30
20
10
0
7/19/09 12:00 PM
7/20/09 12:00 AM
7/20/09 12:00 PM
7/21/09 12:00 AM
7/21/09 12:00 PM
7/22/09 12:00 AM
7/22/09 12:00 PM
7/23/09 12:00 AM
7/23/09 12:00 PM
Date

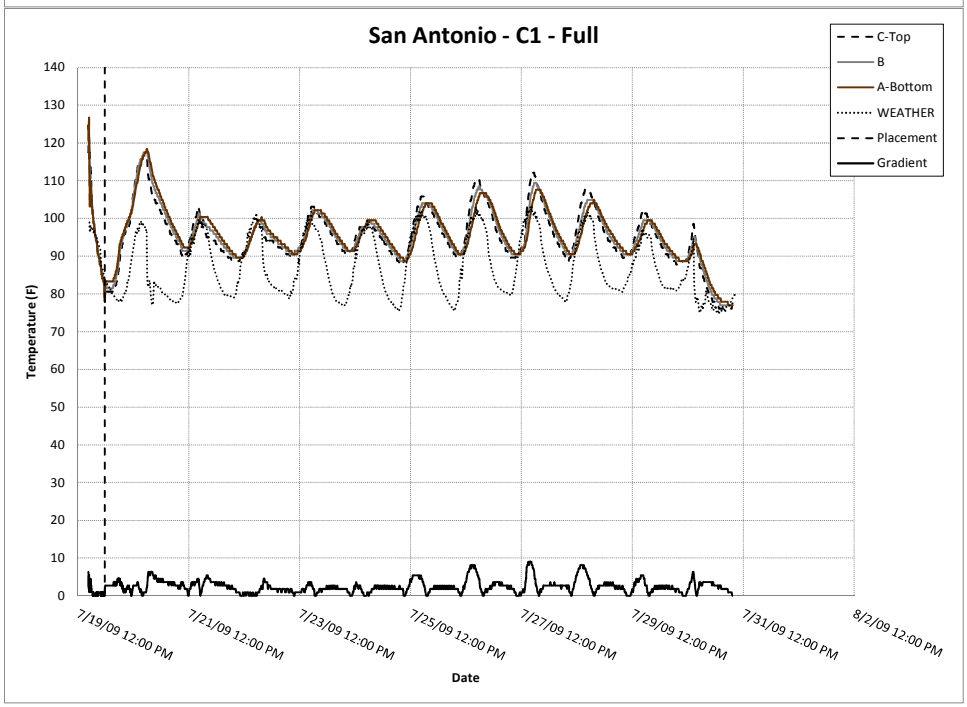
San Antonio - C1 - Full
C-Top
B
A-Bottom
WEATHER
Placement
Gradient
Temperature (F)
140
130
120
110
100
90
80
70
60
50
40
30
20
10
0
7/19/09 12:00 PM
7/21/09 12:00 PM
7/23/09 12:00 PM
7/25/09 12:00 PM
7/27/09 12:00 PM
7/29/09 12:00 PM
7/31/09 12:00 PM
8/2/09 12:00 PM
Date

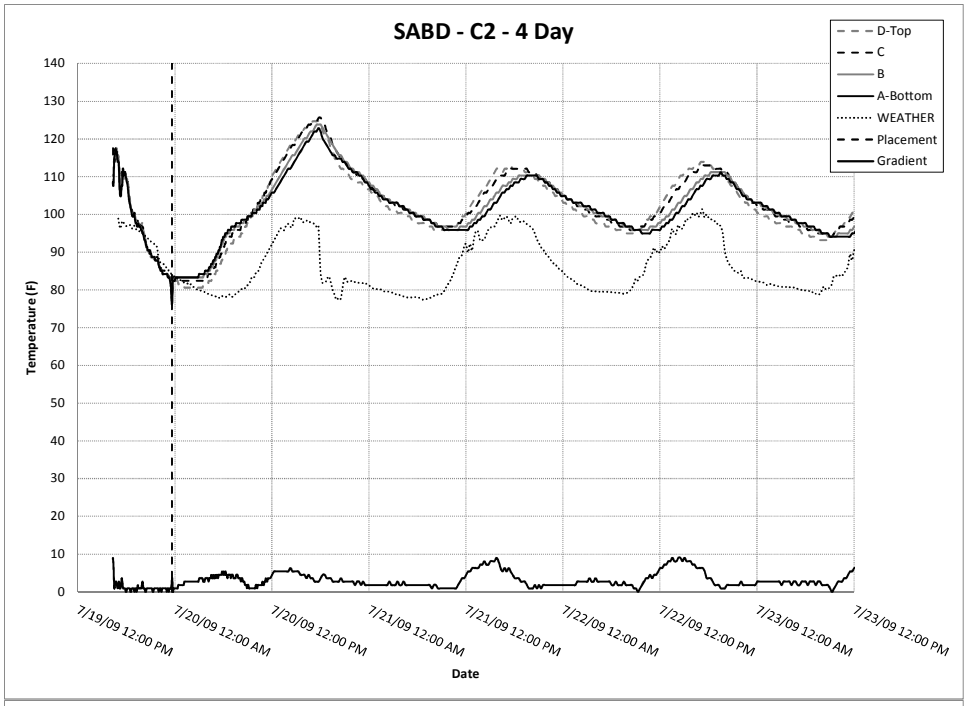
SABD - C2 - 4 Day
D-Top
C
B
A-Bottom
WEATHER
Placement
Gradient
Temperature (F)
140
130
120
110
100
90
80
70
60
50
40
30
20
10
0
7/19/09 12:00 PM
7/20/09 12:00 AM
7/20/09 12:00 PM
7/21/09 12:00 AM
7/21/09 12:00 PM
7/22/09 12:00 AM
7/22/09 12:00 PM
7/23/09 12:00 AM
7/23/09 12:00 PM
Date

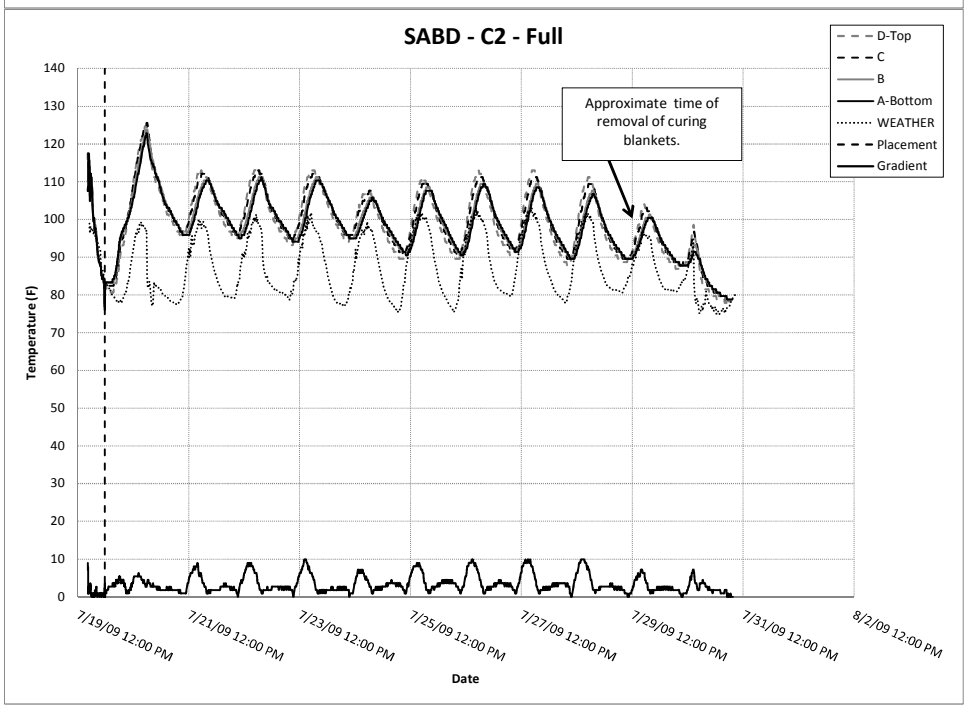
SABD - C2 - Full
Approximate time of removal of curing blankets.
D-Top
C
B
A-Bottom
WEATHER
Placement
Gradient
Temperature (F)
140
130
120
110
100
90
80
70
60
50
40
30
20
10
0
7/19/09 12:00 PM
7/21/09 12:00 PM
7/23/09 12:00 PM
7/25/09 12:00 PM
7/27/09 12:00 PM
7/29/09 12:00 PM
7/31/09 12:00 PM
8/2/09 12:00 PM
Date

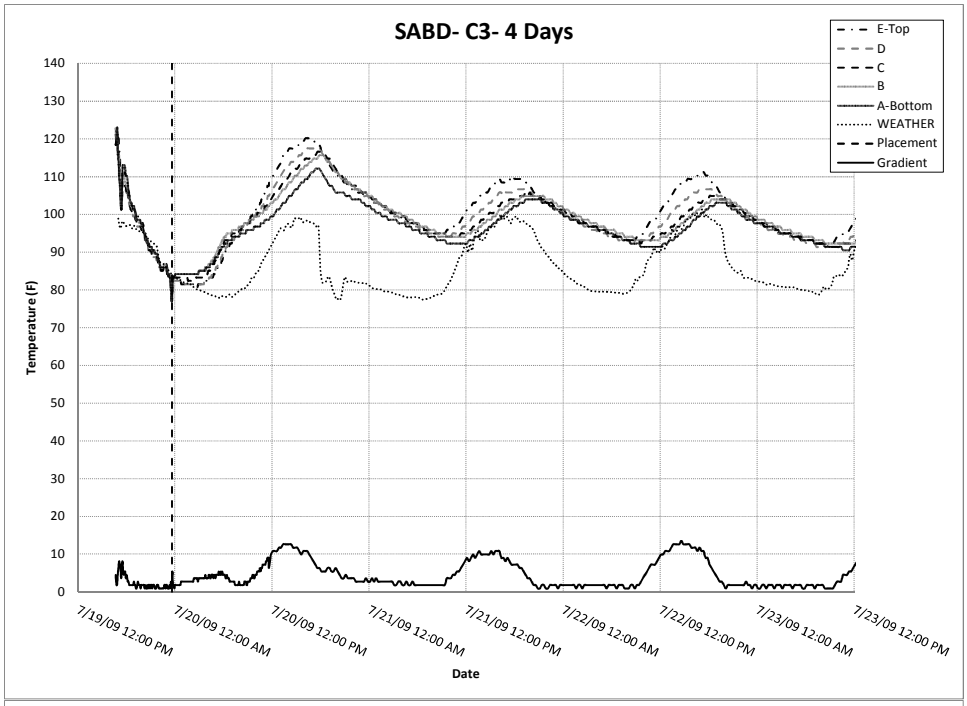
SABD- C3- 4 Days
E-Top
D
C
B
A-Bottom
WEATHER
Placement
Gradient
Temperature (F)
140
130
120
110
100
90
80
70
60
50
40
30
20
10
0
7/19/09 12:00 PM
7/20/09 12:00 AM
7/20/09 12:00 PM
7/21/09 12:00 AM
7/21/09 12:00 PM
7/22/09 12:00 AM
7/22/09 12:00 PM
7/23/09 12:00 AM
7/23/09 12:00 PM
Date

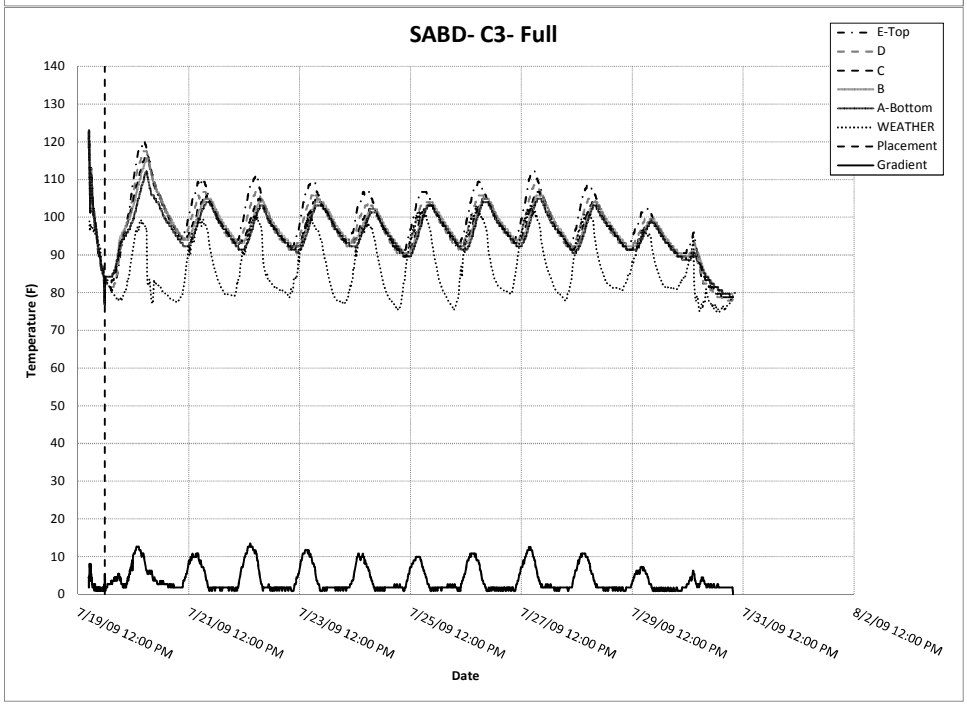
SABD- C3- Full
E-Top
D
C
B
A-Bottom
WEATHER
Placement
Gradient
Temperature (F)
140
130
120
110
100
90
80
70
60
50
40
30
20
10
0
7/19/09 12:00 PM
7/21/09 12:00 PM
7/23/09 12:00 PM
7/25/09 12:00 PM
7/27/09 12:00 PM
7/29/09 12:00 PM
7/31/09 12:00 PM
8/2/09 12:00 PM
Date

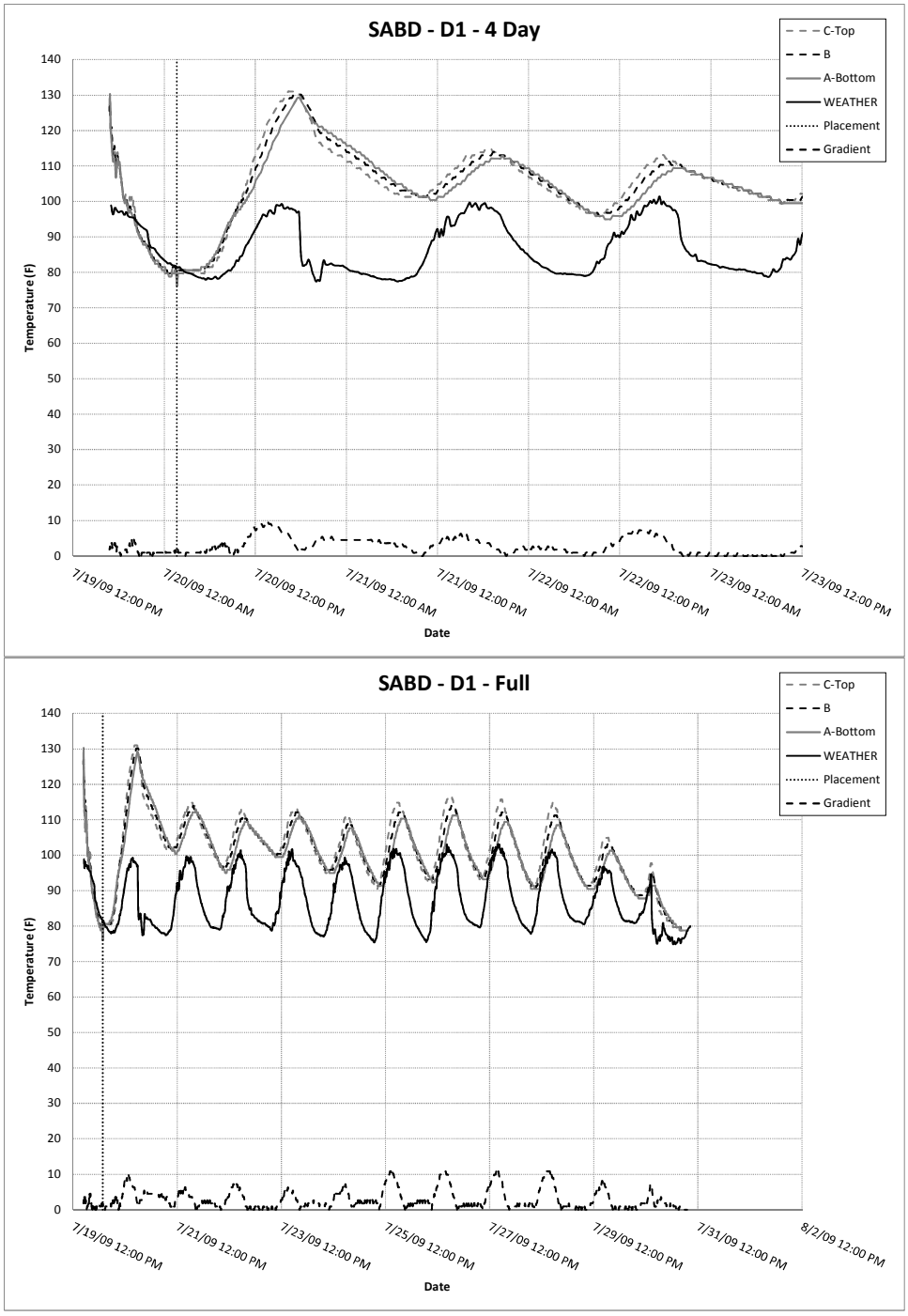
SABD - D1 - 4 Day
C-Top
B
A-Bottom
WEATHER
Placement
Gradient
Temperature (F)
Date
7/19/09 12:00 PM
7/20/09 12:00 AM
7/20/09 12:00 PM
7/21/09 12:00 AM
7/21/09 12:00 PM
7/22/09 12:00 AM
7/22/09 12:00 PM
7/23/09 12:00 AM
7/23/09 12:00 PM
SABD - D1 - Full
C-Top
B
A-Bottom
WEATHER
Placement
Gradient
Temperature (F)
Date
7/19/09 12:00 PM
7/21/09 12:00 PM
7/23/09 12:00 PM
7/25/09 12:00 PM
7/27/09 12:00 PM
7/29/09 12:00 PM
7/31/09 12:00 PM
8/2/09 12:00 PM

B.2 GEORGETOWN BRIDGE DECK: SUMMER POUR

B2.1 iButton String Locations and Placement Times

Locations of iButton strings for this instrumentation, provided in Table B-67, were measured from the South end (beginning of pour) and the West face. iButton placement times, provided in Table B-68, were determined from examination of the iButton temperature data.

Table B-67: iButton string locations- GTBDS.

String	Distance from South end	Distance from West face
A1	13	24
B1	49	30.4
C1	99	22
C2	99	6.67
D1	121	21.9

All values in feet.

Table B-68: Concrete placement times- GTBDS

Strand	Placement Time
A	8/19/09 4:30 AM
B	8/19/09 5:47 AM
C	8/19/09 6:47 AM
D	8/19/09 6:57 AM

B2.2 iButton Depths

Table B-69 provides the heights of the iButtons measured from either the precast, prestressed concrete panel, or the top of the precast, prestressed concrete girder. While the exact depth of the bridge deck is not known, it is assumed that concrete sections are

4” thick over the concrete panels and 11” thick over the concrete girders. Descriptions of the iButton strings are also provided.

Table B-69: iButton depths- GTBDS

Location	String	Buttons	Height from bottom
Start of pour	A1	D	3.250
		C	2.125
		B	1.250
		A	0.375
First line, on panel, middle of deck	B1	D	3.250
		C	2.125
		B	1.125
		A	0.375
Second line, on panel, middle of deck	C1	D	3.500
		C	2.250
		B	1.375
		A	0.250
Second line, on panel, deck overhang	C2	D	3.125
		C	2.125
		B	1.125
		A	0.250
End of pour	D1	D	3.125
		C	2.125
		B	1.125
		A	0.250

All values in inches.

B2.3 Recorded Temperatures

The following figures present the complete set of temperature data for the Georgetown bridge deck summer pour. Figure B-88 presents a comparison of the temperatures recorded for a selected top iButton for each of the strands. The selected iButtons were located in the middle of the bridge deck width, when possible. Figure B-

89 presents a comparison of the gradient recorded across the different strands. As before, each strand is represented by the iButton string located in the middle of the bridge deck width, when possible. In the gradient graph, the iButton gradient, in °F, is presented in on the primary vertical axis, while the ambient air temperature, in °F, is presented on the secondary vertical axis. The graphs following Figure B-89 are labeled with the bridge deck pour name, GTBDS, the iButton string name, and the duration of time presented on that graph. For each string, the first graph presents the 4-day temperature data, such that the first temperature peaks may be examined. The following graph presents the full data set for the iButton string. Due to various factors, some iButton strings may record longer durations than others.

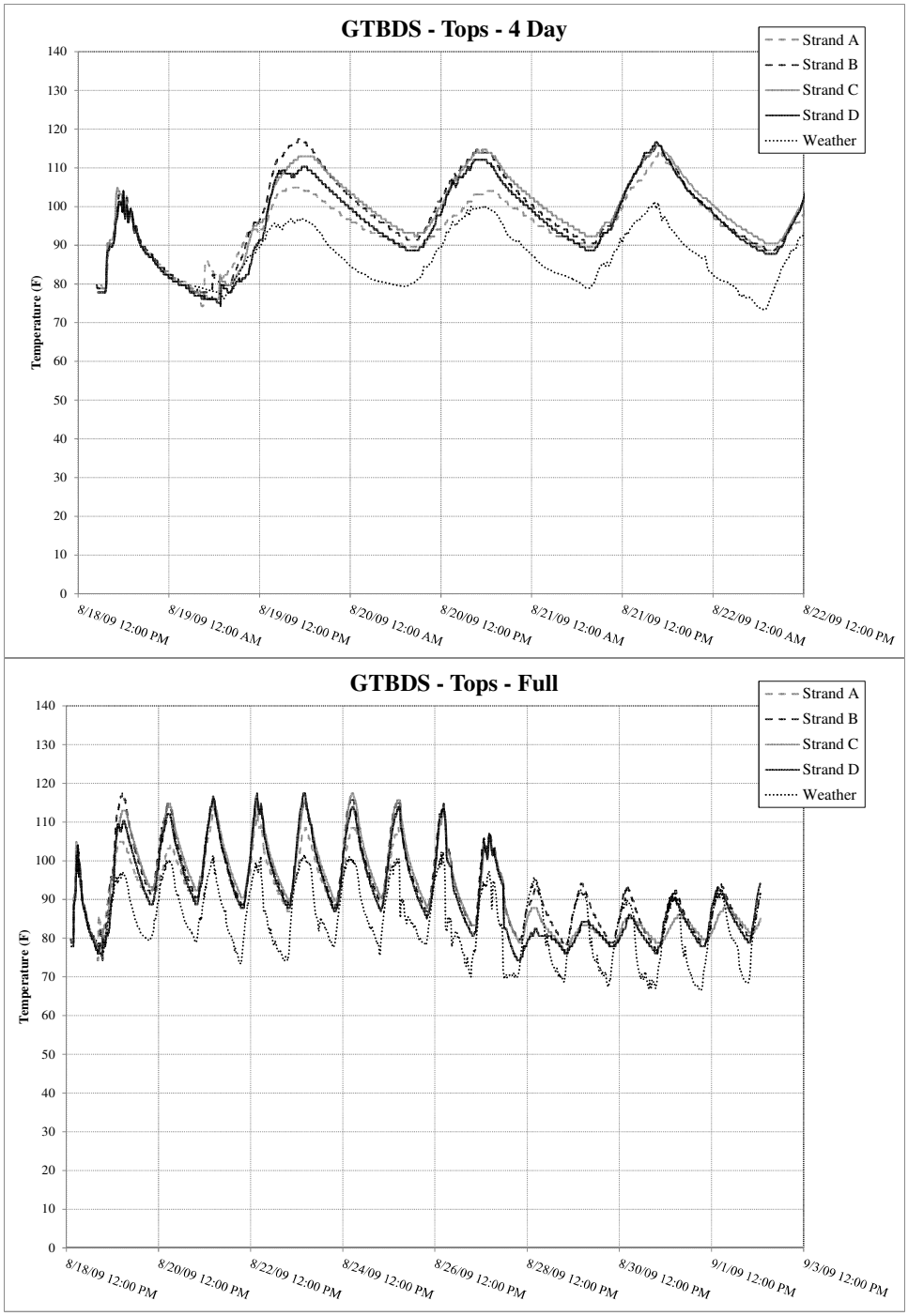

Figure B-88: Comparison of top iButton temperatures- GTBDS

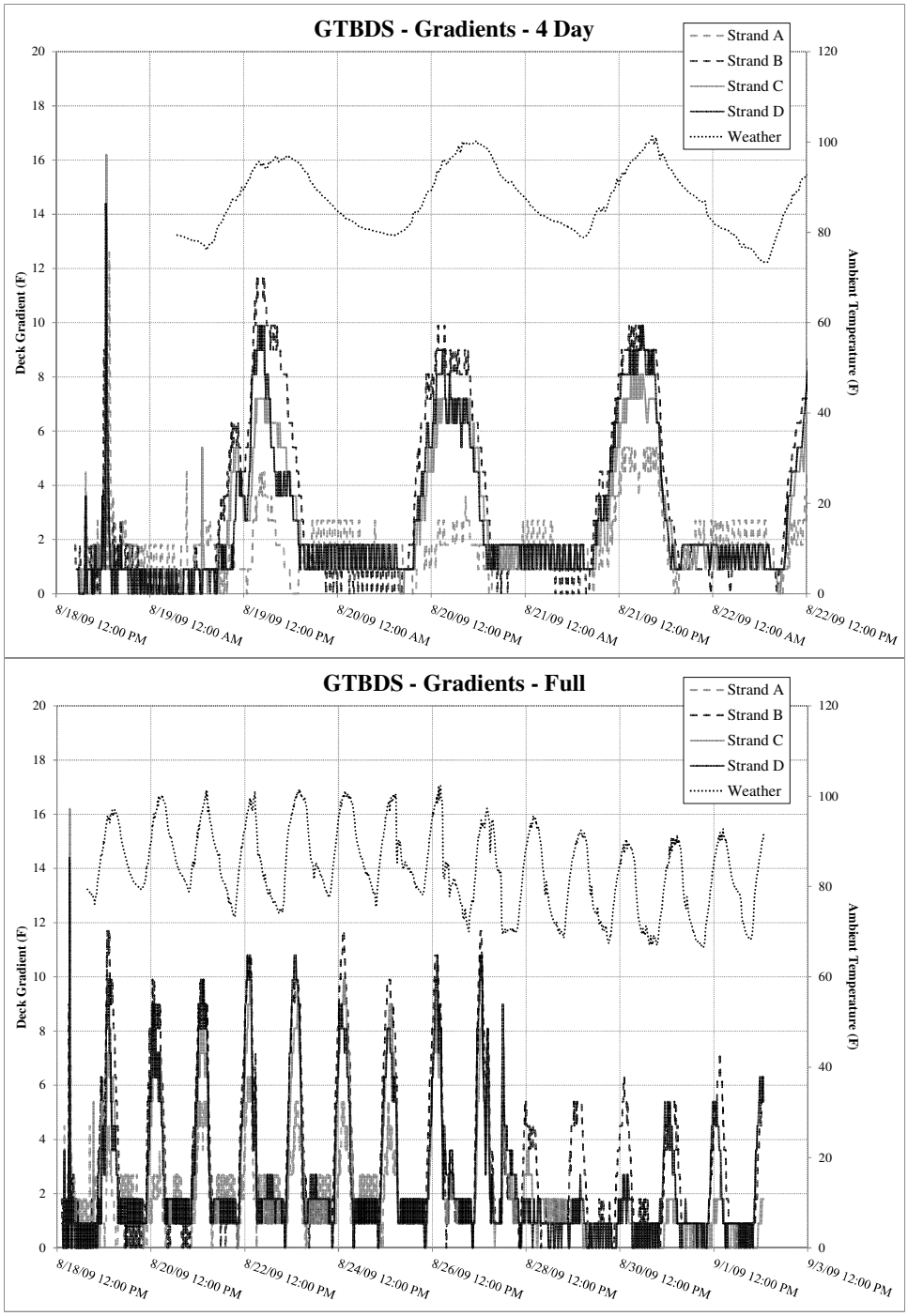

Figure B-89: Comparison of iButton strand gradients- GTBDS

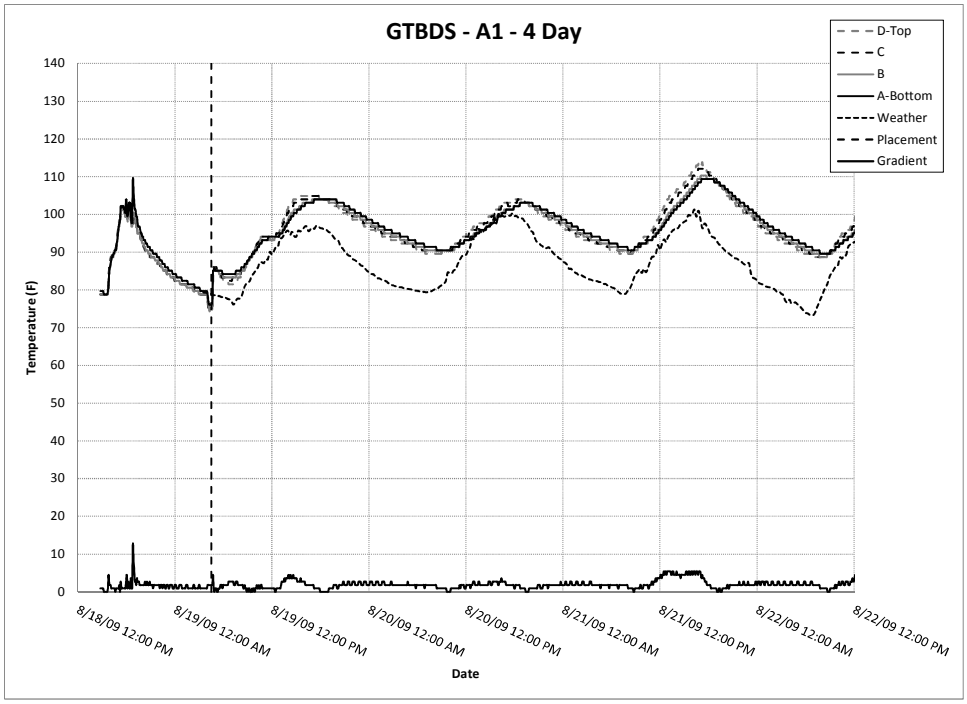
GTBDS - A1 - 4 Day
D-Top
C
B
A-Bottom
Weather
Placement
Gradient
Temperature (F)
140
130
120
110
100
90
80
70
60
50
40
30
20
10
0
8/18/09 12:00 PM
8/19/09 12:00 AM
8/19/09 12:00 PM
8/20/09 12:00 AM
8/20/09 12:00 PM
8/21/09 12:00 AM
8/21/09 12:00 PM
8/22/09 12:00 AM
8/22/09 12:00 PM
Date

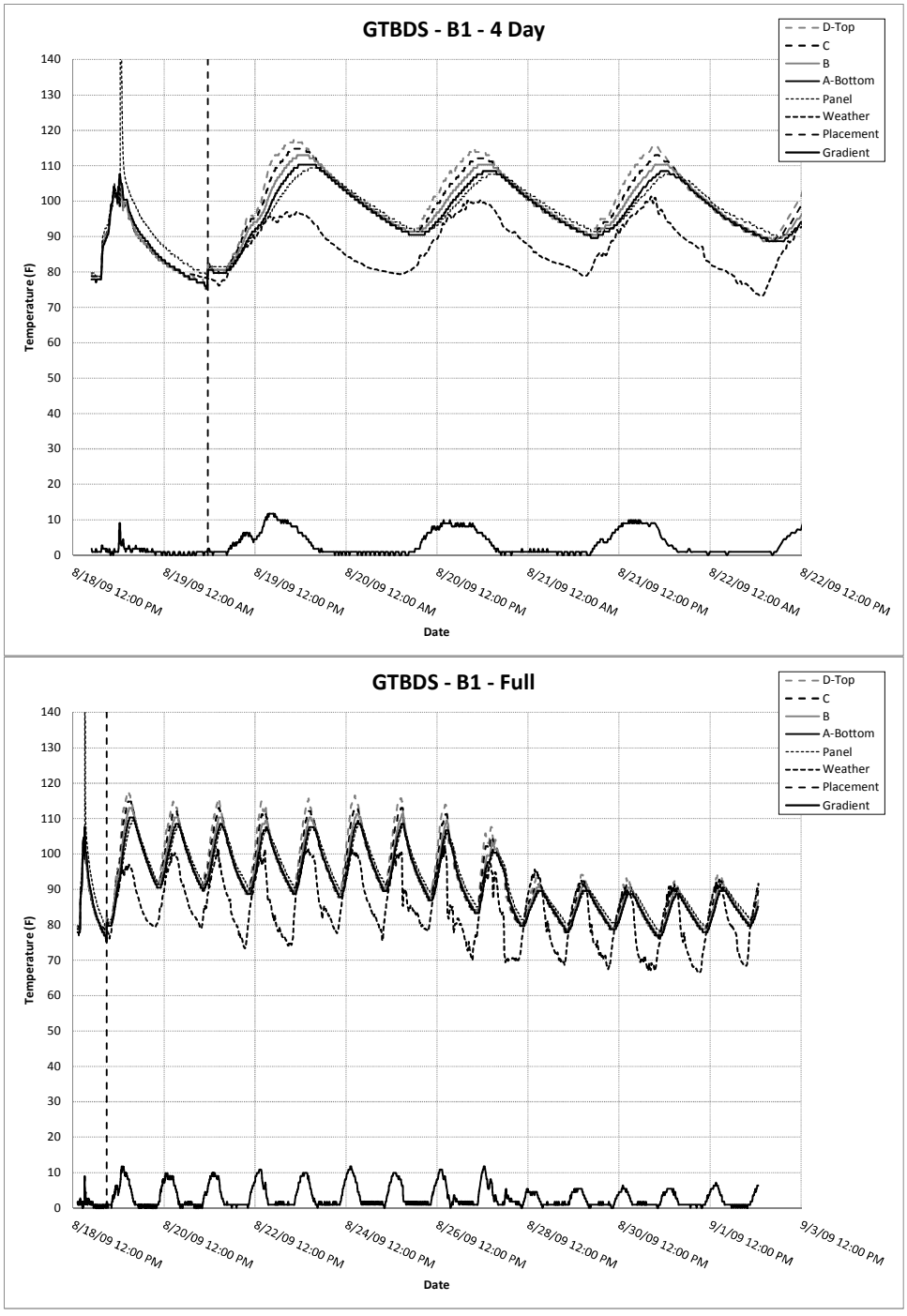
GTBDS - B1 - 4 Day
D-Top
C
B
A-Bottom
Panel
Weather
Placement
Gradient
Temperature (F)
140
130
120
110
100
90
80
70
60
50
40
30
20
10
0
8/18/09 12:00 PM
8/19/09 12:00 AM
8/19/09 12:00 PM
8/20/09 12:00 AM
8/20/09 12:00 PM
8/21/09 12:00 AM
8/21/09 12:00 PM
8/22/09 12:00 AM
8/22/09 12:00 PM
Date
GTBDS - B1 - Full
D-Top
C
B
A-Bottom
Panel
Weather
Placement
Gradient
Temperature (F)
140
130
120
110
100
90
80
70
60
50
40
30
20
10
0
8/18/09 12:00 PM
8/20/09 12:00 PM
8/22/09 12:00 PM
8/24/09 12:00 PM
8/26/09 12:00 PM
8/28/09 12:00 PM
8/30/09 12:00 PM
9/1/09 12:00 PM
9/3/09 12:00 PM
Date

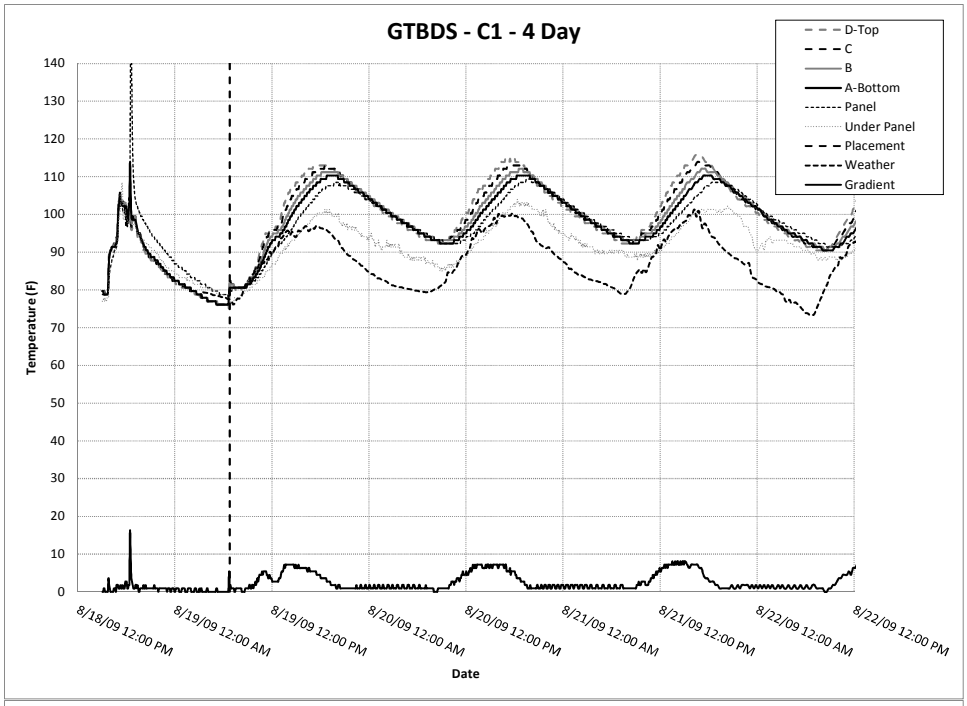
GTBDS - C1 - 4 Day
D-Top
C
B
A-Bottom
Panel
Under Panel
Placement
Weather
Gradient
Temperature (F)
Date
8/18/09 12:00 PM
8/19/09 12:00 AM
8/19/09 12:00 PM
8/20/09 12:00 AM
8/20/09 12:00 PM
8/21/09 12:00 AM
8/21/09 12:00 PM
8/22/09 12:00 AM
8/22/09 12:00 PM

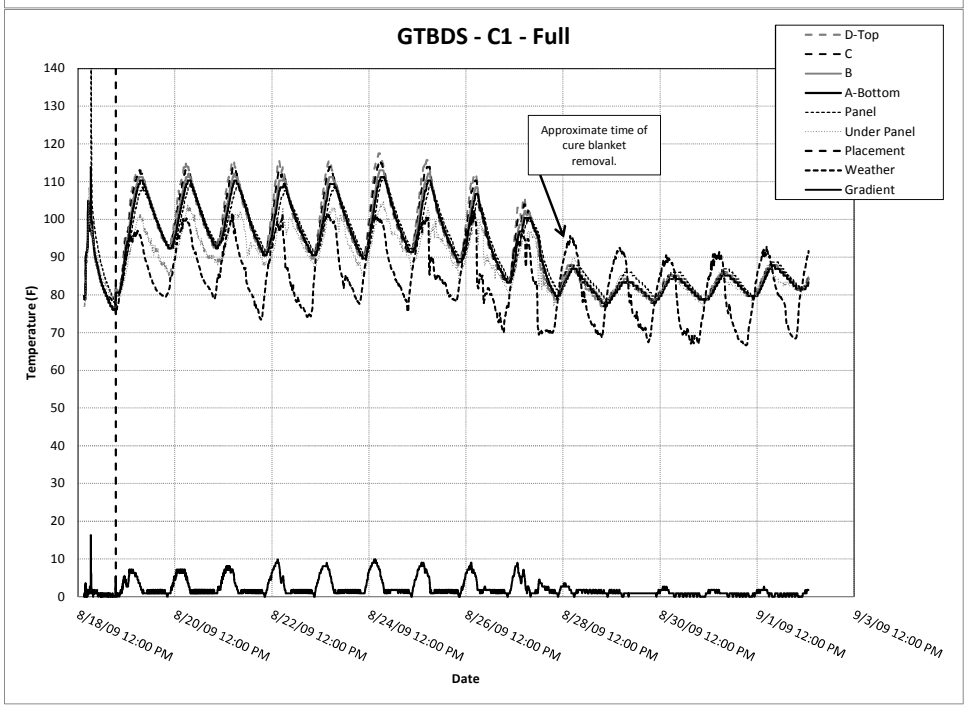
GTBDS - C1 - Full
D-Top
C
B
A-Bottom
Panel
Under Panel
Placement
Weather
Gradient
Approximate time of cure blanket removal.
Temperature (F)
Date
8/18/09 12:00 PM
8/20/09 12:00 PM
8/22/09 12:00 PM
8/24/09 12:00 PM
8/26/09 12:00 PM
8/28/09 12:00 PM
8/30/09 12:00 PM
9/1/09 12:00 PM
9/3/09 12:00 PM

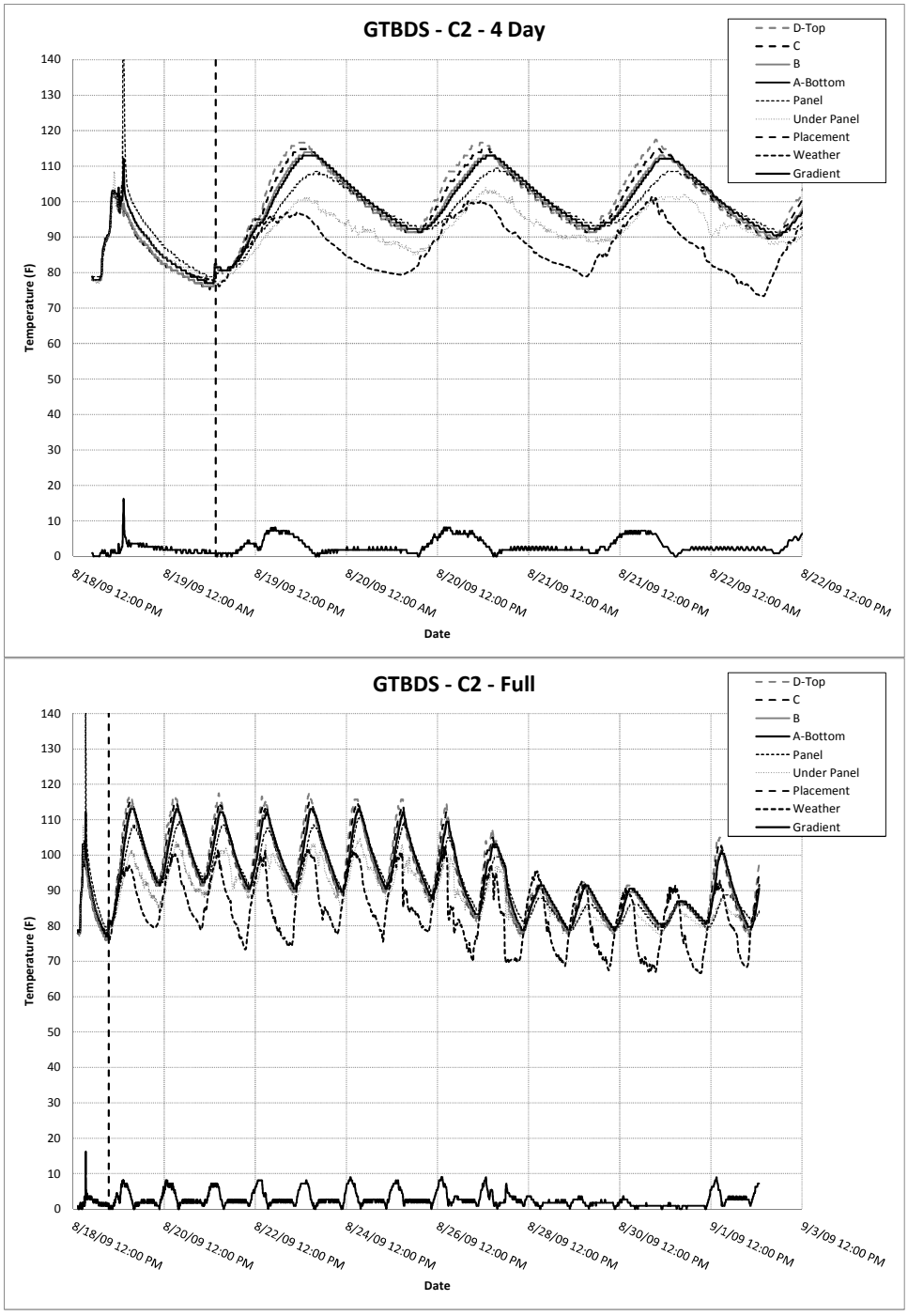
GTBDS - C2 - 4 Day
D-Top
C
B
A-Bottom
Panel
Under Panel
Placement
Weather
Gradient
Temperature (F)
Date
8/18/09 12:00 PM
8/19/09 12:00 AM
8/19/09 12:00 PM
8/20/09 12:00 AM
8/20/09 12:00 PM
8/21/09 12:00 AM
8/21/09 12:00 PM
8/22/09 12:00 AM
8/22/09 12:00 PM
GTBDS - C2 - Full
D-Top
C
B
A-Bottom
Panel
Under Panel
Placement
Weather
Gradient
Temperature (F)
Date
8/18/09 12:00 PM
8/20/09 12:00 PM
8/22/09 12:00 PM
8/24/09 12:00 PM
8/26/09 12:00 PM
8/28/09 12:00 PM
8/30/09 12:00 PM
9/1/09 12:00 PM
9/3/09 12:00 PM

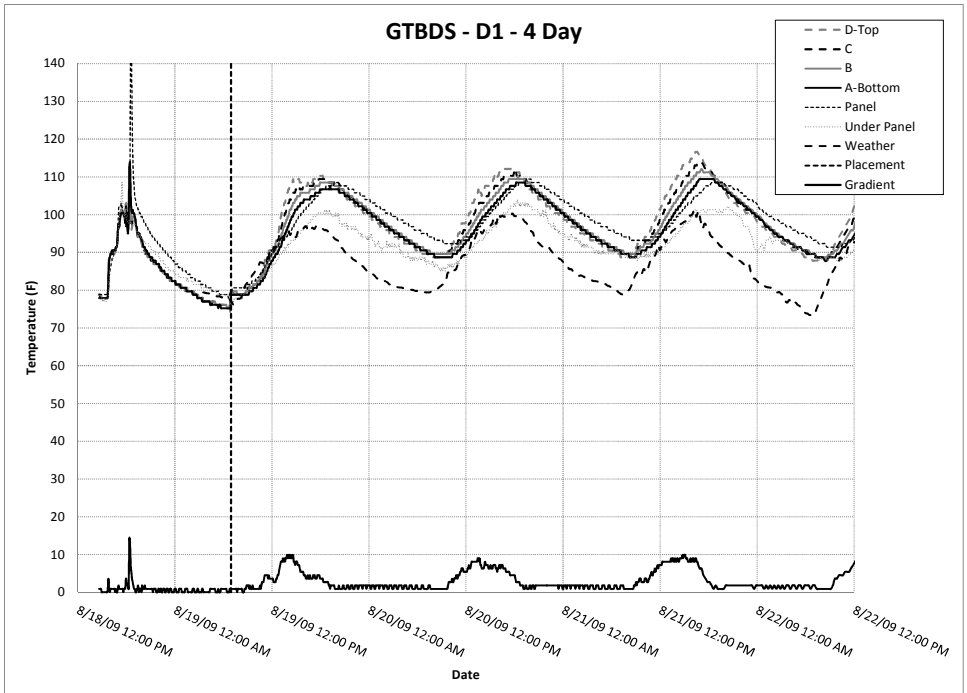
GTBDS - D1 - 4 Day
D-Top
C
B
A-Bottom
Panel
Under Panel
Weather
Placement
Gradient
Temperature (F)
140
130
120
110
100
90
80
70
60
50
40
30
20
10
0
8/18/09 12:00 PM
8/19/09 12:00 AM
8/19/09 12:00 PM
8/20/09 12:00 AM
8/20/09 12:00 PM
8/21/09 12:00 AM
8/21/09 12:00 PM
8/22/09 12:00 AM
8/22/09 12:00 PM
Date

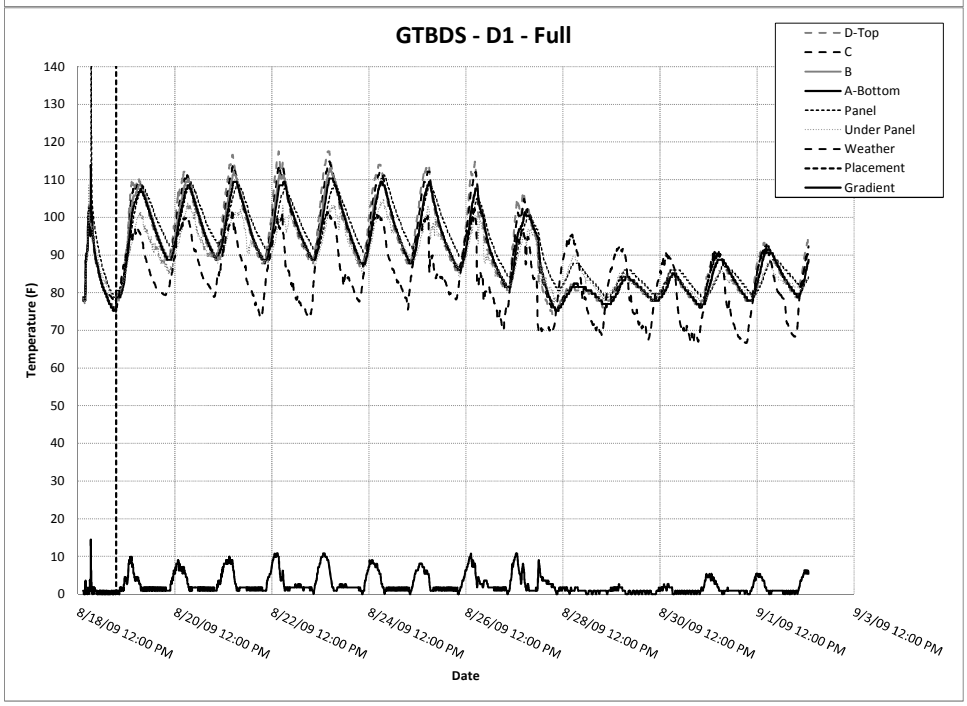
GTBDS - D1 - Full
D-Top
C
B
A-Bottom
Panel
Under Panel
Weather
Placement
Gradient
Temperature (F)
140
130
120
110
100
90
80
70
60
50
40
30
20
10
0
8/18/09 12:00 PM
8/20/09 12:00 PM
8/22/09 12:00 PM
8/24/09 12:00 PM
8/26/09 12:00 PM
8/28/09 12:00 PM
8/30/09 12:00 PM
9/1/09 12:00 PM
9/3/09 12:00 PM
Date

B.3 GEORGETOWN BRIDGE DECK: WINTER POUR

B.3.1 iButton String Locations and Placement Times

Locations of iButton strings for this instrumentation, provided in Table B-70, were measured from the North end (beginning of pour) and the East face. iButton placement times, provided in Table B-71, were determined from examination of the iButton temperature data.

Table B-70: iButton string locations- GTBDW.

String	Distance from North end	Distance from East face
A1	16	22.5
B1	84	24
B2	84	28.5
B3	84	31
C1	170	1
C2	170	19.5
C3	170	23
D1	255	22.5

All values in feet.

Table B-71: Concrete placement times- GTBDW

Strand	Placement Time
A	11/19/09 8:02 AM
B	11/19/09 8:51 AM
C	11/19/09 10:07 AM
D	11/19/09 11:38 AM

B.3.2 iButton Depths

Table B-72 provides the heights of the iButtons measured from either the precast, prestressed concrete panel, or the top of the precast, prestressed concrete girder. While

the exact depth of the bridge deck is not known, it is assumed that concrete sections are 4” thick over the concrete panels and 11” thick over the concrete girders. Descriptions of the iButton strings are also provided.

Table B-72: iButton depths- GTBDW

Location	String	Button	Height from bottom
Start of pour, on panel	A1	D	3.375
		C	2.500
		B	1.250
		A	0.500
First line, mid-width, on panel	B1	D	3.750
		C	2.750
		B	1.750
		A	0.500
First line, West side of deck, on panel	B2	D	3.375
		C	2.375
		B	1.250
		A	0.500
First line, on the girder	B3	F	9.625
		E	8.563
		D	7.625
		C	6.625
		B	3.750
		A	0.500
Second Line, on East overhang, no precast panel	C1	D	6.125
		C	5.000
		B	4.125
		A	3.250
Second line, on girder	C2	F	9.500
		E	8.625
		D	7.500
		C	6.500
		B	3.500
		A	0.500
Second line, mid-width, on panel	C3	D	3.500
		C	2.625
		B	1.625
		A	0.500
End of pour, on panel	D1	D	3.500
		C	2.250
		B	1.250
		A	0.375

All values in inches.

B3.3 Recorded Temperatures

The following figures present the complete set of temperature data for the Georgetown bridge deck winter pour. Figure B-90 presents a comparison of the temperatures recorded for a selected top iButton for each of the strands. The selected iButtons were located in the middle of the bridge deck width, when possible. Figure B-91 presents a comparison of the gradient recorded across the different strands. As before, each strand is represented by the iButton string located in the middle of the bridge deck width, when possible. In the gradient graph, the iButton gradient, in °F, is presented in on the primary vertical axis, while the ambient air temperature, in °F, is presented on the secondary vertical axis. The graphs following Figure B-91 are labeled with the bridge deck pour name, GTBDW, the iButton string name, and the duration of time presented on that graph. For each string, the first graph presents the 7-day temperature data, such that the first temperature peaks may be examined. Seven days was chosen rather than four due to the reduced early-age peaks, and the increased duration of total iButton measurements. The following graph presents the 28-day data set for the iButton string, followed by the full data set. Due to various factors, some iButton strings may record longer durations than others.

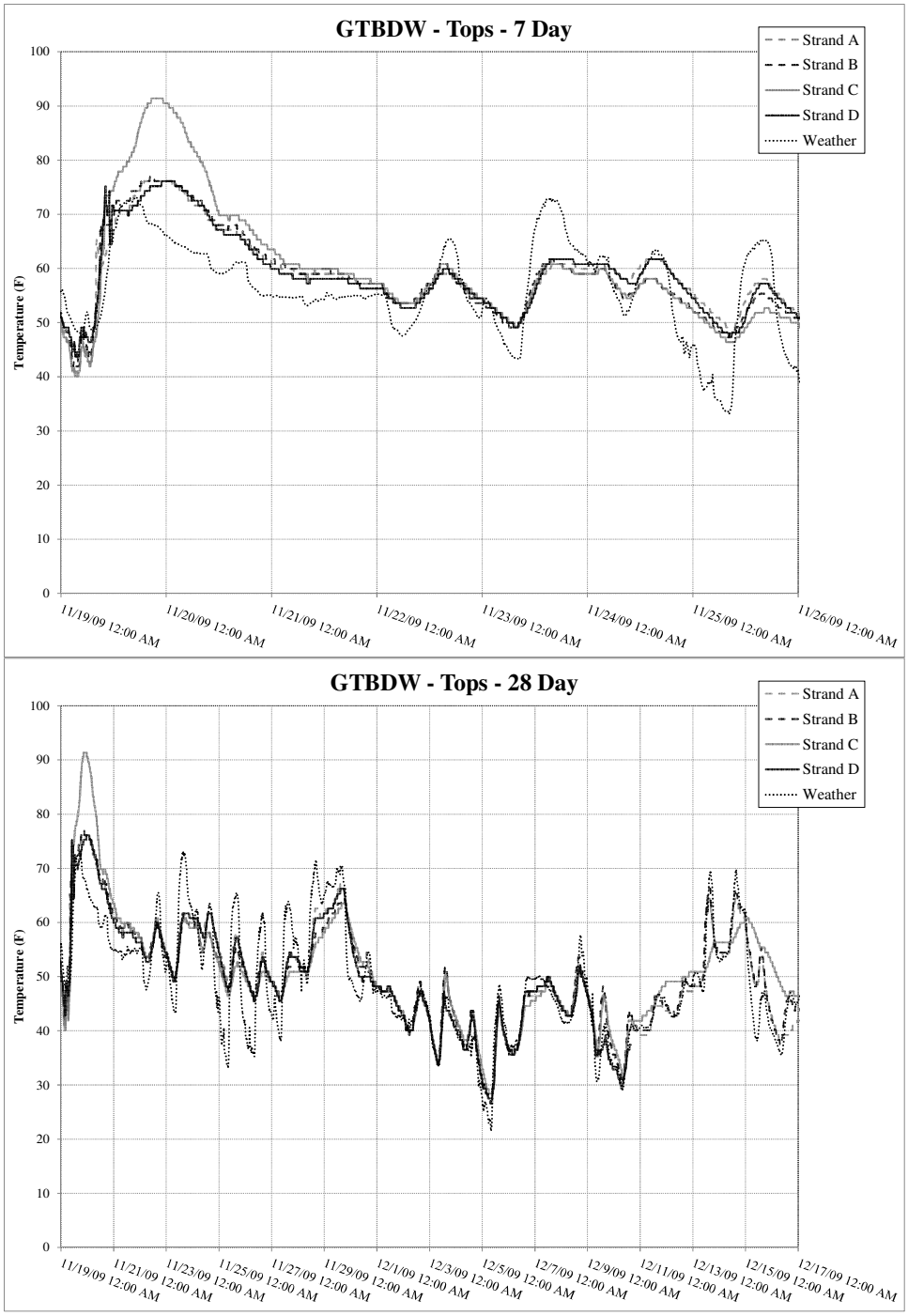

Figure B-90: Comparison of top iButton temperatures- GTBDW

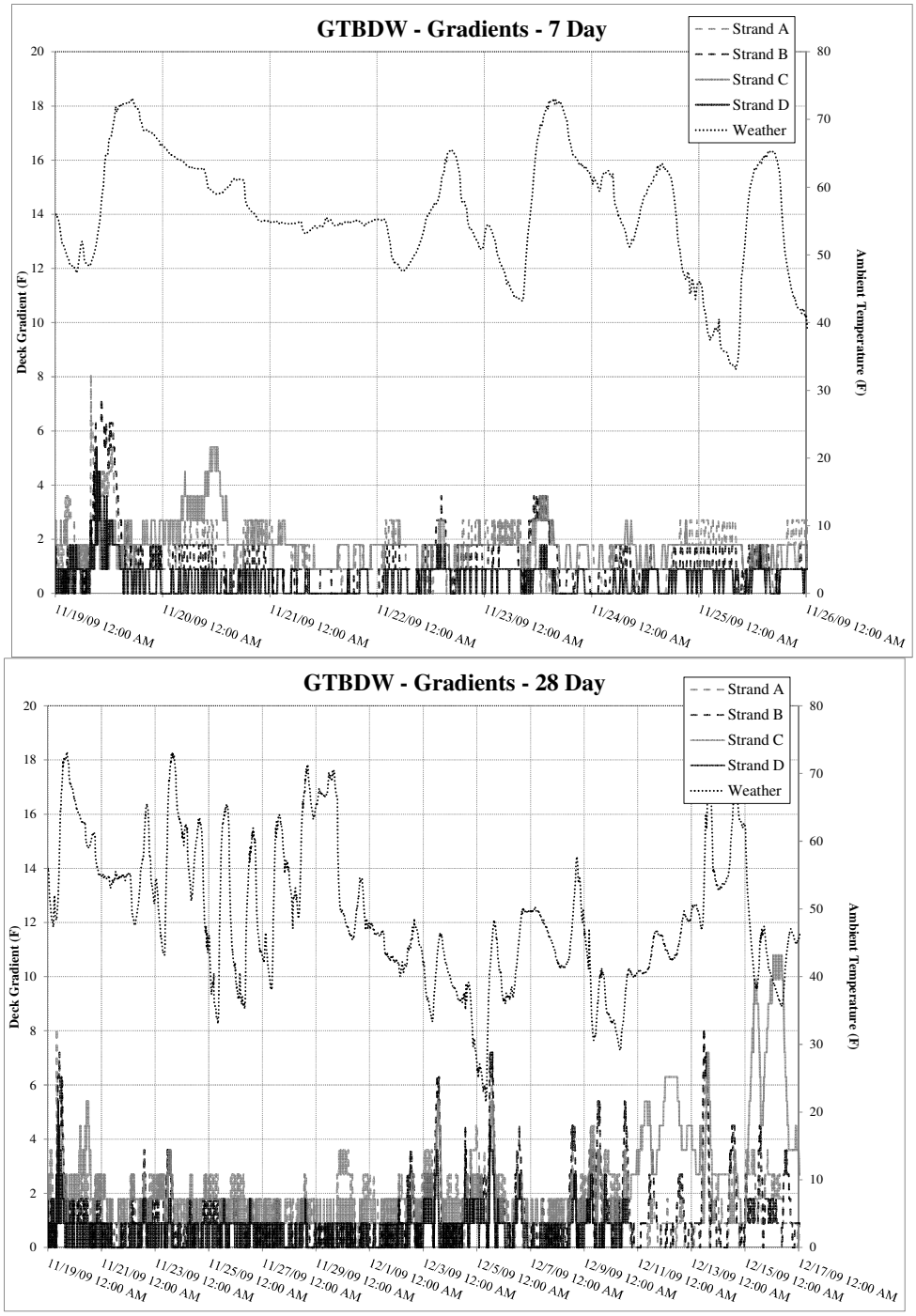

Figure B-91: Comparison of iButton strand gradients- GTBDW

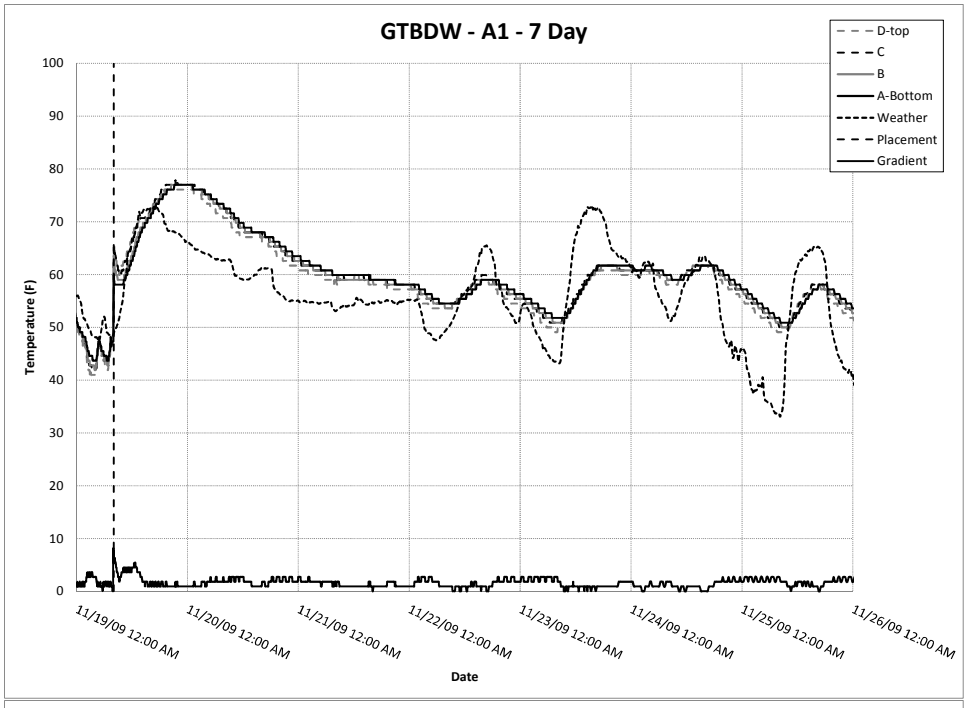
GTBDW - A1 - 7 Day
D-top
C
B
A-Bottom
Weather
Placement
Gradient
Temperature (F)
100
90
80
70
60
50
40
30
20
10
0
11/19/09 12:00 AM
11/20/09 12:00 AM
11/21/09 12:00 AM
11/22/09 12:00 AM
11/23/09 12:00 AM
11/24/09 12:00 AM
11/25/09 12:00 AM
11/26/09 12:00 AM
Date

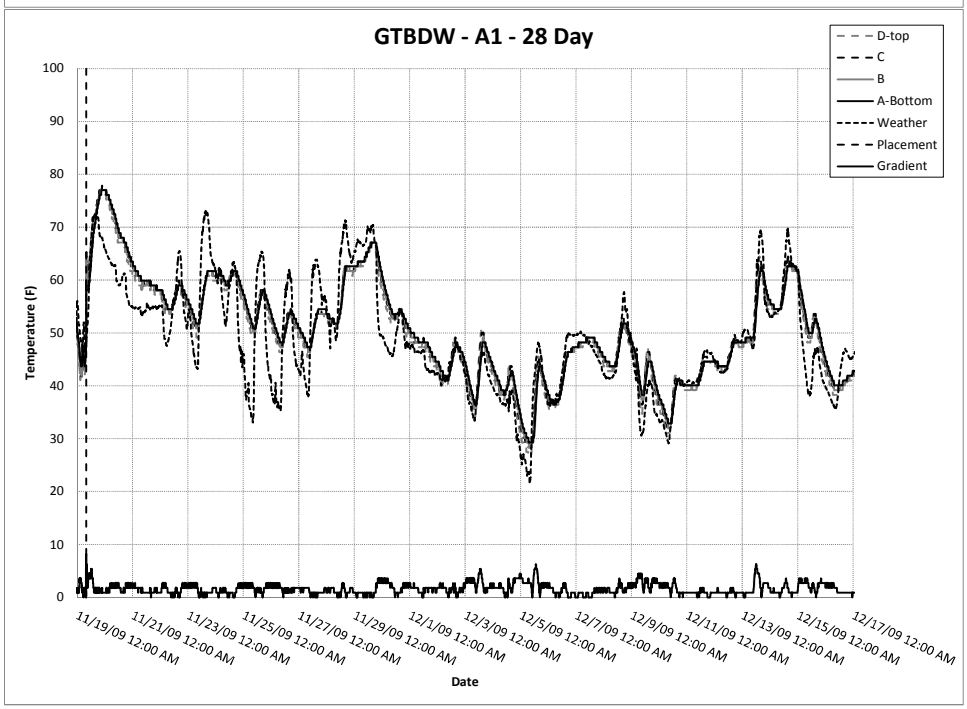
GTBDW - A1 - 28 Day
D-top
C
B
A-Bottom
Weather
Placement
Gradient
Temperature (F)
100
90
80
70
60
50
40
30
20
10
0
11/19/09 12:00 AM
11/21/09 12:00 AM
11/23/09 12:00 AM
11/25/09 12:00 AM
11/27/09 12:00 AM
11/29/09 12:00 AM
12/1/09 12:00 AM
12/3/09 12:00 AM
12/5/09 12:00 AM
12/7/09 12:00 AM
12/9/09 12:00 AM
12/11/09 12:00 AM
12/13/09 12:00 AM
12/15/09 12:00 AM
12/17/09 12:00 AM
Date

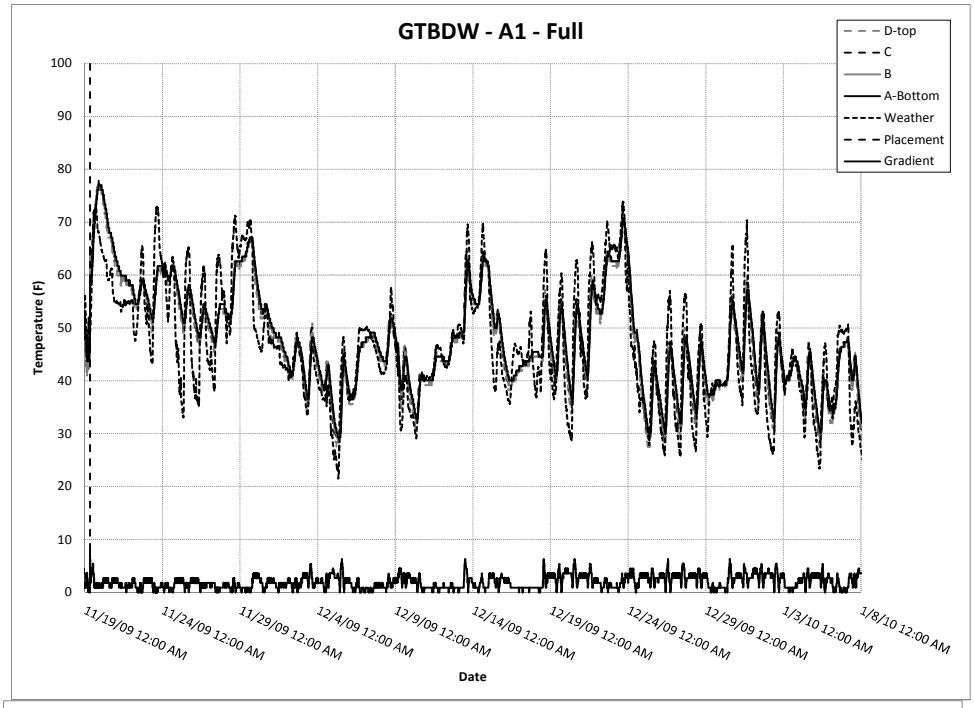
GTBDW - A1 - Full
D-top
C
B
A-Bottom
Weather
Placement
Gradient
Temperature (F)
100
90
80
70
60
50
40
30
20
10
0
11/19/09 12:00 AM
11/24/09 12:00 AM
11/29/09 12:00 AM
12/4/09 12:00 AM
12/9/09 12:00 AM
12/14/09 12:00 AM
12/19/09 12:00 AM
12/24/09 12:00 AM
12/29/09 12:00 AM
1/3/10 12:00 AM
1/8/10 12:00 AM
Date

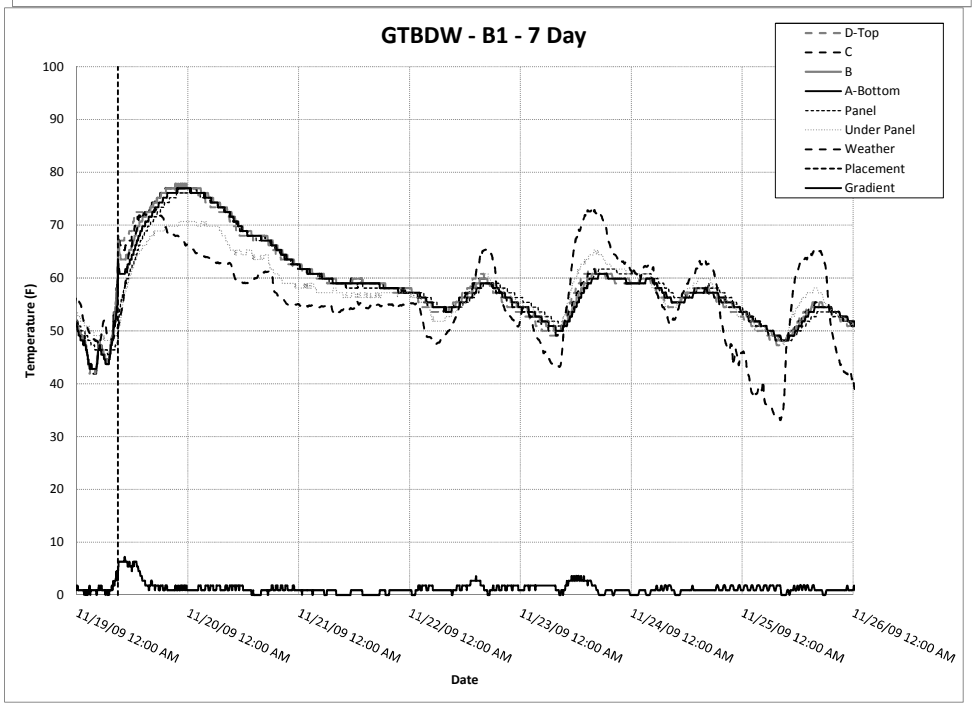
GTBDW - B1 - 7 Day
D-Top
C
B
A-Bottom
Panel
Under Panel
Weather
Placement
Gradient
Temperature (F)
100
90
80
70
60
50
40
30
20
10
0
11/19/09 12:00 AM
11/20/09 12:00 AM
11/21/09 12:00 AM
11/22/09 12:00 AM
11/23/09 12:00 AM
11/24/09 12:00 AM
11/25/09 12:00 AM
11/26/09 12:00 AM
Date

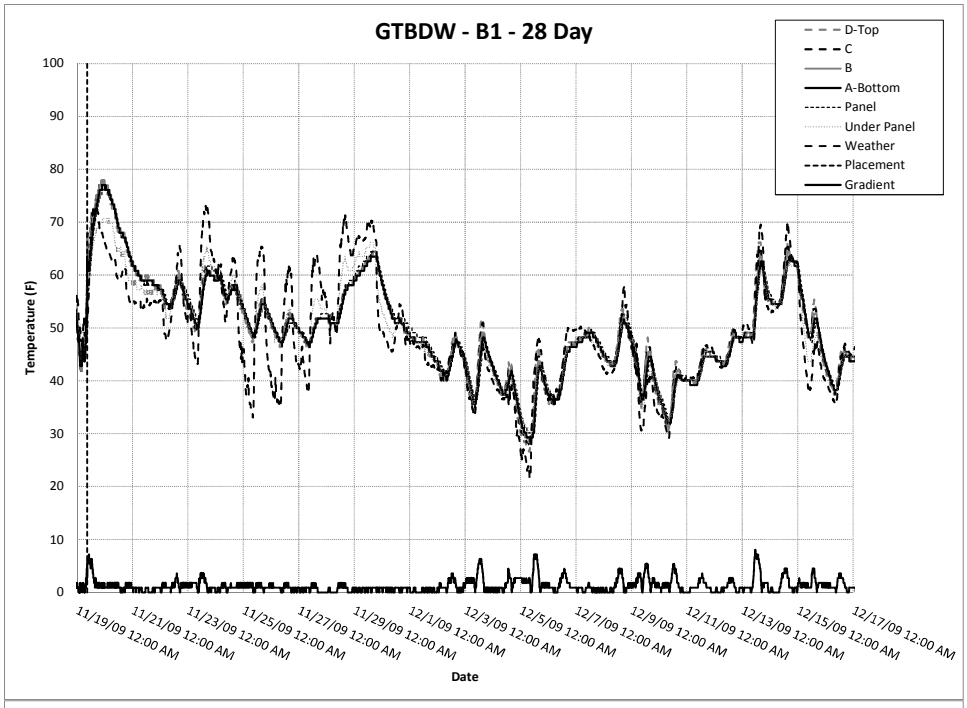
GTBDW - B1 - 28 Day
D-Top
C
B
A-Bottom
Panel
Under Panel
Weather
Placement
Gradient
Temperature (F)
100
90
80
70
60
50
40
30
20
10
0
11/19/09 12:00 AM
11/21/09 12:00 AM
11/23/09 12:00 AM
11/25/09 12:00 AM
11/27/09 12:00 AM
11/29/09 12:00 AM
12/1/09 12:00 AM
12/3/09 12:00 AM
12/5/09 12:00 AM
12/7/09 12:00 AM
12/9/09 12:00 AM
12/11/09 12:00 AM
12/13/09 12:00 AM
12/15/09 12:00 AM
12/17/09 12:00 AM
Date

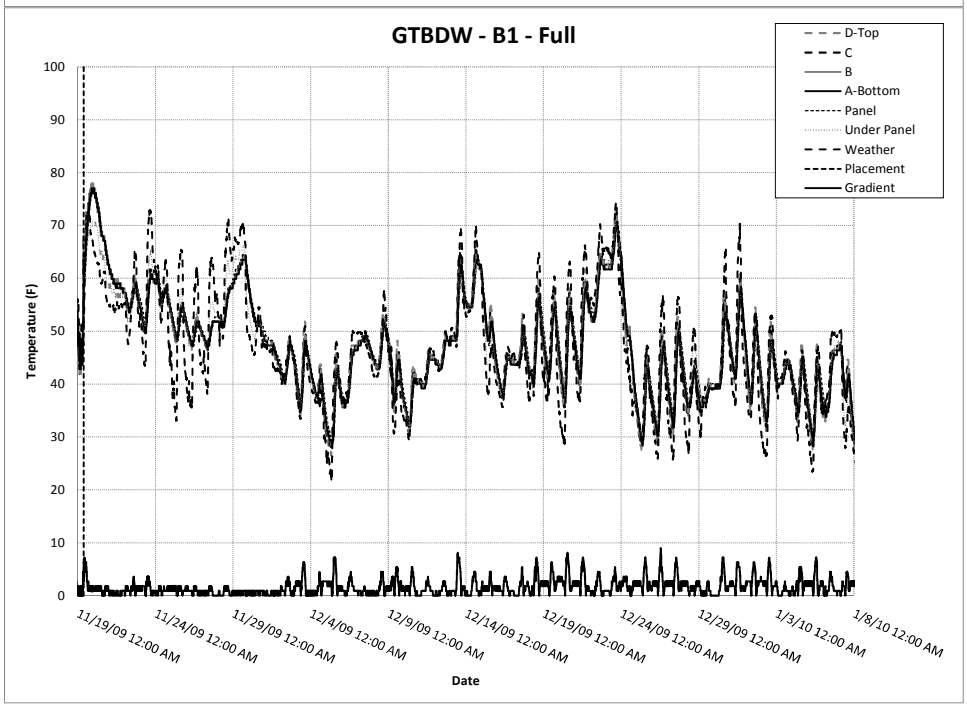
GTBDW - B1 - Full
D-Top
C
B
A-Bottom
Panel
Under Panel
Weather
Placement
Gradient
Temperature (F)
100
90
80
70
60
50
40
30
20
10
0
11/19/09 12:00 AM
11/24/09 12:00 AM
11/29/09 12:00 AM
12/4/09 12:00 AM
12/9/09 12:00 AM
12/14/09 12:00 AM
12/19/09 12:00 AM
12/24/09 12:00 AM
12/29/09 12:00 AM
1/3/10 12:00 AM
1/8/10 12:00 AM
Date

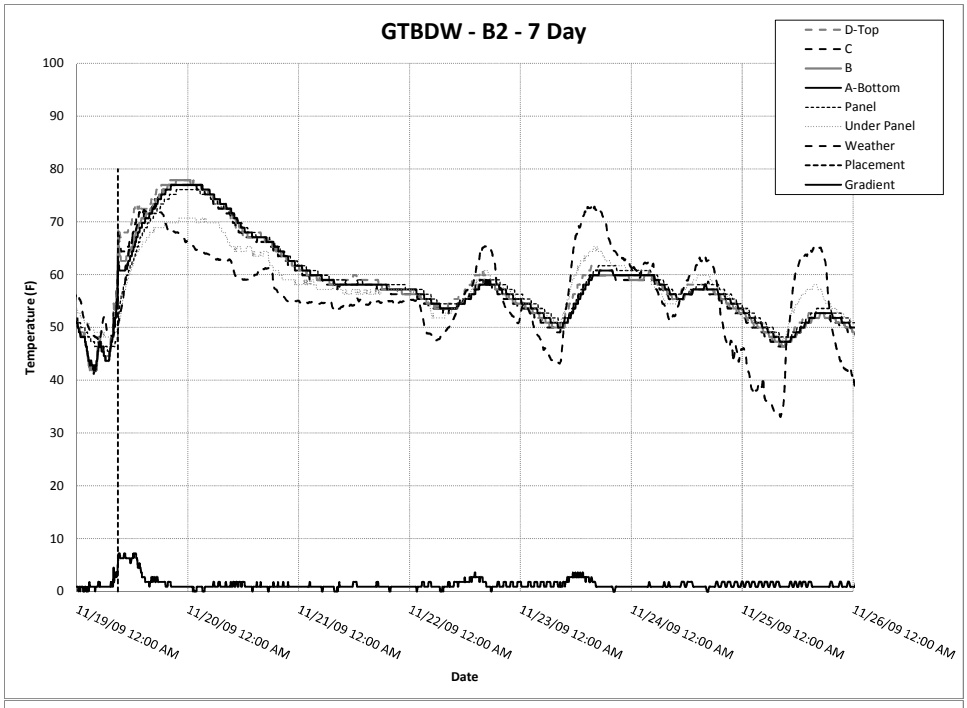
GTBDW - B2 - 7 Day
D-Top
C
B
A-Bottom
Panel
Under Panel
Weather
Placement
Gradient
Temperature (F)
100
90
80
70
60
50
40
30
20
10
0
11/19/09 12:00 AM
11/20/09 12:00 AM
11/21/09 12:00 AM
11/22/09 12:00 AM
11/23/09 12:00 AM
11/24/09 12:00 AM
11/25/09 12:00 AM
11/26/09 12:00 AM
Date

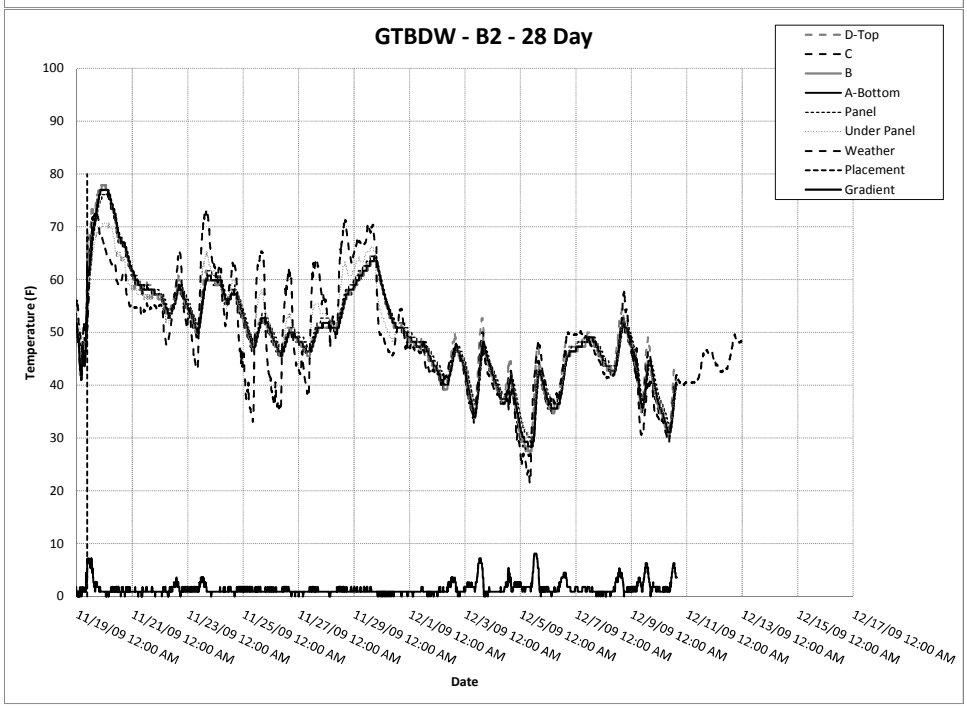
GTBDW - B2 - 28 Day
D-Top
C
B
A-Bottom
Panel
Under Panel
Weather
Placement
Gradient
Temperature (F)
100
90
80
70
60
50
40
30
20
10
0
11/19/09 12:00 AM
11/21/09 12:00 AM
11/23/09 12:00 AM
11/25/09 12:00 AM
11/27/09 12:00 AM
11/29/09 12:00 AM
12/1/09 12:00 AM
12/3/09 12:00 AM
12/5/09 12:00 AM
12/7/09 12:00 AM
12/9/09 12:00 AM
12/11/09 12:00 AM
12/13/09 12:00 AM
12/15/09 12:00 AM
12/17/09 12:00 AM
Date

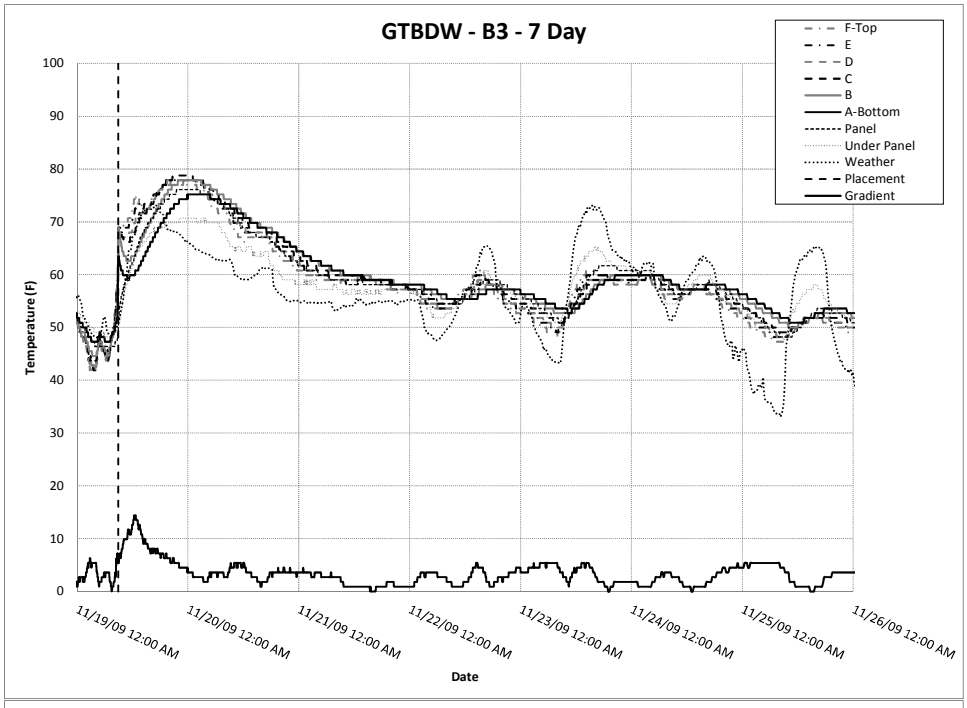
GTBDW - B3 - 7 Day
F-Top
E
D
C
B
A-Bottom
Panel
Under Panel
Weather
Placement
Gradient
Temperature (F)
100
90
80
70
60
50
40
30
20
10
0
11/19/09 12:00 AM
11/20/09 12:00 AM
11/21/09 12:00 AM
11/22/09 12:00 AM
11/23/09 12:00 AM
11/24/09 12:00 AM
11/25/09 12:00 AM
11/26/09 12:00 AM
Date

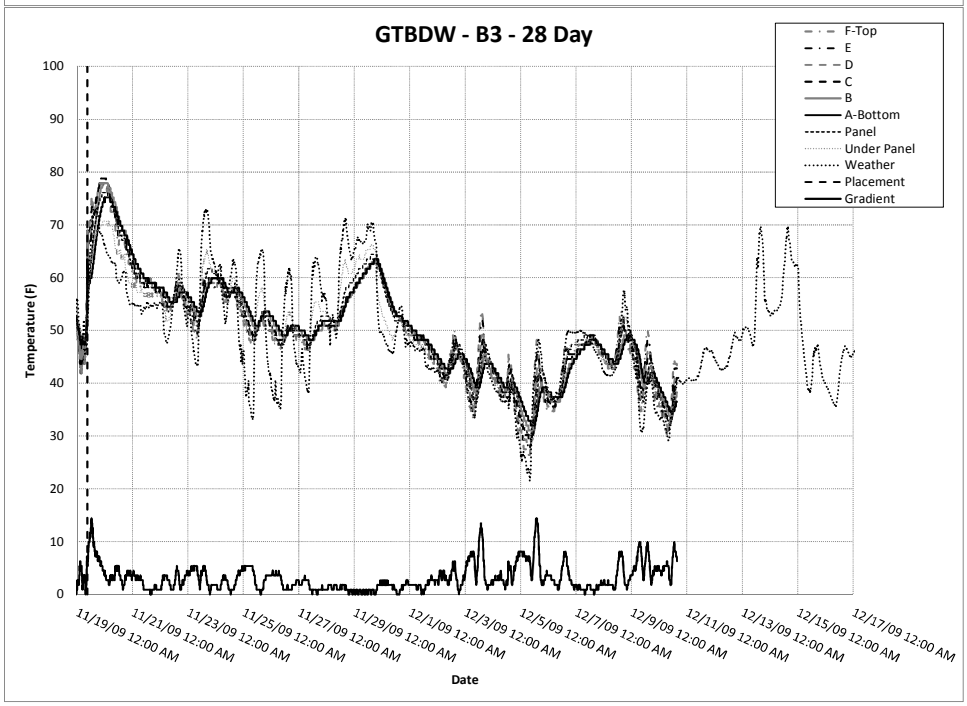
GTBDW - B3 - 28 Day
F-Top
E
D
C
B
A-Bottom
Panel
Under Panel
Weather
Placement
Gradient
Temperature (F)
100
90
80
70
60
50
40
30
20
10
0
11/19/09 12:00 AM
11/21/09 12:00 AM
11/23/09 12:00 AM
11/25/09 12:00 AM
11/27/09 12:00 AM
11/29/09 12:00 AM
12/1/09 12:00 AM
12/3/09 12:00 AM
12/5/09 12:00 AM
12/7/09 12:00 AM
12/9/09 12:00 AM
12/11/09 12:00 AM
12/13/09 12:00 AM
12/15/09 12:00 AM
12/17/09 12:00 AM
Date

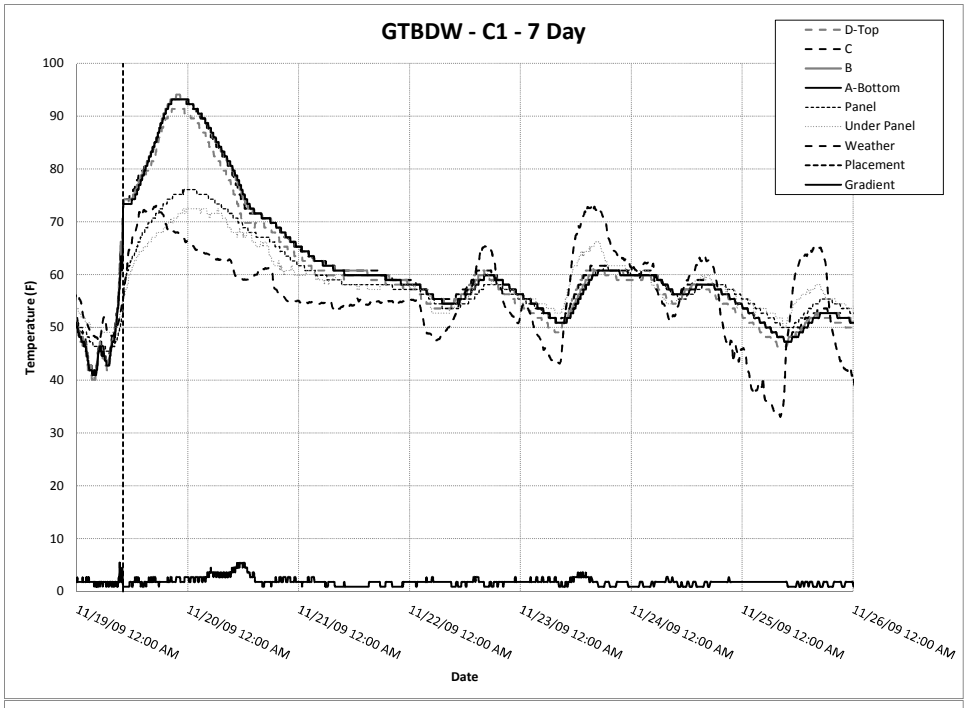
GTBDW - C1 - 7 Day
D-Top
C
B
A-Bottom
Panel
Under Panel
Weather
Placement
Gradient
Temperature (F)
100
90
80
70
60
50
40
30
20
10
0
11/19/09 12:00 AM
11/20/09 12:00 AM
11/21/09 12:00 AM
11/22/09 12:00 AM
11/23/09 12:00 AM
11/24/09 12:00 AM
11/25/09 12:00 AM
11/26/09 12:00 AM
Date

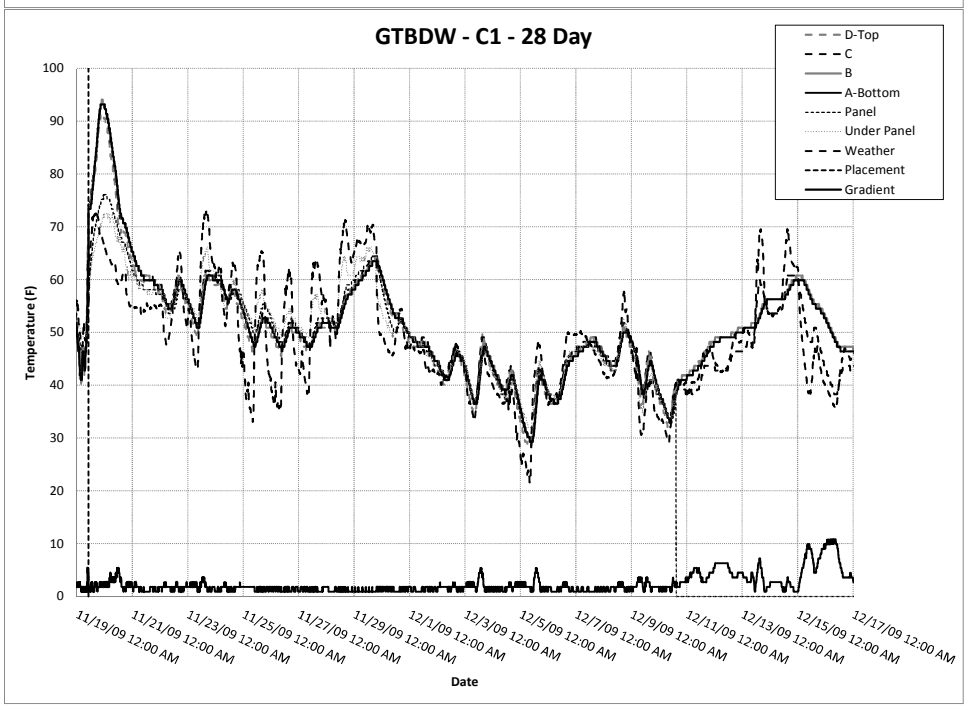
GTBDW - C1 - 28 Day
D-Top
C
B
A-Bottom
Panel
Under Panel
Weather
Placement
Gradient
Temperature (F)
100
90
80
70
60
50
40
30
20
10
0
11/19/09 12:00 AM
11/21/09 12:00 AM
11/23/09 12:00 AM
11/25/09 12:00 AM
11/27/09 12:00 AM
11/29/09 12:00 AM
12/1/09 12:00 AM
12/3/09 12:00 AM
12/5/09 12:00 AM
12/7/09 12:00 AM
12/9/09 12:00 AM
12/11/09 12:00 AM
12/13/09 12:00 AM
12/15/09 12:00 AM
12/17/09 12:00 AM
Date

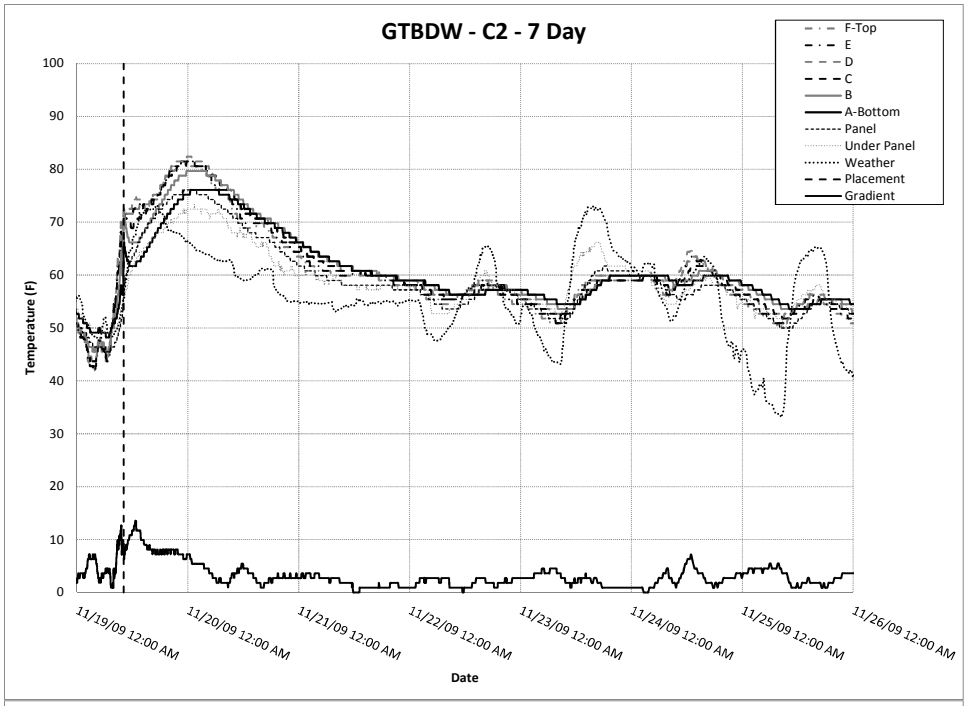
GTBDW - C2 - 7 Day
F-Top
E
D
C
B
A-Bottom
Panel
Under Panel
Weather
Placement
Gradient
Temperature (F)
100
90
80
70
60
50
40
30
20
10
0
11/19/09 12:00 AM
11/20/09 12:00 AM
11/21/09 12:00 AM
11/22/09 12:00 AM
11/23/09 12:00 AM
11/24/09 12:00 AM
11/25/09 12:00 AM
11/26/09 12:00 AM
Date

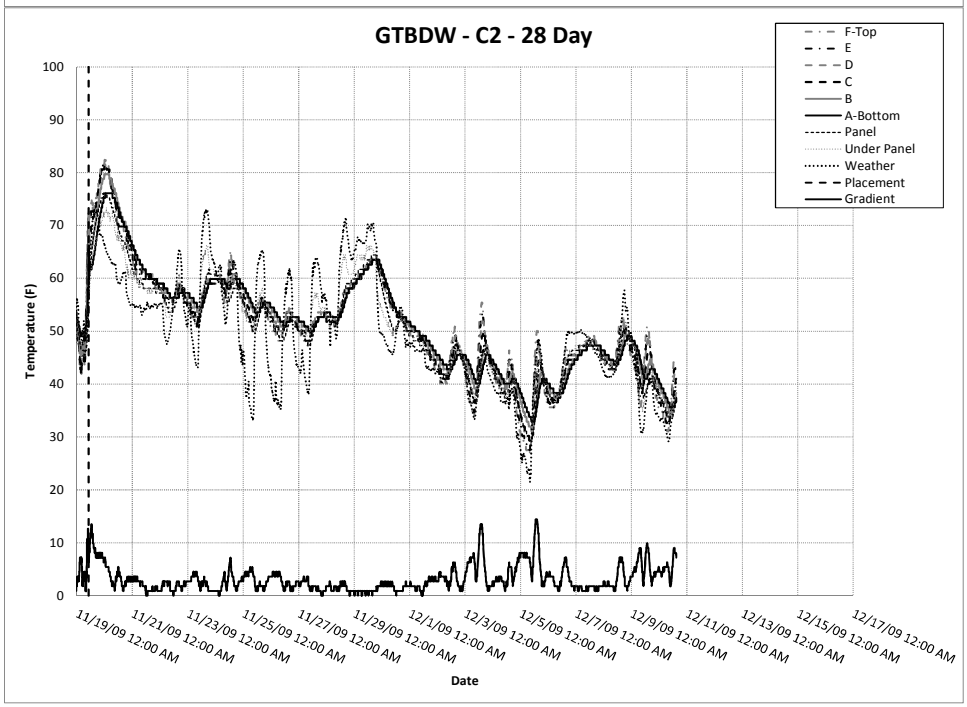
GTBDW - C2 - 28 Day
F-Top
E
D
C
B
A-Bottom
Panel
Under Panel
Weather
Placement
Gradient
Temperature (F)
100
90
80
70
60
50
40
30
20
10
0
11/19/09 12:00 AM
11/21/09 12:00 AM
11/23/09 12:00 AM
11/25/09 12:00 AM
11/27/09 12:00 AM
11/29/09 12:00 AM
12/1/09 12:00 AM
12/3/09 12:00 AM
12/5/09 12:00 AM
12/7/09 12:00 AM
12/9/09 12:00 AM
12/11/09 12:00 AM
12/13/09 12:00 AM
12/15/09 12:00 AM
12/17/09 12:00 AM
Date

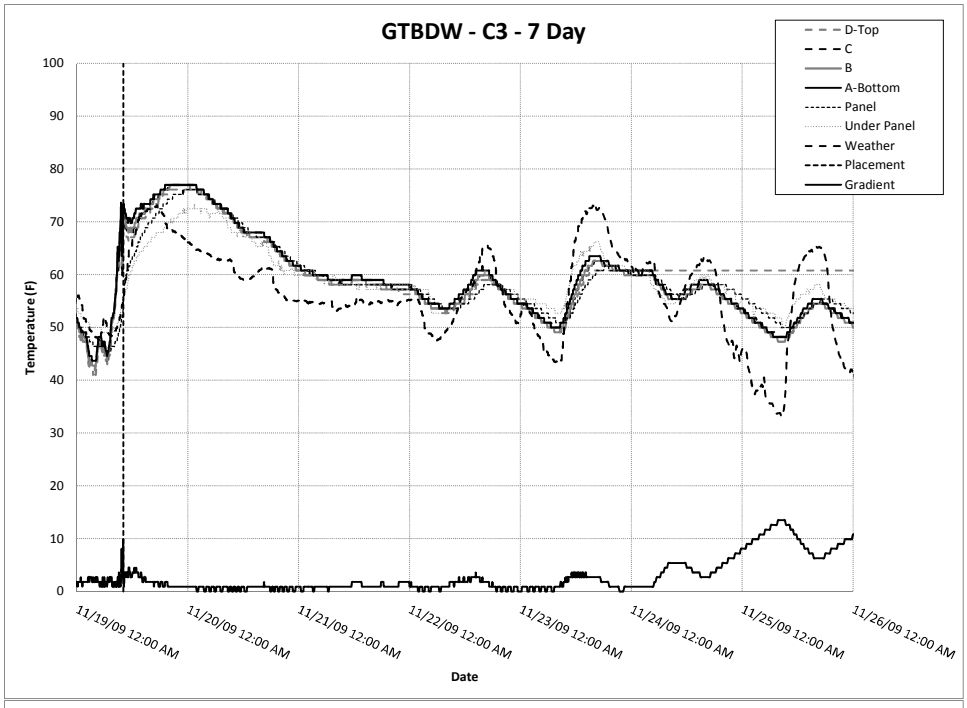
GTBDW - C3 - 7 Day
D-Top
C
B
A-Bottom
Panel
Under Panel
Weather
Placement
Gradient
Temperature (F)
100
90
80
70
60
50
40
30
20
10
0
11/19/09 12:00 AM
11/20/09 12:00 AM
11/21/09 12:00 AM
11/22/09 12:00 AM
11/23/09 12:00 AM
11/24/09 12:00 AM
11/25/09 12:00 AM
11/26/09 12:00 AM
Date

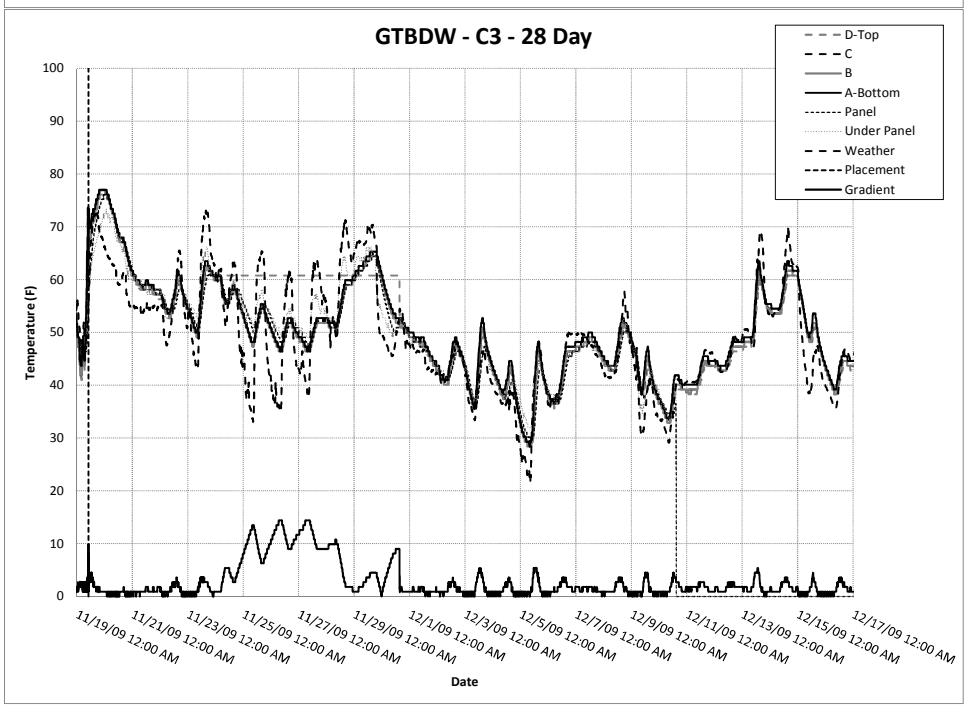
GTBDW - C3 - 28 Day
D-Top
C
B
A-Bottom
Panel
Under Panel
Weather
Placement
Gradient
Temperature (F)
100
90
80
70
60
50
40
30
20
10
0
11/19/09 12:00 AM
11/21/09 12:00 AM
11/23/09 12:00 AM
11/25/09 12:00 AM
11/27/09 12:00 AM
11/29/09 12:00 AM
12/1/09 12:00 AM
12/3/09 12:00 AM
12/5/09 12:00 AM
12/7/09 12:00 AM
12/9/09 12:00 AM
12/11/09 12:00 AM
12/13/09 12:00 AM
12/15/09 12:00 AM
12/17/09 12:00 AM
Date

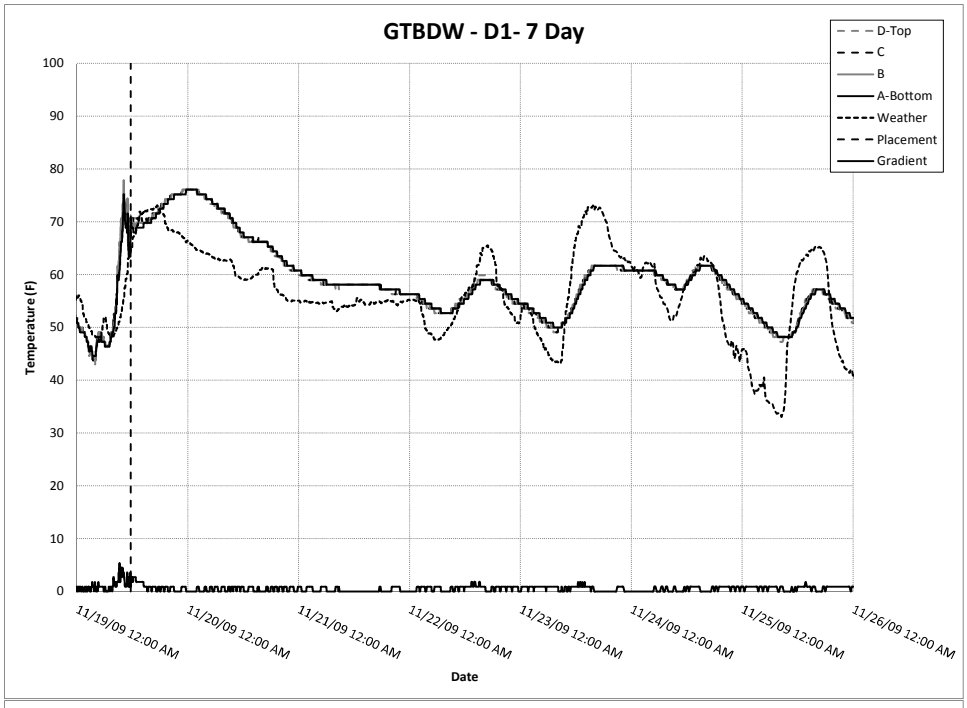
GTBDW - D1- 7 Day
D-Top
C
B
A-Bottom
Weather
Placement
Gradient
Temperature (F)
100
90
80
70
60
50
40
30
20
10
0
11/19/09 12:00 AM
11/20/09 12:00 AM
11/21/09 12:00 AM
11/22/09 12:00 AM
11/23/09 12:00 AM
11/24/09 12:00 AM
11/25/09 12:00 AM
11/26/09 12:00 AM
Date

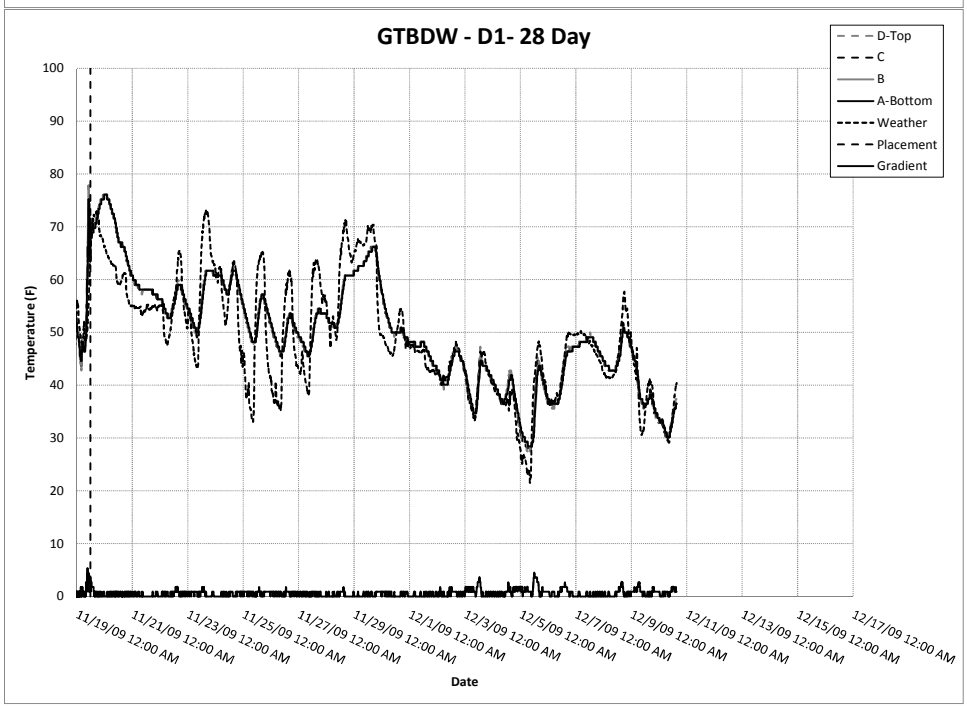
GTBDW - D1- 28 Day
D-Top
C
B
A-Bottom
Weather
Placement
Gradient
Temperature (F)
100
90
80
70
60
50
40
30
20
10
0
11/19/09 12:00 AM
11/21/09 12:00 AM
11/23/09 12:00 AM
11/25/09 12:00 AM
11/27/09 12:00 AM
11/29/09 12:00 AM
12/1/09 12:00 AM
12/3/09 12:00 AM
12/5/09 12:00 AM
12/7/09 12:00 AM
12/9/09 12:00 AM
12/11/09 12:00 AM
12/13/09 12:00 AM
12/15/09 12:00 AM
12/17/09 12:00 AM
Date

B.4 LUBBOCK BRIDGE DECK

B.4.1 iButton String Locations and Placement Times

Locations of iButton strings for this instrumentation, provided in Table B-73, were measured from the North end (end of pour) and the East face. iButton placement times, provided in Table B-74, were determined from examination of the iButton temperature data.

Table B-73: iButton string locations- LBD

String	Distance from North end	Distance from East face
A1	246	28.9
B1	138	51.58
B2	137.33	30
B3	137.5	6.58
C1	137.58	55.5
C2	137.5	25.83
C3	136.5	2.58
D1	13.83	29.75

All values in feet.

Table B-74: Concrete placement times- LBD

Strand	Placement Time
A	7/15/10 11:15 PM
B	7/16/10 1:55 AM
C	7/16/10 1:55 AM
D	7/16/10 5:11 AM

B.4.2 iButton Depths

Table B-75 provides the heights of the iButtons measured from either the precast, prestressed concrete panel, or the top of the precast, prestressed concrete girder. While

the exact depth of the bridge deck is not known, it is assumed that concrete sections are 4" thick over the concrete panels and 11" thick over the concrete girders. Descriptions of the iButton strings are also provided. While their original heights are listed in Table B-75, all 'F' iButtons from the six-button strings were removed at the request of the contractor.

Table B-75: iButton depths- LBD

Location	String	Button	Height from bottom.
Start of pour, above panel	A1	D	3.125
		C	2.250
		B	1.250
		A	0.250
Mid-pour, above panel, West side	B1	D	3.375
		C	2.500
		B	1.375
		A	0.250
Mid-pour, above panel, mid-width	B2	D	3.250
		C	2.250
		B	1.250
		A	0.250
Mid-pour, above panel, East side	B3	D	3.250
		C	2.250
		B	1.250
		A	0.250
End of pour, above panel	D1	D	3.250
		C	2.125
		B	1.125
		A	0.250
Mid-pour, above girder, West side	C1	F	9.500
		E	8.500
		D	7.500
		C	6.250
		B	3.250
		A	0.250
Mid-pour, above girder, mid-width	C2	F	9.375
		E	8.375
		D	7.375
		C	6.375
		B	3.500
		A	0.250
Mid-pour, above girder, East side	C3	F	9.250
		E	8.250
		D	7.500
		C	6.375
		B	3.375
		A	0.250

All values in inches.

B.4.3 Recorded Temperatures

The following figures present the complete set of temperature data for the Lubbock bridge deck. Figure B-92 presents a comparison of the temperatures recorded for a selected top iButton for each of the strands. The selected iButtons were located in the middle of the bridge deck width, when possible. Figure B-93 presents a comparison

of the gradient recorded across the different strands. As before, each strand is represented by the iButton string located in the middle of the bridge deck width, when possible. In the gradient graph, the iButton gradient, in °F, is presented in on the primary vertical axis, while the ambient air temperature, in °F, is presented on the secondary vertical axis. The graphs following Figure B-93 are labeled with the bridge deck pour name, LBD, the iButton string name, and the duration of time presented on that graph. For each string, the first graph presents the 7-day temperature data, such that the first temperature peaks may be examined. Seven days was chosen rather than four due to the reduced early-age peaks, and the increased duration of total iButton measurements. The following graph presents either the 28-day data set for the iButton string or the full data set, depending on how long the iButton was able to record temperatures. Due to various factors, some iButton strings may record longer durations than others.

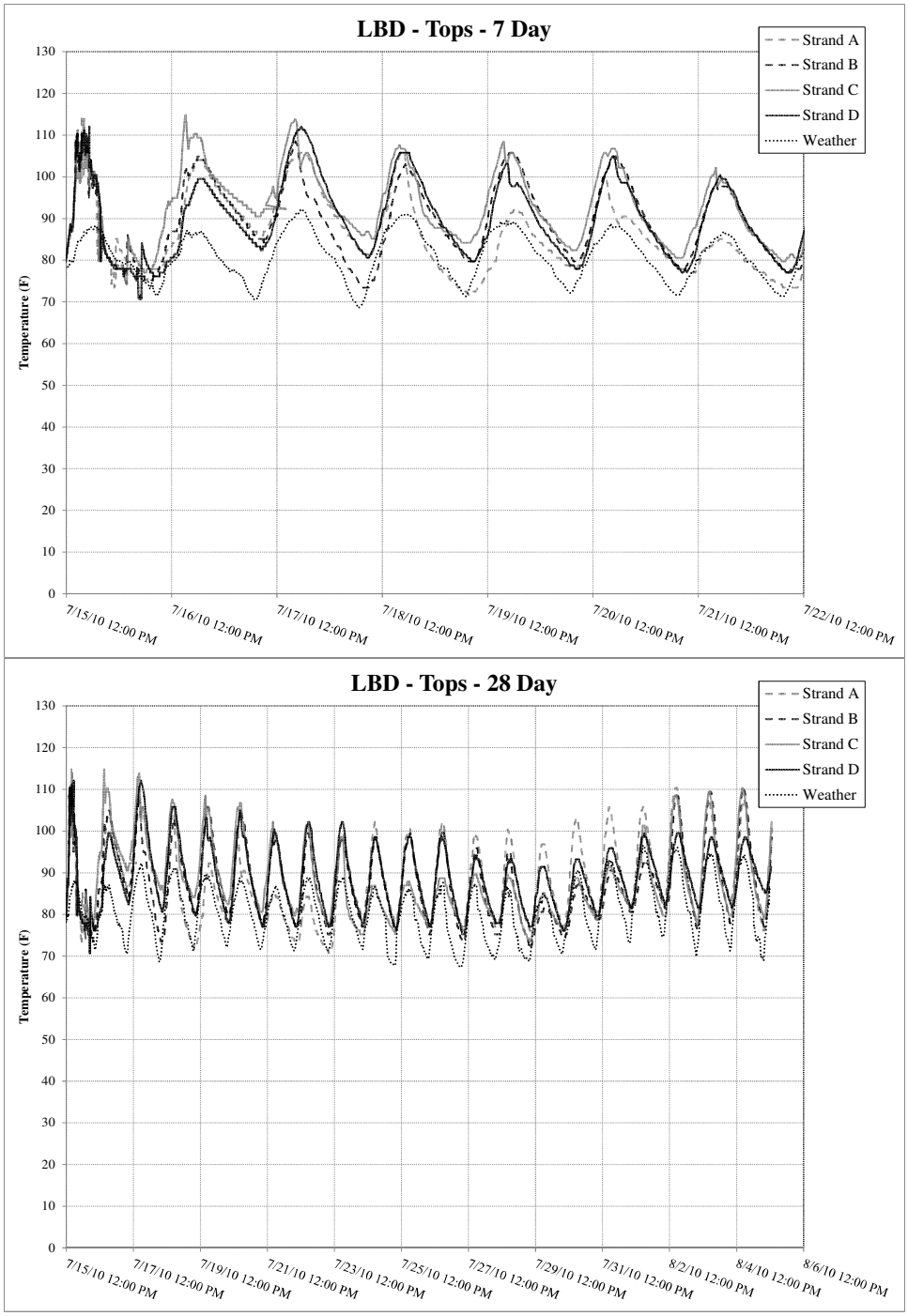

Figure B-92: Comparison of top iButton temperatures- LBD

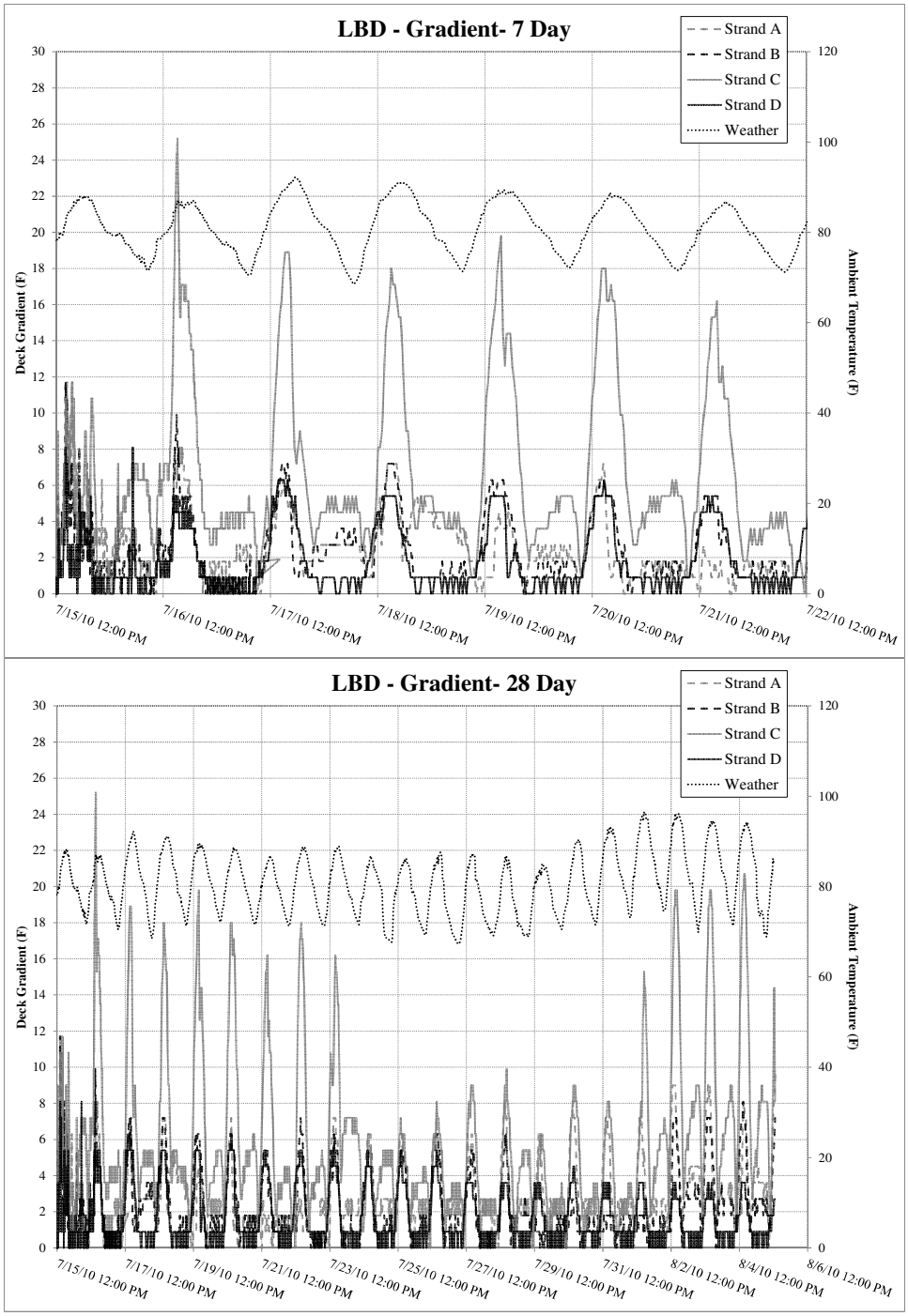

Figure B-93: Comparison of iButton strand gradients- LBD

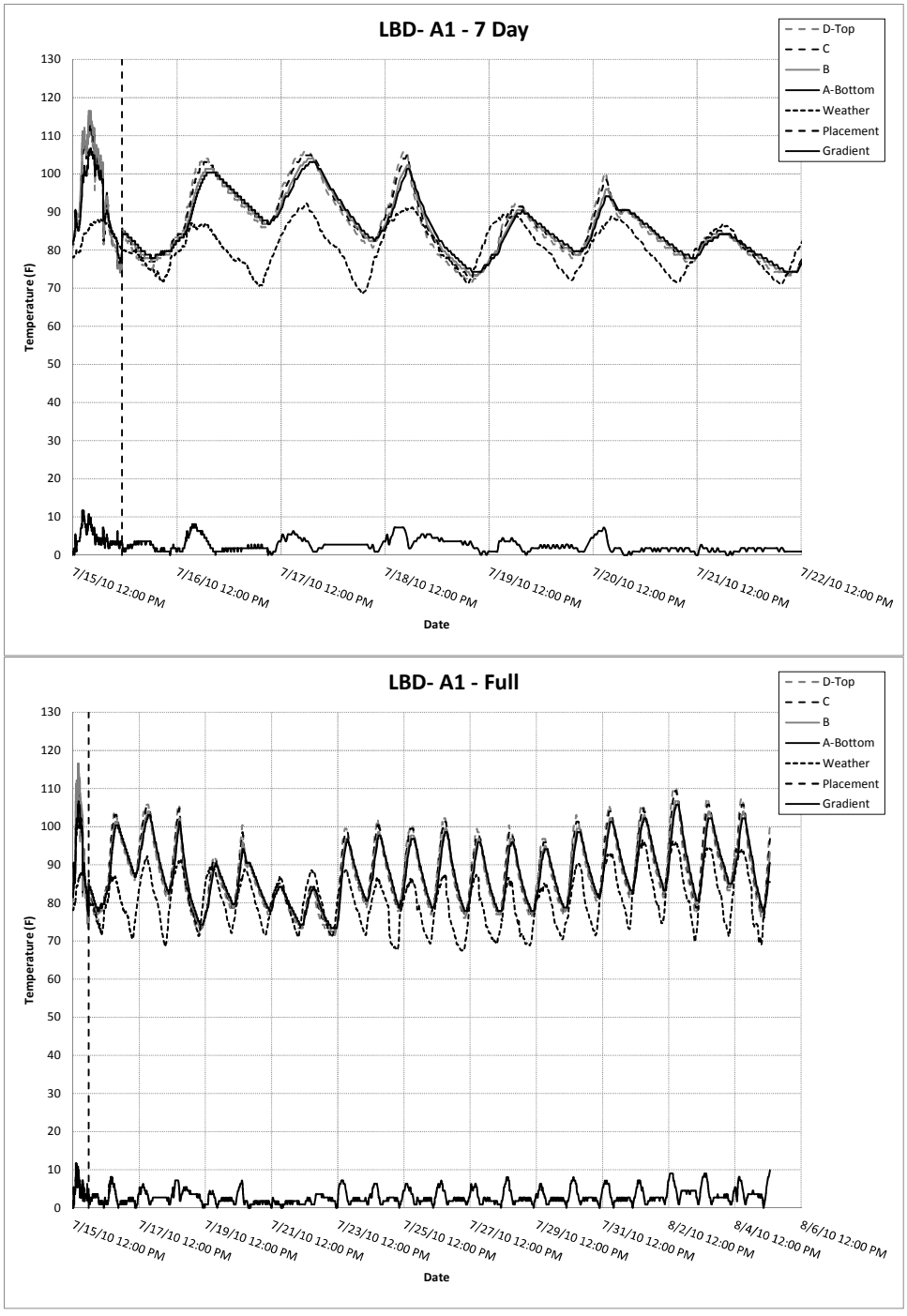
LBD- A1 - 7 Day
D-Top
C
B
A-Bottom
Weather
Placement
Gradient
Temperature (F)
130
120
110
100
90
80
70
60
50
40
30
20
10
0
7/15/10 12:00 PM
7/16/10 12:00 PM
7/17/10 12:00 PM
7/18/10 12:00 PM
7/19/10 12:00 PM
7/20/10 12:00 PM
7/21/10 12:00 PM
7/22/10 12:00 PM
Date
LBD- A1 - Full
D-Top
C
B
A-Bottom
Weather
Placement
Gradient
Temperature (F)
130
120
110
100
90
80
70
60
50
40
30
20
10
0
7/15/10 12:00 PM
7/17/10 12:00 PM
7/19/10 12:00 PM
7/21/10 12:00 PM
7/23/10 12:00 PM
7/25/10 12:00 PM
7/27/10 12:00 PM
7/29/10 12:00 PM
7/31/10 12:00 PM
8/2/10 12:00 PM
8/4/10 12:00 PM
8/6/10 12:00 PM
Date

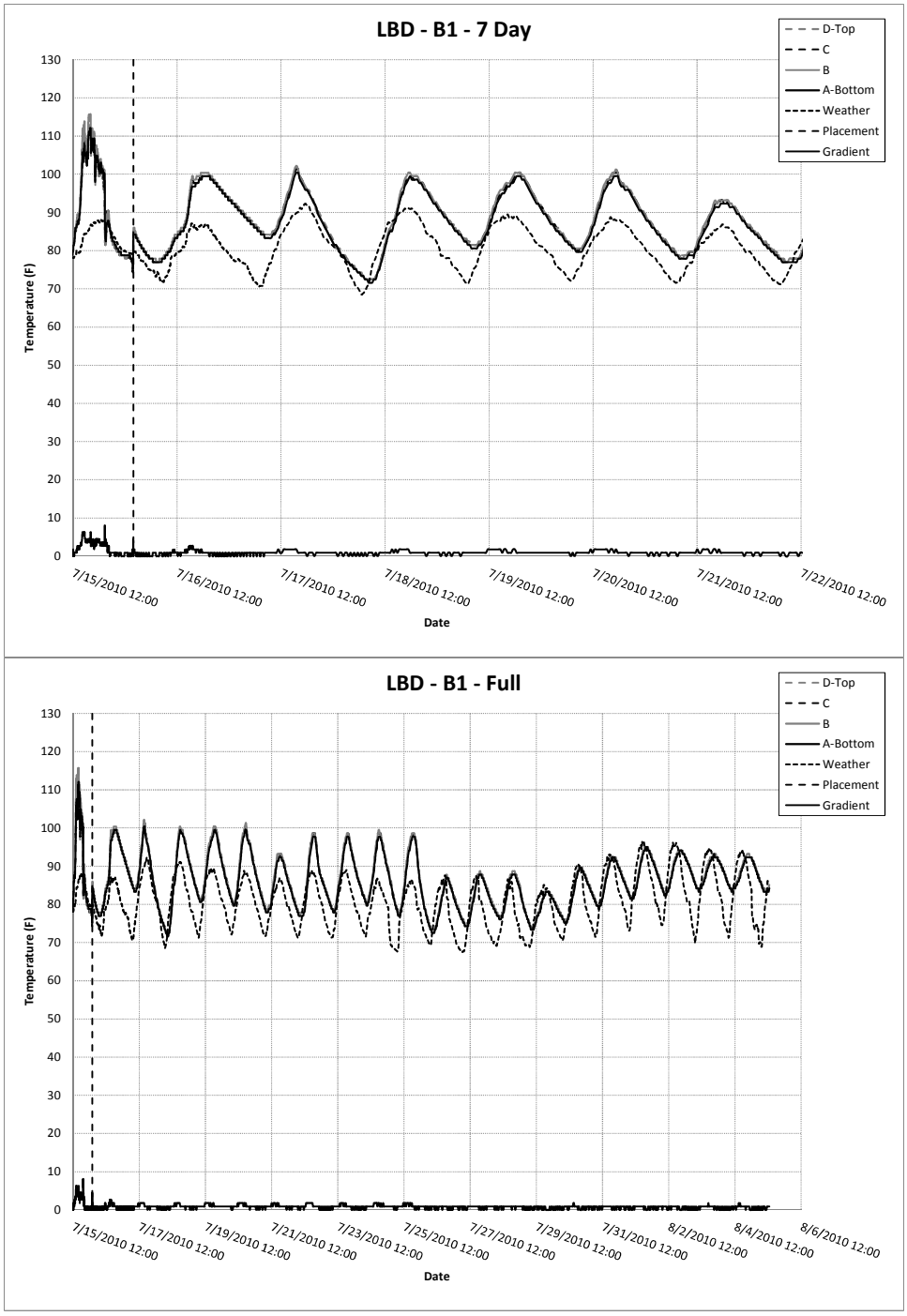
LBD - B1 - 7 Day
D-Top
C
B
A-Bottom
Weather
Placement
Gradient
Temperature (F)
130
120
110
100
90
80
70
60
50
40
30
20
10
0
7/15/2010 12:00
7/16/2010 12:00
7/17/2010 12:00
7/18/2010 12:00
7/19/2010 12:00
7/20/2010 12:00
7/21/2010 12:00
7/22/2010 12:00
Date
LBD - B1 - Full
D-Top
C
B
A-Bottom
Weather
Placement
Gradient
Temperature (F)
130
120
110
100
90
80
70
60
50
40
30
20
10
0
7/15/2010 12:00
7/17/2010 12:00
7/19/2010 12:00
7/21/2010 12:00
7/23/2010 12:00
7/25/2010 12:00
7/27/2010 12:00
7/29/2010 12:00
7/31/2010 12:00
8/2/2010 12:00
8/4/2010 12:00
8/6/2010 12:00
Date

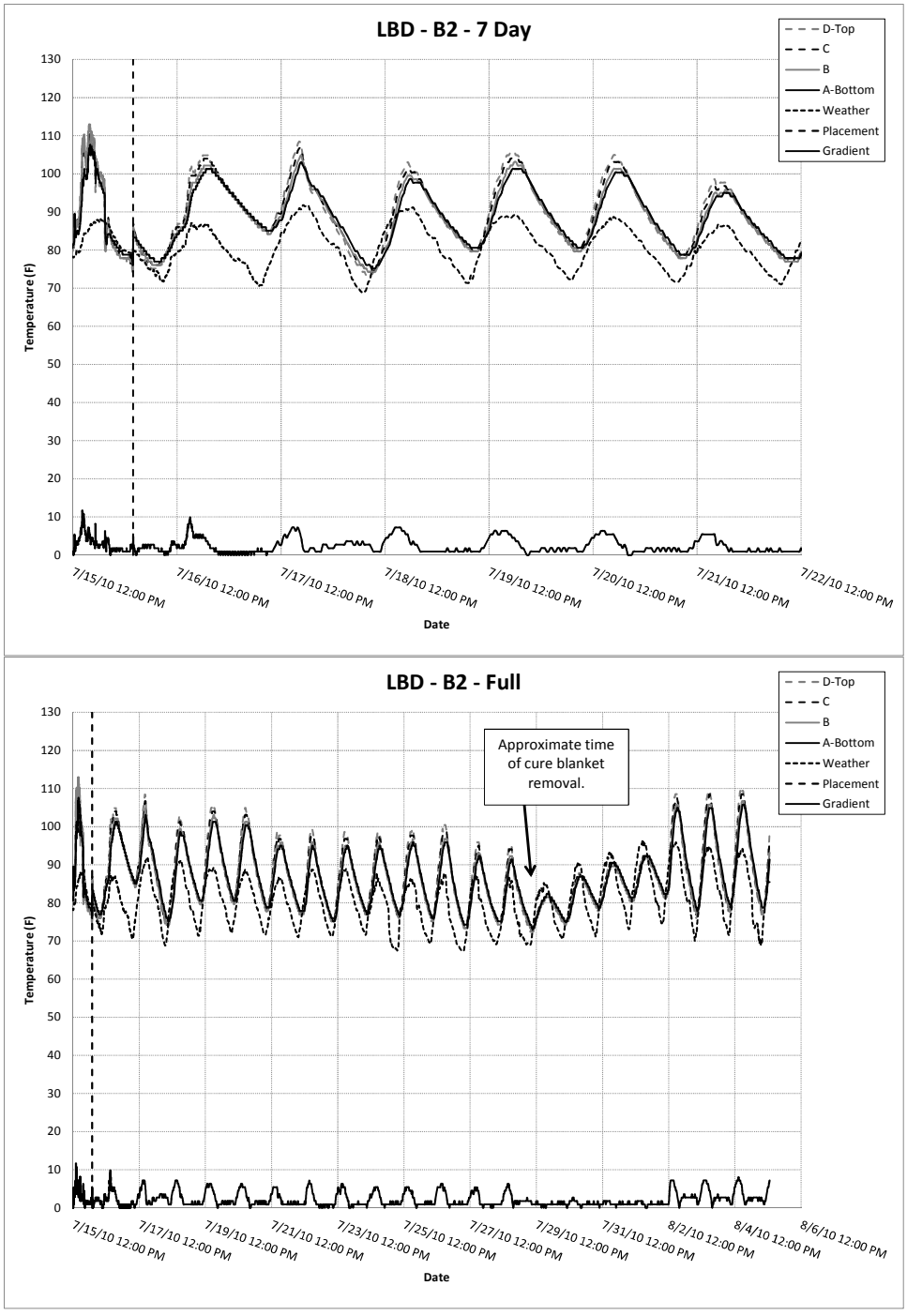
LBD - B2 - 7 Day
D-Top
C
B
A-Bottom
Weather
Placement
Gradient
Temperature (F)
130
120
110
100
90
80
70
60
50
40
30
20
10
0
7/15/10 12:00 PM
7/16/10 12:00 PM
7/17/10 12:00 PM
7/18/10 12:00 PM
7/19/10 12:00 PM
7/20/10 12:00 PM
7/21/10 12:00 PM
7/22/10 12:00 PM
Date
LBD - B2 - Full
Approximate time of cure blanket removal.
7/15/10 12:00 PM
7/17/10 12:00 PM
7/19/10 12:00 PM
7/21/10 12:00 PM
7/23/10 12:00 PM
7/25/10 12:00 PM
7/27/10 12:00 PM
7/29/10 12:00 PM
7/31/10 12:00 PM
8/2/10 12:00 PM
8/4/10 12:00 PM
8/6/10 12:00 PM

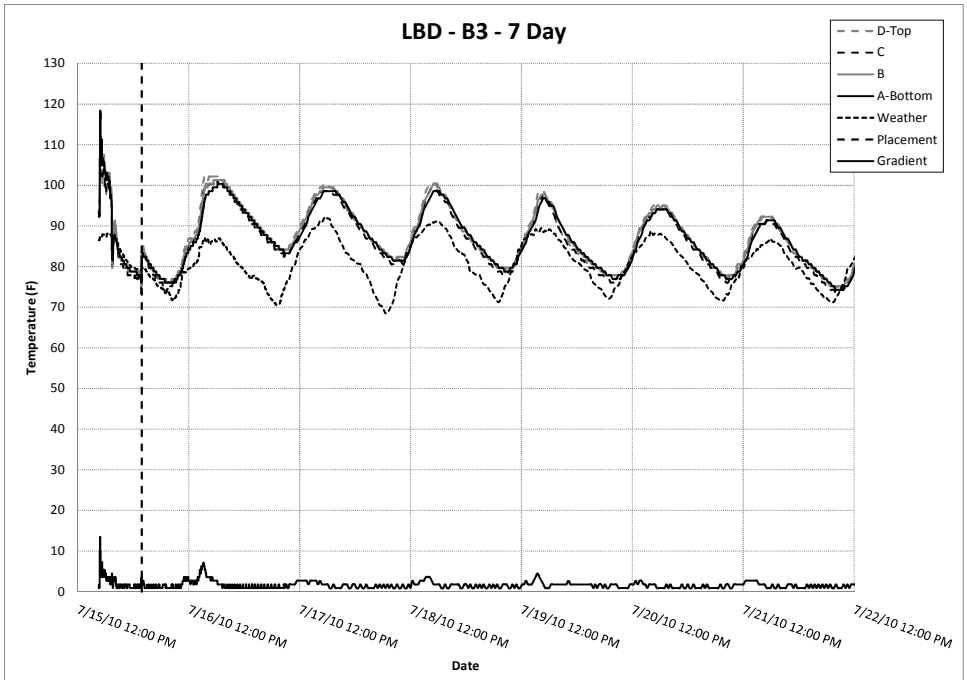
LBD - B3 - 7 Day
D-Top
C
B
A-Bottom
Weather
Placement
Gradient
Temperature (F)
130
120
110
100
90
80
70
60
50
40
30
20
10
0
7/15/10 12:00 PM
7/16/10 12:00 PM
7/17/10 12:00 PM
7/18/10 12:00 PM
7/19/10 12:00 PM
7/20/10 12:00 PM
7/21/10 12:00 PM
7/22/10 12:00 PM
Date

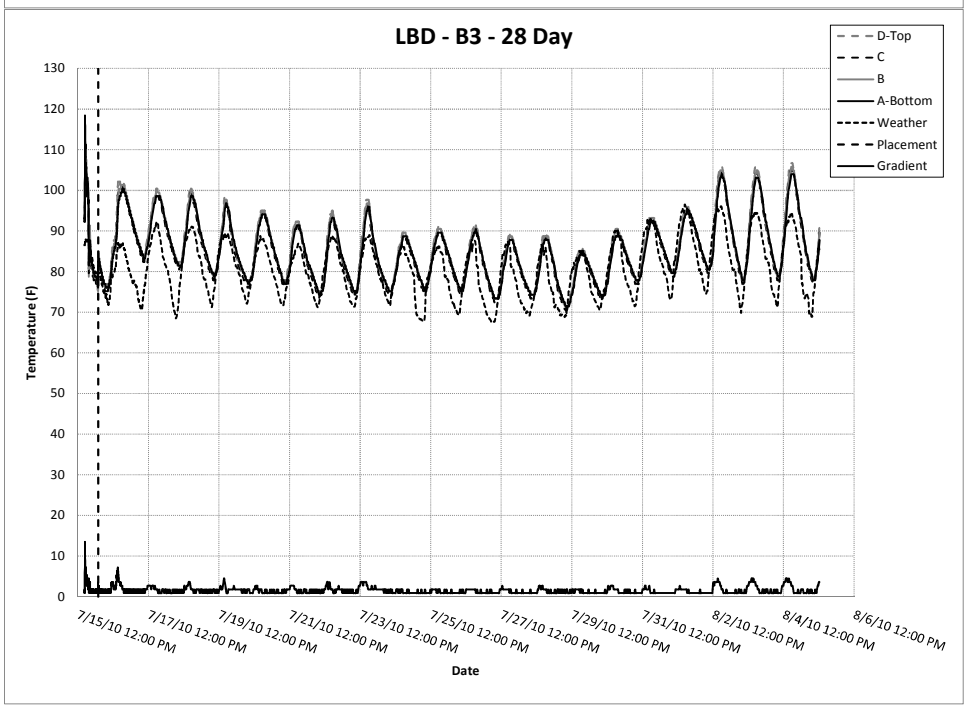
LBD - B3 - 28 Day
D-Top
C
B
A-Bottom
Weather
Placement
Gradient
Temperature (F)
130
120
110
100
90
80
70
60
50
40
30
20
10
0
7/15/10 12:00 PM
7/17/10 12:00 PM
7/19/10 12:00 PM
7/21/10 12:00 PM
7/23/10 12:00 PM
7/25/10 12:00 PM
7/27/10 12:00 PM
7/29/10 12:00 PM
7/31/10 12:00 PM
8/2/10 12:00 PM
8/4/10 12:00 PM
8/6/10 12:00 PM
Date

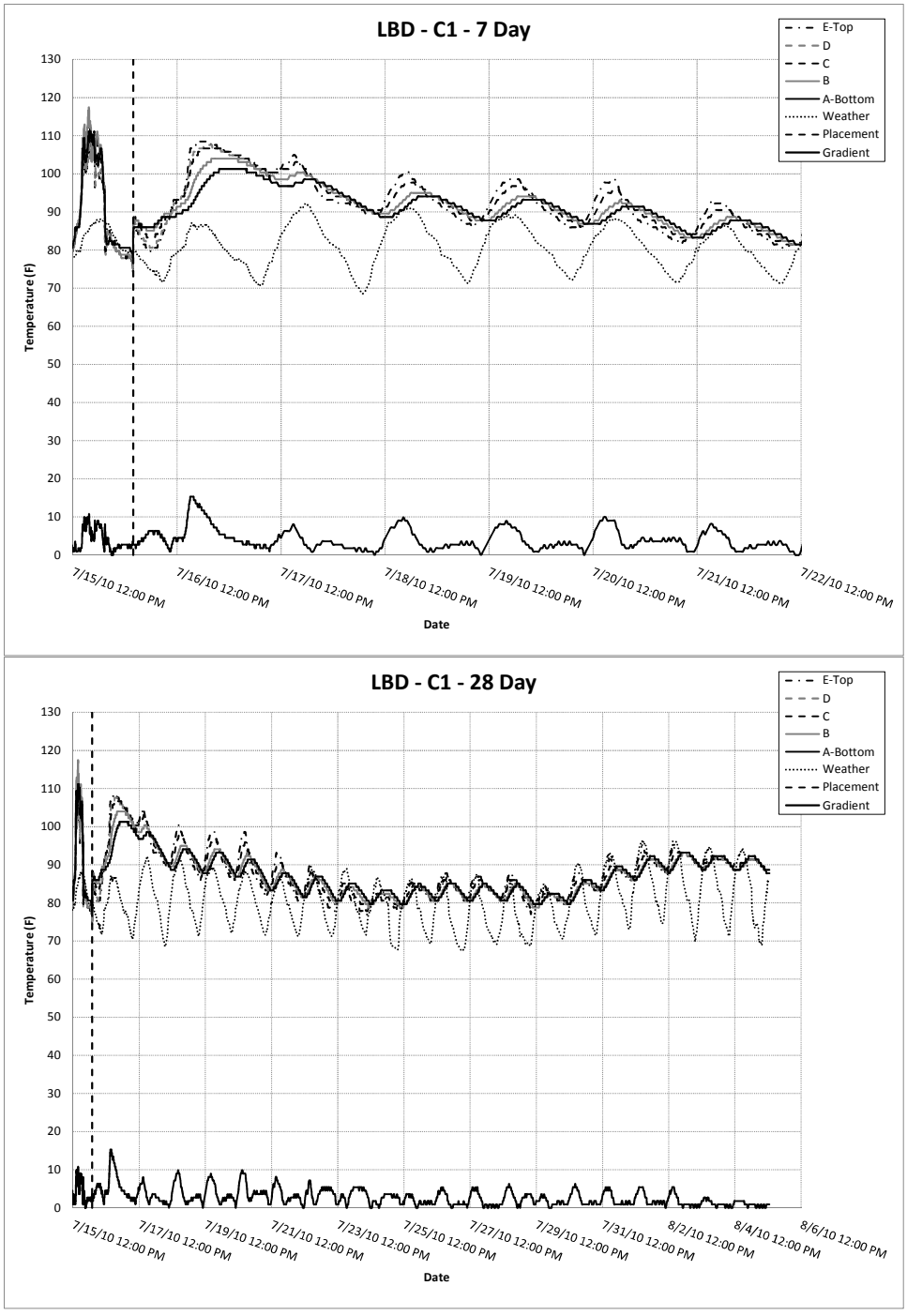
LBD - C1 - 7 Day
E-Top
D
C
B
A-Bottom
Weather
Placement
Gradient
Temperature (F)
130
120
110
100
90
80
70
60
50
40
30
20
10
0
7/15/10 12:00 PM
7/16/10 12:00 PM
7/17/10 12:00 PM
7/18/10 12:00 PM
7/19/10 12:00 PM
7/20/10 12:00 PM
7/21/10 12:00 PM
7/22/10 12:00 PM
Date
LBD - C1 - 28 Day
E-Top
D
C
B
A-Bottom
Weather
Placement
Gradient
Temperature (F)
130
120
110
100
90
80
70
60
50
40
30
20
10
0
7/15/10 12:00 PM
7/17/10 12:00 PM
7/19/10 12:00 PM
7/21/10 12:00 PM
7/23/10 12:00 PM
7/25/10 12:00 PM
7/27/10 12:00 PM
7/29/10 12:00 PM
7/31/10 12:00 PM
8/2/10 12:00 PM
8/4/10 12:00 PM
8/6/10 12:00 PM
Date

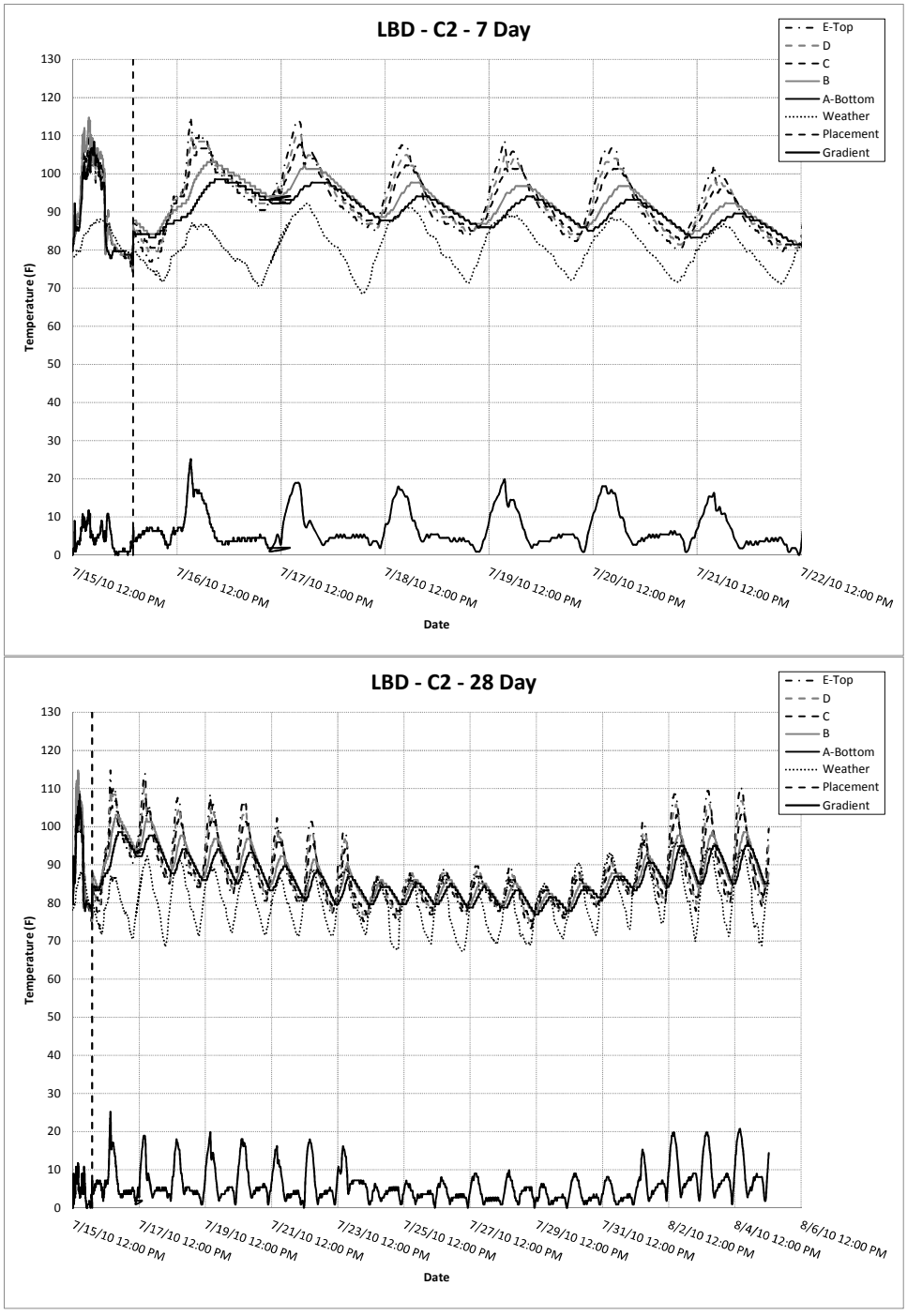
LBD - C2 - 7 Day
E-Top
D
C
B
A-Bottom
Weather
Placement
Gradient
Temperature (F)
130
120
110
100
90
80
70
60
50
40
30
20
10
0
7/15/10 12:00 PM
7/16/10 12:00 PM
7/17/10 12:00 PM
7/18/10 12:00 PM
7/19/10 12:00 PM
7/20/10 12:00 PM
7/21/10 12:00 PM
7/22/10 12:00 PM
Date
LBD - C2 - 28 Day
E-Top
D
C
B
A-Bottom
Weather
Placement
Gradient
Temperature (F)
130
120
110
100
90
80
70
60
50
40
30
20
10
0
7/15/10 12:00 PM
7/17/10 12:00 PM
7/19/10 12:00 PM
7/21/10 12:00 PM
7/23/10 12:00 PM
7/25/10 12:00 PM
7/27/10 12:00 PM
7/29/10 12:00 PM
7/31/10 12:00 PM
8/2/10 12:00 PM
8/4/10 12:00 PM
8/6/10 12:00 PM
Date

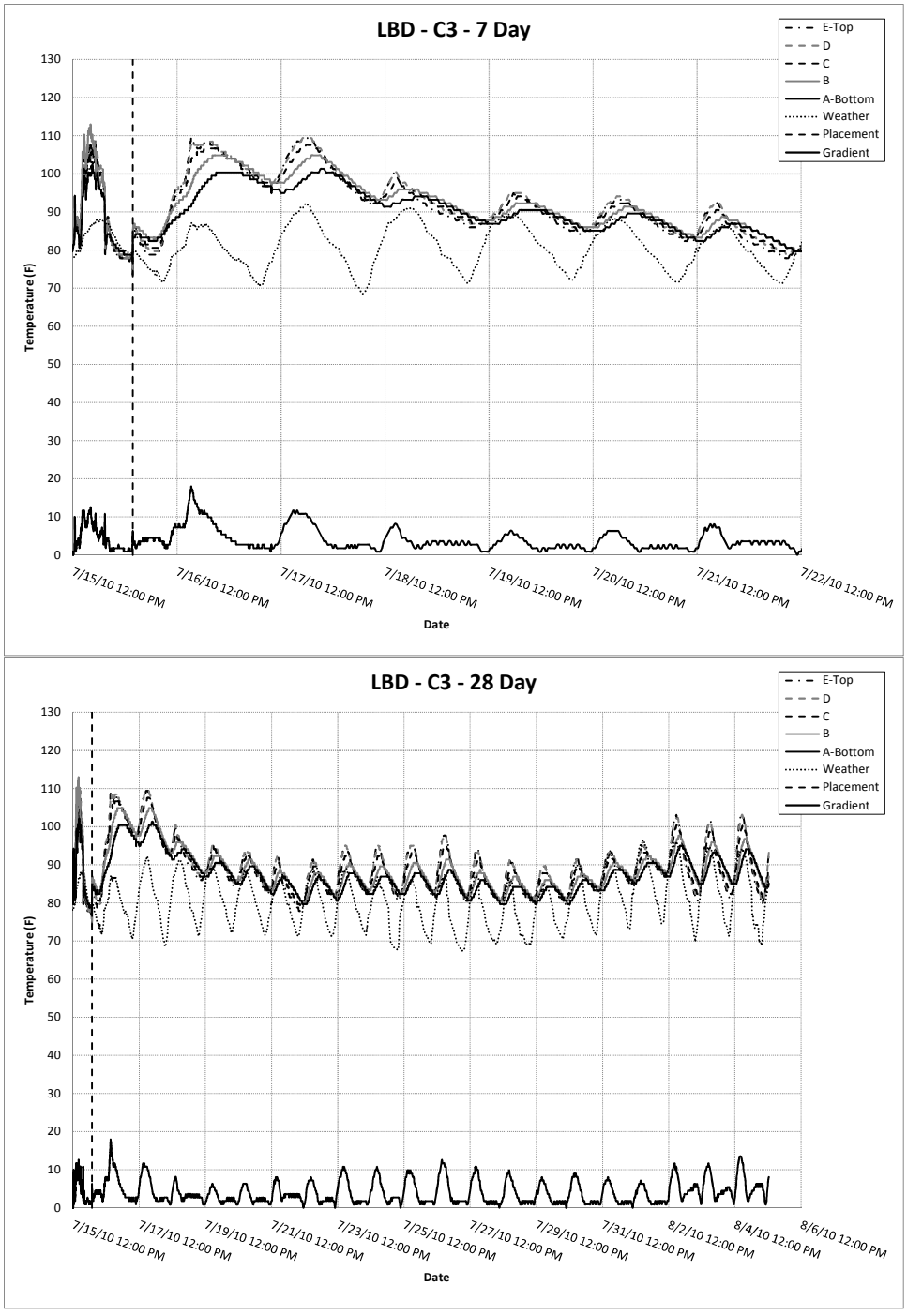
LBD - C3 - 7 Day
E-Top
D
C
B
A-Bottom
Weather
Placement
Gradient
Temperature (F)
130
120
110
100
90
80
70
60
50
40
30
20
10
0
7/15/10 12:00 PM
7/16/10 12:00 PM
7/17/10 12:00 PM
7/18/10 12:00 PM
7/19/10 12:00 PM
7/20/10 12:00 PM
7/21/10 12:00 PM
7/22/10 12:00 PM
Date
LBD - C3 - 28 Day
E-Top
D
C
B
A-Bottom
Weather
Placement
Gradient
Temperature (F)
130
120
110
100
90
80
70
60
50
40
30
20
10
0
7/15/10 12:00 PM
7/17/10 12:00 PM
7/19/10 12:00 PM
7/21/10 12:00 PM
7/23/10 12:00 PM
7/25/10 12:00 PM
7/27/10 12:00 PM
7/29/10 12:00 PM
7/31/10 12:00 PM
8/2/10 12:00 PM
8/4/10 12:00 PM
8/6/10 12:00 PM
Date

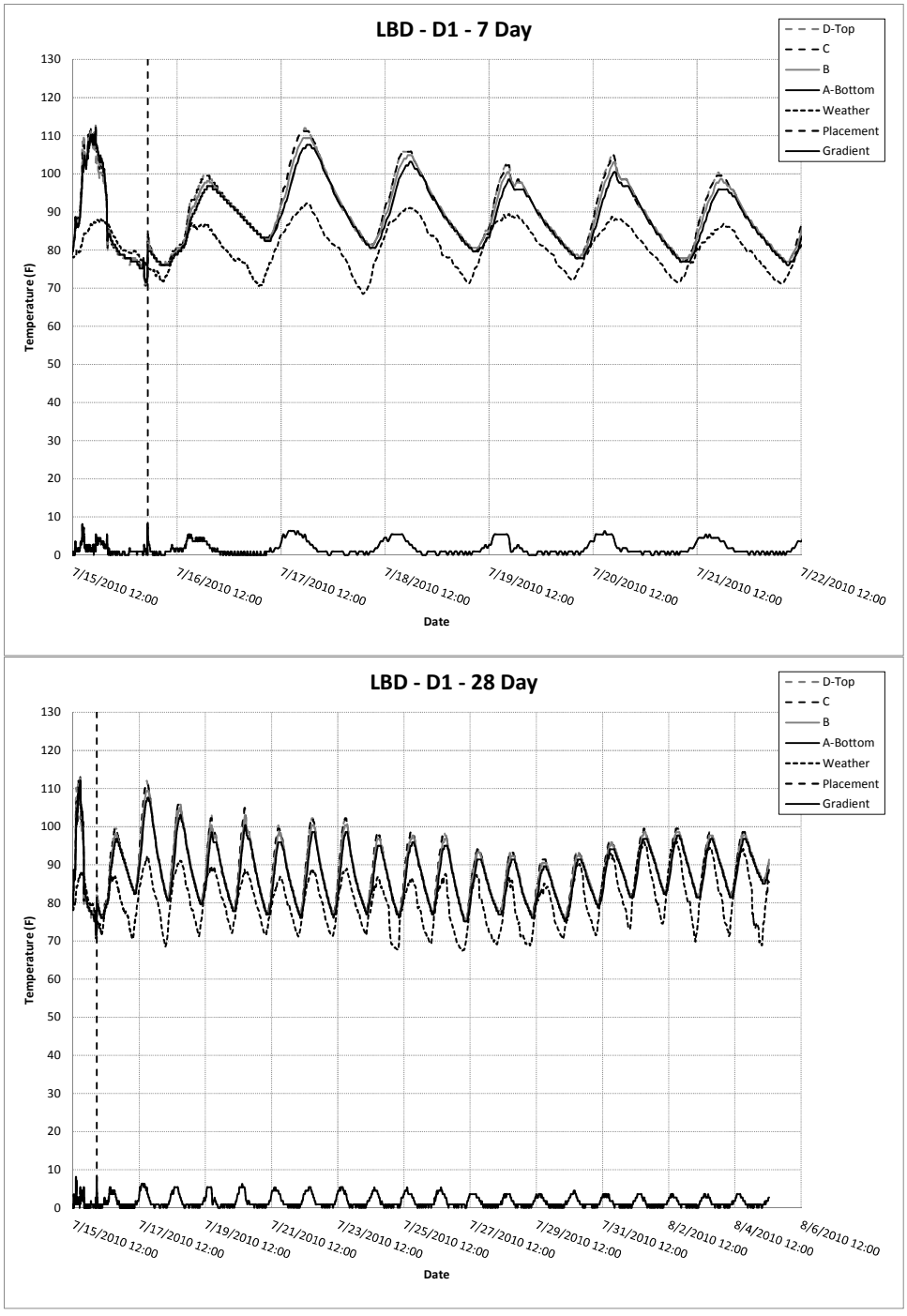
LBD - D1 - 7 Day
D-Top
C
B
A-Bottom
Weather
Placement
Gradient
Temperature (F)
130
120
110
100
90
80
70
60
50
40
30
20
10
0
7/15/2010 12:00
7/16/2010 12:00
7/17/2010 12:00
7/18/2010 12:00
7/19/2010 12:00
7/20/2010 12:00
7/21/2010 12:00
7/22/2010 12:00
Date
LBD - D1 - 28 Day
D-Top
C
B
A-Bottom
Weather
Placement
Gradient
Temperature (F)
130
120
110
100
90
80
70
60
50
40
30
20
10
0
7/15/2010 12:00
7/17/2010 12:00
7/19/2010 12:00
7/21/2010 12:00
7/23/2010 12:00
7/25/2010 12:00
7/27/2010 12:00
7/29/2010 12:00
7/31/2010 12:00
8/2/2010 12:00
8/4/2010 12:00
8/6/2010 12:00
Date

Appendix C: New Rigid Cracking Frame Formwork

Before testing began on TxDOT Project 6332, the formwork that had been previously used for rigid cracking frame testing was replaced with formwork built by the author. After many mixtures and years of testing, the previous wooden formwork had considerable distress including rotting wood, separation of copper flashing, and fatiguing of the walls of the formwork. Fatigue of the sides of the formwork led to the sides shifting during concrete placement in the formwork, which later caused stress concentrations at the formwork-crosshead interface. The new formwork was built with a steel frame, and consists of three separate pieces. The new design was constructed to provide a greater ease of use, and to create formwork that would withstand the rigors of the set-up and removal procedure for many years. The copper flashing used was also approximately twice as thick as that previously used. Pictures of the previously used formwork and pictures taken during the construction of the new formwork are presented below. Further information regarding the dimensions of the steel formwork can be acquired through contacting the laboratory manager at CMRG, or though contacting the author.

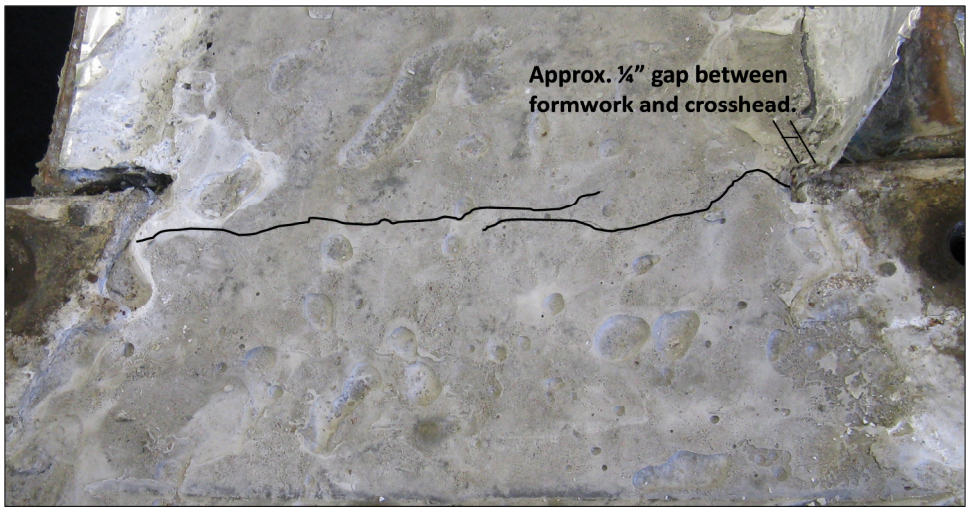

Figure C-94: Stress concentrations from formwork fatigue.

Figure C-95: Separation of copper flashing.

Figure C-96: Deterioration of existing formwork.

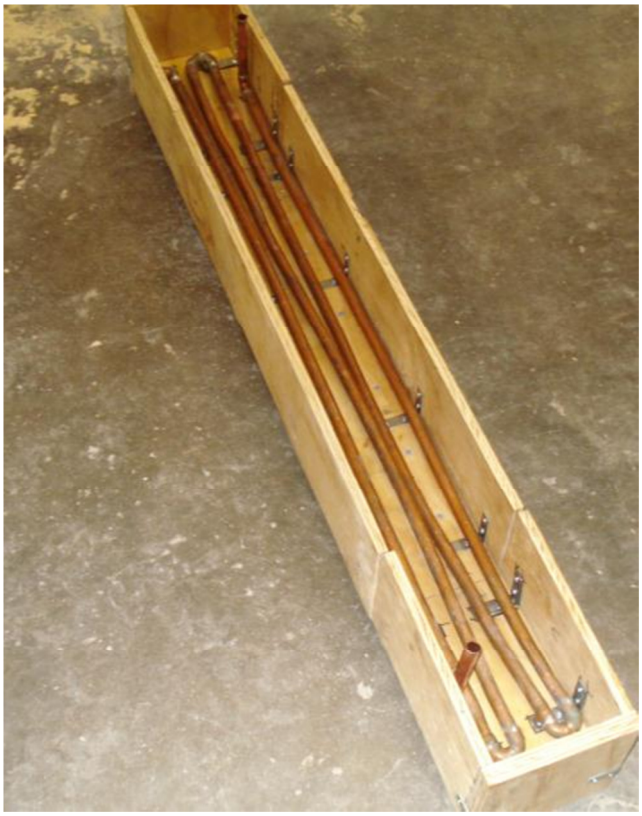

Figure C-97: Formwork for side insulation pouring.

Figure C-98: Fitting of steel formwork.

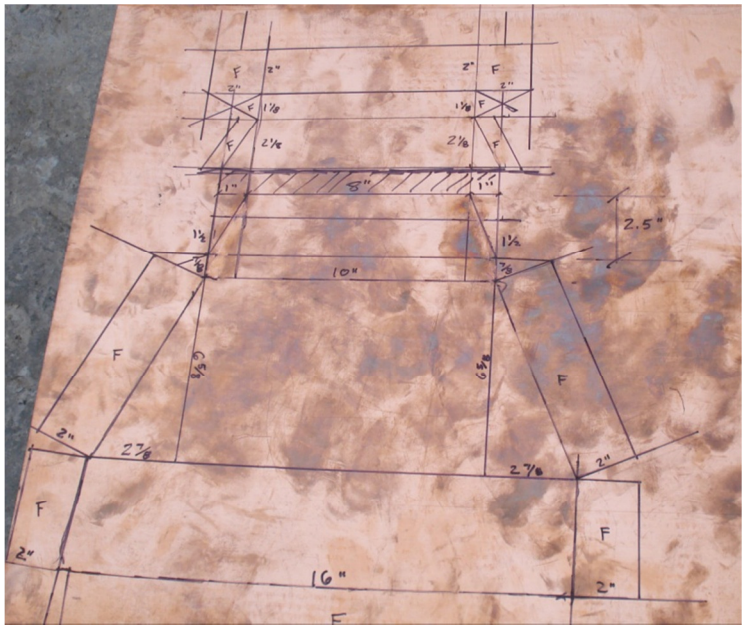

Figure C-99: Measurements for cutting new flashing with fold-over flaps.

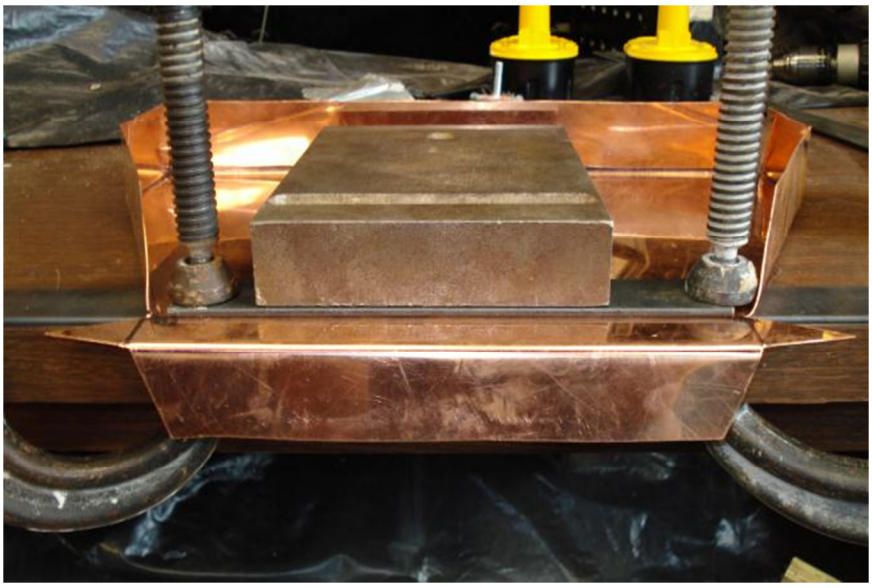

Figure C-100: Bending of copper flashing.

Figure C-101: Painting of steel formwork.

Figure C-102: Side walls prior to application of flashing.

Figure C-103: Bottom formwork before application of flashing.

Figure C-104: Seating of flashing prior to drilling for screw holes.

Figure C-105: Installation process to reduce free edges of flashing.

References

(1993). *CEB-FIP Model Code '90.* Tomas Telford, London: Comite Euro-International du Beton.

Abel, J., & Hover, K. (1998). Effect of Water/Cement Ratio on the Early Age Tensile Strength of Concrete. *Transportation Reserch Record, 1610*.

Abel, J., & Hover, K. (1998). Effect of Water/Cement Ratio on the Early-Age Tensile Strength of Concrete. *Transportation Research Board, 1610*, 33-38.

ACI Committee 209. (2008). *Prediction of Creep, Shrinkage and Temperature Effects in Concrete Structures (ACI209R-92).* Farmington Hills, Mich.: American Concrete Institute.

ACI Committee 224. (2001). *Control of Cracking in Concrete.* Farmington Hills, Mich.: American Concrete Institute.

ACI Committee 318. (2008). *Buidling Code Requirements for Structural Concrete.* Farmington Hills, Mich.: American Concrete Institute.

Akita, H., Fujuwara, T., & Ozaka, Y. (1997). Practical Procedure for the Analysis of Moisture Transfer Within concrete Due to Drying. *Magazine of Concrete Research, 49*(179), 1-7.

Al-Fadhala, M., & Hover, K. (2001). Rapid Evaporation from Freshly Cast Concrete and the Gulf Environment. *Construction and Building Materials, 15*, 1-7.

Al-Manseer, & Lam, J. (2005). Statistical Evaluation of Shrinkage and Creep Models. *ACI Materials Journal, 102*(3).

ASTM C 618. (2008). *Standard Specification for Coal Fly Ash and Raw or Caclined Natural Pozzolan for Use in Concrete.* Pennsylvania: American Society of Testing and Materials.

ASTM C 989. (2010). *Standard Specification for Slag Cement for Use in Concrete and Mortars.* Pennsylvania: American Society of Testing and Materials.

ASTM C138. (2010). *Standard Test Method for Density (Unit Weight), Yield, and Air Content (Gravimetric) of Concrete.* Pennsylvania: American Society of Testing and Materials.

ASTM C143. (2010). *Standard Test Method for Slump of Hydraulic-Cement Concrete.* Pennsylvania: American Society of Testing and Materials.

ASTM C150. (2011). *Standard Specification for Portland Cement.* Pennsylvania: American Society of Testing and Materials.

ASTM C157. (2008). *Standard Test Method for Length Change of Hardened Hydraulic-Cement Mortar and Concrete.* Pennsylvania: American Society of Testing and Materials.

ASTM C231. (2010). *Standard Test Method for Air Content of Freshly Mixed Concrete by the Pressure Method.* Pennsylvania: American Society of Testing and Materials.

ASTM C33. (2011). *Standard Specification for Concrete Aggregates.* Pennsylvania: American Society of Testing and Materials.
ASTM C39. (2010). *Standard Test Method for Compressive Strength of Cylindrical Concrete Specimens.* Pennsylvania: American Society of Testing and Materials.
ASTM C403. (2008). *Standard Test Method for Time of Setting of Concrete Mixtures by Penetration Resistance.* Pennsylvania: American Society of Testing and Materials.
ASTM C469. (2010). *Standard Test Method for Static Modulus of Elasticity and Poisson's Ratio of Concrete in Compression.* Pennsylvania: American Society of Testing and Materials.
ASTM C494. (2010). *Standard Specification for Chemical Admixtures for Concrete.* Pennsylvania: American Society of Testing and Materials.
ASTM C496. (2004). *Standard Test Method for Splitting Tensile Strength of Cylindrical Concrete Specimens.* Pennsylvania: American Society of Testing and Materials.
Babaei, K., & Fouladgar, A. (1997). Solustions to Concrete Bridge Deck Cracking. *Concrete International, 19*(7), 34-37.
Bazant, Z. (1995). Creep and Shrinkage Prediction Model for Analysis and Design of Concrete Structures- Model B3. *Materials and Structures, 28*, 357-365.
Bentz, D., Garboczi, E., & Quenard, D. (1997). Modeling Drying Shrinkage in Reconstructed Porous Materials: Application to Vycor Glass. *Modeling and Simulation in Material Science and Engineering, 6*, 211-236.
Byard, B. (2011). (Personal Communication).
Edson, A. (2007). *Effects of Supplementary Cementing Materials on the Setting Time and Early Strength of Concrete.* University of Texas at Austin.
Emborg, M. (1998). Models and Methods for Computation of Thermal Stresses. In R. Springenschmid (Ed.), *Prevention of thermal cracking in concrete at early ages : state of the art report prepared by RILEM Technical Committee 119, Avoidance of Thermal Cracking in Concrete at Early Ages*, (pp. 178-230).
Emmanuel, J., & Hulsey, J. (1977, April). Prediction of the Thermal Coefficient of Expansion of Concrete. *Journal of the American Concrete Institute, 74*(4), 149-155.
Folliard, K., & Berke, N. (1997). Properties of High-Performance Concrete Containing Shrinkage-Reducing Admixture. *Cement and Concrete Research, 27*(9), 1357-1364.
Folliard, K., Smith, C., Sellers, G., Brown, M., & Breen, J. (2003). *Evaluation of Alternative Materials to Contorl Drying-Shrinkage Cracking in Concrete Bridge Decks.* Texas Department of Transportation.
Folliard, K., Smith, C., Sellers, G., Brown, M., & Breen, J. (2003). *Evaluation of Alternative Materials to Control Drying-Shrinkage Cracking in Concrete Bridge Decks.* Texas Department of Transportation. Center for Transportation Reserach.
Gardner, N., & Lockman, M. (2001, March-April). Design Provisions for Drying Shrinkage and Creep of Normal-Strength Concrete. *ACI Materials Journal*, 159-167.

Grasley, Z., & Lange, D. (2004). Modeling Drying Shrinkage Stress Gradients in Concrete. *Cement, Concrete, and Aggregates, 26*(2), 115-122.

Hedlund, H. (2000). *Hardening Concrete. Measurements and Evaluation of Non-Elastic Deformation and Associated Restraint Stresses.* PhD Thesis, Lulea University of Technology, Division of Structural Engineering.

Holt, E. (2001). *Early Age Autogenous Shrinkage of Concrete.* Technical Research Centre of Finland , VTT Building and Transport. VTT Publications 446.

Jensen, O., & Hansen, P. (2004). Autogenous deformation and RH-change in perspecitve. *Cement and Concrete Research, 31*, 1859-1865.

Krauss, P., & Rogalla, E. (1996). *Transverse Cracking in Newly Constructed Bridge Decks.* National Cooperative Higway Research Program (NCHRP). Transportation Research Board.

Larson, M., & Jonasson, J. (2003). Linear Logarithmic Model for Concrete Creep. II: Prediction Formulas for Description of Creep Behaviour. *Journal of Advanced Concrete Technology, 1*(2), 188-200.

Maxim. (2011). *DS1921G Thermochron iButton*. Retrieved from http://www.maxim-ic.com/datasheet/index.mvp/id/4023

Meadows, J. (2007). *Early-Age Cracking of Mass Concrete Structures.* Masters Thesis, Auburn University.

Mehta, P., & Monteiro, P. (2005). *Concrete: Microstructure, Properties, and Materials* (3rd ed.). McGraw-Hill.

Mindess, S., Young, J., & Darwin, D. (2002). *Concrete.* Englewood Cliffs, N.J.: Prentice Hall.

Mokarem, D. (2002). *Development of Concrete Shrinkage Performance Specifications.* PhD Thesis, Virginia Polytechnic Institute and State University, Civil and Enviromental Engineering.

National Instruments. (2006, Sept.). *Measuring Position and Displacement with LVDTs*. Retrieved from NI Developer Zone: http://zone.ni.com/devzone/cda/tut/p/id/3638

Poole, J. (2007). *Modeling Temperature Sensitivity and Heat Evolution of Concrete.* PhD Thesis, University of Texas at Austin.

Rao, A. (2008). *Evaluation of Early-Age Cracking Sensitivity in Bridge Deck Concrete.* Masters Thesis, Auburn University.

Raphael, J. (1984, March). Tensile Strength of Concrete. *ACI Journal, 81*(2), 158-165.

Riding, K. (2007). *Early age concrete thermal stress measurement and modeling.* PhD Thesis, University of Texas at Austin, Civil Engineering.

Schindler, A. (2004). Prediction of Concrete Setting. In J. Weiss, K. Kovler, J. Marchand, & S. Mindess (Ed.), *International RILEM Symposium on Concrete Science and Engineering.* RILEM Publications SARL.

Schindler, A., & Folliard, K. (2005). Heat of Hydration Models for Cementitious Materials. *ACI Materials Journal*, 24--33.

Shilstone, J. (1990, June). Concrete Mixture Optimization. *Concrete International, 12*(6), 33-39.

TxDOT. (2011). *Chemical Admixtures for Concrete.* Retrieved from Material Producer List: http://ftp.dot.state.tx.us/pub/txdot-info/cmd/mpl/admixtur.pdf
TxDOT. (2011, April). *Hydraulic Cement.* Retrieved from Materials Producer List: http://ftp.dot.state.tx.us/pub/txdot-info/cmd/mpl/cement.pdf
Viviani, M. (2005). *Monitoring and Modeling of Construction Materials During Hardening.* PhD Thesis, Swiss Federal Institute of Technology, Lausanne, Switzerland.
W.R. Grace. (2007). *Eclipse Plus.* Retrieved from Concrete Products: http://www.buildsite.com/dbderived/wrgrace/derived_files/derived320838.pdf
W.R. Grace. (2009). *WRDA 64.* Retrieved from Concrete Admixtures: http://www.na.graceconstruction.com/concrete/download/CMD-366G.pdf
Whigham, J. (2005). *Evaluation of Restraint Stresses and Cracking in Early-Age Concrete with the Rigid Cracking Frame.* Masters Thesis, Auburn University.
Wittman, F., & Roelfstra, P. (1980). Total Deforamtion of Loaded Drying Concrete. *Cement and Concrete Research, 10*, 601-610.